

University of  
**Strathclyde**  
Engineering

Department of Biomedical Engineering

Monitoring of antimicrobial coatings and biofilm formation on  
in vitro model of medical implant surfaces

Alyssa Reis

A thesis presented in the fulfilment of the requirements for  
the degree of Doctor of Engineering

January 2025

## Declaration of Authenticity and Author's Rights

This thesis is the result of the author's original research. It has been composed by the author and has not been previously submitted for examination which has led to the award of a degree.

The copyright of this thesis belongs to the author under the terms of the United Kingdom Copyright Acts as qualified by University of Strathclyde Regulation 3.50. Due acknowledgement must always be made of the use of any material contained in, or derived from, this thesis.

Signed:

Date: 1/7/25

# Abstract

Medical implant infections pose significant treatment challenges due to biofilm formation on the device surface, which is difficult to eradicate and can become antibiotic resistant. There are a range of antimicrobial strategies in use to prevent biofilm formation including development of biodegradable coatings loaded with antibiotics which enable controlled release of antibiotics to inhibit biofilm formation. This study evaluates the feasibility of utilizing Electrical Spectroscopy (ES) to non-invasively monitor medical implant-like surfaces along with polymer-antibiotic coatings for real-time monitoring of biofilm formation.

ES was used to monitor PLGA-Rifampicin coating degradation on stainless steel electrodes over 6-months. A novel system was developed to allow for monitoring of coating degradation and bacterial growth within the same system, and PLGA-Rifampicin-coated stainless steel and cobalt-chrome electrodes were challenged with *Staphylococcus aureus* and *Pseudomonas aeruginosa*, with bacterial growth and coating degradation monitored over six months.

The results showed that stainless steel and cobalt-chrome electrodes could measure bacterial growth on the electrode surface, with a significant decrease in impedance at 10 Hz and 100 Hz. ES could also detect the degradation of PLGA-Rifampicin coatings over a 6-month incubation period, with noticeable decreases in the whole impedance spectra correlating to drug release and polymer degradation. The novel system developed in this study could not distinguish between bacterial growth and coating degradation, as the coating's insulating properties overshadowed bacterial impedance signals leading to 80%

reduction in impedance at 10 Hz and 100 Hz for all different coating formulas with or without bacteria growth.

These findings highlight the potential of ES for characterizing bacterial growth on medical devices, though a technical challenge of the coatings insulating properties needs to be further studied to help further this work. Future work could refine this technique to support the development of advanced antimicrobial strategies.



# Acknowledgements

The first acknowledgements go to my two project supervisors Christopher McCormick and Michelle Maclean. They both provided invaluable guidance and encouragement that helped complete this project.

I must also thank Craig for teaching the tedious art of electrode production and Sandy with so much AFM guidance. As well as Stephen and Stewart for help in creating parts for my testing systems.

I thoroughly enjoyed my PhD experience, and I enjoyed everyone in lab. Many thanks to David and Lucy for all the bacteria help and thanks to all other friends and lab mates through the years, as it made the long days in lab bearable with some company.

Finally, a special thanks for all my family, but specifically all of my parents for supporting me going abroad for this experience and supporting me through it.

# List of Figures

Figure 1.1 – Depiction of bacteria attachment to surface

Figure 2.1 – Randles equivalent circuit model

Figure 2.2 – AC sin wave diagram

Figure 2.3 – Bode, phase, and Nyquist plot example

Figure 2.4 – Potential and responses of different types of voltammetry

Figure 3.1 – Schematic of dip coating and measurement points

Figure 4.1 – Impedance data for metals in PBS and different Rifampicin concentrations

Figure 4.2 – Phase angle at 10 Hz and 10 kHz of different Rifampicin concentrations of PBS with medical device metals as electrodes

Figure 4.3 – Representative impedance spectra of Rifampicin in stirred and non-stirred conditions

Figure 4.4 – Impedance and phase angle of SS in PBS at range of temperatures

Figure 4.5 – Impedance spectra, impedance and phase angle at 10Hz and 10kHz of Translumina stent and 50:50 PLGA: Rifampicin coated SS wire incubated for 10 hours

Figure 4.6 – Concentration curve with linear fit equation for sirolimus and Rifampicin

Figure 4.7 – Cumulative mass of drug released and total % drug released of Translumina stent and 50:50 PLGA: Rifampicin coated SS wire incubated for 10 hours

Figure 4.8 – Total impedance spectra for SS, Ti, CoCr, and Rifampicin coated wires incubated in PBS of fixed system

Figure 4.9 – Impedance at 10 and 100Hz and phase angle at 10 Hz and 10 kHz of SS, Ti, CoCr and Rifampicin coated wires in fixed system

Figure 4.10 – Changing rate of impedance at 10Hz and 10KHz and changing rate of phase angle at 10 Hz and 10 kHz for SS, Ti, CoCr and Rifampicin coated wires in fixed system

Figure 4.11 – Impedance spectra of PLGA, 75:25, 60:40, and 50:50 PLGA: Rifampicin coated wires incubated in PBS in fixed system

Figure 4.12 – Impedance and phase angle at 10Hz and 10kHz for PLGA, 75:25, 60:40, and 50:50 PLGA: Rifampicin coated wires incubated in PBS in fixed system

Figure 4.13 – Changing rate of impedance and phase angle at 10Hz and 10 kHz for PLGA, 75:25, 60:40, and 50:50 PLGA: Rifampicin coated wires incubated in PBS in fixed system

Figure 4.14 - Impedance spectra of PLA, 75:25, 60:40, and 50:50 PLA: Rifampicin coated wires incubated in PBS in fixed system

Figure 4.15 – Impedance and phase angle at 10 Hz and 10 kHz for PLA, 75:25, 60:40, and 50:50 PLA: Rifampicin coated wires incubated in PBS in fixed system

Figure 4.16 – Changing rate of impedance and phase angle at 10 Hz and 10 kHz for PLA, 75:25, 60:40, and 50:50 PLA: Rifampicin coated wires incubated in PBS in fixed system

Figure 4.17 – Cumulative and Total % Rifampicin released from PLA: Rifampicin and PLGA: Rifampicin samples over 1 week incubation in PBS

Figure 4.18 – Impedance measurements of samples incubated in 37°C fixed system at 10 Hz and 10 kHz

Figure 4.19 – Phase angle measurements of samples incubated in 37 °C fixed system at 10Hz and 10kHz

Figure 4.20 – Cumulative and % total Rifampicin released from PLGA: Rifampicin samples over 2-month period

Figure 4.21 – SEM Images at 0 hour and 1 week for SS, PLGA, 50:50 PLGA: Rifampicin and 50:50 PLA: Rifampicin

Figure 4.22 – SEM Images of remaining samples at time point 0 hour

Figure 4.23 – AFM 3D renderings of height data with height retrace of SS, PLGA, 75:25 PLGA: Rifampicin, 60:40 PLGA: Rifampicin, and 50:50 PLGA: Rifampicin

Figure 4.24 – AFM 3D renderings of height data with phase retrace of SS, PLGA, 75:25 PLGA: Rifampicin, 60:40 PLGA: Rifampicin, and 50:50 PLGA: Rifampicin

Figure 4.25 – AFM average roughness root mean square of coated samples

Figure 4.26 – Thickness measurements of each sample type

Figure 4.27 – DPV and SWV of Rifampicin with concentrations from 0  $\mu$ M to 6  $\mu$ M

Figure 5.1 – Schematic of xCelligence system

Figure 5.2 – Schematic of Lee et al, Pan et al, and Xu et als systems

Figure 5.3 – Schematic of Paredes et al systems

Figure 5.4 – Schematic of Turick et al patterned electrode for non-contact measurements

Figure 5.5 – Schematic of Holland et al's design

Figure 5.6 – Impedance and normalised impedance profile of Nutrient broth over 24 hours

Figure 5.7 – Impedance and normalised impedance profiles of *S. aureus* and *P. aeruginosa* compared to broth incubated on gold electrodes over 24 hours with a starting population of  $10^5$

Figure 5.8 – Phase angle and normalised phase angle profiles of *S. aureus* and *P. aeruginosa* compared to broth incubated on gold electrodes over 24 hours with a starting population of  $10^5$

Figure 5.9 – Impedance of nutrient broth versus *S. aureus* and *P. aeruginosa* normalised to nutrient broth at 10 Hz and 100 Hz, phase angle of nutrient broth versus *S. aureus* and *P. aeruginosa* normalised to nutrient broth at 1 Hz and 1000 Hz

Figure 5.10 – Normalised impedance of nutrient broth full spectra and 23 Hz and 100Hz compared to supernatants of *S. aureus* and *P. aeruginosa*

Figure 5.11 – Crystal violet-stained electrodes after 24 hour incubation period of *S. aureus* and *P. aeruginosa*

Figure 5.12 - *S. aureus* and *P. aeruginosa* biofilm formation after 24 hour incubation at 37°C with  $10^5$  starting population

Figure 5.13 – Planar device design for new system

Figure 5.14 – Vertical device design for new system

Figure 5.15 – Pictures of vertical device design

Figure 5.16 – Impedance of device design for validation

Figure 5.17 – Phase angle of device design for validation

Figure 6.1 – Normalised impedance and phase angle of samples incubated for 6 months in new system

Figure 6.2 – Normalised frequency at 10 Hz and 10 kHz for samples over 6 months in new system

Figure 6.3 – Normalised phase angle at 10 Hz and 10 kHz for samples over 6 months in new system

Figure 6.4 – Total and % total Rifampicin released from samples of new system over 6 months

Figure 6.5 - % Total Rifampicin released over 6-month incubation versus normalised impedance at 10 Hz for samples

Figure 6.6 – Impedance at 10 Hz and 10 kHz for all samples over 6 months

Figure 6.7 – Normalised impedance and normalised phase angle of sterile nutrient broth incubated over 24 hours

Figure 6.8 – Normalised impedance and normalised phase angle of nutrient broth with  $10^2$  to  $10^9$  S. aureus concentrations

Figure 6.9 – Normalised Z and phase angle of *S. aureus* grown on SS over 24 hours, 48 hours, and 72 hours

Figure 6.10 – Bacteria count of different incubation times

Figure 6.11 -Normalised Z at 10 Hz and 100 Hz and normalised phase angle at 1000 Hz and 10000 Hz of *S. aureus* grown over 24 hours

Figure 6.12 – Normalised Z and phase of *S. aureus* grown on Titanium electrodes

Figure 6.13 – Impedance and phase angle of *S. aureus* grown on PLGA coated SS electrodes

Figure 6.14 – Relative variation of normalised impedance at 10 Hz in % and bacteria count for *S. aureus* and *P. aeruginosa* grown over 24 hours on SS, PLGA, Rifampicin, and 50:50 coated electrodes

Figure 6.15 – Relative variation of normalised impedance at 100 Hz in % and bacteria count for *S. aureus* and *P. aeruginosa* grown over 24 hours on SS, PLGA, Rifampicin, and 50:50 coated electrodes

Figure 6.16 – Relative variation of normalised phase angle at 1000 Hz in % and bacteria count for *S. aureus* and *P. aeruginosa* grown over 24 hours on SS, PLGA, Rifampicin, and 50:50 coated electrodes

Figure 6.17 – Relative variation of normalised phase angle at 10,000 Hz in % and bacteria count for *S. aureus* and *P. aeruginosa* grown over 24 hours on SS, PLGA, Rifampicin, and 50:50 coated electrodes

Figure 6.18 – Bacteria count versus normalised impedance at 10 Hz and 100 Hz and versus normalised phase angle at 1000 Hz and 10 kHz for *S. aureus* and *P. aeruginosa*

Figure 6.19 – Biofilm inhibition versus drug remaining on Rifampicin and 50:50 coated electrodes



# List of Tables

Table 1.1 – List of metals used within medical implants, advantages and disadvantages, and devices they are used in

Table 1.2 – Common medical device and their infection rates

Table 1.3 – Most common bacteria species and prevalence in medical device infections

Table 1.4 – Common polymers and their properties

Table 1.4 – EIS designs with bacteria type, frequency range, and chosen analysis method

Table 3.1 – Summary details of impedance experiments for chapter 3

Table 4.1 – Coating type and total mass gained after coating

Table 5.1 – Needs analysis for new electrode design

Table 5.2 – Table of different types of EIS electrodes designs with advantages and limitations

Table 5.3 – Table of relevant frequency parameters

# List of Abbreviations

AFM	Atomic Force Microscope
AC	Alternating Circuit
CoCr	Cobalt chrome
CRFK	Crandall-Rees feline Kidney
DPV	Differential pulse voltammetry
<i>E. coli</i>	<i>Escherichia coli</i>
ECIS	Electrical Cell-Substrate Impedance Sensing
EIS	Electrochemical impedance spectroscopy
ES	Electrical Impedance Spectroscopy
EPS	Extracellular polymeric substance
GCE	Glassy Carbon electrode
<i>P. aeruginosa</i>	<i>Pseudomonas aeruginosa</i>
PBS	Phosphate Buffered saline (0.1M)
PDLA	Polymer D-lactic acid
PJI	Prosthetic join infection
PLA	Poly(lactic Acid
PLGA	Poly(lactic-co-glycolic acid)
PLLA	Poly-L-lactic acid
RMS	Mean average roughness
<i>S. aureus</i>	<i>Staphylococcus aureus</i>
<i>S. mutans</i>	<i>Streptococcus mutans</i>
SEM	Scanning electron microscopy
SS	Stainless Steel
SWV	Square wave voltammetry
Ti	Titanium
v/v	Volume per volume
w/v	Weight per volume
<i>S. epidermidis</i>	<i>Staphylococcus epidermidis</i>

## Contents

1	Introduction .....	21
1.1	Clinical Challenges.....	22
1.1.1	Medical Devices.....	22
1.1.2	Biofilms.....	25
1.1.3	Medical Implant Infections .....	27
1.1.4	Antibiotic Resistance .....	29
1.2	Medical Implant Antimicrobial Techniques.....	30
1.2.1	Antibiotic/antiseptic treatments .....	30
1.2.2	Surface Modifications .....	32
1.2.2.1	Coatings .....	32
1.2.2.2	Surface Roughening.....	36
1.3	Biofilm Monitoring/Antimicrobial testing techniques .....	38
1.3.1	Invasive Techniques.....	38
1.3.2	Non-Invasive Techniques.....	39
1.4	Clinical and Research Needs .....	40
1.5	Electrical Impedance Spectroscopy.....	41
1.5.1	Bacteria Monitoring .....	42
1.5.2	Drug Monitoring .....	45
1.5.3	Polymer Degradation .....	46
1.5.4	Surface Modification.....	47
1.5.5	Biomedical Applications.....	<b>Error! Bookmark not defined.</b>
1.6	Commercially available EIS electrodes.....	49
1.7	EIS Analysis Methods .....	50

1.8	Study Hypothesis and Aims .....	52
2	Theory .....	54
2.1	EIS .....	54
2.2	DPV and SWV .....	60
2.3	AFM .....	62
2.4	Biofilm recovery methods .....	63
3	General Methodology.....	65
3.1	Materials .....	65
3.2	Equipment .....	66
3.3	Section Aim and Objectives .....	66
3.4	Methods .....	67
3.4.1	Dip Coating .....	67
3.4.2	Electrochemical Impedance Spectroscopy.....	71
3.4.2.1	Variable testing .....	71
3.4.2.2	Translumina Stent vs Dip Coated Wires.....	72
3.4.2.3	Fixed system work .....	73
3.4.3	Characterization of Polymer and drug coatings .....	73
3.4.3.1	Coating Analysis.....	73
3.4.3.2	UV Spectrophotometry .....	74
3.4.3.3	Differential Pulse Voltammetry and Square Wave Voltammetry .....	75
3.4.3.4	Characterization of coating surface .....	75
3.5	Data Analysis .....	76
3.5.1	Data Presentation and Statistics .....	76
3.5.2	Experimental data inclusion.....	76
4	Chapter 4 Results of Polymer-drug Coating Development and EIS evaluation ....	78
4.1	EIS System Characterization of Variables .....	78
4.1.1	Impact of Rifampicin .....	78

4.1.2	Impact of Temperature and non-turbulent flow .....	81
4.2	Impedance characterization of Translumina Stent vs Dip Coated Wires .....	83
4.3	Impedance Characterization of Fixed System .....	86
4.3.1	Short term room temperature work .....	86
4.3.2	Long term 37°C temperature work .....	101
4.3.3	Polymer Degradation Characterisation .....	106
4.3.4	Non-invasive Drug Detection .....	116
4.4	Discussion .....	117
4.4.1	Characterisation of EIS System .....	117
4.4.2	Impedance of polymer-drug coatings .....	120
4.4.3	Polymer Evaluation .....	126
4.4.4	Drug Detection .....	128
4.5	System Limitations .....	130
4.6	Future Work .....	131
4.7	Summary .....	132
5	Chapter 5 Novel ES System Development .....	134
5.1	Introduction .....	134
5.1.1	Electrode Designs .....	134
5.1.1.1	Planar .....	135
5.1.1.2	Vertical .....	137
5.1.1.3	Non-contact .....	140
5.1.2	Bacteria ES analysis methods .....	141
5.2	Section Aims and Objectives .....	143
5.3	Methods .....	144

5.3.1	General Materials .....	144
5.3.2	General Equipment.....	144
5.3.3	Device 1 Design Fabrication .....	145
5.3.4	Bacteria test device design 1 .....	146
5.3.4.1	Bacteria Preparation.....	146
5.3.4.2	EIS of Biofilm.....	146
5.3.4.2.1	Measurement of nutrient broth alone.....	146
5.3.4.2.2	Measurement of biofilm formation.....	147
5.3.4.2.3	Measurement of bacteria byproducts .....	147
5.3.4.2.4	Evaluation of Biofilm .....	148
5.4	Bacteria Results from Chamber 1 .....	149
5.4.1	Bacteria ES chamber 1 .....	149
5.4.2	Biofilm Evaluation on device design 1 .....	157
5.5	Discussion .....	159
5.5.1	Electrical impedance spectroscopy on electrode design 1 .....	159
5.5.2	Biofilm Evaluation method.....	162
5.6	Limitations.....	163
5.7	System Development.....	164
5.7.1	Needs Analysis.....	164
5.7.2	Device designs .....	169
5.7.3	Design selection .....	171
5.8	Device Design 2 Methods .....	173
5.8.1	Electrode Fabrication .....	173
5.8.2	Design Evaluation .....	174
5.9	Results .....	174

5.10	Discussion.....	178
5.11	Limitations.....	180
5.12	Future Work.....	181
5.13	Summary.....	182
6	Chapter 6 Impedance based characterisation of drug release and biofilm formation using a novel <i>in vitro</i> platform.....	183
6.1	Aims and objectives .....	183
6.2	Methods .....	184
6.2.1	Characterisation of impedance properties of polymer-drug coatings on medical implant-like surfaces .....	184
6.2.2	Characterisation of impedance properties of biofilm formation on medical implant-like surfaces .....	185
6.2.2.1	ES of biofilms .....	185
6.2.2.2	Direct Enumeration from sonication.....	186
6.2.3	Data Presentation and analysis.....	186
6.3	Results .....	188
6.3.1	Characterisation of impedance characteristics of polymer-drug coatings on medical implant materials .....	188
6.3.1.1	Impedance Analysis.....	188
6.3.1.2	Rifampicin drug release characterisation.....	195
6.3.2	Impedance characterisation of model biofilms on electrodes .....	199
6.3.3	ES of polymer-drug and biofilms over time .....	207
6.4	Discussion .....	219
6.4.1	Impedance profiles of polymer-drug coatings within new system .....	219
6.4.2	Impedance using medical device metals to detect biofilm formation.....	223

6.4.3	Characterize polymer-drug coatings and biofilm formation in same system over time.....	226
6.5	Limitations.....	229
6.6	Future Work .....	230
6.7	Summary .....	231
7	General Discussion.....	233
7.1	Introduction .....	233
7.2	Impedance monitoring of the medical implant surfaces.....	234
7.3	Development of novel system for near continuous monitoring of the medical implant-bacteria interface.....	236
7.4	An optimised system for exploring antimicrobial medical implant-bacteria interfaces .....	236
7.5	General Study Limitations and Future Work .....	238
7.6	Summary of Contribution.....	239
8	Appendix .....	240
9	References .....	244



# 1 Introduction

The use of medical implants has increased significantly in recent decades because of both technological advancements and the larger proportion of the population that is living to an older age. Medical implants are devices meant to replace or support a damaged biological structure and include joint replacements, fracture fixation devices, dental implants, and vascular devices. While there have been many advancements in these devices, there are still a number of limitations that impact their effectiveness. One of the more problematic and persistent of such limitations is implant infection. Of all hospital infections, upwards of 25.6% of all infections are related to implants (Bryers, 2008, Magill et al., 2014) creating a strain on the patient and creating a larger cost for the healthcare sector. The current treatment for medical implant infections is often a full removal of the implant, cleaning of the wound, then replacement of the device with a new implant. Industry has developed a range of preventative antibacterial treatments with surface modifications being widely used in an attempt to reduce bacterial colonisation of implant surfaces (Zheng et al., 2022). Orthopaedic implants and vascular grafts have been developed that utilize drug coatings paired with biodegradable polymers, bone cement, or hydrogels to have a prolonged release (Pan et al., 2018). However, these approaches have not fully addressed the infection challenge. The design and implementation of these different antibacterial technologies has been limited by a number of technical challenges that remain to be overcome (Pan et al., 2018). One important challenge is the current inability to continuously monitor in real time the interaction between bacteria and medical implant surfaces in conditions that mimic the *in vivo* environment, including materials that

are actually used in medical implants, coatings used on those implants, and the combined growth of cells and bacteria. Electrochemical impedance spectroscopy (EIS) is a non-destructive and non-invasive measurement method that has been used to characterise mammalian cell cultures (Shedden et al., 2010, Holland et al., 2018, Szulcek et al., 2014), with some recent reports indicating its potential for monitoring bacterial adhesions and biofilm formation (Begly et al., 2020, Gutierrez et al., 2016, Kim et al., 2011a). However, such studies have been exclusively performed on model electrode surfaces, such as gold or platinum, which are not representative of the typical materials used within medical implants. This study therefore set out to address these knowledge gaps and develop new ES-based technologies for monitoring bacterial colonisation of medical surfaces. It focused on identifying a quick analysis method that could simultaneously monitor changes to an antimicrobial coating and differentiate those changes from biofilm growth of different bacteria species. In so doing, it is intended to accelerate progress towards more effective prevention of medical implant infection in future through screening many different antimicrobial coatings and determining their effectiveness in real-time.

## **1.1 Clinical Challenges**

### **1.1.1 Medical Devices**

Over one million vascular devices are implanted each year including stents, grafts, heart valves, and pacemakers (Darouiche, 2004). Of these, over 4% are predicted to experience an infection, with high mortality and morbidity rates (Darouiche, 2004). Vascular devices are used to treat and repair parts of the vascular system including heart and blood vessels.

Vascular grafts have one of the higher rates of infection at 4% (Darouiche, 2004). They are used to treat aneurysms, a part of an artery wall that has stretched and created a bubble-like structure with thin walls. Grafts are placed to avoid rupture by creating an alternative route for blood to flow. These grafts are made of biostable polymers such as Dacron, with endovascular grafts also including a wire mesh made of Nitinol alloy for a self-supporting structure that prevents slipping of the graft along the artery wall (Jackson and Carpenter, 2009).

Total hip arthroplasty is one of the most common joint replacements worldwide, with more than 790,000 procedures recorded in the National Joint Registry in England from 2012 to 2016 (Hu and Yoon, 2018). Total hip arthroplasty relieves pain and improves function of those with arthritis of the hip joint (Ferguson *et al.*, 2018). For the procedure, the femoral head of the femur is replaced with a metal femoral stem and head while the acetabulum is replaced with an acetabular cup which could be made of several different materials (Hansen, 2020). The common materials used in for the femoral stem and acetabular cup are stainless steel, cobalt-chromium alloys, and titanium alloys (Hu and Yoon, 2018). Polyethylene and ceramics are also used within the acetabular cup and femoral head, but for the acetabular cup they are placed within a metal jacket that is in direct contact with the bone for better securement. This study will focus on the metals used within medical devices as they are electrically conductive, therefore will be more likely to measure bacterial attachment..

**Table 1.1** List of metals used within medical implants, the advantages and disadvantages, devices they are used in, and reference

<b>Metal</b>	<b>Advantages</b>	<b>Disadvantages</b>	<b>Device</b>	<b>Reference</b>
Stainless Steel	Malleability, corrosion, and fatigue resistance	Not inherently biofunction	Stents, grafts, artificial joints, support screws	(Bekmurzayeva <i>et al.</i> , 2018), (Hu and Yoon, 2018)
Cobalt-Chromium alloys	Strength, corrosion, wear resistance, biocompatibility	Biocorrosion, allergic reactions, Cardiotoxicity with wear	Artificial joints, stents, grafts	(Hu and Yoon, 2018)
Titanium Alloys	Low density, high corrosion resistance, specific strength, biocompatibility	Poor wear resistance, hypersensitivity	Artificial joints, Bone fixators	(Hanawa, 2012, Akshaya <i>et al.</i> , 2022)

Stainless steel and cobalt-chromium alloys are the most common metals used in stent and orthopaedic implants. Nitinol is common in graft designs. Cobalt-chrome and titanium alloys are more frequently used in artificial hips, with stainless steel being used less frequently apart from the United Kingdom (Hu and Yoon, 2018). Stainless steel is widely used because of its easy machining and low cost but fell out of favour because of its mechanical properties and need to be altered to have good blood compatibility, osteoconductivity, and bioactivity which makes it less ideal for long term implants. Cobalt-chromium alloys are the most favourable metal with artificial hips and stents because of its strength, biocompatibility, and wear resistance (Hu and Yoon, 2018).

Titanium alloys have benefits including low density, high corrosion resistance, biocompatibility, and higher strength. It has also been shown that titanium may be more resistant to biofilm formation, compared to stainless steel (Connaughton *et al.*, 2014). The main disadvantage comes from its poor wear resistance so when used within a hip implant, it releases wear particles more often than other metals. Each of these metals are commonly used within medical implants and have therefore been associated with bacterial infections following implantation (VanEpps and Younger, 2016, Jiao *et al.*, 2021).

### **1.1.2 Biofilms**

Medical device infection accounts for 25.6% of all healthcare associated infections (Magill *et al.*, 2014). Bacterial infections are problematic as 65% of cases form a biofilm, which are very difficult, and often impossible, to eradicate with antibiotics due to various factors (del Pozo and Patel, 2007). A biofilm comprises of an aggregation of bacteria that secrete an extracellular polymeric substance (EPS) (Figure 1.1). There are several stages to bacteria attachment and biofilm formation, which can be sectioned into two categories: reversible and irreversible. In the reversible category, which occurs when bacteria are initially introduced into the environment, the bacteria attach to the surface with non-specific binding. This can occur within seconds of the bacteria being introduced to the surface and its surrounding environment (Khatoon *et al.*, 2018).

The irreversible stage takes place when the bacteria begin to form clusters and secrete the EPS to adhere to the surface and protect the bacteria within from the environment (Kargupta *et al.*, 2014). This continual formation leads to a microcolony that creates a full mature biofilm. Maturation can vary depending on the bacteria type but typically occurs

within 24 hours and drops off after 72 hours (Babushkina *et al.*, 2020). Once a biofilm is matured, it will eventually begin to disperse planktonic bacteria, thereby spreading the infection further.

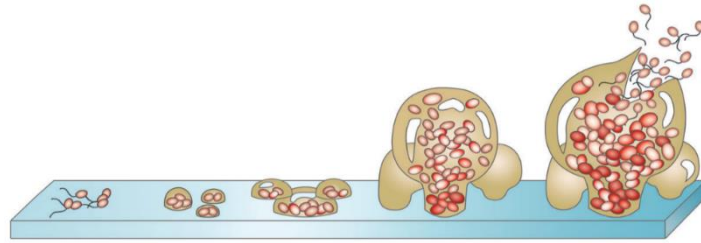


**Figure 1.1** Depiction of bacteria attachment to surface. Aggregation of bacterial cells to the surface and the secretion of the EPS. Maturation of the biofilm, leading to a release of bacteria into the environment. Replicated from Kargupta *et al* (Kargupta *et al.*, 2014).

The EPS holds an important role in the biofilm life cycle as it protects the bacteria in several ways. It creates a barrier that inhibits penetration of antibiotics and provides protection against the immune cells thereby shielding the bacteria within. It also slows down the metabolism of the bacteria within the biofilm, making the antibiotics that do penetrate less effective (Arciola *et al.*, 2018). This leads to severe difficulty in treating bacterial infections on medical implants.

Infections can occur at several different points after implantation of medical devices: early, delayed, or late. The most at-risk time for bacterial infection is within 3 months after placement which are called early infections. These are thought to occur from contamination during implantation. Delayed infections occur within 3 to 12 months after

placement and are usually coagulase-negative staphylococci that are very resistant to antibiotics (Kargupta *et al.*, 2014). The last and most difficult to treat infections are late infections that can occur several years after implantation and can be hard to detect as symptoms can be misdiagnosed as another cause (Huotari *et al.*, 2015). Most of these infections occur due to another infection within the body that spreads through the bloodstream (Surgeons, 2023). This is why it is important to have an antimicrobial treatment or indeed surface, that is effective in long term and short term, and to have studies on antimicrobial effectiveness in the long and short term.

### **1.1.3 Medical Implant Infections**

Every implanted medical device is susceptible to bacterial infections, but some are more susceptible than others due to the body's foreign body reaction to inorganic material.

Table 1.2 lists common medical devices that have metal and their rate of infection.

**Table 1.2** Table of common medical devices with metals and their infection rates in percentage

Vascular/Cardiac Devices	Infection Rate (%)	Reference
Stent	1	(Ayyubi <i>et al.</i> , 2023)
Vascular graft	4	(del Pozo and Patel, 2007) (Darouiche, 2004)
Left ventricular assist device	40	(Darouiche, 2004)
Heart Valve	4	(del Pozo and Patel, 2007)
Cardiac implantable electronic device	5-20	(del Pozo and Patel, 2007)
<b>Prosthetic Joints</b>		
Hip	0.5-1.7	(Stewart and Bjarnsholt, 2020) (VanEpps and Younger, 2016)
Knee	1-4	(Stewart and Bjarnsholt, 2020)
Shoulder	1-1.5	(Stewart and Bjarnsholt, 2020) (VanEpps and Younger, 2016)
Elbow	5	(VanEpps and Younger, 2016)
<b>Others</b>		
Fixation screws	5	(del Pozo and Patel, 2007)

Vascular and cardiac devices tend to have higher infection rates, especially the assist device and cardiac implantable electronic device which start at 5% and going as high as 40%. The prosthetic joints have a smaller range of infection rates from 0.5 to 5% but prosthetic joints are more difficult to treat as they need longer periods of antibiotic therapy and typically need revision surgery which can cause other complications (Darouiche, 2004).



The most common bacterial infections come from Gram-positive species like *S. aureus* and *S. epidermidis* as seen in Table 1.3, but Gram-negative infections can also occur (Davidson *et al.*, 2019). *P. aeruginosa* is the most prevalent Gram-negative species, but it is still significantly lower in occurrence, at only 6%, than the Gram-positive species in orthopaedic implant (Arciola *et al.*, 2018).

**Table 1.3** Table of most common bacteria species split between positive species (top) and negative species (bottom) and the prevalence in medical device infections adapted from (Arciola *et al.*, 2018)

Species	Prevalence in medical device infections (%)
<i>Staphylococcus aureus</i>	31.7
<i>Staphylococcus epidermidis</i>	39
<i>Streptococcus spp. &amp; Enterococcus spp.</i>	10.3
<i>Enterococcus faecalis</i>	2.4
<i>Pseudomonas aeruginosa</i>	6.1
<i>Escherichia coli</i>	2.4

#### 1.1.4 Antibiotic Resistance

The most common treatment method for bacterial infections is antibiotics. When a full biofilm forms on an implant, the implant is removed, and the area cleaned to ensure the biofilm is eradicated followed by a treatment of antibiotics. Infection thus will often necessitate surgery to remove the implant, with a further separate surgery needed to replace the implant. All of this introduces physical pain and mental anguish to the patient and their relatives. The success of such revision and replacement surgery is lower than the primary surgery and has a higher rate of infection associated with the surgery. The

challenge is further exacerbated by the potential development of antibiotic resistance, with *S. aureus* infections having the highest propensity to develop resistance (Bhattacharya *et al.*, 2015).

Many factors play into antibiotic resistance, gene mutations associated with planktonic bacteria and others that are biofilm specific. *S. aureus* has an increase in antibiotic minimum inhibitory concentrations when in a biofilm compared to planktonic bacteria, indicating enhanced antibiotic tolerance when in a biofilm state (Bhattacharya *et al.*, 2015). Horizontal gene transfer also occurs within biofilm at a faster rate, increasing antibiotic resistance, especially if the treatment is not lethal to all bacteria and a few dormant “persister” bacteria cells remain that have developed a resistant gene (del Pozo and Patel, 2007). Biofilms can upregulate stress-response genes when a biofilm bacteria is exposed to a certain type of drug, going on to express phenotypes that are more resistant to that drug (del Pozo and Patel, 2007). All these factors make treatment of biofilms especially difficult and antibiotic resistance a major concern in the treatment of biofilms.

## **1.2 Medical Implant Antimicrobial Techniques**

### **1.2.1 Antibiotic/antiseptic treatments**

Antibiotic treatment remains the most common practice to treat infections and is used as pre-emptive treatment as well. For treatment of existing biofilms, antibiotics are given and, in most cases, surgical debridement with retention of implant is also performed (Bhattacharya *et al.*, 2015). Since implant infections are usually concentrated at the implant site, oral antibiotics are ineffective as the drug is dispersed throughout the body and not concentrated enough at the infection site. An established biofilm is hard to

eradicate even with the combined protocol and exposes the patient to increased pain and cost. Due to this, pre-emptive treatments are being widely investigated for use in medical implant surgery. These have been recently reviewed by Fearing et al (Fearing et al., 2022), in the field of orthopaedics and Arciola et al (2018), in the field of vascular implants and medical devices more generally.

Pre-emptive use of antiseptics and antibiotics like iodine or vancomycin can be directly applied to the implant using a simple dip coating (Li *et al.*, 2023a). Vancomycin is a widely used drug treatment for *S. aureus* biofilm-associated infections. However, because *S. aureus* can develop resistance easily as described in Section 1.1.3 vancomycin is often used in combination with other drugs like Rifampin (also known as Rifampicin) or linezolid to minimise the risk of drug resistance. The drug that remains most effective against biofilm-associated staphylococci is Rifampin, as it is effective against even difficult-to-treat dormant bacteria (Bhattacharya *et al.*, 2015). It is currently used by some surgical teams to prevent infection following graft implantation for treatment of aortic aneurysms (Mufty *et al.*, 2022), although it is not generally used alone within orthopaedic implant applications. Other drugs that are used for biofilm treatment include oxacillin and tigecycline, which are generally used in combination with Vancomycin or Rifampin. A study by Lew and Moore (2011), explored the coating of gentamicin onto vascular grafts to prevent infection but the antibiotic did not bind to the Teflon and thus did not provide consistent protection clinically. Simple antibiotic coatings seem to only be effective in the very short-term time providing some prevention of infection from surgical contamination but only if the antibiotic can bind to the implant. However, infections can occur as far as

years after implantation and so other methods are being explored for long term effect and methods of binding the antibiotic, or other antimicrobial compounds, to the surface.

### **1.2.2 Surface Modifications**

There are currently a wide range of antimicrobial treatments for medical implants with either a passive or active surface modification. Passive modifications change the surface properties like the hydrophobicity, while active modifications have interactions based on different uses of biological molecules. The goal of these modifications is to prevent infections while also promoting implant integration by promoting cell growth. The ‘race to the surface’ suggests that if the surface can be colonised by mammalian cells then that in itself prevents bacteria adhesion and biofilm formation.

#### ***1.2.2.1 Coatings***

As discussed, antibiotics are most effective against bacterial infections. A method of binding antibiotics to the surface that has significant potential is the use of coatings that are loaded with a drug, allowing for sustained release over a variety of durations and profiles. Such coatings have found widespread successful application within coronary drug-eluting stents (O’Brien *et al.*, 2015), with similar approaches under development within orthopaedic devices and vascular grafts, as a means of providing protection against infection. Such coatings can consist of polymers, or sol-gel composites with the typical antibiotics of gentamicin, Rifampicin, and vancomycin (Li *et al.*, 2023b) (Eltorai *et al.*, 2016). Hydroxyapatite coatings have also been used within orthopaedics, but the effectiveness of the antibiotics bound has yet to be fully demonstrated (Davidson *et al.*, 2019).

Permanent polymers were briefly used on stents but were linked to inflammation and delayed healing (Wu et al., 2015). Biodegradable polymers are often used within these coatings as they provide a steady release profile that can be easily manipulated. Table 1.4 shows the common polymers used and their typical properties relevant to coatings. Polylactic Acid (PLA) and Poly-L-lactic acid (PLLA) are both semi-crystalline. They have some structured sections of polymer and some unstructured sections, that have unique combination of properties including a set melting point. Poly(lactic-co-glycolic acid) (PLGA) and Polymer D-lactic acid (PDLA) are amorphous polymers which have a gradual glass transition temperature versus a set temperature at which they melt. PLGA is more common in medical device applications as it allows for more control in the ratio of the acids for controlled degradation rates.

**Table 1.4** List of common polymers, their crystallinity, typical degradation time, their glass transition temperature, and their tensile strength. Replicated from (Gentile *et al.*, 2014)

<b>Polymer Material</b>	<b>Crystallinity</b>	<b>Degradation Time (days)</b>	<b>Glass Transition Temperature (°C)</b>	<b>Tensile Strength (MPa)</b>
PLGA	Amorphous	12-18	50	65
PLA	Semi-crystalline	18-30	60	65
PLLA	Semi-crystalline	Over 24	60-65	60-70
PDLLA	Amorphous	3-4	55-60	40

Biodegradable polymers have four stages of degradation: water diffuses into the polymer matrix, oligomers with acidic end- groups autocatalyze, and then diffuse out from polymer, creating micropores for the drug to release. With further water uptake into the increasingly porous polymer matrix, degradation accelerates and continues until complete degradation and dissolution of the polymer (Engineer *et al.*, 2011).

There are many studies within the scientific literature that have been developed on a variety of different antimicrobial drug-polymer coatings (Lu *et al.*, 2021), but very few such coatings are approved for use, with applications limited to vascular stents, catheters, and titanium tibia nails (Li *et al.*, 2023b, Zhu *et al.*, 2022). The precise reasons for the

limited translation of promising drug-polymer coatings into more widespread clinical application are complex. Within orthopaedics, Busscher et al has suggested there is a translational deadlock comprising a number of interlinking factors that sit across academia, industry and regulatory bodies (Busscher et al., 2019). Importantly, the costs involved in product development and regulatory approval are substantial, which can impede the investigation of new coating technologies. The same factors also mean that our understanding of the precise causal factors driving biofilm formation following implant surgery remains incomplete, with significant gaps in understanding of the interaction between bacteria and surface coatings.

Another common surface modification that has antimicrobial properties is the impregnation of metals onto the surface through plasma spraying or sputtering metals. Silver, copper oxide, zinc oxide, titanium dioxide, and tungsten oxide all have antimicrobial properties (Kargupta *et al.*, 2014). Silver is the most common used within medical implants but has been linked to cytotoxicity, so it is challenging to find a balance that achieves antimicrobial effectiveness whilst minimising cell toxicity (Li *et al.*, 2023a). In one study of a copper and titanium modified surface, copper was found to prevent bacteria, with the titanium helping to bind the copper to the stainless steel implant. Another study also looked at Si attachment which also had high antimicrobial properties, which was attributed to its nano roughness (Braceras et al., 2014). While metal impregnation does have the benefit of being relatively easy to control in the production of the surface, the potential toxicity from the metals makes it a higher risk antimicrobial treatment.

#### ***1.2.2.2 Surface Roughening***

The most common passive surface roughening techniques are 3D polishing, electropolishing, plasma spraying, and chemical etching. There also has been research into nanopatterning and self-assembled monolayers or multilayers which both have antibacterial properties (Romanò *et al.*, 2015, Singh *et al.*, 2011). Each creates a different roughness profile, from the nano to macro scale. Bohinc *et al* showed that while bacterial adhesion increased with increased roughness it did not depend on the roughening technique, although this study only examined a limited number of different roughening techniques (Bohinc *et al.*, 2016). A surface with micro scale alterations has greater chance of bacterial adhesion versus a nano roughness (Georgakopoulos-Soares *et al.*, 2023, Mu *et al.*, 2023).

Surface roughness and chemical composition influence biofilm formation, with Medilanski *et al* finding an average roughness of 0.16  $\mu\text{m}$  measured over 1  $\text{mm}^2$  for different metals being ideal to prevent bacteria adhesion (Bekmurzayeva *et al.*, 2018, Medilanski *et al.*, 2002). Many different studies try to find an ideal roughness, and going above or below the ideal roughness will cause an increase in bacterial attachment so the right balance needs to be found (Eltorai *et al.*, 2016).

Smart hydrogels are stimuli responsive and have been loaded with antibiotics and applied directly to an implant surface to prevent surgical infection (Bordbar-Khiabani and Gasik, 2022). Such hydrogels undergo hydrolytic degradation *in vivo* releasing the antibiotic that was trapped within for a sustained release over 72 hours for prevention of infection (De Meo *et al.*, 2021). There are more studies on prophylactic efficacy of hydrogels than the



therapeutic strategies like targeted antibiotic therapy. There are many studies on antibiotic-loaded hydrogels but only a few are currently used commercially. The current ones are mainly utilized in wound dressing including ActivHeal, DermaSyn, NU-GEL, and a few more are examples of commercial products (Aswathy et al., 2020).

It is clear that a vast volume of research has been produced in the pursuit of the development of more effective technologies for prevention of implant-associated infections. Whilst there are substantial differences in the proposed antimicrobial mechanism in each case, they are all united by what has been very limited translation into clinical practice or indeed new devices. Numerous studies are published in academia each year, but in recent years only a few have made it to commercial use (Busscher et al., 2019). Many factors limit such translation, but common to many of these is a still fairly limited understanding of the interaction between bacteria and the implant surface coating. This in turn limits the extent to which such surface coatings can be optimised. A new technique that would permit near real-time monitoring of the implant surface coating would therefore be of substantial value. Specifically, a monitoring system that would be able to detect surface modification as well as bacteria attachment may allow for the correct selection of antimicrobial treatments and/or surface modifications, thereby providing new knowledge to help accelerate development of more effective antimicrobial implant coatings in future.

## **1.3 Biofilm Monitoring/Antimicrobial testing techniques**

### **1.3.1 Invasive Techniques**

In vivo techniques for researching and evaluating antimicrobial technologies involve implantation of the prototype device into an animal model for a certain amount of time, following which the animal is killed, allowing complete removal of the implant and subsequent inspection (Xi et al., 2021). There are several important limitations associated with such in vivo studies, with significant ethical concerns and their high cost, meaning that they are generally reserved for final characterisation of the safety and potential efficacy of the proposed device. This means that data gathered is generally limited to a single end-point analysis. Li et al 2019 evaluated several animal studies to determine the effectiveness of various antimicrobial coatings against *S. aureus* in orthopaedic implants/femur fractures. Importantly, in vivo animal studies do not allow detailed assessment of the mechanisms driving biofilm formation at various stages following implantation.

Once a device has successfully passed through in vivo evaluation in animal models, it can be considered for first evaluation in humans. Such clinical studies provide critical information on the potential safety and efficacy of the proposed device. This involves patients being implanted with the device and monitored post operatively for a variety of indicators, including infection and other possible side effects. While this gives the most accurate data on device performance and is essential before the device can be approved for more widespread use, it remains limited in the temporal nature of the information that can be gained. Such limitations are, at least in part, responsible for the continuing

uncertainty surrounding the precise factors responsible for implant-associated infections (Fearing et al., 2022).

### **1.3.2 Non-Invasive Techniques**

In vitro techniques for testing antimicrobial coatings includes elution studies if the coating involves antibiotic loading. The coating is placed in an appropriate media and the concentration of drug released over time is measured. This can then be compared to drug effectiveness to determine how long the effectiveness against bacteria will be (Zhao et al., 2009).

Antibacterial assays have the coated implant incubated in a bacterial suspension and left for certain time periods. Once the chosen time has been reached, the solution is removed and the bacteria counted to determine kill (Jahanmard *et al.*, 2020). This provides data on how effective the coating is in preventing bacterial attachment or causing bacteria death, but again is limited to certain time points and does not show real time data on how the antibacterial mechanisms responsible.

A real time monitoring of *S. aureus* and *P. aeruginosa* biofilm was tested through bioluminescent bacteria using a multi-photon laser scanning microscope (Bryers, 2008). This was effective in tracking the biofilm and its dispersal or accumulation, along with various steps of biofilm formation but it required bacteria that were manipulated to be bioluminescent. This requires bacteria species that can produce the fluorescent protein, limiting its usefulness in terms of in vivo work. None of these techniques allows an easy real time monitoring of bacteria on an implant-like surface.

## 1.4 Clinical and Research Needs

Medical implants have revolutionised healthcare, with the use of cardiac valves, coronary stents and vascular grafts saving millions of lives each year. Likewise, within orthopaedics, the development of joint replacement surgery has helped restore pain-free movement to similar numbers of people. However, implant surgery presents a small, but persistent, risk of infection, which when it takes hold can be devastating for the patient. It also increases the financial burden on healthcare systems.

There are many new antimicrobial methods being developed each year (Akshaya et al., 2022, Li and Webster, 2018). Industry is exploring how local drug release from the implant surface may help improve implant integration and reduce infection (Acharya and Park, 2006). Efforts are under way to exploit alternative alloys and new surface treatments to promote cell adhesion and growth to promote better integration of the implant within surrounding tissue (O'Brien *et al.*, 2015). Progress in all of these areas has relied on the use of a variety of experimental methods, ranging from in vitro through to in vivo (section 1.3). Typically, these methods include an in vitro model that does not mimic the real environment the implant would be exposed in the non-invasive techniques. This limitation is addressed to some extent by in vivo models, but the need for removal of the implant for characterisation means that the number of data points gathered is very limited. This limits understanding of the implant-tissue interface, meaning that innovation is limited as industry does not fully understand the reactions in the body (Busscher et al., 2019).

The precise factors governing biofilm formation on medical implant materials remain poorly understood. In turn, this knowledge and technology gap, limits industry in their

efforts to improve device design using advanced materials and drug delivery strategies. Moreover, there is currently no accurate way to non-invasively characterize the degradation of the polymer or drug release of these coatings while simultaneously understanding the effect of these coatings on biofilm growth. . At present, industry and clinicians do not know the optimal release kinetics for polymer-drug coatings for the prevention of infection whilst preserving cell viability and function within the surrounding environment. The full potential of polymer coatings and local drug delivery strategies for the prevention of infection therefore remains to be realised.

This study explores the use of ES as a non-destructive real time monitoring technique that would more accurately model an antibacterial coated implant. It is intended that the system provide near real-time, non-invasive simultaneous measurement of drug release/polymer degradation and bacterial colonization on medical implant surfaces. Ideally, this system will be able to provide real time analysis on the presence of a biofilm and help with screening for new antimicrobial coatings quickly. This will provide new knowledge and technical capability to help inform future design of implant surfaces that are more resistant to biofilm formation.

## **1.5 Electrical Impedance Spectroscopy**

ES has been used within a large range of applications from corrosion monitoring to biosensors. ES provides a non-invasive means of monitoring bacteria adhesion, drug monitoring, polymer degradation, and surface modification. To date, these have almost exclusively been monitored separately or in isolation. ES holds great potential for

providing the enhanced understanding of the device-cell-bacteria interface necessary to optimise future implant design.

### 1.5.1 Bacteria Monitoring

There are many different electrical techniques used to monitor bacterial attachment and other electrode surface effects from cyclic voltammetry (CV) to differential pulse voltammetry (DPV) to square-wave voltammetry (SWV) to ES. ES has been used in many ways to detect different bacteria strains and to determine the maturation of biofilms and will be the focus of this review.

Hannah *et al* used a three-electrode cell using a DropSens SPE chip to measure bacteria growth following modification. They used both EIS and DPV on a gold electrode to see growth profiles of *S. aureus* and Methicillin Resistant *S. aureus* on different agarose gels containing different antibiotic concentrations of amoxicillin and oxacillin, at 8 and 50  $\mu\text{g/ml}$ . They found that impedance at 100 kHz the measurements showed no growth with antibiotic and growth in low antibiotic concentrations (Hannah *et al.*, 2019), with the impedance increasing noticeably upwards of 20  $\Omega$  from baseline after 90 minutes with no antibiotic compared to with amoxicillin or oxacillin the impedance which decreased slightly by 4  $\Omega$ . This shows that in an ideal setting, impedance can be used to detect bacteria growth based on different antibiotic concentrations effectively.

Ward *et al* used carbon ink electrodes on disposable sensor with impedance readings that were normalised to the initial measurement to measure *P. aeruginosa* strain PA14 and *S. aureus* strain RN4220 individually and in a co-culture. They found that after 24 hours

incubation there were changes in phase angle and impedance that were clearly observed dropping from 4.7 M $\Omega$  to 100 k $\Omega$  at 0.1 Hz for *P. aeruginosa*. *S. aureus* did not show a significant difference in impedance throughout the experiment, though they do show a difference in their impedance curve, they believe the lack of significance was due to the large baseline impedance reading effecting results and that an electrode with a lower starting impedance would help that (Ward *et al.*, 2014). This would be important to consider during experimentation, if the electrodes had a large starting impedance that would overshadow bacteria reading results. This shows both *S. aureus* and *P. aeruginosa* can be detected by impedance measurements, though not always giving a significant result depending on the electrode.

There are many studies on EIS and ES with different bacteria which are listed in Table 1.5. The main points to take from the table are most of the designs include gold, carbon, platinum, or silver-silver chloride electrodes. They also generally start at a high bacterial starting population of 10<sup>6</sup> CFU/ml, with a frequency range from around 1Hz and going as high as 1MHz. There are many different analysis methods which will be discussed in Section 2.1.

**Table 1.5** List of different EIS and ES designs used to monitor bacteria, the type of bacteria tested, the frequency range used in the system, and their chosen analysis method for bacteria growth

EIS and ES Design	Bacteria Type with Population (CFU/ml)	Frequency Range	Chosen Analysis	Reference
Gold (Au) screen-printed with agarose gel deposit	<i>S. aureus</i> x 10 <sup>7</sup>	0.1 Hz – 100 kHz	Z vs time @ 100kHz Change in Z over time (in %)	(Hannah <i>et al.</i> , 2019)
Carbon ink with acrylic cylinder chamber on top	<i>P. aeruginosa</i> and <i>S. aureus</i> x 10 <sup>6</sup>	0.1 Hz – 1 Mhz	Below 1000 Hz Phase v Frequency Impedance versus frequency Normalized resistance vs Frequency	(Ward <i>et al.</i> , 2014)
Silver-silver chloride suspended vertically in vial	<i>S. aureus</i> x 10 <sup>6</sup>	0.1 Hz- 100 kHz	Normalized Phase vs Fre Normalized Z vs Fre Peak in normalized phase vs Frequency	(Farrow <i>et al.</i> , 2012)
Interdigitated microelectrode sensors of goldvertically placed in petri dish	<i>S. epidermidis</i> x 10 <sup>6</sup>	1, 10, 100, 1000 Hz	Relative variation % at 10Hz and 100hz	(Paredes <i>et al.</i> , 2014a)
Platinum disk electrodes insulated with polychlorotetrafluoroethylene	<i>P. aeruginosa PA14 wild type</i> x 10 <sup>6</sup>	1-100,000 Hz	% Change in double-layer capacitance ZvsF Cim vsCre	(Kim <i>et al.</i> , 2011c)
Graphite rods with silver-silver chloride reference	<i>Ureolytic microorganisms</i>	10 kHz to 1 mHz	Equivalent circuit	(Romero <i>et al.</i> , 2021)
Anti-fouling and polyurea coated steel coupons	<i>Sulfate reducing bacteria</i>	1 MHz to 1 Hz	Equivalent Circuit	(Permeh <i>et al.</i> , 2019)



### 1.5.2 Drug Monitoring

There are certain types of drugs that are electroactive, meaning when subject to an electric field they undergo chemical reactions, in this case oxidation, and this change can be monitored through different voltammetry techniques (Kul, 2020). The theory behind voltammetry will be discussed in chapter 2. The combined use of voltammetry with an ES system would be useful as it could potentially measure drug concentration while simultaneously taking ES measurements. Rifampicin is a common electroactive antibiotic that is used to treat many different bacterial infections, specifically *S. aureus*, one of the most prevalent bacterial infections for medical devices as discussed in Section 1.1.3.

There have been many studies into using voltammetry to detect Rifampicin concentrations in different media for quick detection. They mainly use modified glassy carbon electrodes (GCE) or carbon paste electrodes. Amidi *et al* used a GCE vs Ag/AgCl reference electrode that was modified with poly-melamine and gold nanoparticles to investigate Rifampicin oxidation using CV. They found potential peaks at 0.09 V and 0.7 V that allowed for a linear detection range for Rifampicin of 0.08-15  $\mu\text{M}$  (Amidi *et al.*, 2017). Kul *et al* used a GCE modified with multi-walled carbon nanotubes vs Ag/AgCl reference electrode to detect Rifampicin using CV, DPV and SWV. They found peaks at around 0.2 V (Kul, 2020). While these coated electrodes would be useful within a laboratory setting, investigation into other electrode materials like those within a medical implant need to be performed to determine if they have the same sensitivity to detect Rifampicin concentrations.

### 1.5.3 Polymer Degradation

Many medical devices employ a polymer coating to release drugs from the surface or provide antimicrobial properties itself, so it is important that there is a way to monitor how this affects the healing as well as infection prevention. There have been a few studies on the use of EIS and ES in detecting polymer degradation, most recently Zhong *et al.* They used a stainless steel electrode coated with a PLGA polymer and correlated the change in impedance to mass loss of the polymer from the surface of the electrode across a large frequency range (Zhong *et al.*, 2015). They found a large decrease in impedance across the whole frequency range with larger differences observed in the 1-10 Hz range. They correlated that data to a coated stent and found similar decreases in impedance over 50 days of incubation.

Another study by Fan *et al* looked at an epoxy coating on galvanized steel and its EIS behaviour when placed in an acidic environment. They evaluated different analysis methods, finding that the phase angle at 10 kHz provided a rapid approach to evaluate degradation of the polymer coating, finding that the delamination of the polymer corresponded with a decrease in phase angle (Fan *et al.*, 2021).

Advancing on this work that ES could monitor polymer degradation, the present study also sought to investigate impedance spectra of polymer-drug coatings to understand if ES could differentiate between polymer degradation and drug release on a medical implant-like surface.

#### 1.5.4 Surface Modification

Another property that will be common to medical implants are surface modifications that help promote cell growth or to stop bacteria attachment. The use of ES in characterizing these surface modifications and their effect on cell adhesion or prevention of bacteria adhesion has not been explored extensively. There has been investigation into how surface modifications alone effect impedance measurements but not surface modifications along with bacteria growth at the same time.

One study by Rahman *et al* showed how plasma sprayed coatings on titanium caused an increase in impedance compared to uncoated titanium due to the contact area of the electrode being higher and resulting in a higher charge transfer and lower overall impedance (Rahman et al., 2016). This was also proven by Holland *et al* when they added a platinum black coating to gold electrodes, which decreased the impedance measurements of the gold electrode which they attributed to the increase in surface area (Holland *et al.*, 2018). Olmo *et al* looked at impedance to characterize titanium samples with different levels of porosity and found 500 MHz the frequency of interest to see impedance differences linearly correlate to porosity based on normalised  $|Z|$  (Olmo *et al.*, 2020). A study also found that impedance changed with the addition of a titanium oxide to the surface of titanium implants (Basiaga *et al.*, 2016). Navarro *et al* furthered this study, they used a titanium disk with different pitting and performed impedance measurements from 150 MHz to 500 MHz and compared the impedance and phase angle values at different percentages of pitting using femtosecond laser (Navarro et al., 2022). They found that samples treated with the femtosecond laser had a large increase in

impedance compared to untreated samples. They also performed impedance measurements after cell seeding and saw impedance increased significantly after being treated, specifically at 500 MHz.

These studies show that a modified titanium surface could be monitored using impedance measurements and could be used in combination to monitor cell growth but little work has been explored in bacterial monitoring on altered surfaces.

### **1.5.5 Impedance Used with Medical Devices**

There have been many studies of the use of EIS and ES within biomedical applications, but relatively few using impedance to monitor infection of medical implants. Lin *et al* used impedance to measure the healing of a fracture. A separate sensor was implanted next to the broken tibias of mice and the fracture had an external fixator around the leg. They did linear regression analysis and found a significant positive relationship between resistance and time on 0.5 mm defects but no correlation on 2 mm defects that they attribute to the formation of bone on the 0.5 mm but not on the 2 mm. The electrodes had some initial trouble with the electrode being too big compared to the fracture, so they switched to smaller electrodes and got better results. They also normalized their data to ensure electrode to electrode differences were accounted for. They found that 14 kHz had the largest spread, indicating the most functional frequency for detecting the fracture healing (Lin *et al.*, 2019).. This showed the potential for impedance spectroscopy in future smart devices, but this study utilized a separate electrode feature for the impedance studies. The current study would look at using the actual device as an electrode versus needing separate electrodes.

Arpaia *et al* used impedance spectroscopy to look at osteointegration for orthopaedics. They used two bone screws placed in a cow femur bone and found that spectroscopy could detect the presence of connective tissue and could determine the thickness through polarization between -2 to +2 V (Arpaia *et al.*, 2007). This method utilized the bone screw as the electrode.

Fox and Miller conducted a study on pure titanium with a Ag/AgCl reference implanted into a baboon tibia. EIS measurements were performed for 60 minutes at 0 V conditioning potential. They found the growth of surface oxides formed over 20 minutes causing a rapid decrease in double layer capacitance and formed a steady state within 40 minutes (Casey Fox and Miller, 1993).

These are just a few examples of how EIS and ES could be used within a smart system to detect implant performance. Many of these studies focus on cell/bone regrowth and do not investigate possible infections or performance of antibacterial coating, hence this studies main goal.

## **1.6 Commercially available spectroscopy electrodes**

There are many commercially available EIS and Electrical Cell-Substrate Impedance Sensing (ECIS) electrodes. Many of these are screen printed electrodes that are disposable like xCelligence and Dropsens. These systems offer a range of gold, platinum, or carbon small electrodes that are plugged into a system. A downside to xCelligence is that it only gives a cell index from one frequency, so all other data from the frequency sweep of the ECIS is lost and potential other interesting data overlooked. While these are advantageous for high throughput drug screening or detection for different aspects, they would not be

used within a medical device and do not give a realistic simulation of *in vivo* conditions, including size, metal type and possible coating or surface modifications.

An example of an ECIS system that has a reusable electrode would be Applied BioPhysics Trans-epithelial/endothelial electrical resistance (TEER) systems. This system mainly utilizes gold electrodes, but can also be stainless steel, graphite or platinum. This system focuses on measurement of the resistance of the cell barriers. ECIS can measure different things related to cells including attachment of cells to the surface, as well as the movement of the cells (Giaever and Keese, 1986, Giaever and Keese, 1993).

There are currently no available commercial electrodes that use medical implant metals as the working electrode specific for biofilm formation. All of these systems are made by the researchers for specific purposes.

## **1.7 Spectroscopy Analysis Methods**

This study will focus on ES used in coating analysis and biofilm attachment, which can utilize different analysis methods other than equivalent circuit fitting in order to account for electrode-to-electrode differences. An equivalent circuit model for this type of system would be very complicated and might not accurately account for what is happening as shown by Hannah *et al* (Hannah *et al.*, 2019).

There are many different types of plots that can be used to display impedance data including impedance vs frequency, phase vs frequency, and Nyquist plots  $Z'$  vs  $-Z''$ . The main plots used for bacteria analysis and coating analysis are select frequencies versus impedance or phase angle and changing rate of impedance or phase angle. The change in

rate is the impedance at a given frequency subtracted by the next impedance at the next frequency, divided by the difference between those frequencies given below.

$$\Delta rate = \frac{|Z|_{f_i} - |Z|_{f_{i-1}}}{f_i - f_{i-1}}$$

Paredes *et al* used a range of frequencies for analysis of *S. epidermidis* on interdigitated microelectrode sensors in 4 different orientations including a 96-well microtiter plate, petri dish, modified biofilm reactor, and a lab-tester device. They found that the low range of frequency 10-100 Hz had the most sensitive range for all different set ups and could show marked differences with biofilm growth regardless of electrode orientation (Paredes *et al.*, 2014).

Xia *et al* used the changing rate of impedance in 1-100 Hz range to determine the degree of organic coating degradation and found that it is a fast evaluation method to determine how much of the coating has disbanded from the metal (Xia *et al.*, 2012). Fan *et al* used several methods to analyse coating effectiveness including 10 Hz, 10 kHz, changing rate of phase angle, and equivalent circuit modelling(Fan *et al.*, 2021). They demonstrated the use of several impedance analysis methods for evaluating steel with an epoxy coating exposed to an acidic environment, focusing on the corrosion characteristics once the epoxy coating started to show defects. They found that the changing rate of impedance and the phase angle at 10 kHz both represented the epoxy coating delamination quite well. The phase angle approach was taken in this study for a fast analysis approach also demonstrated by Zhang (Zhang *et al.*, 2023). Zhang *et al* demonstrated that the phase angle at 10 Hz could be a fast evaluation method for monitoring the degradation process

of the polymer coating on a metal substrate. Mahdavian and Attar used the phase angle at 10 kHz to fast evaluate paint coating defects (Mahdavian and Attar, 2006). Bing used a fast evaluation method for organic coating performance and showed that the decreasing phase angle at 10 Hz and 10 kHz correlated to coating performance (Bing, 2012).

Most of these methods have been used on biofilm growth on ideal electrodes of gold or simplified circuits. This study will look at utilizing a fast evaluation method on polymer-drug combination coatings and biofilm growth on non-ideal surfaces. A fast evaluation method was preferred over circuit modelling and intensive mathematical modelling based evaluation methods as circuit modelling can be associated with great error as multiple circuits can be fitted to the same data. This is also a complicated system where the circuit would need to change as the polymer degraded and the drug released making its fitting difficult and changing with many assumptions needing to be made that could be inaccurate.

## **1.8 Study Hypothesis and Aims**

Hypothesis: Electrical impedance spectroscopy can potentially be used to monitor polymer degradation and drug release on common medical implant surfaces and determine effectiveness against bacterial adhesion and biofilm formation.

The aims of this study are summarized below.

- Investigate the feasibility of using impedance spectroscopy to non-invasively characterizing polymer degradation and drug release on common medical device metals.



- Stainless Steel (SS)
  - Cobalt Chrome (CoCr)
  - Titanium (Ti90)
- Design and develop an in vitro test system using medical device metals as electrodes that can non-invasively characterize biofilm formation on metal surface.
- Investigate the feasibility of using impedance spectroscopy to non-invasively characterize polymer-drug effectiveness on biofilm formation over clinically relevant time periods.

## 2 Theory

Materials and methodological information will be provided within a General Methodology chapter, with study specific details provided within the relevant results chapter. In advance of this, the present chapter will introduce the basic theory underpinning the main techniques being exploited in this work. This will therefore serve to both explain the key features of each of the main methods and the context in which they have been selected.

### 2.1 Impedance Spectroscopy

When a voltage is applied to a circuit, the resultant current ( $I$ ) will be equal to the voltage applied ( $E$ ) divided by the impedance of the system ( $Z$ ). Within a Direct Current (DC) circuit with an ideal resistor, the impedance is equal to the resistance ( $R$ ), according to Ohm's Law.

Electrical Impedance Spectroscopy utilizes an alternating current (AC), which is a sinusoidal wave shown in Figure 2.1. In AC circuits, the current response ( $I(t)$ ) is driven by the voltage ( $E(t)$ ) and the electrical impedance,  $Z$ , of the system. The impedance has a magnitude,  $|Z|$ , phase shift,  $\phi$ , and angular frequency,  $\omega$  ( $=2\pi f$ ), with the relationship between each shown in equation 2.1 below. The phase shift is the shift in time of the sine wave, Figure 2.1. The phase difference between an applied voltage and a measured current for a capacitor (Figure 2.1), with a current leading the voltage, is due to the capacitor charging/discharging

$$Z = \frac{E_t}{I_t} = \frac{E_0 \sin(\omega t)}{I_0 \sin(\omega t + \varphi)} = |Z| \frac{\sin(\omega t)}{\sin(\omega t + \varphi)}$$

**Equation 2.1** Impedance, the magnitude, phase shift, and angular frequency relationship.

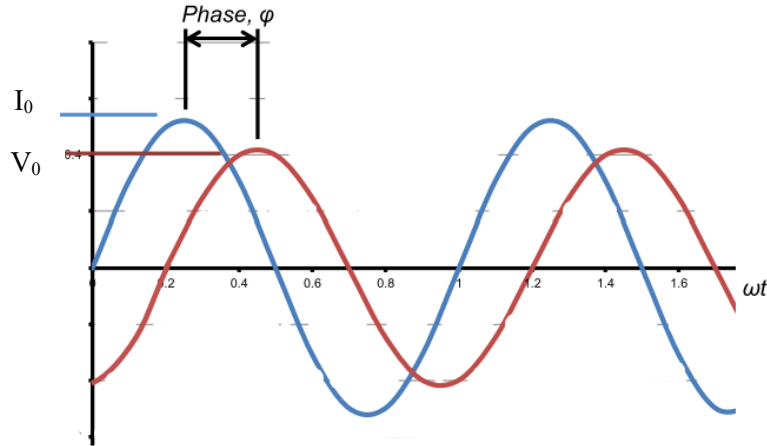


**Figure 2.1** AC sine wave showing the phase shift in relation to current and voltage versus angular frequency

Impedance spectroscopy refers to characterisation of impedance responses over a range of frequencies. This technique is used within a large range of applications from corrosion monitoring and optimization of battery performance through to biosensor development and characterisation. In each case it is often useful to use an equivalent circuit in order to describe the system response, with a variety of combinations of resistors and capacitors used in series and parallel arrangements (Metrohm, Gamry, 2022). There are a multitude of such models, although a simple model of bacteria growth on a metal electrode is usually represented as a resistor in series with a single resistor and capacitor in parallel as seen in Figure 2.2 (Kim *et al.*, 2011a).  $R_1$  represents the solution resistance,  $C_1$  represents the

double layer capacitance of the biofilm, and R2 represents the charge-transfer resistance between the biofilm and electrode.

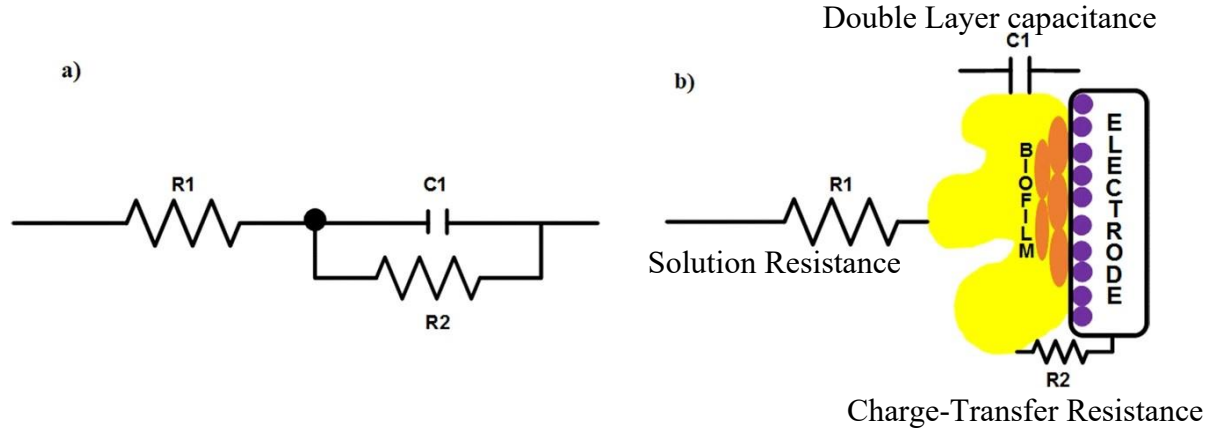


**Figure 2.2** a) Randles equivalent circuit model with resistor and capacitor in parallel for impedance monitoring system b) Physical representation of the ES measurement system

The impedance of the Randles circuit can be broken down into components based on Equation 2.2. When frequencies are low, an alternating current acts like a direct current, which makes  $1/\omega C1$  close to zero making  $|Z| \approx R1+R2$ . At high frequencies,  $(\omega C)^2$  is much larger than 1 so  $|Z|$  is approximately  $R1-1/(\omega C1)$  (Zhong *et al.*, 2015). Resistive features are prevalent at low frequencies and capacitive features are prevalent at high frequencies. Resistive features of the impedance response describe the electrolyte and electrode-electrolyte interface while the capacitive features refer to the electrode and electrode surface (Shedden *et al.*, 2010). The double layer capacitance is the interface between the electrode and the rest of the system that consists of an electrical double layer. The electrical double layer forms due to charge separation between the electrode surface

and the electrolyte. When a biofilm forms on the electrode, it can influence the ions that are absorbed onto this surface and affects the double layer capacitance directly.

$$i. \quad Z(\omega) = R_1 + \frac{1}{\frac{1}{R_2} + j\omega C_1}$$

$$ii. \quad |Z| = \frac{1}{\sqrt{\frac{1}{R_1^2} + \omega^2 C_1^2}}$$

**Equation 2.2** i. impedances of a  $R_1$  and  $R_2$  and  $C_1$  in parallel; ii. Magnitude of impedance of  $R_1$  and  $C_1$  in parallel

Randles equivalent circuit model is widely used within impedance research, allowing fundamental parameters such as solution resistance, charge transfer resistance, and double layer capacitance to be extracted from the frequency response. The Randles circuit may also have a Warburg impedance element in series with the  $R_2$ . The Warburg Impedance is an element that accounts for the diffusion process that could occur in a system.

There are several graph types that can be created from EIS information including a Bode Plot, Phase Plot and Nyquist plot seen in Figure 2.3.

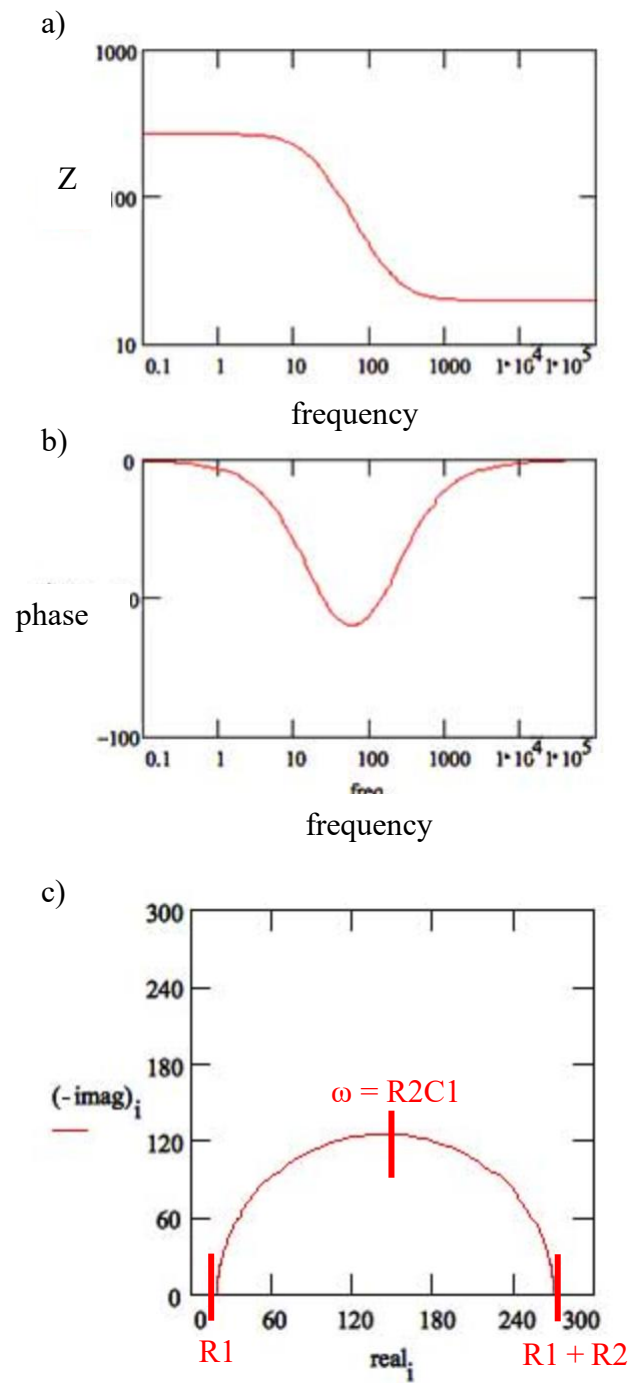


**Figure 2.3** a) Bode Plot b) Phase Plot c) Nyquist Plot of a Randles circuit replicated from (Gamry, 2022)

The bode plot has the frequency versus the impedance. The phase plot has the frequency versus the phase angle. The Nyquist plot has the imaginary part of impedance versus the real part of impedance. Each gives a unique insight into the impedance data.

The bode plot focuses on the frequency response of the system and shows the magnitude of the impedance. The phase plot also gives a total frequency response but for the phase shift/delay of the system. These plots give insight into the system as a whole, with bode focusing on impedance and phase focusing on the phase shift. The Nyquist plot is mainly used to determine the stability of the system and can give some insight into the different imaginary and real parameters of the system but does not give any data on the frequency recorded for those parameters limiting its use for frequency dependent changes. One consideration when trying to decipher meaning from these plots is potential noise associated with the system. This is a common problem in the lower frequency range as there can be system drift as the impedance is higher at lower frequencies and can lead to lower currents which can also lead to low signal-to-noise ratio. An open circuit potential adjustment can minimize drift but there is still some drift due to the nature of high impedance and low currents.

## 2.2 DPV and SWV

Voltammetry studies the current response of a chemical under an applied potential difference in an electrolyte solution. It can provide information regarding the kinetics and thermodynamics of reduction and oxidation of chemical species. Cyclic Voltammetry investigates reduction and oxidation of molecular species through a full potential sweep. Differential Pulse Voltammetry (DPV) is a pulse waveform that increases along a linear baseline after being held for a specific period. The current is sampled before the pulse, the potential applied and current sampled again after the pulse. This is to minimize measurements of background currents by allowing time for non-Faradaic current to decay so only the current arising from Faradaic reactions is present allowing for lower detection limits.



Square Wave Voltammetry (SWV) is also a pulse waveform that minimizes background current but is faster due to a shorter potential period and can analyse reversible and quasi-reversible electrode processes. The potential of the working electrode is stepped through a series of forward and reverse pulses from an initial potential to a final potential.

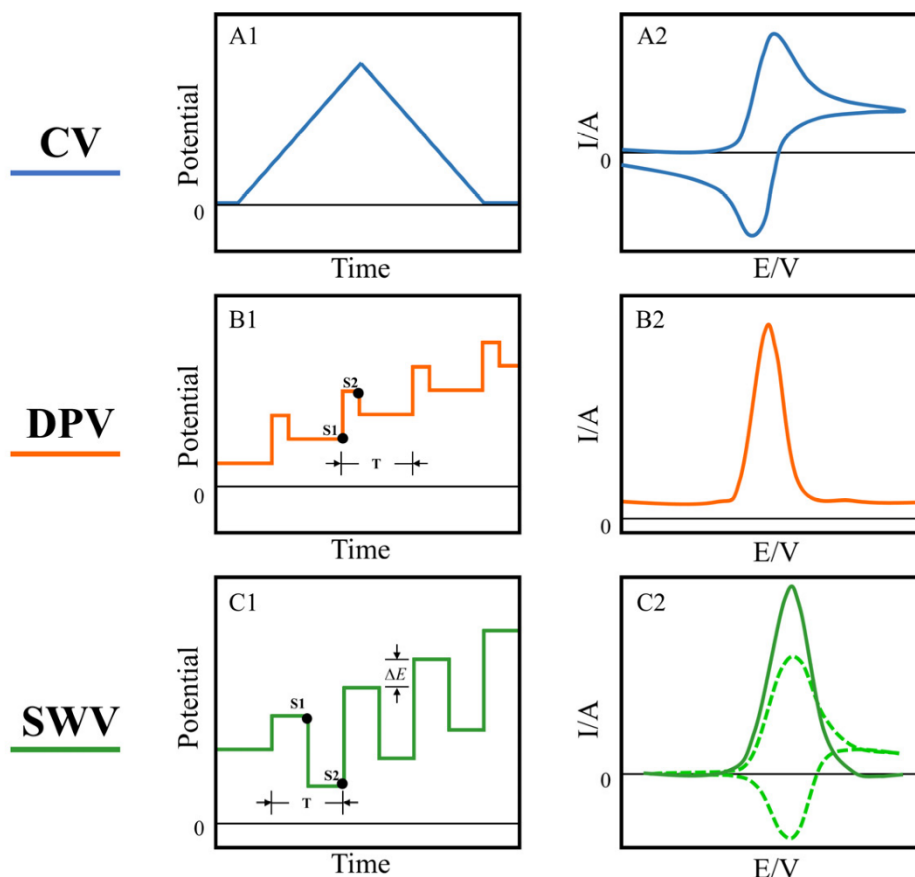


**Figure 2.4** Each of the figures represents how the potential is applied to the circuit and the response of that potential. Cyclic voltammetry has a steady increase to a peak then decrease in potential (A1) and typical response current that has a oxidation and reduction peak(A2).Differential pulse voltammetry has a potential (B1) with T waveform period , S1 and S2 being two sampling points and a single peak response (B2). Square wave

*voltammetry typical potential with  $\Delta E$  as potential increment (C1) and current response of a single peak(C2) (replicated from (Liu et al., 2022))*

A voltammogram shows current curves of oxidation and reduction processes of the electroactive species by showing peak value, peak width and peak potential that allows for electrochemical properties to be analysed. For reversible reactions, a peak for both the anodic indicating the oxidation and cathodic indicating the reduction of the species will occur at similar potentials (voltage). A reference electrode is used in this setup to provide a stable and known reference point regardless of the solution. The three electrode set-up allows for more stability and control over the measurement set-up.

### **2.3 AFM**

Atomic force microscopy (AFM) is a scanning probe microscopy technique that uses a cantilever and tip to probe the surface of a sample for imaging at the nanometre scale. The force sensor consists of a sharp tip mounted on a flexible cantilever that has a laser focused on the back of the cantilever that reflects onto a photodetector. The photodetector then measures the displacement of the laser light which translates to height measurements to allow for topographic imaging. There are various different imaging modes including contact, tapping, and non-contact mode. The contact mode has the tip dragging along the surface to detect the contours of the surface. Tapping mode is where the tip is oscillating at a given frequency and produces an image based on the force of the intermittent contacts. This can be used for ambient conditions or in liquids. Non-contact mode does not contact the surface and measures van der Waals forces and is best for measurements made in liquids.

There is a substantial amount of data collected from these measurement methods, and several ways to analyse it. Surface roughness is often calculated, with height analysis, grain analysis, and particle analysis also useful techniques. Surface roughness can be calculated according to equation 2.3 below.

$$\text{Eq. 1. Surface Roughness: } S_a = \frac{\sum_i^N |Z_i - \bar{Z}|}{N}, \bar{Z} = \frac{\sum_i^n Z_i}{N}$$

$$\text{Eq. 2. Root Mean Square: } S_q = \sqrt{\frac{\sum_i^N (Z_i - \bar{Z})^2}{N}}$$

$$\text{Eq. 3. Peak to Peak: } S_r = Z_{max} - Z_{min}$$

$$\text{Eq. 4. Mean Value: } S_m = \bar{Z} - Z_{min}$$

**Equation 2.3** Surface roughness, root mean square, peak to peak, and mean value roughness equations based on Z axis value

Root mean square (RMS) roughness is the value of height irregularities and allows for most accurate roughness and local peaks leading it to be the most common used value for analysis of polymer-drug coatings (Vo *et al.*, 2018). Tapping mode allows for phase imaging that can provide information on differences in material composition, adhesion, and other surface factors (Babcock and Prater, 1995)

## 2.4 Biofilm recovery methods

Biofilms can be quantified in many different ways. There are biomass assays, viability assays, and matrix quantification assays. Crystal violet is a biomass quantification that is a dye that binds to negatively charged surface molecules and polysaccharides in the extracellular matrix (Tripathi and Sapra, 2024). This stains both living and dead cells and

is therefore not suitable for evaluating biofilm kill. In contrast, viability assays can be used that only stain viable bacteria cells based on their metabolic activity (Welch et al., 2012). Finally, there are stains that bind to the extracellular matrix for matrix quantification. In each assay type, the stains require staining and removal of the biofilm for quantification (Peeters *et al.*, 2008), meaning only a single time point analysis can be performed. They also require UV light detection for quantification, and as the study used Rifampicin the dye may be altered based on the Rifampicin colour.

Direct enumeration is another method of quantification of a biofilm growth which generally requires disruption of the biofilm through sonification. The need for titration and plating of the biofilm makes this a time-consuming and laborious method (Donlan and Costerton, 2002). In common with other conventional methods, such enumeration does not permit repeated measurements on the sample.

### 3 General Methodology

This chapter will cover general methodology used within this thesis. PLGA and PLA were taken forward as the polymers of interest to determine the difference between amorphous and semi-crystalline release profiles as well as impedance differences. PLGA is one of the most common polymers used for drug release studies as it is very easy to manipulate release time through polymer ratios. Rifampicin was taken forward as the antibiotic as it is again one of the more common and effective antibiotics but also has a different effect on gram positive versus gram negative bacteria.

#### 3.1 Materials

Material	Company	Location
Translumina sirolimus eluting coronary stent, 4mm diameter and 32 mm length	Translumina	UK
Rebel Monorail PtCr coronary stent, 3.5mm diameter and 28mm length	Rebel	UK
Stainless steel (SS) (316L, 1mm diameter) wires	Goodfellow	Cambridge, UK
Titanium/aluminium/vanadium (Ti) (Ti90/Al6/V4) wires	Goodfellow	Cambridge, UK
cobalt/chromium/iron/nickel/molybdenum/manganese (CoCr) (Co60/Cr20/Fe15/Ni15/Mo7/Mn2/C/Be) alloy wires	Goodfellow	Cambridge, UK
Poly(lactic-co-glycolic acid) (PLGA) MW 40000-75000	Sigma-Aldrich	St Louis
Polylactic acid (PLA) Viscosity 4 dL/g	Sigma-Aldrich	St Louis
AFM silicon cantilever tips (TAP150AI-G)	Oxford Instruments	UK
Single Glassy Carbon Electrode (GCE)	Palmsens	(Houten, Netherlands)
Rifampicin, ≥97% (HPLC), powder (or crystals), RNA polymerase inhibitor, Calbiochem, MW 822.94	Sigma-Aldrich	Poole, UK
All chemicals used were reagent grade	Sigma-Aldrich	Poole, UK

### 3.2 Equipment

Equipment	Company	Location
AutoLab PGSTAT302N with Nova 2.0 computer program	Metrohm	Herisau, Switzerland
PalmSens4 with PStace 5.0 computer program	PalmSens	Houten, Netherlands
Ultraviolet Spectrophotometry (UV Spectrophotometry): Multiskan Go	Thermo-Fisher	UK
Scanning Electron Microscope (SEM): TM-1000 Tabletop Microscope with Swift ED-TM computer program	Hitachi	UK
Atomic Force Microscope (AFM): MFP-3D with Argyle Light 3D viewer	Asylum Research	UK

### 3.3 Chapter Aim and Objectives

Section 1.8 (Study Hypothesis and Aims) defined the study's aim with respect to characterizing polymer-drug coatings as follows.

- Investigate the feasibility of using impedance spectroscopy to non-invasively characterizing polymer degradation and drug release on common medical implant metals.
  - Stainless Steel (SS)
  - Cobalt Chrome (CoCr)
  - Titanium (Ti)

This chapter focuses on this first study aim. The specific objectives for the experiments used to address this aim are detailed below.

- Investigate the influence of factors related to experimental testing on impedance measurements.
  - Drug Concentration
  - Stirring conditions
  - Temperature
- Investigate the feasibility of using common medical implant metals as electrodes within an electrical impedance system.
- Investigate the feasibility of using impedance spectroscopy to non-invasively characterize polymer-drug coatings compared to stent polymer-drug coating.
- Determine which analysis methods can be applied to polymer-drug coatings.
- Investigate the feasibility of using differential pulse voltammetry and square wave voltammetry to non-invasively monitor drug concentration.
- Investigate different coating methods and verifying ways to characterize the polymer-drug coating as it degrades.

## **3.4 Methods**

### **3.4.1 Dip Coating**

All sample wires were cut to 25 mm in length before dip coating or use within the impedance system. Solutions of 10% weight per volume of separate PLGA, PLA, and Rifampicin were prepared in chloroform, these were then portioned into different volume ratios together as described below for different experiments. When PLGA, PLA, or Rifampicin is referred to in text it refers to the original 10% w/v.

There are three separate experiments performed for coating degradation: room temperature, fixed room temperature, and fixed 37 °C. Set-ups for these are further described in table 3.1.

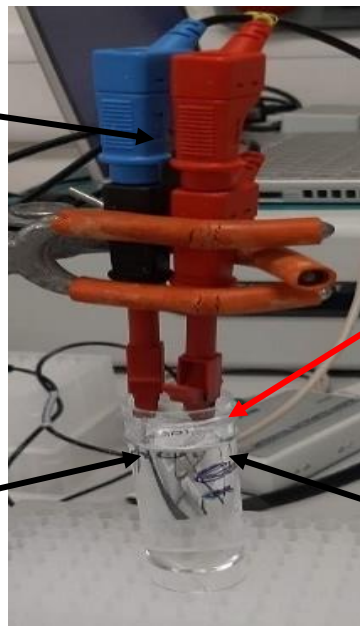
SS wire samples used for room temperature work where the electrodes were connected to the alligator clips for ES measurements then removed and incubated in a different vial (SS wire non-fixed work Table 3.1) were dipped into either PLGA, PLA, or 50:50 v/v of PLGA: Rifampicin solutions, as indicated in Table 3.1. Non-fixed work refers to electrodes that were held in place only by the alligator clips and were re-secured after incubation. Samples were dipped into solution for 15 seconds, then left to air dry for one minute before dipping again. All samples were dip coated a total of five times for all experiments, unless stated otherwise.

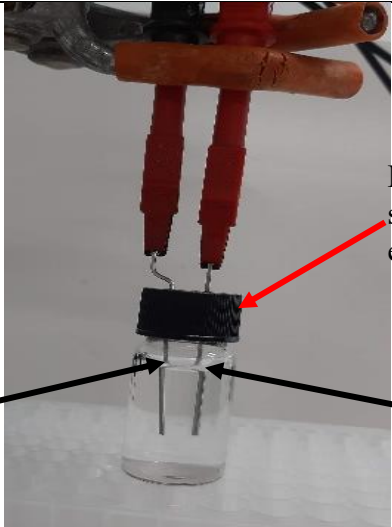
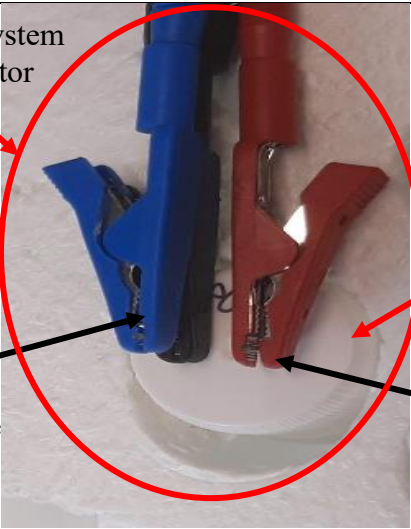
SS wire samples used for room temperature fixed work where electrodes were fitted into vial lid were dipped into PLGA, PLA, 50:50 v/v PLGA: Rifampicin, 75:25 v/v PLGA: Rifampicin, and 60:40 v/v PLGA: Rifampicin. Fixed work refers to electrode samples that were secured into lid of incubation jar. Samples were dipped into solution for 15 seconds. They were then connected to a standing drill with the coated side facing down and spun to dry for 30 seconds. This was repeated for two coatings.

SS wire samples used for 37 °C fixed work were dipped into same solutions used in room temperature fixed work using the air-dry method. They were dipped a total of 6 times. A replica set of samples were also produced for the AFM/SEM work (Section 3.4.3.4).



**Table 3.1** Summary details of coating types and methods, impedance analyser used, and picture of set-up for the impedance experiments outlined in the next section.

Experiment	Coating Solutions	Coating Method	No. of Coatings	Impedance Analyzer	Picture
SS wire non-fixed	10% w/v PLGA 10% w/v PLA 50:50 v/v of PLGA: Rifampicin	Air Dry	5	Autolab	 <p>Leads to Autolab</p> <p>Counter Electrode</p> <p>Working Electrode</p> <p>Non-fixed wires connected to leads each time experiment performed.</p>

SS wire fixed room temperature	10% w/v PLGA 10% w/v PLA 50:50 v/v of PLGA: Rifampicin 60:40 v/v of PLGA: Rifampicin 75:25 v/v of PLGA: Rifampicin	Spin Dry	5	Autolab	
SS wire fixed 37°C temperature	10% w/v PLGA 10% w/v PLA 50:50 v/v of PLGA: Rifampicin 60:40 v/v of PLGA: Rifampicin 75:25 v/v of PLGA: Rifampicin	Air Dry	6	PalmSens	

### **3.4.2 Electrical Impedance Spectroscopy**

A two-electrode system was used to make all impedance measurements in this study. In all experiments, the material under investigation was used as the working electrode, with a counter electrode being selected from either SS or platinum (selection of this is detailed within each study description). The platinum electrode was used for the stent versus wire measurements for an electrode that was a common material to ensure minimum drift. All other experiments performed with SS counter electrode to determine impedance using only medical device metals as both working and counter electrode. Temporal impedance measurements were performed at a voltage (50 mV vs open circuit potential) with an AC sine wave, across a frequency range of 1 Hz to 100k Hz as per the method described by Holland (2018) and Kim (2011) (Kim et al., 2011b, Holland, 2017). The open circuit potential adjustment first measures the open circuit value. Then the wanted voltage (50 mV) is then applied on top of the measured value. These conditions were used for all impedance measurements in this study, unless stated otherwise.

#### ***3.4.2.1 Variable testing that could impact ES measurements***

Several initial variables were tested to determine their influence on ES measurements including Rifampicin concentration, stirring conditions, and temperature. These experiments were conducted using the Autolab system with non-fixed electrodes an example of which is shown in Table 3.1 (SS wire non-fixed).

Each working wire and the SS counter electrode were submerged in 25 ml of Phosphate Buffered Saline (PBS) used throughout this study as 0.1M solution with a range of Rifampicin concentrations from 0.001 mg/ml to 0.1 mg/ml solution in a 25 ml centrifugal

tube. ES measurements were taken on the Rifampicin concentration range in static conditions and non-turbulent stirring conditions using a magnet and stir table. SS, CoCr, and Ti wires were all tested within these conditions.

ES measurements were also performed on a range of measurement temperatures from 8 °C to 32 °C using a SS working electrode, with a SS counter electrode.

#### ***3.4.2.2 Translumina Stent vs Dip Coated Wires***

In order to assess the potential of using impedance for monitoring coronary stent drug coatings, a method similar to that first reported by Shedden *et al* 2010 was used. A Translumina Choice PES polymer-sirolimus coated stent was investigated since these stents had been the subject of substantial interest due to the potential for provision of dose-controlled drug release profiles and potentially enhanced endothelialisation (Acharya and Park, 2006).

The Translumina stent and the platinum counter electrode were submerged in 25 ml PBS containing 10% Ethanol, with impedance measurements taken at various time points over six hours using the Autolab system. The Ethanol was used because sirolimus does not dissolve in aqueous solutions.

This was repeated using the dip coated 50:50 v/v PLGA: Rifampicin wires as the working electrode and PBS solution as the solution. These were both non-fixed electrodes, meaning they were not fixed in place throughout the entire measurement.

#### **3.4.2.3 *Fixed system work***

A fixed system was employed after initial experiments to maintain a consistent immersion depth and minimize discrepancies between samples as seen in Table 3.1 picture for the SS wire fixed. The electrodes were secured within 1mm holes drilled in the container lid at a depth of 15 mm that was replicated for each sample. There were two different fixed system experiments performed, one at room temperature (~20 °C) using the Autolab that was performed up to one week and the other at 37 °C within an incubator using the PalmSens performed up to two months. The Autolab was changed to a PalmSens because the PalmSens's size allowed it to fit within an incubator, it had better connections leading to less data exclusions from faulty measurements, and had quicker measurement times.

### **3.4.3 Characterization of Polymer and drug coatings**

#### **3.4.3.1 *Coating Analysis***

The initial mass of the SS wires were weighed using a laboratory balance (sensitive to 0.0001g) and then weighed after the dip coatings were dried to obtain the mass difference. Thickness was also measured before and after dip coating using callipers at three different locations: tip, middle, and end.

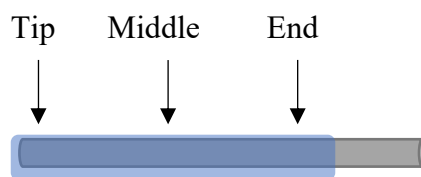


**Figure 3.1** Schematic of SS wire, represented by grey cylinder, with coating of polymer or polymer-drug, represented by blue shading, and the 3 points at which the thickness were measured using callipers.

### 3.4.3.2 UV Spectrophotometry

Drug release for each experiment was measured using UV spectrophotometry. Infinite sink conditions were approximated, according to recommendations of an expert consensus group (Schwartz *et al.*, 2008). Infinite sink condition refers to having a dissolution media that removes dissolved drug at a faster rate than it dissolves, allowing continuous dissolution. An absorption calibration curve was produced for Rifampicin using 350 nm light (Khan *et al.*, 2021, Angiolini *et al.*, 2019) and a range of concentrations from 0.1 mM to 1 mM. Total drug released for the incubated samples was determined by taking 1ml samples from the solvent solution at each time point. The absorbance of the 1 ml samples taken from the experiments were then measured at the same wavelength, with reference to the calibration curve allowing estimation of the drug content. A similar approach was used for sirolimus from the Translumina stent, with the key differences being the wavelength of the light source was 278 nm light and the calibration curve drug concentrations range was from 1  $\mu$ M to 10  $\mu$ M.

#### ***3.4.3.3 Differential Pulse Voltammetry and Square Wave Voltammetry***

DPV and SWV were performed to determine if electrochemical means could find Rifampicin concentration without need for a modified electrode. This was to determine if a simple surface could still detect drug concentration, allowing for a fully autonomous measurement system measuring biofilm formation, polymer degradation, and drug concentration all non-invasively. An unmodified GCE was used as the working electrode, a silver/silver chloride as the reference electrode, and a platinum wire as the counter electrode. The GCE was electrochemically cleaned, and surface activated by performing 10 cyclic voltammetry scans from 0 V to 1.4 V at 0.1 V/s in 20 mM of NaCl. A DPV was performed at pulse amplitude 50 mV, pulse width 50 ms and scan rate of 2 mV s<sup>-1</sup>. A SWV was performed at pulse amplitude 25 mV, frequency 10 Hz, and step potential of 1 mV (Kul, 2020). These were both started at -0.3 V and stopped at 0.6 V. A range of Rifampicin concentrations from 0.1 µM to 7 µM was tested in PBS. The results were baseline corrected before plotting.

#### ***3.4.3.4 Characterization of coating surface***

Characterization of coating surfaces was performed using an AFM in open-air tapping mode at room temperature with a soft mid to soft silicon tip with 5 N/m spring. The samples used for AFM were also used for SEM imaging. Coating surfaces were imaged using an SEM at 250X magnification up to 1 week for most samples.

Data for the AFM was collected from a range of sizes 10 µM – 1 µM and 5 µM chosen as the ideal size (Bian *et al.*, 2012), which was used for all other images. Images were

flattened to the 0 order and plane fit in the XY plane to the 1st order. The mean average roughness (RMS) was taken from the height data for all sample types.

### **3.5 Data Analysis**

#### **3.5.1 Data Presentation and Statistics**

Unless stated otherwise all statistical analysis was performed in Origin. Impedance results were plotted as a mean with error bars representing  $\pm$  standard error mean. Statistical significance of phase angle at 10 Hz and 10 kHz and impedance variations at 10Hz and 10 kHz was determined using one-way ANOVA analysis followed by Tukey's or Bonferroni's post-hoc multiple comparison tests. Values of  $p < 0.05$  were considered statistically significant. All one-way ANOVA used these parameters unless stated otherwise.

The results of the SWV and DPV used smooth wave function and correction for the baseline. A one-way ANOVA with Tukey's post hoc was performed for statistical significance.

The root mean square (RMS) roughness data from AFM had one-way ANOVA with Tukey's post hoc performed for each sample between samples.

#### **3.5.2 Experimental data inclusion**

Throughout experimentation some results were excluded from data analysis due to clear discrepancies and excessive noise in the data, as compared to well-established outputs and calibration measurements, although the precise reason for these discrepancies remains



unclear. In the majority of cases, such erroneous data recordings could be attribute to a compromised electrode connection.

## **4 Chapter 4 Results of Polymer-drug Coating Development and ES evaluation**

### **4.1 ES System Characterization of Variables**

#### **4.1.1 Impact of Rifampicin concentration on ES measurements**

Before performing impedance measurements on coatings, the first experiments focused on a range of experimental factors that could influence the impedance readings when experiments were performed. The coatings would comprise of a polymer and Rifampicin mixture. As the polymer degraded, Rifampicin would therefore be expected to release into the surrounding media. In order to investigate the potential impact of such release, impedance data was collected from a range of Rifampicin concentrations in PBS using SS, Ti, and CoCr as working electrodes. The results generated are displayed in Figure 4.1. As described in the ES theory section (2.1), at higher frequencies, the solution resistance tends to become more dominant, according to the assumed Randle's circuit model. For this reason, the 1000 Hz to 100 kHz range has been magnified to showcase the Rifampicin influence. In order to clearly indicate differences in impedance characteristics of the three electrode materials, a separate plot of the absolute impedance ( $|Z|$ ) at 10 kHz for the Rifampicin concentrations were examined (Figure 4.1 (c)).

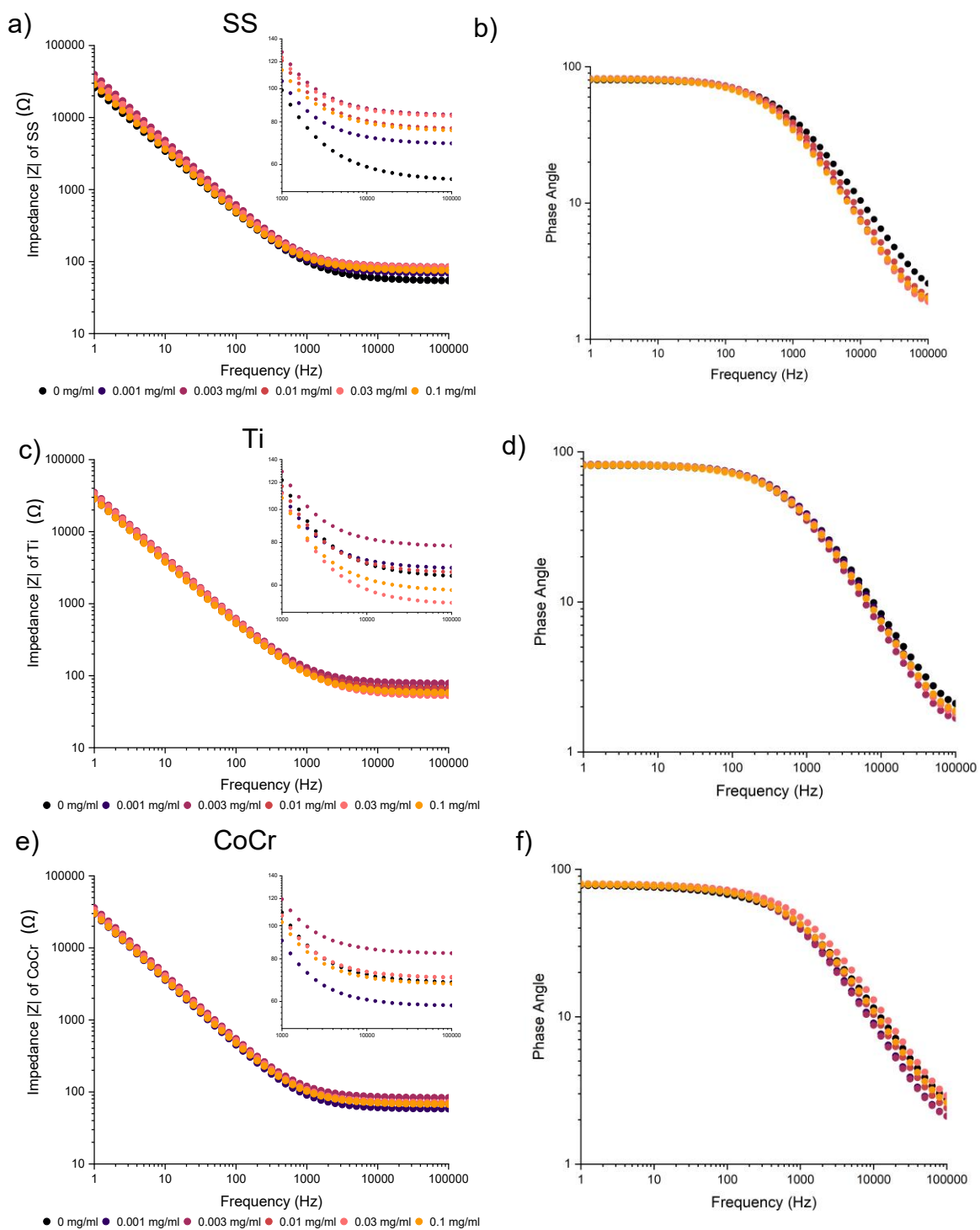


**Figure 4.1** Data with an enlargement of the higher impedance range 1000 Hz to 100 kHz collected from Rifampicin concentrations ranging from 0-0.1 mg/ml in PBS .**a)** Modulus of impedance of SS working electrode ( $n=1$ ), **b)** Phase angle of SS, **c)** Modulus of

*impedance of Ti working electrode ( $n=1$ ), d) Phase angle of Ti , e) Modulus of impedance of CoCr working electrode ( $n=1$ ). f) Phase angle of CoCr*

In the modulus of impedance data, a larger difference in impedances can be seen in the higher frequency range, with the impedance appearing to increase as the Rifampicin concentration increases. When analysing this further at the selected 10 kHz frequency, there is clearly a sharp increase in impedance at the lowest Rifampicin concentrations (0.001 to 0.01 mg/ml), an effect that was relatively consistent. In contrast, at higher concentrations (0.3 to 0.1 mg/ml), there was a general decrease in impedance, with the nature of this being inconsistent between the different electrode types. The SS impedance remains relatively stable at these elevated concentrations while the CoCr and Ti decrease was more marked. This follows a similar trend for the phase angle analysis, with a decrease in phase angle with increase in concentration at first in the higher frequencies but then back to the original phase angle as a continued increase in concentration.

As mentioned in Section 2.1, a key metric for determining coating performance include the phase angle at 10 Hz and 10 kHz (Zuo *et al.*, 2008, Zhang *et al.*, 2023, Mahdavian and Attar, 2006). The influence of different Rifampicin concentrations on phase angle was found to be relatively small, as seen in Figure 4.2, with the phase angle not changing noticeably with the increase in Rifampicin concentration for all electrode types.

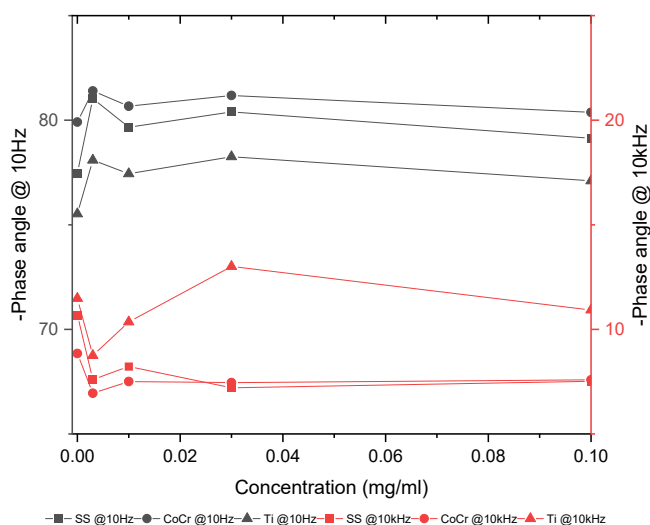
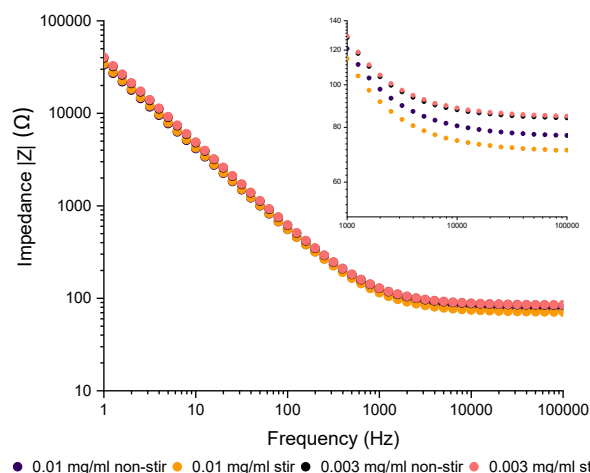


**Figure 4.2** Negative phase angle at 10Hz (left axis) and 10kHz (right axis) of different concentrations of Rifampicin in PBS with SS, CoCr, and Ti as working electrodes.

#### 4.1.2 Impact of Temperature and non-turbulent flow

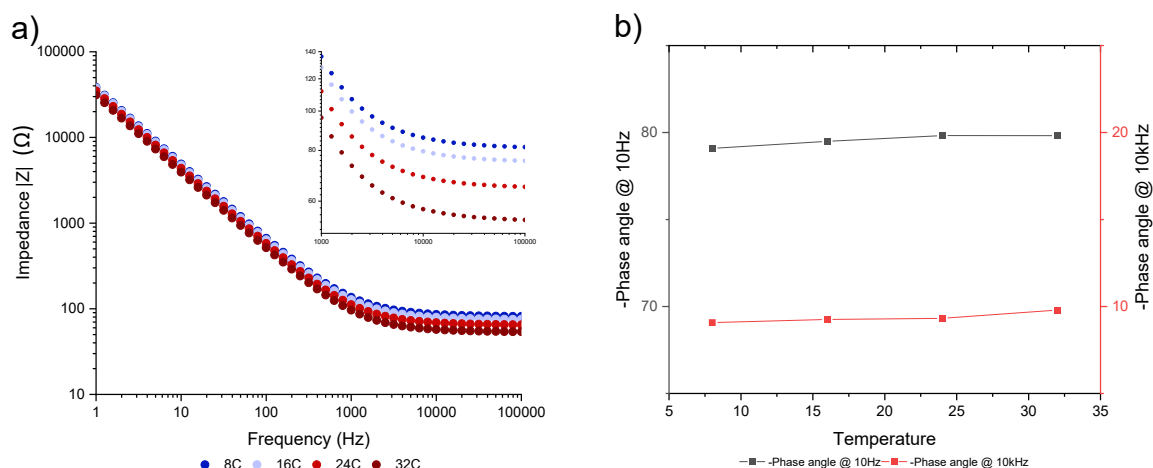
The first polymer-drug experiments were performed at room temperature but to grow bacteria and to mimic in vivo conditions the samples ideal conditions would be performed at 37 °C and have flow conditions, therefore the effect of temperature and stirring on impedance needed to be evaluated.

Figure 4.3 showed negligible influence of stirring on the impedance at various Rifampicin concentrations on SS. The other electrode types displayed the same trend, with stirring having very little effect on the impedance measurements.



**Figure 4.3** Representative impedance spectra of select Rifampicin concentrations in non-stirred and stirred conditions using SS wire electrodes (non-turbulent) ( $n=1$ )

Impedance can be seen to decrease as temperature increases in Figure 4.4 a, specifically in the higher frequency range that is influenced by solution resistance. The phase angle for temperature shows no change over temperature variances.



**Figure 4.4 a)** Total Impedance spectra and **b)** negative phase angle at 10 Hz and 10 kHz of PBS in a range of temperatures 8-32 °C ( $n=1$ ) with SS as working electrode

## **4.2 Impedance characterization of Translumina Stent vs Dip Coated Wires**

This project creates a model of polymer-drug coated medical implants with the goal to accurately represent the implants qualities. A Translumina stent coated in sirolimus and PLA, a manufactured medical device, was compared to our model of stainless steel coated with PLGA: Rifampicin (50:50) to determine how similar the impedance profiles matched and if the model was an accurate representation.

The impedance spectra of the Translumina stent and of the PLGA: Rifampicin coated SS, recorded over a 7-hour immersion period, are shown in Figure 4.5 a) and b). The spectra for both samples was characterised by a maximum impedance at the lowest frequency which reduced in a linear manner as frequency increased to 1000 Hz before stabilizing at higher frequencies. Both experienced an initial decrease in impedance over the first 3 hours followed by a rapid increase in impedance, highlighted by Figure 4.5 c) and d), with the stent having larger impedance variations. The experiment had to be stopped after 10 hours due to inconsistent connections with the stent, with attempts to resolve the issue discussed in Section 4.2.

The plots of impedance at 10 Hz and 10 kHz both had similar trends for each of the samples, in contrast to the phase angles at the two chosen frequencies. The phase angle had opposite trends with the lower frequency increasing over time and the higher frequency decreasing. The phase trendlines had more gradual changes over time compared to the impedance.

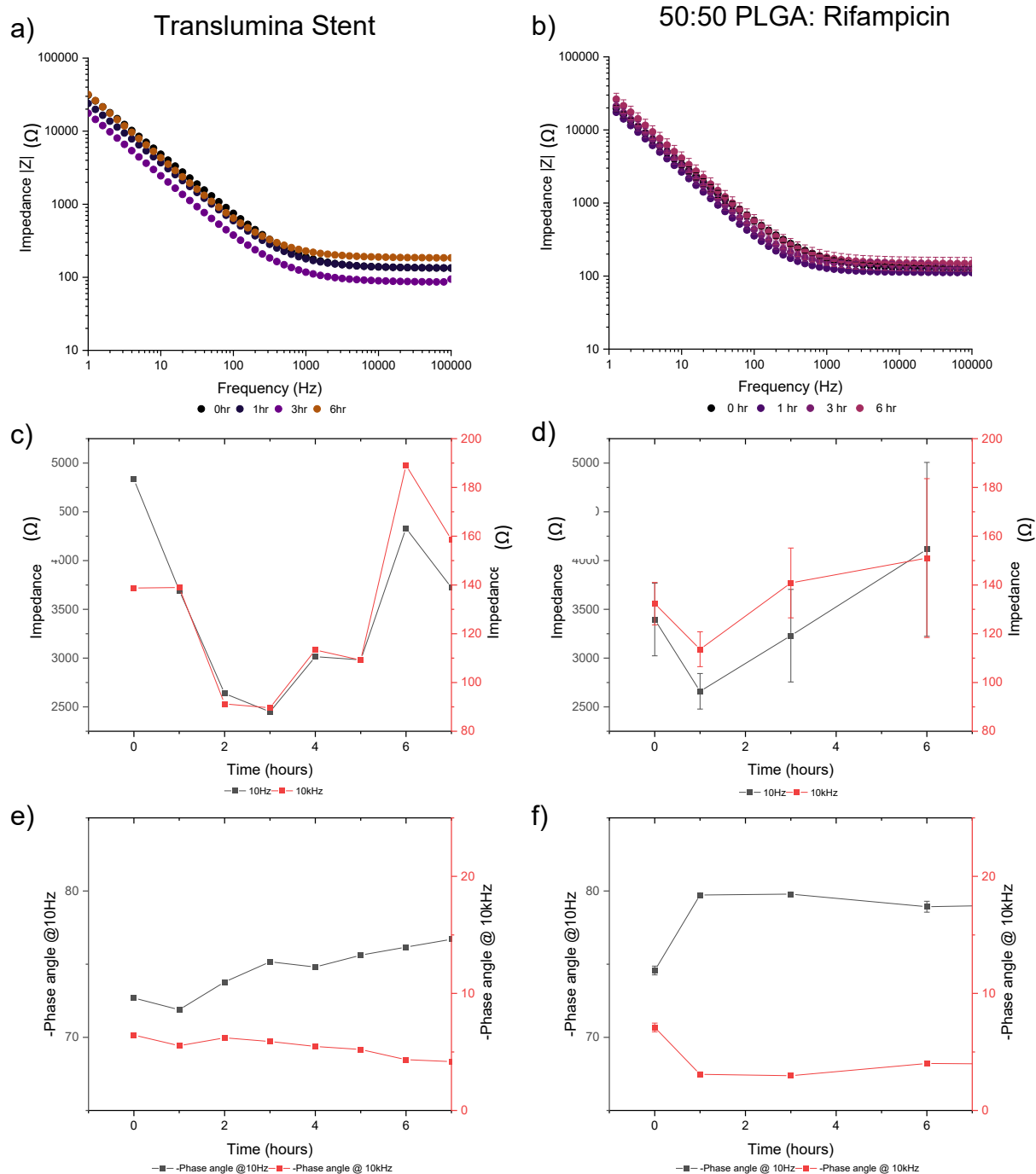


**Figure 4.5 a)** Modulus of impedance spectra of a Translumina stent submerged in PBS containing 10% ethanol ( $n=1$ ) and **b)** 50:50 PLGA: Rifampicin coated wires ( $n=3$ )



submerged in PBS. A plot of the impedance at 10 Hz (left axis) and 10 kHz (right axis) for **c)** the Translumina stent and **d)** 50:50 coated wire. Then the negative phase angle at 10 Hz and 10 kHz of **e)** a Translumina stent and **f)** 50:50 coated wire.

A calibration curve was constructed for each drug type using absorbance measurements, and an equation derived from the curve to determine the concentration of drug released based on the samples seen in Figure 4.6.

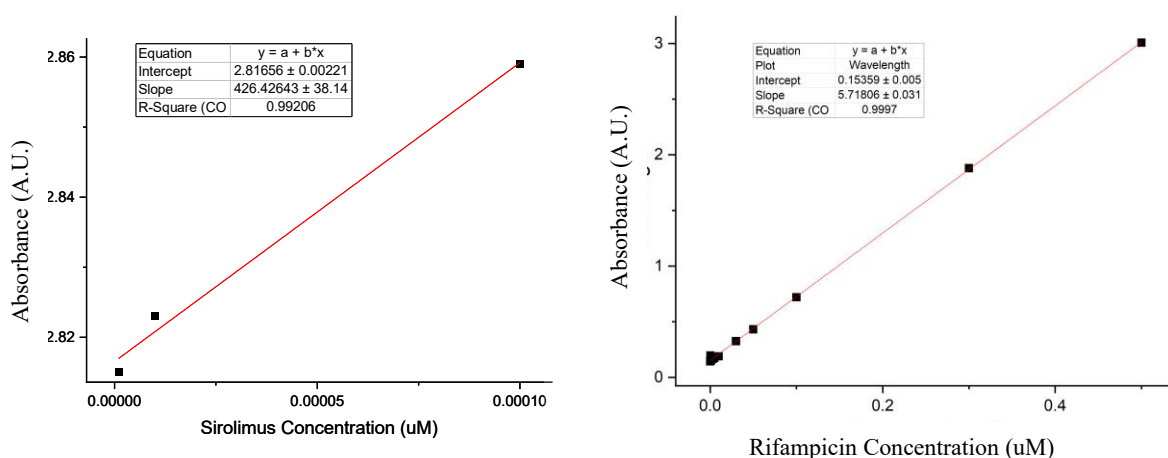


**Figure 4.6** Concentration curve with linear fitted equation of **a)** sirolimus from 10  $\mu\text{M}$  to 1  $\mu\text{M}$  in 10% ethanol at 278 nm light ( $n=1$ ) and of **b)** Rifampicin from 0.1 mM to 1 mM in PBS at 350nm light ( $n=1$ )

Each concentration curve was fit with a linear equation, the sirolimus equation  $y = 426x + 2.81$  and the Rifampicin equation  $y = 3.36x + 0.1$ . The equations were used to calculate the concentrations reported in Figure 4.7. Any calculation that resulted in a negative concentration was recorded as zero.

A large difference was seen between the stent and the model coating in terms of drug release. The stent released a total 80.7  $\mu\text{mol}$  of sirolimus over the 10 hours while the SS sample released a total of 1.33  $\mu\text{mol}$  over 10 hours. They also had different release rates with the Rifampicin releasing in the first 3 hours and the sirolimus releasing near the 9-hour time point.

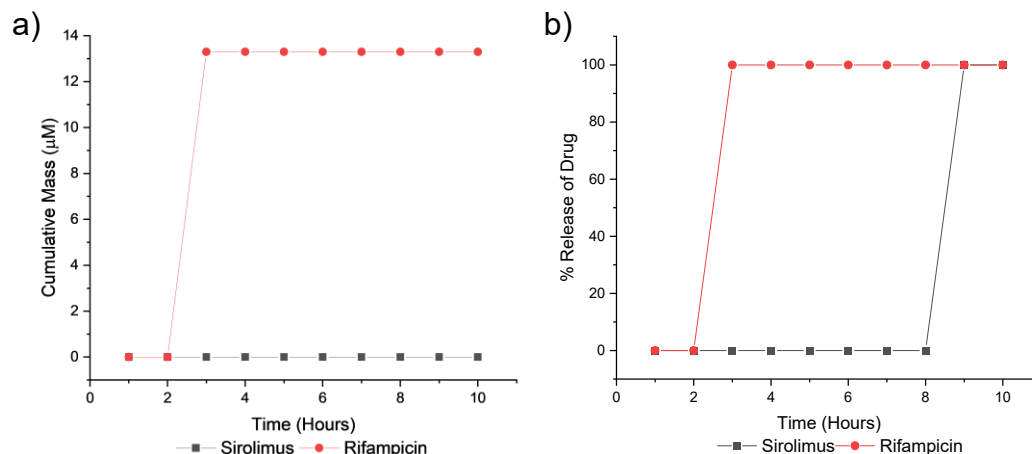


**Figure 4.7 a)** Cumulative mass of drug released from samples of Translumina stent (Sirolimus) immersed in 10% ethanol solution and from 50:50 PLGA: Rifampicin coated wires immersed in PBS at 20 °C. **b)** Total % of drug release by hour of the samples over the incubation period ( $n=1$ )

### 4.3 Impedance Characterization of Fixed System

#### 4.3.1 Short term room temperature work

The metals chosen for this study each metal has different properties, specifically pertaining to the formation of oxide layers. A short-term study was performed to determine the metals stability over time and how the formation of different oxide films

influences impedance. It was also investigated how the different coatings would influence impedance compared to the bare metals.

The following results are from the experiments performed at room temperature in the fixed system shown in table 3.1, with SS, Ti, CoCr, 10% Rifampicin, 10% PLGA, 10% PLA, 75:25, 60:40 and 50:50 formulations for PLGA/ PLA and Rifampicin. It is clear that each metal has a similar impedance spectrum (Figure 4.8) with the most noticeable differences shown in CoCr's increase in impedance over time, specifically in the higher frequency range and Ti's increase in impedance over time in the lower frequency range looked at closer in the next figure with statistical analysis performed. The Rifampicin coated samples have a distinct impedance spectrum from the metals, Figure 4.8 (d), with the total impedance increasing over time as the drug releases from the surface and becoming more linear across the whole frequency range over time.

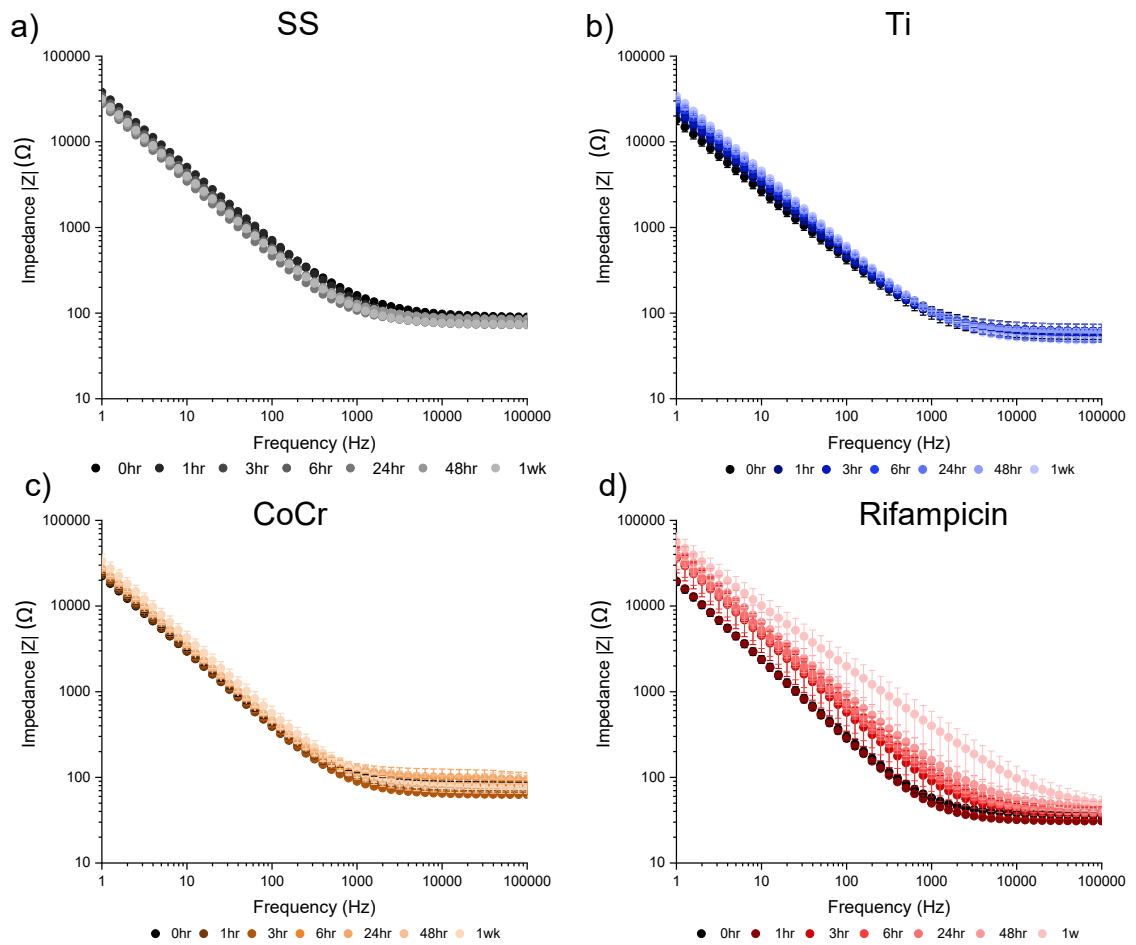


**Figure 4.8** The total Impedance spectra of **a) SS** **b) Ti**, and **c) CoCr** wires and **d) 10% Rifampicin** covered SS wires ( $n=3$ ) incubated in PBS on the room temperature fixed system pictured in Table 3.1.

At the chosen frequency, one way ANOVA statistical analysis was performed on all datasets with two different post hoc tests. Bonferroni post hoc compared each impedance at different time points to time zero. Tukey post hoc compared the variances of the mean of the entire trendline and corrected the confidence interval and p-value based on the number of comparisons. The impedance did not change significantly over time for any samples, however there were a few significant differences between samples. At 10 Hz and

10 kHz (Figure 4.9 (a) and (b)), the impedance of the Rifampicin coated samples were significantly different from SS and Ti. The SS was also significantly different from CoCr at 10 Hz and Ti at 10 kHz. From Figure 4.8 it was noted that the impedance profiles were different for the different metals which reflects in their significance at different chosen frequencies.

The phase angle of these experiments had more significant differences shown than the impedance profiles in Figure 4.9 (c) and (d). Ti had many significant differences at 10 Hz for most time points. Rifampicin was significantly different at the 1-week time point at both 10 Hz and 10 kHz.

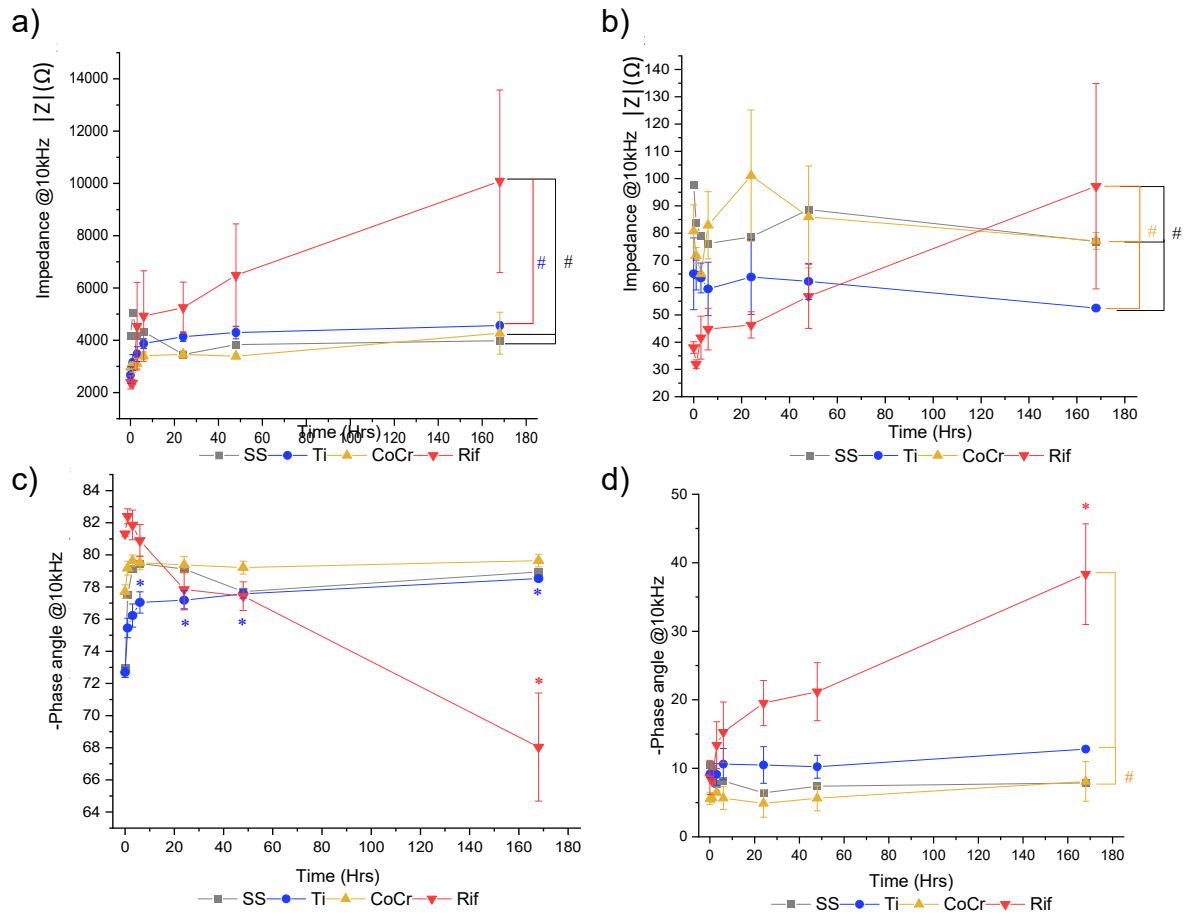


**Figure 4.9** Temporal impedance measurements of **a)** SS, Ti, CoCr wires ( $n=3$ ) and Rifampicin coated wires ( $n=3$ ) at 10 Hz **b)** and 10 kHz. **c)** The negative phase angle for same samples at 10 Hz and **d)** 10 kHz. Significance was determined by ANOVA analysis, with Bonferroni post hoc between time 0 and subsequent time points (Shown by \*Ti, \*Rif) and Tukey post hoc between trendlines (Shown by # SS, # CoCr, #Rif).

Very little change can be seen in the changing rate of impedance and phase angle, for both chosen frequencies (Figure 4.10). This follows what is seen in Figure 4.8, the slopes of the impedance profiles appear to be similar at each time point, all be it with evident

changes in over-all magnitude. The Rifampicin samples rate of change does decrease below the metals in the impedance 10 Hz and phase angle 10 kHz but not noticeably so.

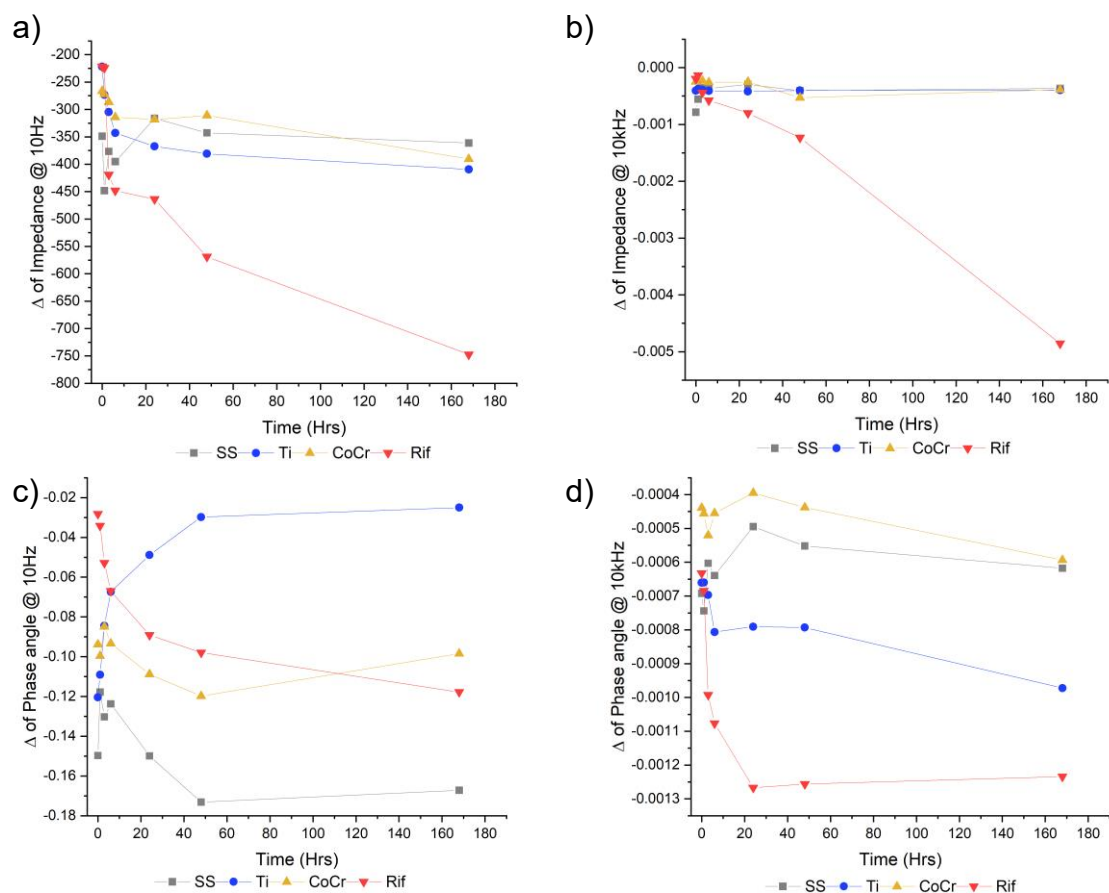


**Figure 4.10** The changing rate of impedance at **a)** 10 Hz and **b)** 10 kHz of bare SS, Ti, and CoCr and Rifampicin coated wires ( $n=3$ ) incubated in fixed system with PBS at room temperature and the changing rate of phase angle at **c)** 10 Hz and **d)** 10 kHz

The PLGA samples and the highest concentration of PLGA-drug ratio 75:25 in Figure 4.11 have very similar impedance profiles, with a small negative slope across the whole frequency range and larger standard error than the other samples. The magnitude of their impedance is also noticeably higher than an uncoated SS wire. The 60:40 and 50:50 ratio have more similar impedance spectrums to each other, with a steep slope in the smaller

frequency range and a zero slope in the higher frequency range closely resembling the bare SS spectrum. The 0-hour time point stands out above the rest of the time points for the 60:40 and 50:50. The magnitude of the impedance decreases over time for all the different samples with larger decreases corresponding to higher polymer concentration.

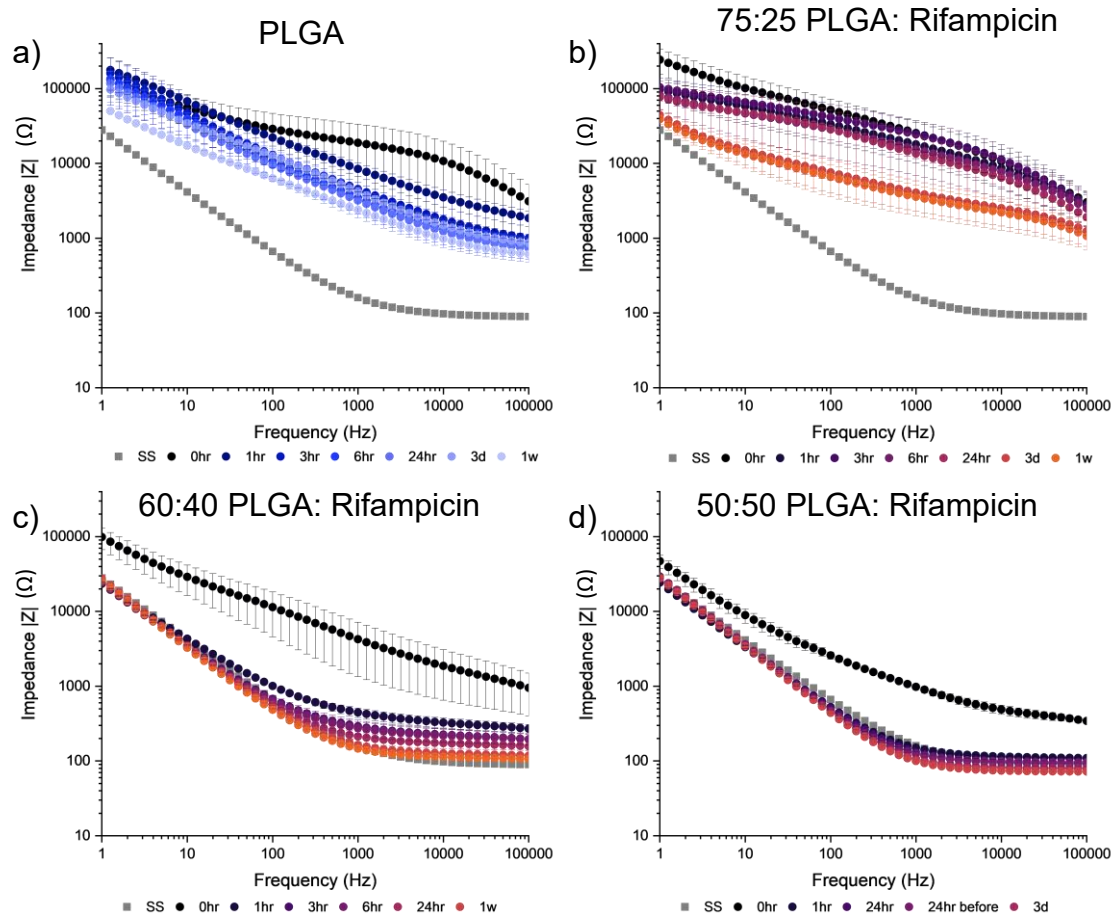


**Figure 4.11** The **a)** Impedance spectra of PLGA **b)** 75:25 v/v PLGA: Rifampicin **c)** 60:40 v/v PLGA: Rifampicin and **d)** 50:50 v/v PLGA: Rifampicin coated wires ( $n=3$ ) incubated in PBS in the fixed system



The impedances of PLGA and 75:25 had similar decreases in impedance over the 1-week period at 10 Hz (Figure 4.12), with them having the largest decrease in impedance of all sample types but not significant differences. They were statistically different from SS based overall trendline. The 60:40 and 50:50 formulations had statistically significant differences between all time points at the phase angle and impedance at the lower frequency. The phase angle had more statistical significances for samples than the impedance in both chosen frequencies.

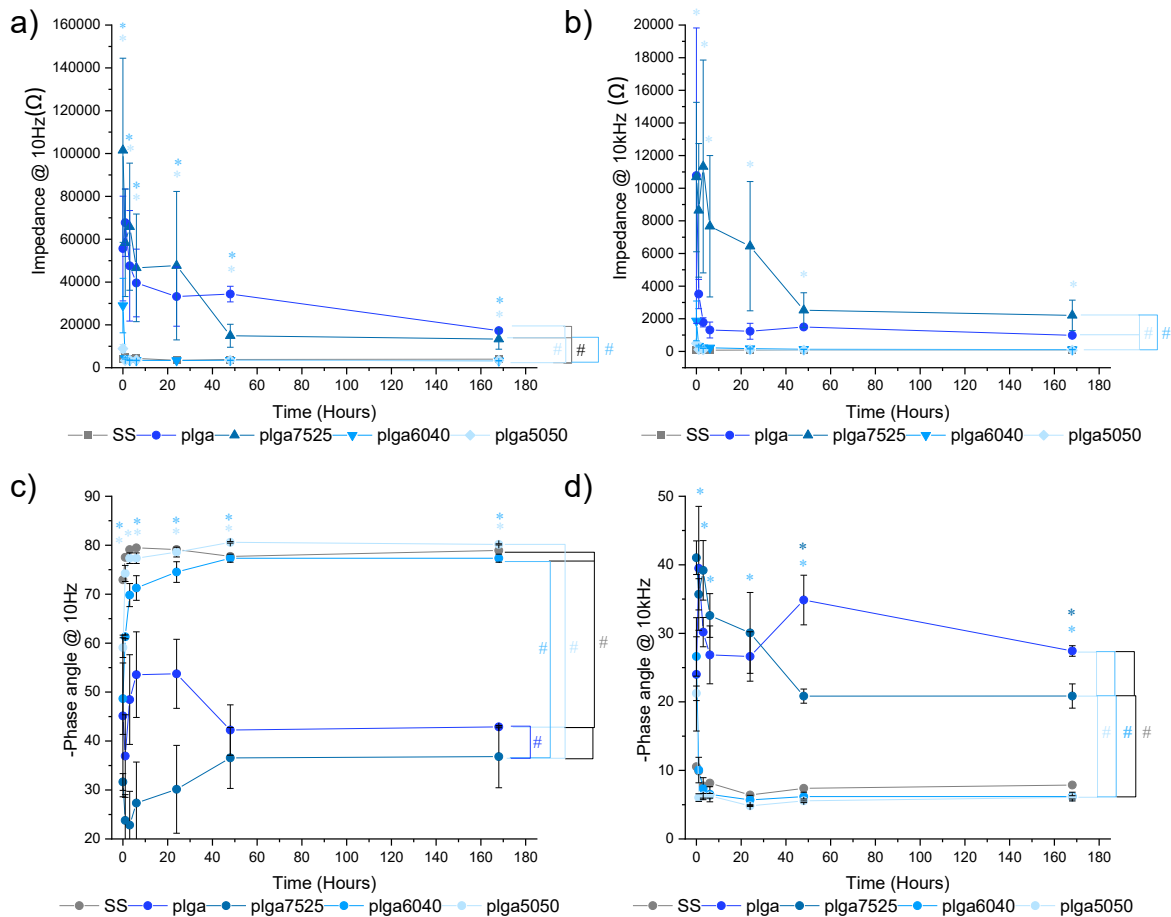


**Figure 4.12** Temporal impedance measurements at **a)** 10 Hz and **b)** 10 kHz of SS, PLGA, 75:25 v/v PLGA: Rifampicin, 60:40 v/v PLGA: Rifampicin and 50:50 v/v PLGA:

*Rifampicin coated wires (n=3) incubated in fixed system with PBS at room temperature and the negative phase angle at c) 10 Hz and d) 10 kHz. Significance was determined by ANOVA analysis, with Bonferroni post hoc between time points and time 0 (shown by \* 50:50, \*60:40, \*75:25) and Tukey post hoc between trendlines. (shown by # SS, # 50:50, #60:40, #75:25)*

The changing rate of impedance in Figure 4.13 has little change in all the samples except for PLGA. It has a variable changing rate of impedance that doesn't follow a clear pattern. The changing rate of phase angle shows a more difference between the different polymer drug formulations. This is especially clear in the changing rate of phase at 10kHz, with SS at the lowest, then 50:50, 60:40, 75:25 and PLGA at the highest.

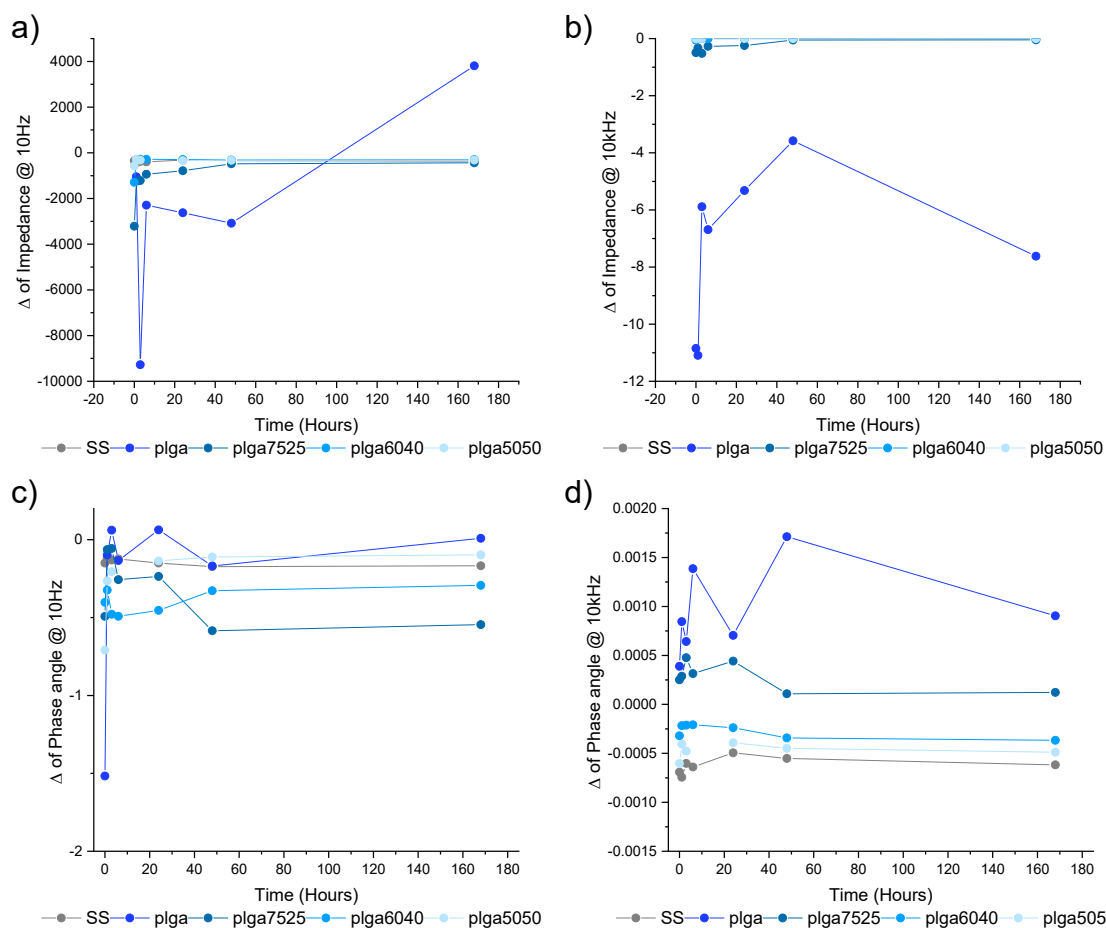


**Figure 4.13** The changing rate of impedance at **a)** 10Hz and **b)** 10 kHz of of SS, PLGA, 75:25 v/v PLGA: Rifampicin, 60:40 v/v PLGA: Rifampicin and 50:50 v/v PLGA: Rifampicin coated wires ( $n=3$ ) incubated in fixed system with PBS at room temperature and the changing rate of phase angle at **c)** 10 Hz and **d)** 10 kHz

Each of the PLA samples (Figure 4.14) had a similar impedance profile with a small negative slope across the whole frequency range and much higher magnitude than the bare SS spectrum for all sample types. They all experience a decrease in impedance over the 1 week.

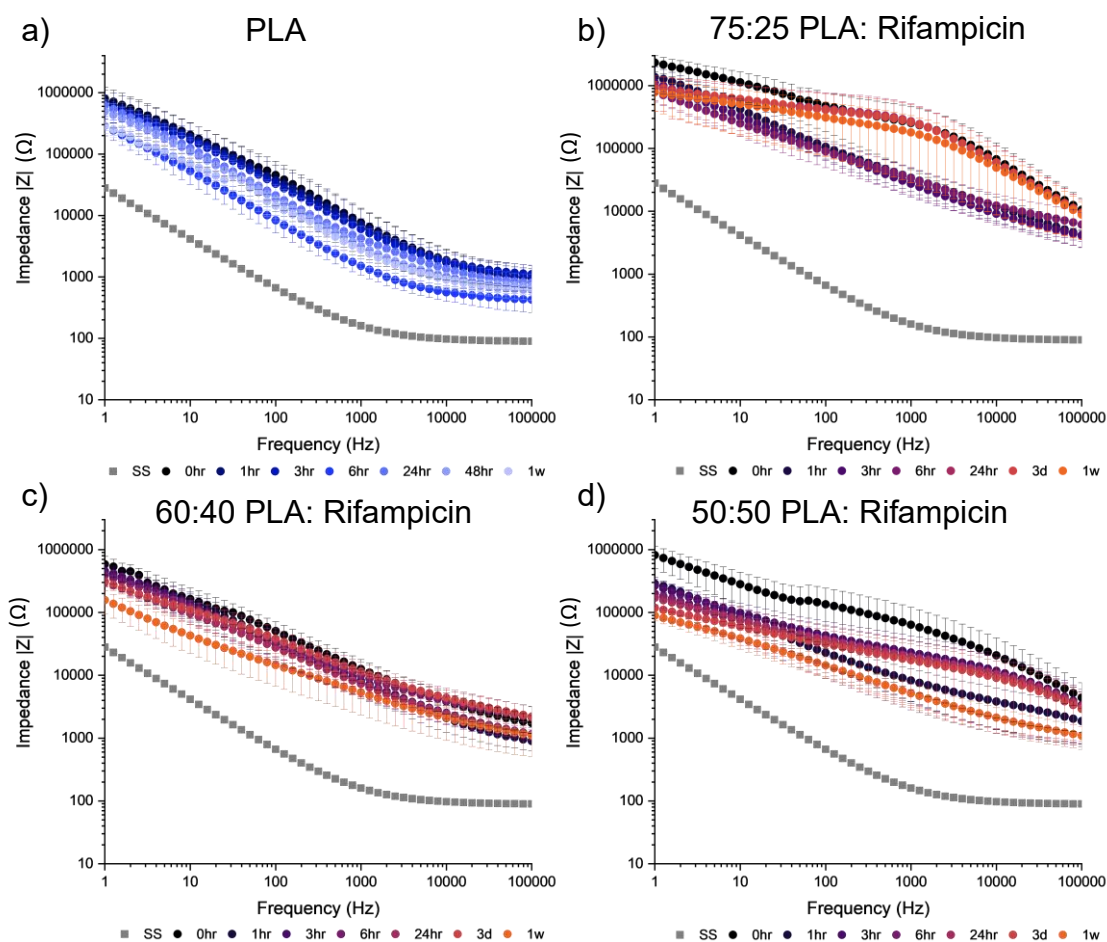


**Figure 4.14** The **a)** Impedance spectra of PLA, **b)** 75:25 v/v PLA: Rifampicin **c)** 60:40 v/v PLA: Rifampicin and **d)** 50:50 v/v PLA: Rifampicin coated wires ( $n=3$ ) incubated in PBS on the fixed system

There were no statistical differences between any time points for any of the samples in either the impedance or phase angle (Figure 4.15). The 75:25 formulation was statistically significant from all other samples at the 10 Hz impedance. The SS was statistically different from all other samples at 10 Hz phase angle. The error bars were large in these datasets as the PLA created a thick coating and larger thickness coating differences.

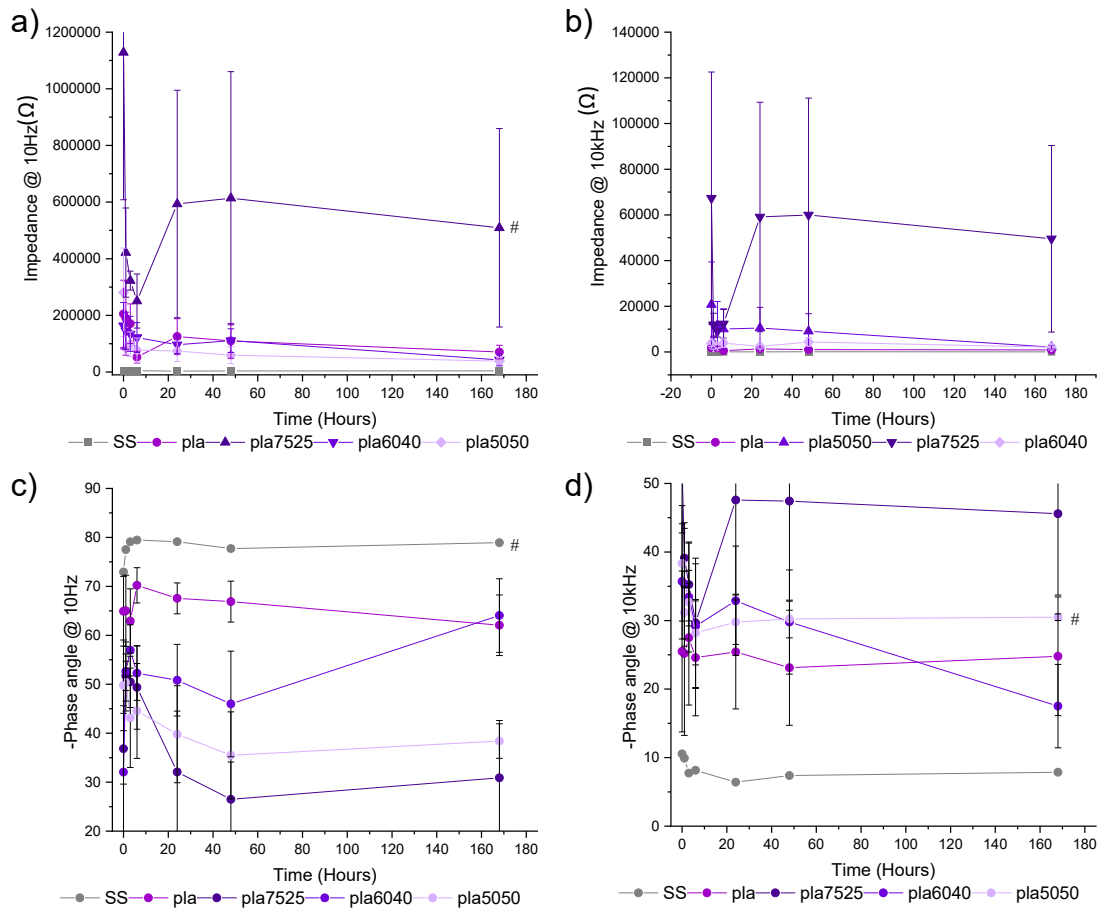


**Figure 4.15** Temporal impedance measurements at **a) 10Hz** and **b) 10 kHz** of SS, PLA, 75:25 v/v PLA: Rifampicin, 60:40 v/v PLA: Rifampicin and 50:50 v/v PLA: Rifampicin coated wires ( $n=3$ ) incubated in fixed system with PBS at room temperature and the negative phase angle at **c) 10Hz** and **d) 10kHz**. Significance was determined by ANOVA

analysis, with Bonferroni post hoc between time points and time 0 and Tukey post hoc between trendlines. # signifies significance from all other trendlines.

The changing rate of impedance and phase angle had no significant change over time and no visual difference between sample types seen in Figure 4.16.

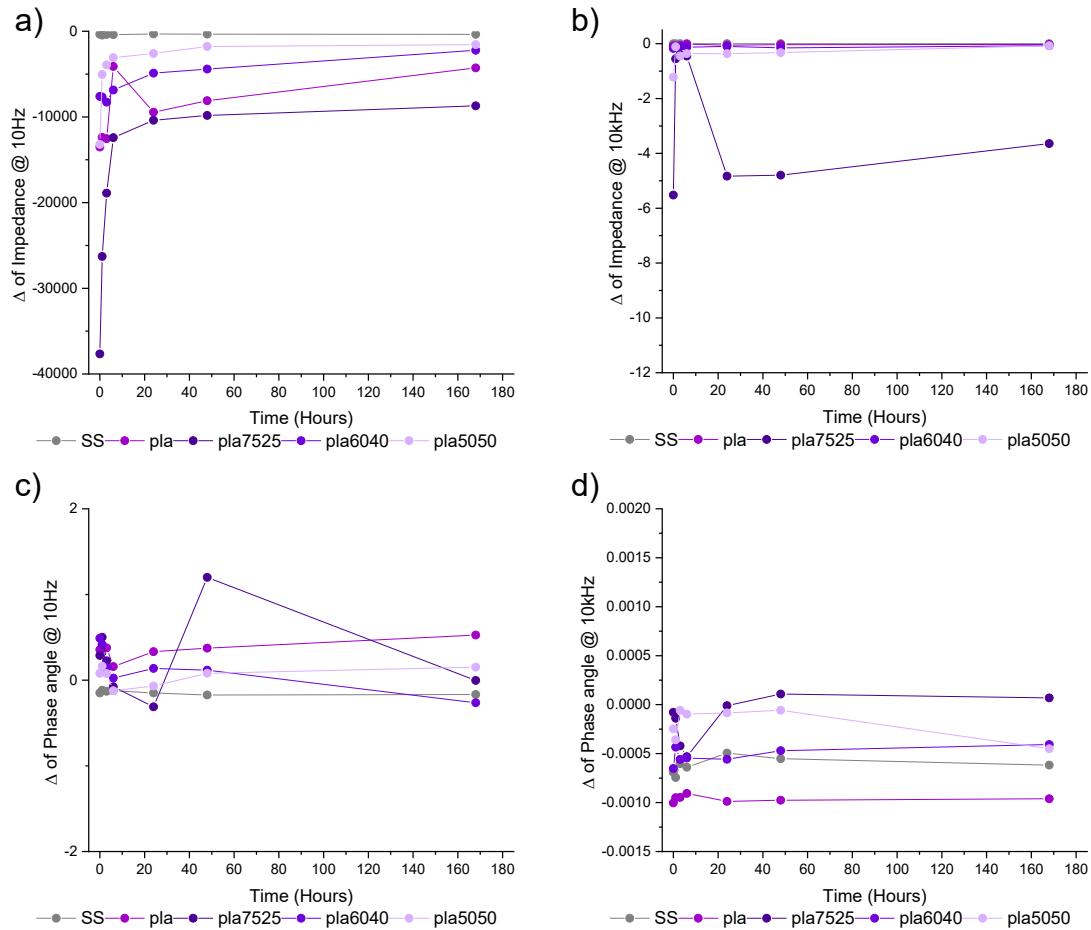


**Figure 4.16** The changing rate of impedance at **a)** 10 Hz and **b)** 10 kHz of SS, PLA, 75:25 v/v PLA: Rifampicin, 60:40 v/v PLA: Rifampicin and 50:50 v/v PLA: Rifampicin coated wires ( $n=3$ ) incubated in fixed system with PBS at room temperature and the changing rate of phase angle at **c)** 10 Hz and **d)** 10 kHz

A concentration curve was created using a known set of Rifampicin concentrations. The equation fit to the curve was  $y = 3.36x + 0.2$ . The concentration curve was used to find drug elution of the all the samples used in the above study. All negative values calculated were assumed 0. The cumulative Rifampicin released, and percent total Rifampicin released were plotted in Figure 4.17.

Testing for statistical significance using ANOVA with Tukey post hoc, the PLGA: Rifampicin 50:50 and 75:25 are significantly different from each other but none of the other samples differ. The cumulative release of Rifampicin shows that the PLGA: Rif 50:50 releases the most Rifampicin within a week compared to the other PLGA formulations, with the 60:40 formulation releasing the second largest amount and 75:25 releasing the least. With the PLA formulations, the PLA: Rif 75:25 released the most Rifampicin all together with PLA 60:40 coming second and PLA 50:50 having the least amount released.

The room temperature work was repeated at 37°C with a longer incubation period of 1 week to be more biologically relevant and only one polymer (PLGA) was taken forward for all further testing as it had the most consistent impedance results with small variations between samples. It also allowed for more release of drug in a shorter time period which would allow quicker release periods to see differences in biofilm growth. The following figures represent the results from this work.

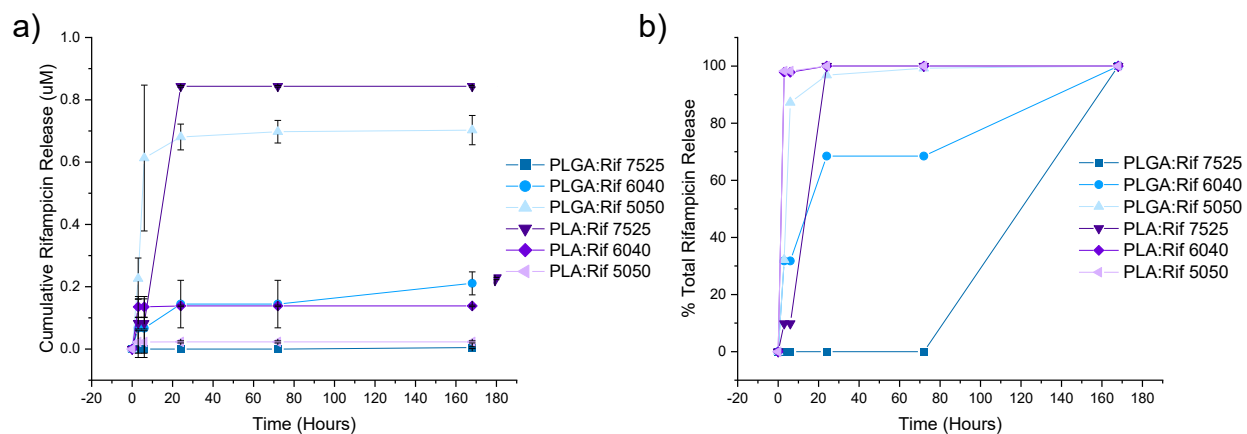


**Figure 4.17 a)** Cumulative Rifampicin released in  $\mu\text{mol}$  and **b)** % Total Rifampicin released from the samples ( $n=3$ ) over the 1-week period for PLGA: Rifampicin samples and PLA: Rifampicin samples



### **4.3.2 Long term 37°C temperature work**

The previous experiments were performed at room temperature for 1 week, but many typical implants will be in the body for extended periods of time therefore the next experiments focused on impedance measurements performed at 37°C for 2 months. These were performed in the fixed system as shown in table 3.1.

The impedance at 10 Hz and 10 kHz were plotted in Figure 4.18 and compared to the room temperature work in Figure 4.12. The metal's impedance at 10 Hz increased over the month period before stabilizing between month 1 and 2. This impedance increased more than it did at room temperature. The metals were all significantly different from one another, and different from Rifampicin. The 10 kHz had overall lower impedances than the room temperature work. The metal impedances did not change as significantly in the higher frequency than the lower frequency, with Rifampicin having the most noticeable change over time.

PLA had the highest impedance with large standard error and the most change over time. The PLGA samples and 75:25 samples had higher overall impedances and impedance changes than the other 2 polymer drug formulations. Compared to the room temperature work, the 10kHz showed an overall lower impedance again, similar to the metal samples. The 10Hz did not have much difference from the room temperature work. Only the PLGA sample and 75:25 samples were significantly different from the SS, 50:50, and 60:40 samples.

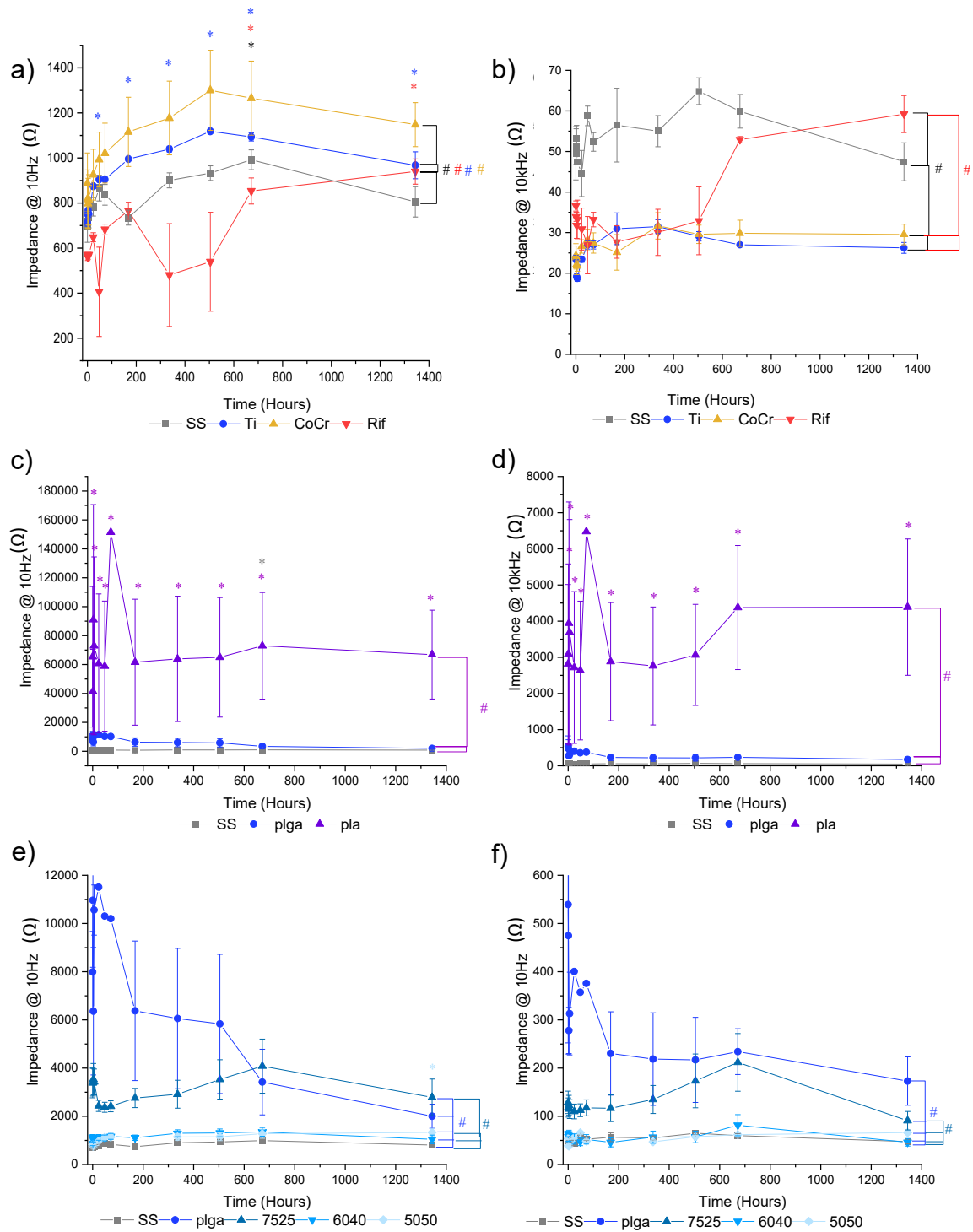


**Figure 4.18** Temporal impedance measurements of samples incubated in 37°C fixed system of **a)** metals SS, Ti, CoCr, and Rifampicin coated samples at 10 Hz and **b)** 10 kHz, **c)** SS, PLGA, and PLA coated wires at 10 Hz and **d)** 10kHz, **e)** SS, PLGA, 75:25, 60:40,

*and 50:50 v/v PLGA: Rifampicin coated samples (n=3) at 10 Hz, and f) 10 kHz. Significance was determined by ANOVA analysis, with Bonferroni post hoc between time points (shown by \*SS, \*Rifampicin, \* Ti, \*PLA, \*50:50) and time 0 and Tukey post hoc between trendlines (shown by # SS, # 50:50, #60:40, #75:25)*

The metal impedance changed more over the 2 months than the phase angle. There were also less differences seen between the metals in this work than the room temperature. The Rifampicin samples were significantly different from the metals at both chosen frequencies.

Both polymers were significantly different from each other and SS. At 10 Hz, there was a noticeable decrease in phase angle over the 2 months for both polymers.

The polymer-drug formulations are more distinguishable between each other with the phase angle than the impedances. It is also noted that there is a significant difference between SS and all formulations except for the 50:50, but the 50:50 is significantly different from all other formulations. There is a larger decrease in phase angle at the lower frequency and a smaller increase in phase angle at the higher frequency for all the polymer and polymer-drug samples.

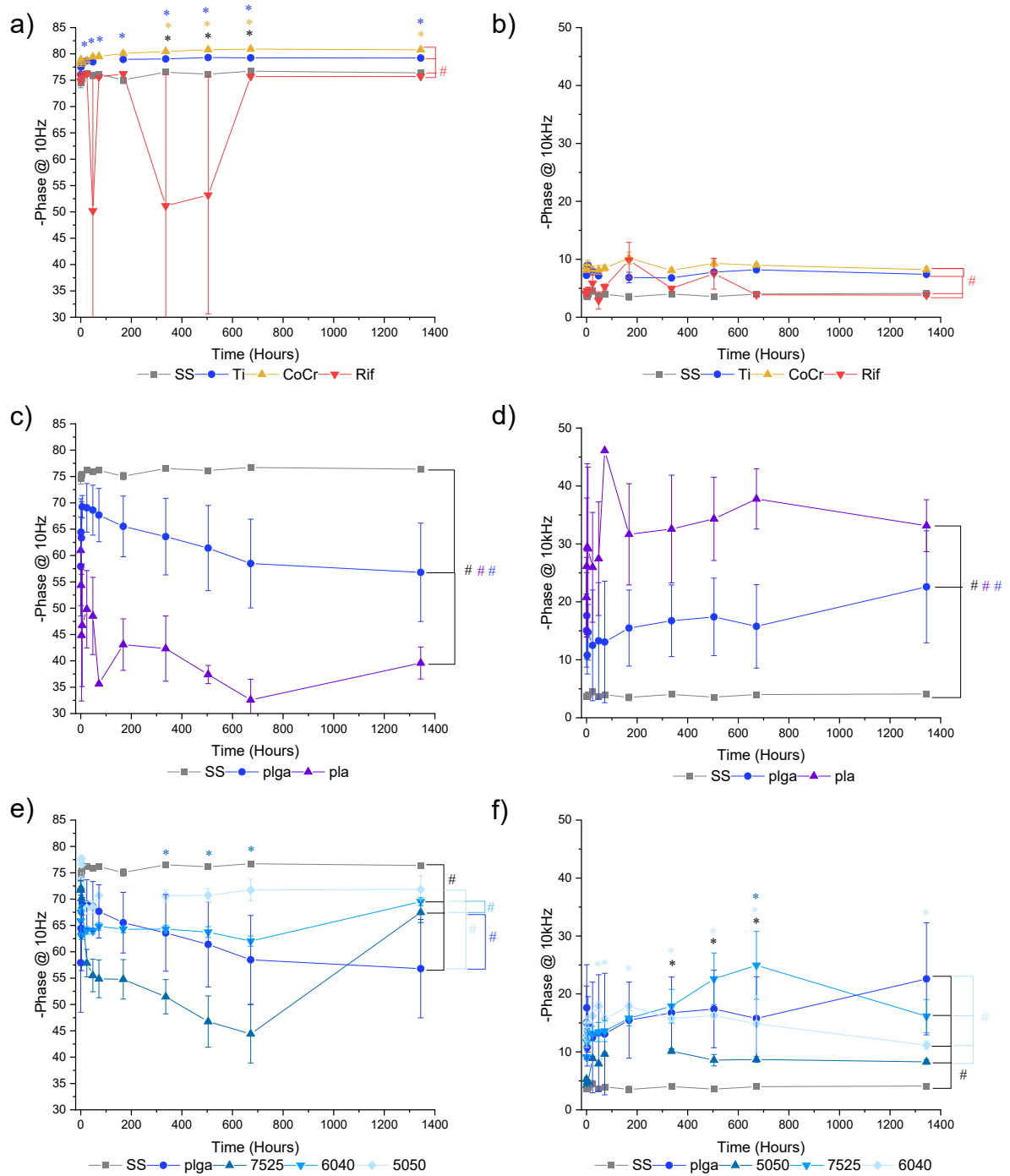


**Figure 4.19** Temporal negative phase angle measurements of samples incubated in 37°C fixed system of **a)** metals SS, Ti, CoCr, and Rifampicin coated samples at 10Hz and **b)** 10kHz, **c)** SS, PLGA, and PLA coated wires at 10Hz and **d)** 10kHz, **e)** SS, PLGA, 75:25,

60:40, and 50:50 v/v PLGA: Rifampicin coated samples ( $n=3$ ) at 10 Hz, and **f**) 10 kHz. Significance was determined by ANOVA analysis, with Bonferroni post hoc between time points (shown by \*SS, \*Rifampicin, \*Ti, \*PLA, \*50:50) and time 0 and Tukey post hoc between trendlines (shown by #SS, #50:50, #60:40, #75:25)

The 50:50 PLGA: Rifampicin samples had the most Rifampicin released at 1.75mg, followed by 60:40 v/v then 75:25 v/v. The 50:50v/v had the quickest release with over 90% released in the first 3 hours, while 60:40 had a slower steadier release with 60% released in the first week. The 75:25 formulation had no drug release until the 2-month reading.

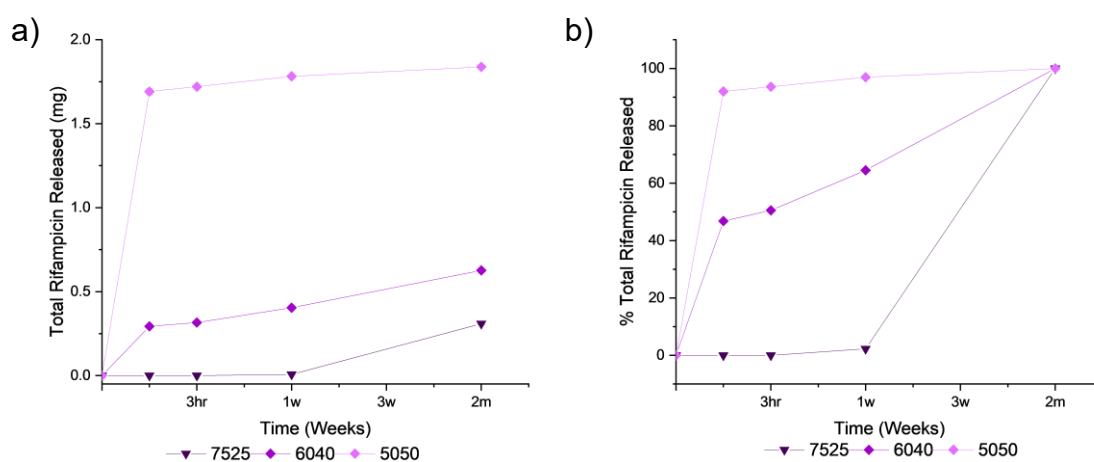


**Figure 4.20 a)** Cumulative Rifampicin released and **b)** % Total Rifampicin released from the samples( $n=3$ ) over the 2-month period for 75:25, 60:40, and 50:50 PLGA: Rifampicin samples

### 4.3.3 Polymer Degradation Characterisation

There were several ways that could be used to characterize the degradation of the polymer/polymer-drug coatings. The first proposed method was through mass loss degradation. The samples were measured before and after coating with the mass gained calculated and shown in the table below.

**Table 4.1** *The coating type and the total mass gained after coating(mg)(n=3)*

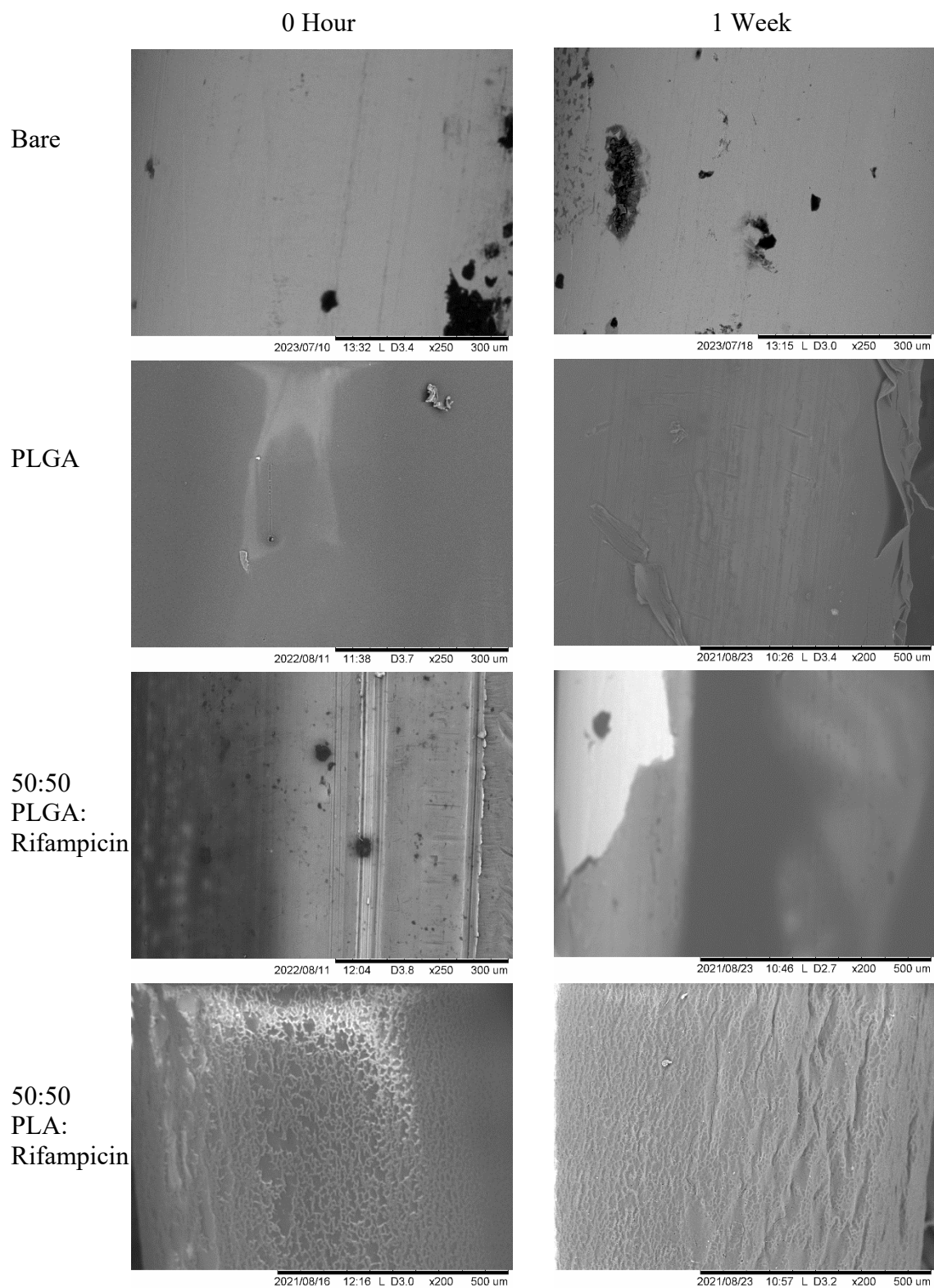
Sample	Mass Gain after Coating (mg)
Rifampicin	0.2
PLGA	2.5
PLA	4.9
75:25 PLGA	1.4
60:40 PLGA	0.4
50:50 PLGA	1.7
75:25 PLA	4.8
60:40 PLA	2.3
50:50 PLA	1.8

Table 4.1 shows that the samples had very little mass difference with the addition of the coatings. The largest difference was seen in the PLA coating with ~4.9 mg. The PLGA mass differences were even smaller with the highest being PLGA ~2.5 mg. Because of such small differences, using mass loss as a characterization of degradation did not seem fitting as it could lead to inaccurate data therefore alternative ways were explored.

SEM imaging was explored as an alternative from 120 to 1000 magnification as it would give visual clues as to what was happening on the surface as the polymer degraded that

could potentially be linked to impedance and phase changes. SEM images in Figure 4.21 showed the surface of the coatings at 0 hour and 1 week for bare, PLGA, 50:50 PLGA: Rifampicin and 50:50 PLA: Rifampicin.

Small metal deformities can be seen on the bare samples at both time points, with no noticeable difference. The PLGA sample at 0 hour has a very smooth surface, almost shiny with no deformities. At 1 week, the polymer had lost the shininess and there were ripples along the whole surface with only a few places where the coating had degraded all the way through to the metal. The 50:50 PLGA: Rifampicin coating did not have the same smoothness as the PLGA coating, with visible striations along the surface and dulled visuals of the metal deformities underneath. At 1 week there were large deformities in the coatings, with many places where the metal was showing through the coating and less striations along the surface. The 50:50 PLA: Rifampicin coating was a very solid looking coating, not as smooth as PLGA but looked unbroken and covered the SS all the way. Over the week there were ripples on the surface but not very deep ridges and no breaks in the coating.



**Figure 4.21** SEM images at time points 0 hour and 1 week for bare, PLGA, 50:50 PLGA:



*Rifampicin, and 50:50 PLA: Rifampicin.*

The SEM images had to be stopped and not all samples were able to get a 1-week time point image because the imaging method damaged the polymer coating at 1 week causing deformations or leading it to peel off the samples. This is believed to be due to the coating integrity lessening as it degraded. Below are pictured the samples that only had the 0-hour time point.

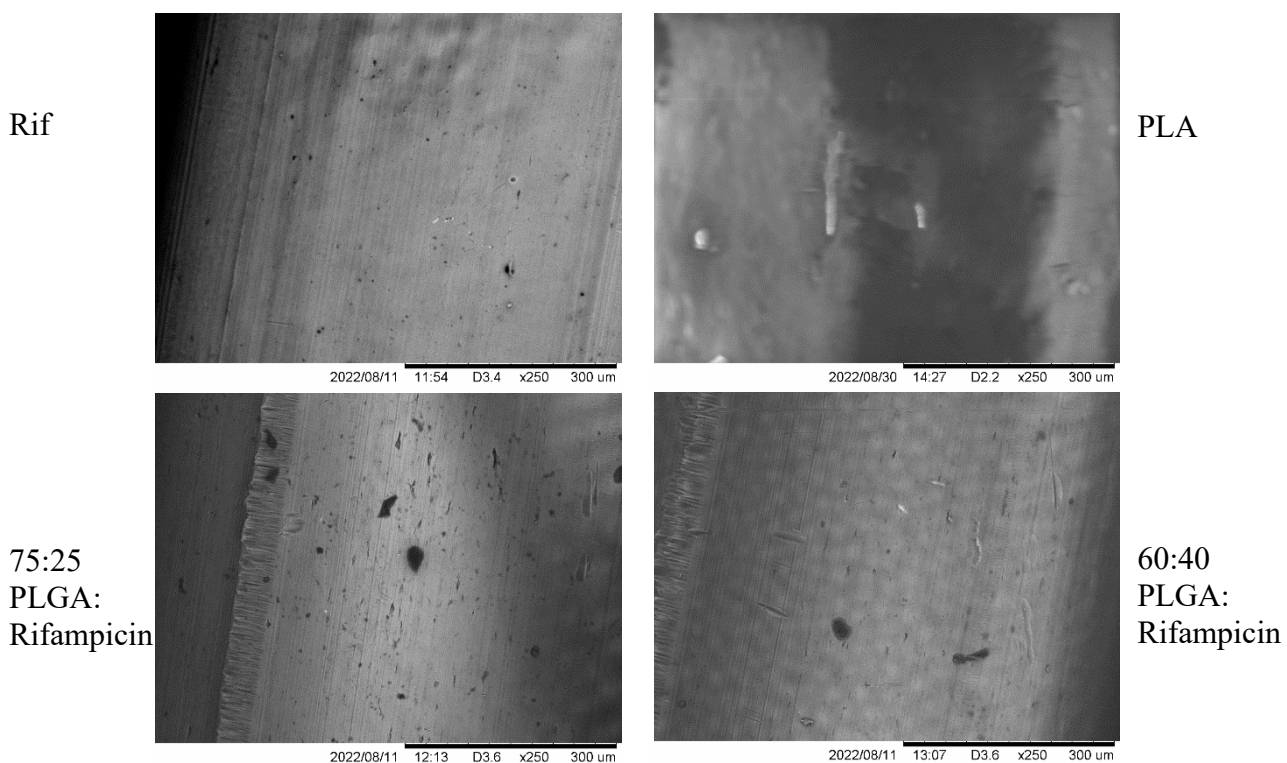


**Figure 4.22** SEM images of remaining samples only at time point 0 hour. Rifampicin, PLA, 75:25 PLGA: Rifampicin, and 60:40 PLGA: Rifampicin.

The Rifampicin coating did not have the striations that are seen in each of the PLGA: Rifampicin coatings. The different polymers had noticeable differences, with the PLGA having a smoother surface than the PLA. There was not a noticeable visual difference between the different polymer drug formulations.

While SEM was a good visualization tool, it had problems with imaging past the 1-week time point and did not give any quantifiable data. The last method explored to show polymer degradation was AFM measurements.

The colour scales show that the height for the bare SS ranges from -240 to +218 nm which is the largest variation in height for all the samples. The PLGA has the smallest range of height which follows since the SEM images showed a very smooth surface for the PLGA. The 50:50 formulation has the second largest height variation from -20 to +36 nm. Visually, all the coatings have more peaks across the surface than the bare SS.

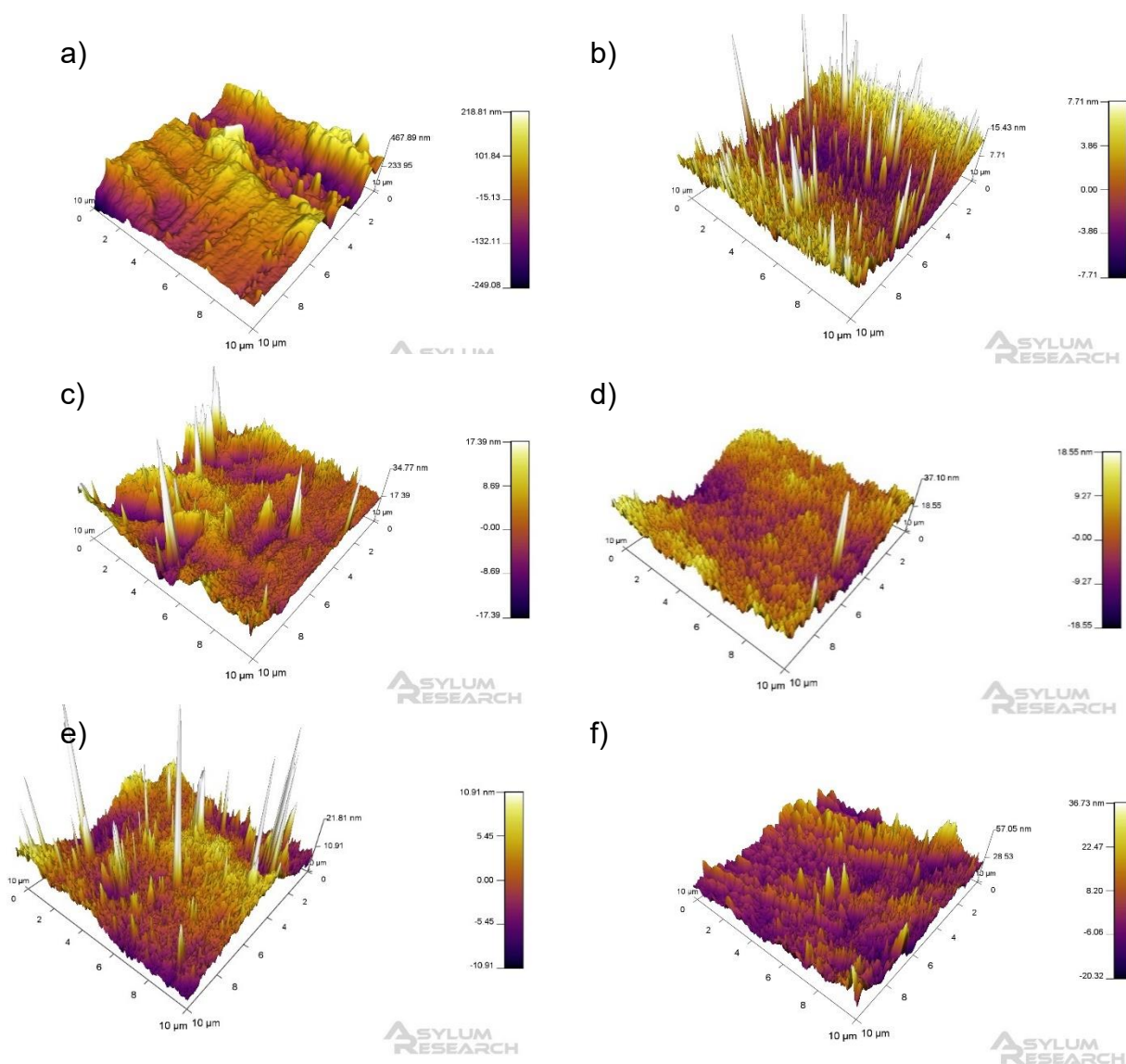


**Figure 4.23** AFM 3D renderings of height data with height retrace of **a)** bare SS **b)** PLGA **c)** Rifampicin **d)** 75:25 PLGA: Rifampicin **e)** 60:40 PLGA: Rifampicin **f)** 50:50 PLGA: Rifampicin. Other renderings attached in appendix.

The phase data gives us a different insight into the AFM data from a materials mechanical perspective including if there is a change in stiffness, adhesion, or viscoelasticity. Each of the samples has a quite distinct phase profile as seen by the difference in colour for each of the samples. The SS sample had a generally smooth surface with quite large pitting of

-700 nm. More notable differences can be seen between the different polymer drug formulations. The 75:25 formulations looks like it has quite consistent variations of the light and dark regions signifying different compositions across the whole sample. The 50:50 has less variations but still a range of different compositions on the surface. The Rifampicin coating is quite consistent with the range staying within one colour over most of the surface.

The AFM data was sample over three samples, with two sections each. Each of the renderings had similar profiles, with the polymer-drug coatings having the distinct pattered surface.

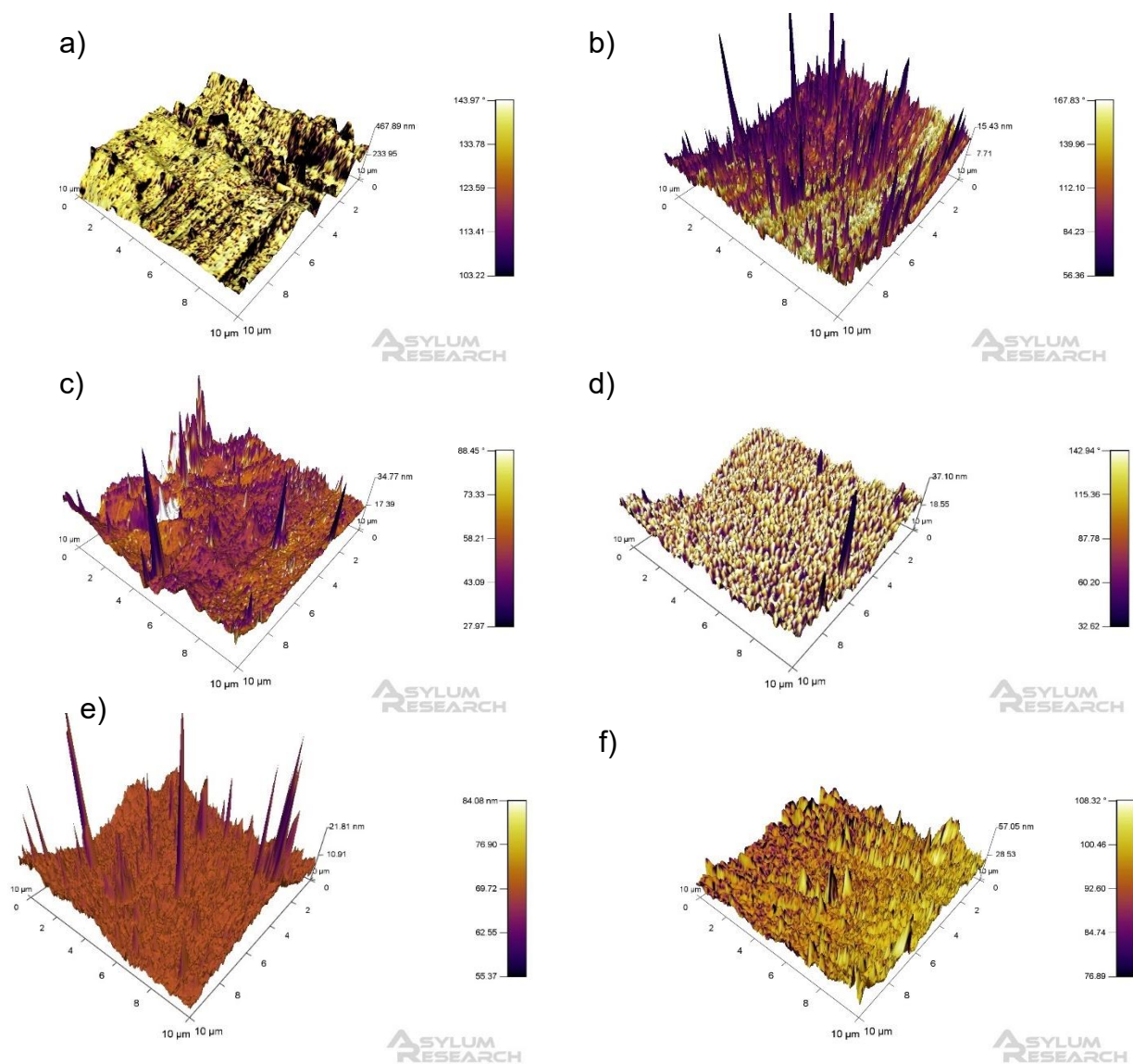


**Figure 4.24** AFM 3D renderings of height data with phase retrace of **a)** bare SS **b)** PLGA **c)** Rifampicin **d)** 75:25 PLGA: Rifampicin **e)** 60:40 PLGA: Rifampicin **f)** 50:50 PLGA: Rifampicin

The root mean square roughness (RMS) is the most used roughness parameters as discussed in AFM theory Section (2.4) (Raposo *et al.*, 2007). Figure 4.25 plots the root mean square roughness for each of the different coating types. The bare SS has the highest

roughness while all the coatings are slightly below 10nm average roughness with very small error. All of the coatings are significantly different from the bare SS.

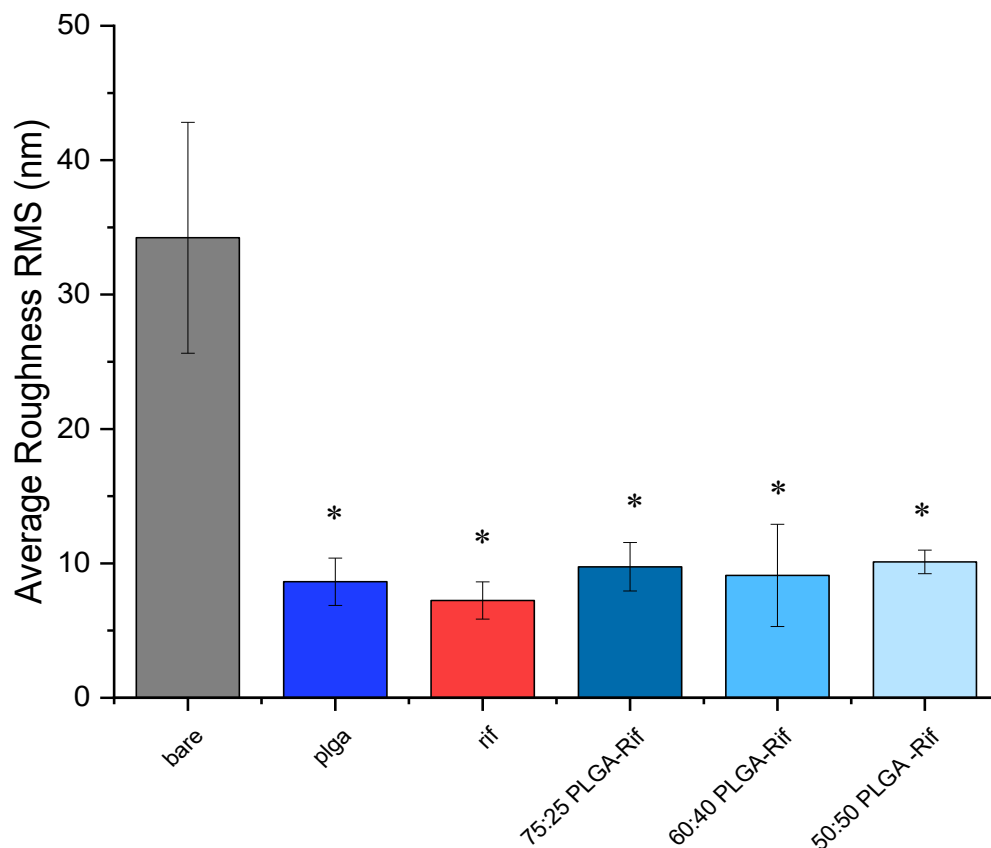


**Figure 4.25** AFM average roughness root mean square of SS, PLGA, Rifampicin, 75:25 PLGA: Rifampicin, 60:40 PLGA: Rifampicin, and 50:50 PLGA: Rifampicin. One way ANOVA performed with Tukey post hoc, \* represents significantly different from bare SS ( $n=3$ , with total of 6 samplings).

A possible problem with the dip coating method for the samples was when coated there was a noticeable unevenness between the top of the coating and the bottom. To determine

how much of a difference occurred across the coating, measurements were taken along the length of the coating as described in Section 3.4.3.1 coating analysis and plotted below.

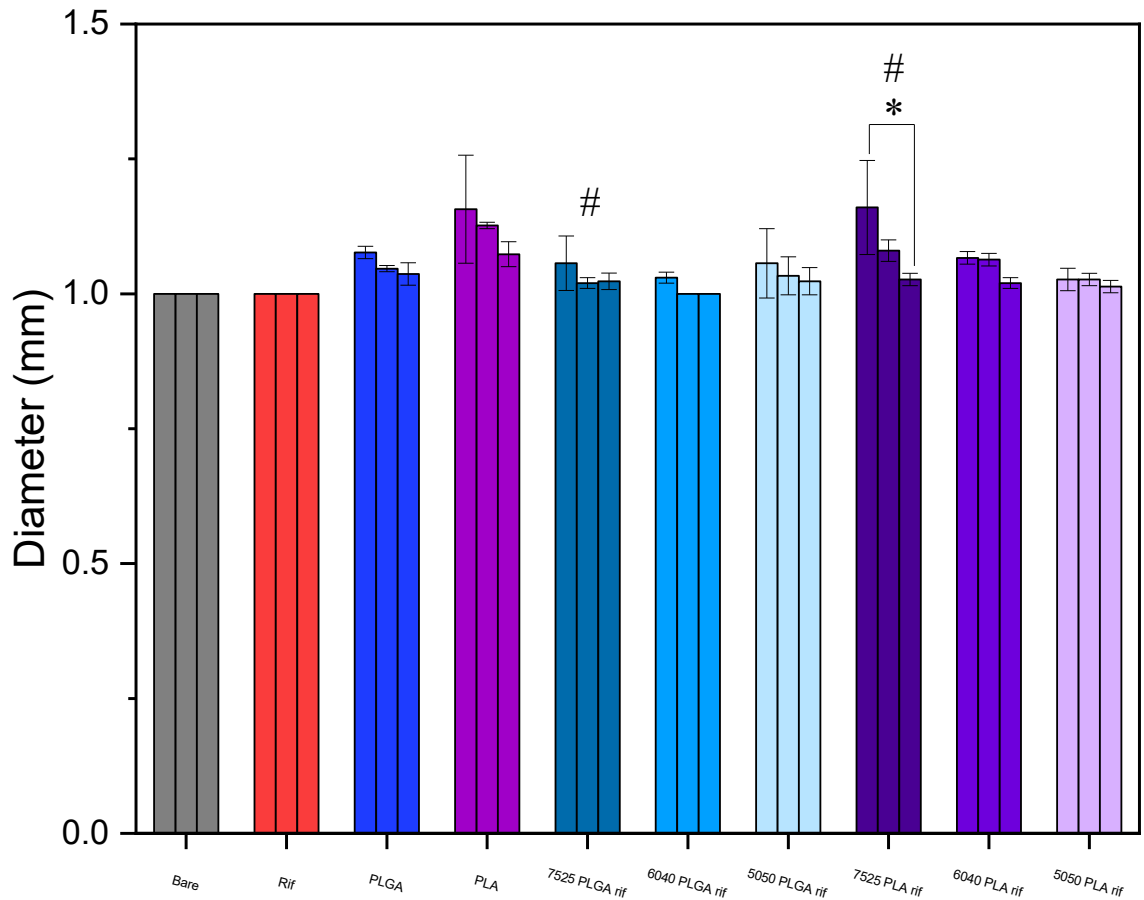


**Figure 4.26** Thickness measurements for each sample type, with columns representing average thickness ( $n=3$ ) of (starting at left): tip, middle and end of coating. \* Representing statistically significant difference between measured spots on same coating while # represents significant difference between coating type and a bare SS wire using ANOVA with Tukey post hoc

The samples show a similar trend of the tip of the coating have a larger coating diameter than the end of the coating. This is consistent through all the coating types. The only ones

significant were the 75:25 coating formulations for both the PLGA and PLA samples. Also, the only significant difference between the tip and end was the 75:25 PLA coating.

#### 4.3.4 Non-invasive Drug Detection

A large advantage to electrochemical impedance spectroscopy is the ability to monitor non-invasively. A potential non-invasive drug monitoring method would be differential pulse voltammetry and square wave voltammetry. A test was conducted on Rifampicin concentrations in PBS using both these test methods, Figure 4.27.

It can be seen there is a clear increase in current as the Rifampicin concentration increased, occurring around 0.05 V for both differential pulse and square wave voltammetry. The current raised from 0 to approximately  $0.6 \times 10^{-7}$  amps, when the concentration raised from 0  $\mu\text{M}$  to 6  $\mu\text{M}$ .

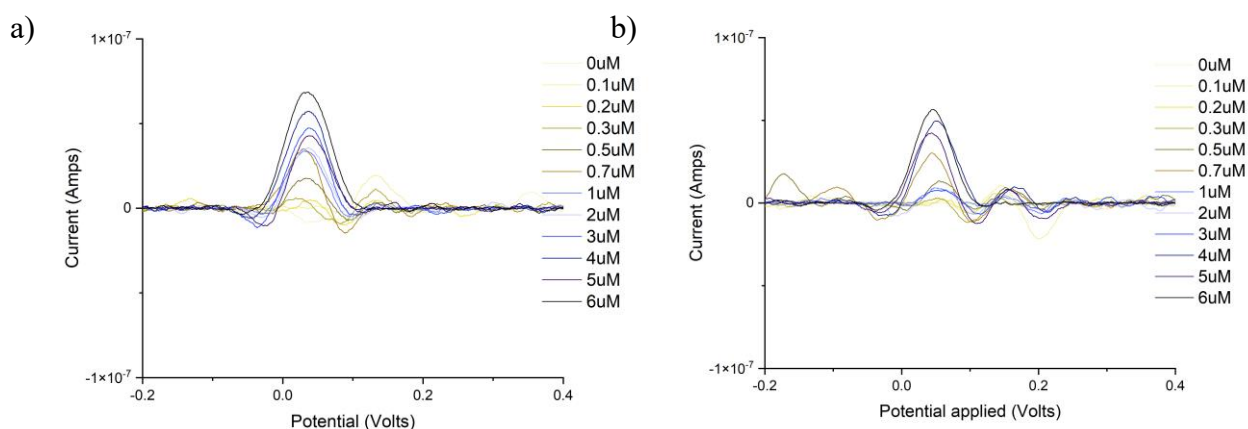


**Figure 4.27 a)** Differential pulse voltammetry and **b)** square wave voltammetry for range of Rifampicin concentrations from 0  $\mu\text{M}$  to 6  $\mu\text{M}$  in PBS solution ( $n=1$ )



## 4.4 Discussion

Each section will be discussed individually regarding the Chapter 1 aims (Section 3.3) before discussing contribution to the overall study aim (Section 1.8) this chapter addresses.

The key aims of this chapter were to determine what factors would influence impedance measurements, if medical implant metals could be used as electrodes for impedance measurements, if polymer-drug coating degradation could be characterized using ES, feasibility of using DPV and SWV to measure drug concentrations, and how to characterize polymer-drug coatings as it degrades.

### 4.4.1 Characterisation of ES System

Initial impedance experiments were focused on experimental factors that could influence impedance measurements. This study focused on biodegradable polymer-drug coatings as described in the coating selection section (Section 2.2). As the polymer degrades, it will release the drug, and it therefore needed to be determined how various drug concentrations within the incubation media may influence impedance measurements. In Figure 4.1, it is shown that as Rifampicin concentration increases there was minimal influence on the impedance in the lower frequency range (1-100 Hz). However, a larger difference in impedances can be seen in the higher frequency range (1000-100,000 Hz). Based on what is known of the impedance behaviour of systems like the one used here (Section 2.1), the solution resistance becomes more prevalent at higher frequencies according to the Randle's equivalent circuit model previously used to model this system (Shedden *et al.*, 2010). The impedance at 10kHz in Figure 4.1 d), shows a sharp increase in impedance at

the first introduction of Rifampicin which can be seen for all electrode types which could be due to the change in solution charge from the first addition of Rifampicin, as Rifampicin is an electroactive species (Metrohm). The subsequent drop in impedance and stabilization even with increasing Rifampicin concentration could mean that Rifampicin does not influence the solution resistance.

The effect of temperature and stirring on the impedance measurements were also investigated. Implant materials will typically be exposed to a temperature of 37° C in vivo. The surface of the implant is also likely to experience fluid forces, with the nature of these being dependent upon the implant location.

It was found that gentle stirring caused minor changes to the impedance measurements as seen in Figure 4.3, with an overall minor decrease observed of around 10  $\Omega$  for  $|Z|$ . An earlier study, using a rotating microdisk voltammetry experiment, showed that low ionic strength solution species show decreasing voltametric currents as the angular velocity increases (Gao and White, 1995). Gao and White hypothesized this may be due to the removal of ions from the electrode surface. However, given the minor differences observed in the present study, and the overall focus of the work being on the investigation of impedance measurements in low-flow applications such as orthopaedics, it was decided that the addition of flow added a complexity to the analysis that was not justified. This also permitted easier drug concentration measurements to be made, which was an essential feature of the subsequent bacteria experiments.

The temperature of the solution did appear to influence the impedance measurements, with increased temperature decreasing the overall impedance. This effect was most marked at

higher frequencies, where such solution effects would be expected to be most dominant. As the solution temperature increases, the molecules speed up leading to a reduction in overall resistance and ultimately the total impedance (Gamry, 2022). The phase angle was less sensitive to temperature changes than the impedance. Given these findings, it was concluded that experiments performed at different temperatures could not be directly compared.

This study focused on the feasibility of using medical implant metals as the electrode. Therefore, the metals needed to be investigated for their ES properties. The metals used for this study are SS, Ti, and CoCr all common metal implant materials (Section 1.1.1). Each metal has different formations of oxide layers, therefore a short-term study was performed to determine the metals stability over time and how the formation of different oxide films influences impedance.

The first experiment was performed at room temperature for 1 week in the fixed system to lessen sample variations. The total impedance spectra of each metal as seen in Figure 4.8 have similar impedance profiles with very minimal changes over 1 week. CoCr had more variation across the whole impedance spectra than the other metals, while Ti had variations in the lower frequency range. Each of these metals can form different oxide layers that depend on temperature and the environment which could attribute to the different impedance spectra seen in this study (Kurup *et al.*, 2021, Jelovica Badovinac *et al.*, 2019, Wang *et al.*, 2020) When compared to a Rifampicin coated sample, the metals are stable and not significantly different from each other. The Rifampicin coated samples had a large increase in impedance across the whole frequency range as the drug was

released from the surface of the metal as seen in Figure 4.8 d. This difference is highlighted in Figure 4.9, with Rifampicin having a significant change over 1 week in phase angle, at high and low frequencies while also being significantly different from the metals in impedance at high and low frequencies. These results show the metals can be used as an electrode within the system without needing significant consideration of their properties or different oxide layer formations significantly affecting the impedance.

#### **4.4.2 Impedance of polymer-drug coatings**

Most impedance studies focus on an idealized system that uses gold or platinum electrodes as described in commercially available EIS and ES (Section 1.7). Since the central aim of this thesis is to investigate the utility of impedance measurements as a means of monitoring the bacteria-implant interface, it was decided to move beyond the simplified wire-electrode measurements outlined above. Inspired by the previous work of Shedden *et al*, 2010, these experiments investigated the impedance characteristics of commercially available implants. The first implant material investigated was a PLA-sirolimus coated stent, which was compared to a 50:50 PLGA: Rifampicin coated wire model.

Figure 4.5 a and b shows the total impedance spectra for the stent and the wire model are very similar in magnitude and shape. In Figure 4.5 c and d, an initial decrease in impedance over the first 3 hours is observed, followed by a gradual increase over the next 3 hours. This early reduction in impedance likely reflects water uptake immediately following immersion of the coated stent (Engineer *et al.*, 2011, Gentile *et al.*, 2014). Once the PLA on the stent has absorbed water, conductivity will increase due to a decrease in density leading to an increase in impedance

The differences between the stent and PLGA: Rifampicin coated wire model can be seen in Figure 4.5 c and d with the stent having a larger initial decrease in the first 3 hours followed by an increase in impedance over the following 3 hours. PLGA and PLA have different crystalline structures, with PLGA being amorphous and PLA having a semi-crystalline structure as described in Section 1.2.2.1. PLGA's amorphous nature allows for quicker degradation times and quicker release of imbedded drug while PLA allows for more water absorption and slower degradation. Another difference between the two polymers can be seen in Figure 4.7, with the PLGA: Rifampicin model having released most of the drug within 3 hours of incubation and having 13X more drug released than the PLA sirolimus stent. This could be due to the stent having a thinner coating and slower degradation time with PLA. While the stent and model had two different polymer-drug combinations the impedance profiles were comparable, lending to the model being accurate for manufactured medical device surfaces.

Once it was established that the wire model could be used, long term studies were performed using different polymer-drug formulations. SS was used as the base metal for all the polymer-drug experiments as it had the most stability over time, seen in Figure 4.8. The bare metal impedance results were compared to PLGA and PLA formulation coated samples. The PLGA formulations had two distinct impedance profiles. In Figure 4.11, the first two graphs had higher polymer concentrations, and their impedance profiles were more linear across the whole impedance spectra. A thicker polymer coating had more overall resistance as described by Zhong(Zhong *et al.*, 2015). The lower polymer concentrations had impedance profiles that were more similar to the metal profiles, with

the main difference being the magnitude of the impedance decreased over time. This occurs for all PLGA samples, correlating to the degradation of polymer leading to a decrease in resistance. Zhong compared impedance of a model PLGA-coated stainless-steel sample to a PLGA-coated stent, and related EIS to mass loss. He saw a clear decrease in impedance over 50 days for both his model and stent, that followed a clear change in mass when incubated in PBS and changes in the microstructure of the coating. The work in this study shows that the addition of drug does influence the impedance spectra, but the polymer degradation still dominates the impedance changes over time. The impedance and phase data have similar trends at both the 10 Hz and 10 kHz for the PLGA samples. Figure 4.12 shows that PLGA and 75:25 have the highest impedance and the most change over time likely attributed to the thicker coating which created more resistance, shown by their significant differences between them and the SS and lower polymer formulations.

The PLA samples had very thick coatings due to PLA's higher viscosity. The impedance profiles shown in Figure 4.14 do not show consistent decreases in impedance over time. The standard error was larger for PLA than PLGA, more likely related to variations in coatings. More in depth look at the impedances can be seen in Figure 4.15, where there were no significant differences in impedance between PLA formulations.

A fast evaluation method was preferred over circuit modelling and intensive maths evaluation methods for this study. This is because circuit modelling can be associated with great error as multiple circuits can be fitted to the same data. This study used a complicated system where the circuit would need to change as the polymer degraded and the drug released making its fitting difficult (Loveday, 2004). Many assumptions would also need

to be made as the circuit changes which could lead to an inaccurate model or inaccurate conclusions based off the assumptions.

As described in Section 2.1, there are many theoretical methods for fast evaluation of coating effectiveness. This Section looked at the different fast evaluation methods including impedance at 10 Hz and 10 kHz, phase angle at 10 Hz and 10 kHz, and changing rate of impedance and phase angle at 10Hz and 10kHz (Zuo *et al.*, 2008, Bing, 2012, Xia *et al.*, 2012).

The impedance at 10 Hz and 10 kHz showed obvious decreases in impedance over time for the higher PLGA concentrations. The 50:50 and 60:40 PLGA: Rifampicin concentrations had significant differences in impedance over time and were significantly different from the bare electrode. This trend was also repeated in the phase angle data for both frequencies.

The PLGA results are supported by Zuo's and Mahdavian's analysis method where they compared equivalent circuit analysis to phase angle at 10 Hz and 100 Hz for epoxy coatings. They found that 10 Hz and 10 kHz for phase angle had similar variations compared to the coating resistance which reflected the coating performance (Zuo *et al.*, 2008) (Mahdavian and Attar, 2006). Zhang also used phase angle at 10 Hz and 10 kHz to evaluate polymer coatings on metal substrates (Zhang *et al.*, 2023).

The current study showed the potential use of impedance and phase angle at certain frequencies as a fast evaluation method for polymer-drug coatings. The changes seen in impedance and phase angle correlated to the expected time it takes for the polymer to

degrade and drug release. This is shown in the drug measurement results, Figure 4.17. The 50:50 PLGA: Rifampicin had the most drug released over the 1-week period with 60:40 releasing the next highest amount. These formulations released drug rapidly in the first 24 hours and then had a slower release over the week. The impedance data followed this trend, with Figure 4.12 showing the most change in impedance over the first 48 hours followed by a smaller change over the rest of the week.

The changing rate of impedance and phase angle did not show the same trends in the polymer-drug samples. Figure 4.13 and 4.16 showed the changing rate for phase angle and impedance for both the PLGA and PLA samples, but there were no significant changes over time. When looking at the full impedance spectra in Figures 4.11 and 4.14, the shape of the impedance spectra does not change over time, only the magnitude of the impedance changed. Therefore, the rate of change fast evaluation method was not suitable for this type of study. It had previously been used for fast corrosion organic coatings on metals. Xia (Xia *et al.*, 2012) studied an organic epoxy coating submerged in “functional beverage”, as described by the source, over 254 days and looked at changing rate of phase angle. The epoxy coating only had three stages of degradation: penetration, corrosion initiation, and delamination of coating leading to complete degradation. As discussed in Section 1.2.2.1, biodegradable polymers have four stages of degradation: water diffusion, oligomers with acidic end- groups autocatalyzing, oligomers diffuse out from polymer and create micropores for the drug to release with water taking spot of drug, and then the polymeric matrix becoming highly porous and degradation continues (Engineer *et al.*, 2011). The very different degradation processes and length of incubation could explain



why the changing rate of impedance and phase angle could not be used as a fast evaluation method for these polymer-drug coatings.

The PLGA samples showed promising results of reliable changes in impedance and phase angle to drug release and polymer degradation, especially in short time periods. The PLA samples did not have many significant differences in any of the samples for impedance or phase angle. Due to the large standard error between PLA samples and the lack of significant differences between formulations, PLA was not taken forward in further testing.

The experiment was repeated in 37°C with only PLGA: Rifampicin formulations for 2 months to determine how temperature and longer time periods affected the degradation rate and impedance changes.

The metal's impedance at 10 Hz increased until the 4-week time point but had little change at 10 kHz, Figure 4.18 a) and b). The change at 10 Hz could be associated with the oxide layer formation as discussed in the previous section. Oxide layers form faster at higher temperatures, therefore the larger changes seen at 37°C versus room temperature could be related to the faster formation of an oxide layer (Evans, 2001). The Rifampicin samples were significantly different from the metals at 10Hz. It also had significant changes at the 4 week and 2-month time points correlating to when the drug would be completely dispersed from the surface.

The impedance of the PLGA: Rifampicin formulations showed less significant change for the lower formulation samples, 60:40 and 50:50, at the longer time points compared to the

shorter room temperature work. This could be due to the quicker degradation of the polymer leading to faster changes. The phase angle was more informative with changes being more noticeable for the longer degradation times and significant differences being seen between all the different PLGA: Rifampicin formulations especially at the 10Hz frequency seen in Figure 4.19.

Fan *et al* (Fan *et al.*, 2021) performed a similar experiment analysing an epoxy coating on steel in an acidic environment and related corrosion characteristics to several fast evaluation methods and the gold standard of equivalent circuit modelling. They found that the phase angle at 10 kHz represented the delamination of the coating.

#### **4.4.3 Polymer Evaluation**

To interpret the impedance measurements for the polymer-drug coatings, the polymer was evaluated for changes over time. There were several proposed methods on how to characterize the polymer degradation: mass loss, SEM, and AFM.

The mass measurements were gold standard for determining how much polymer had degraded as demonstrated by Zhong (Zhong *et al.*, 2015). In Table 4.1, the mass gain was minor, with less than 5mg for any sample type. These mass measurements were too small, and the equipment used not sensitive enough to gain any understanding into the polymer degradation. There was a higher chance of inaccurate data for such small masses therefore alternative ways were explored.

SEM images were taken at two different time points, time 0 and 1 week. Figure 4.24 shows side by side images of bare metal, PLGA, 50:50 PLGA: Rifampicin, and 50:50 PLA:

Rifampicin at the two different time points. The PLGA and 50:50 PLGA: Rifampicin samples had noticeable surface deformations after 1 week. PLGA has a degradation period of 12-18 days while PLA has over 24 days, which could account for PLA not showing obvious deformations (Gentile *et al.*, 2014). Imaging could not be taken forward after one week due to the securement method for imaging damaged the coating once the coating had been compromised through degradation.

AFM was used in tapping mode to gain information on roughness and phase imaging of the polymer-drug coatings as discussed in Section 2.4. Roughness was used as a polymer degradation evaluation based on Silva *et al.*, as the polymer degrades roughness should change and give indication to degradation (Silva *et al.*, 2023). A visual assessment of the height and phase was performed on Figures 4.26 and 4.27. The polymer and polymer-drug coatings had a noticeable difference in height profiles from the bare metal. In Figure 4.26 a) the bare metal had a smooth surface with little pitting and the largest height variation compared to the other samples. The coated samples had smaller height variations but had a structured pattern across the surface, more likely attributed to the polymer.

The phase images gave a different outlook on the AFM data, as discussed in Section 2.4 relating to composition and adhesion. The bare metal had a more uniform image with higher phase angle, while the other samples had a larger range in angle with noticeable peaks that could relate to the polymer and drug differences. Wu *et al.* used AFM to characterize the surface of a PLA Everolimus stent and an EVAL Everolimus stent (Wu *et al.*, 2010). They also saw two phase separated structures with circular domains on the stents, with data showing initial drug covered surface compared to the bulk properties.

After elution there was a rapid loss of material from the surface followed by slow degradation of the polymer. Marques used AFM to differentiate between bioactive coatings on Ti (Marques *et al.*, 2015).

The RMS was plotted for each of the different surfaces in Figure 4.28. Each of the coatings was significantly different from the bare control metal. This showed promising results for using AFM to characterize the surface of the coatings and could potentially be used in the future to gain insights into surface changes when compared to impedance changes. This study was to determine how well AFM characterized the surface of polymer-drug coatings and how to optimize the methodology of the AFM measurements.

A potential problem with the measurements could be un-evenness of the coating through the dip method. Thickness measurements were performed at various points to determine how much variation was within the coatings. In Figure 4.29, it showed there was a noticeable difference between the tip and end of the coatings leading to some inconsistencies but there were only significant differences in the thicker coatings. As these formulations would not be taken forward into later experiments, the coating method was deemed usable for later experiments with consideration to mitigation efforts to eliminate variations including controlled amount of coating put onto the surface and even application using a tool

#### **4.4.4 Drug Detection**

In the ES discussion Section 4.2.1, UV spectrophotometry is used to determine drug released from the samples. This is a commonly used method for drug detection and works well for larger drug release, specifically in the beginning of the release period that these

initial experiments focused on. The longer drug release experiments would be more difficult to detect due to smaller drug concentrations. This method also requires samples to be taken out from the incubation media and measured at later time points, leading to the potential of the drug to degrade. A new real time analysis method of drug detection was looked at for this experiment.

As discussed in Section 2.2, Rifampicin was chosen for its superior antimicrobial qualities, especially against *S. aureus*. Another key feature of this drug is its electroactive nature, meaning it can be electrochemically detected through its oxidation reaction (Kul, 2020). This oxidation reaction is mainly studied using modified glassy carbon electrodes (Amidi *et al.*, 2017, Kul, 2020, Radhi *et al.*, 2019). This study looked at using an un-modified glassy carbon electrode to determine if it was sensitive enough to still detect the Rifampicin concentration through DPV and SWV.

Initial experiments seen in Figure 4.30 had a clear increase in current, ranging from 0 to  $7 \times 10^{-8}$ , with increasing Rifampicin concentration. This result provided similar results to Kul and Amidi (Kul, 2020, Amidi *et al.*, 2017). They both used a modified GCE with poly-melamine and carbon nanotube to measure Rifampicin concentrations and saw a clear linear increase in current with increased concentration at approximately 0.17 V. When this study was repeated, variable results were given using the un-modified GCE.

When this experiment was performed on nutrient broth, there was no correlation between concentration and the produced curves (Yu *et al.*, 2011). Broth did not follow a pattern for the DPV most likely due to the other proteins including peptone (Saeed *et al.*, 2017) within that overpowers the Rifampicin electrochemical signal.

## 4.5 System Limitations

This experimental work had many limitations that are discussed in this section.

Initial variable experiments were performed with an  $n$  of 1, which did not constitute enough data points to run statistical analysis on the results. The electrodes were also not securely fixed in the initial experiments, allowing for minor variations in data collection that could cause some minor differences in impedance data. The later fixed system also had a few variations between setups that could have small variations in impedance measurements because the counter electrode was used for all experiments meaning it was moved between each measurement.

The stent measurements had insecure connections that did not allow for long experimental times. The experiment had to be stopped after 10 hours because the clamp that held the stent was causing deformities in the coating. An attempt at attaching a wire for stable connection was unsuccessful therefore long incubation studies were not carried out on the stent.

The analysis methods for impedance, the changing rate of impedance and changing rate of phase full spectra did not allow for statistical analysis. This presented a significant challenge in using it as an analysis method in comparison to a single chosen frequency.

The chosen coating method presented a few challenges. Uneven coatings could lead to variations in measurements and uneven degradation. There could be variations from sample to sample, leading to surface characterization to be inaccurate. All efforts were

implemented to minimize these variations through steady dipping, drying methods, and coating measurements.

When measuring drug release, the total amount of drug or polymer from the samples was not fully determined as the total amount of drug was not released in the short time span and could not be calculated based on the dip method. Therefore, total drug released was measured in relation to the final time point and not total drug in the coating.

The SEM as discussed had limitations to its measurements. The fixation that held the samples for imaging damaged the coating once the coating had started to degrade, not allowing for later time points to be imaged. The AFM also had limitations including the limited size of the area measured when compared to larger surface morphology. While the surface could be measured, and certain aspects of the coating obtained specifically through phase imaging, differences could only be determined after long degradation periods. There are impedance changes that need to be accounted for before the polymer starts to degrade that need to be determined before major surface morphological changes.

#### **4.6 Future Work**

A few limitations were spotted in the experiments performed. The stent impedance measurements had to be stopped after only 10 hours. A different experimental method would be beneficial to perform long term experiments on the stent including a connection method that would allow full submersion and not damage the stent. An investigation of other medical implants as electrodes would also add to the feasibility of using medical implants as self-reporting on infections.

This study limited focus to polymer-drug coatings as an antimicrobial coating but as discussed in Section 1.2, there are many new developments in antibacterial techniques being applied to medical implants. Testing many of the different techniques and determining their influence on impedance would be necessary to further the validation of using ES as a non-destructive evaluation of antimicrobial performance.

This study also limited the scope to stable conditions to allow for drug measurements. To mimic the *in vivo* conditions of the medical device more accurately, flow conditions would need to be investigated on how it influences polymer degradation and drug release as well as biofilm growth in later experiments.

This experimental work looked at using an unmodified GCE to make drug concentration measurements. A further experimentation would be looked at in using other metals to measure the drug concentrations and see how small of concentrations could be measured using a non-ideal surface. It would also be beneficial to determine if drug concentrations could be detected in more complex media, like blood.

#### **4.7 Summary**

From this study, it can be stated that impedance spectroscopy may be able to non-invasively characterise degradation of polymer-drug coatings on some common medical device metals. The impedances profiles of varying polymer-drug formulations show distinct variations, with the higher PLGA concentrations having overall higher impedances and the lower PLGA concentrations having a similar profile to bare electrodes, with the exception of a decrease in impedance over time as the polymer degrades. The significant differences are seen in both impedance and negative phase angle



in the higher and lower frequency range, with the 50:50 and 60:40 formulations always being significantly different from the control electrode.

Impedance spectroscopy could be a potential method to non-invasively characterise the effectiveness of antibacterial coatings for medical implants in real time. The results show that ES can be used in vitro to characterize different types of polymer-drug coatings and monitor the degradation of the polymer. With further development, this can inform device manufacturers and clinicians about how much polymer may be expected to degrade in vivo and can give more real time data as to how different polymer-drug formulations perform and how much drug is released. As discussed in Section 1.5 (Clinical and research needs) there is a lack of knowledge surrounding the real time performance of antibacterial coatings, therefore more knowledge on how the coatings perform in real time and their effectiveness would be of great benefit in creating new technology and perfecting existing technologies.

The work described has provided a platform upon which to go on to investigate the extent to which the impedance measurements system can be deployed for monitoring bacterial growth on medical device-like surfaces. This forms the basis of the next results chapter.

## **5 Chapter 5 Novel ES System Development**

### **5.1 Introduction**

In the first results chapter, a conventional measurement system was used to investigate if ES could be used as a means of monitoring polymer-drug coating degradation on common medical implant metals. It was shown that impedance variations of 50:50 and 60:40 formulations were significantly different than the control electrode and had a decrease in impedance over time as the polymer degrades and the drug is released. However, the ES system used would not allow for easy assessment of bacterial growth, and also displayed high variability and low repeatability with the wire electrodes. The present chapter details investigations made to address these limitations, leading to the development of a device that used medical device metals as the working electrode, being modified with an antibacterial coating and thereby enabling measurement of biofilm formation on such surface coatings. The next step was to test the effect of the polymer-drug coatings on bacteria. In order to achieve this overall aim, it was necessary to review the electrode configurations used within existing devices reported in the literature before going on to detail how they have been used for measurement of cell and bacterial growth. This provides a framework for identification of opportunities to develop a novel system to address the specific challenges set out in this study.

#### **5.1.1 Electrode Designs**

In Section 1.6, the commercially available EIS and ES systems were discussed in some detail, with reference to their applications within relevant literature. Most of these existing systems have a planar electrode orientation. Most planar electrode orientations do not have

a removable electrode which within this study would make modification of the electrode difficult as well as direct enumeration less accurate. Given this limitation, a series of non-commercial systems have also been investigated within this research. Both are discussed in the following sections, with systems grouped according to the electrode orientation used.

#### **5.1.1.1 Planar**

A planar orientation refers to the electrodes being on the bottom of a culture area. This is a common orientation for commercial impedance systems, used in both bacteria and cell impedance measurements.

A widely used commercially available system is the xCelligence real time cell analyser (RTCA) as discussed in Section 1.6. This microelectrode array uses a 96-well or 16-well plate orientation with the gold microelectrodes on the bottom of the wells and uses a cell index reading, which is the ratio of the impedance at time 0 versus the current measurement, at 10kHz for impedance analysis, shown in Figure 5.1. A number of studies used this system to measure bacterial biofilm formation. Gutierrez *et al* grew *Streptococcus mutans* in the presence of varying glucose and sucrose concentrations over a 24 hour time period (Gutierrez *et al.*, 2016). They found significant bacterial strain differences began in the cell index following an 8-hour incubation period versus controls. They found a larger biofilm production correlated with a larger increase in the cell index with populations above  $10^4$  CFU/ml. They also tested the inhibition of biofilm growth with endolysin LysH5 and found a significant decrease in cell index at the 8-hour time point. This shows that a significant difference in impedance readings can occur within a

24-hour time period, specifically a difference when a biofilm inhibitor is added versus no inhibitor. Van Duuren *et al* also used the xCelligence system to investigate the effectiveness of L-arginine, ciprofloxacin, tobramycin and meropenem on *P. aeruginosa* biofilms over 70 hours and found that the slope of the cell index over time increased as drug concentration increased, which also affected the biofilm growth (van Duuren *et al.*, 2017). The higher the concentration of the drugs the less bacteria, leading to a higher slope in the cell index. A range of drug concentrations would need to be tested in order to determine when drug effectiveness decreased and how it affected bacterial growth as well as impedance measurements.

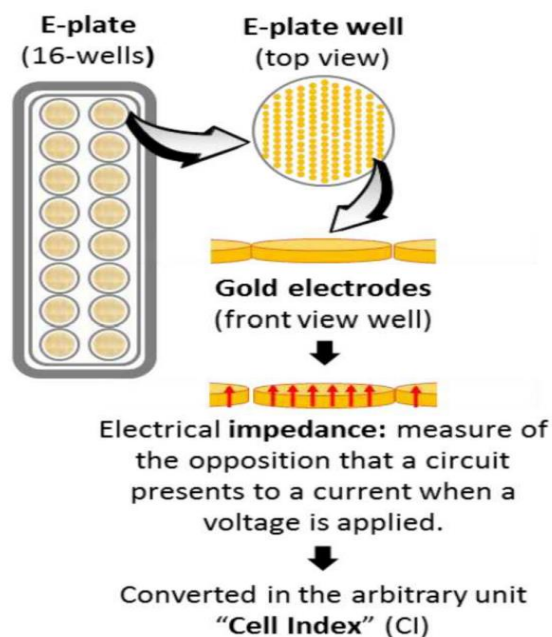


**Figure 5.1** Schematic of xCelligence RTCA system from Gutierrez *et al* (Gutierrez *et al.*, 2016). E-plates (16-wells) where bacteria are cultured in a planar system with view of individual well gold electrode orientation.

Ward *et al* created a novel impedance-based biosensor with carbon ink to create a low cost, point of care, disposable sensor (Ward *et al.*, 2018). It was shown to detect *P. aeruginosa* in nutrient broth, with some noted differences when bacteria formed a pellicle, a floating biofilm, at the surface air contact versus attaching to the electrode. The formation of this pellicle on the surface may increase the solution resistance and could influence the impedance readings. This would need to be considered when taking impedance readings and analysing results, either through separate tests of potential pellicle formation or ensuring pellicle was fully removed at some point in the experimental process.

Holland *et al* used electroplated gold electrodes to measure different vascular cell lines in culture. It was reported that the impedance characteristics were cell-type dependent with endothelial cells, HUVECs and smooth muscle cells displaying distinct reactance profiles. The ES system used by Holland *et al* is very easy to reproduce, low cost and can be used with a range of electrode materials (Holland *et al.*, 2018). This system also used a relatively wide frequency range (1-100 kHz) versus the xCelligence system that only uses 10 kHz, thereby potentially missing important frequency dependent information. Therefore, Hollands planar electrode orientation with gold electrodes was taken forward in this study as the known system with common electrode materials.

#### **5.1.1.2 Vertical**

Another common orientation, more often used in novel devices such as Lee *et al*'s matrix of vertical electrodes (Figure 5.2 (a)), Pan *et al*'s single channel 3D sensor unit (Figure 5.2 (b)), and De Agua *et al*'s poly (3,4-ethylenedioxythiophene) xanthan gum

electroactive scaffold (Figure 5.2 (c)), is the vertical orientation. This refers to the electrodes being vertical and placed within the culture media surrounded by bacteria culture. This was more common in 3D cell measurement systems, for spatial readings.

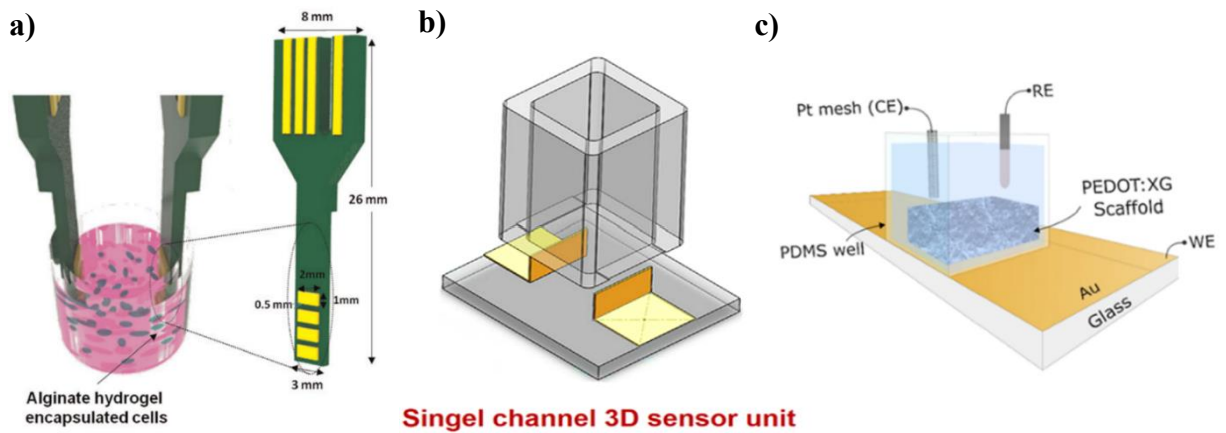


**Figure 5.2** Schematic for **a)** Lee *et al*'s matrix of vertical electrodes used on alginate hydrogel with cells, **b)** Pan *et al*'s single channel 3D sensor unit, and **c)** De Agua *et al*'s PEDOT sensor. (Lee *et al.*, 2016, Pan *et al.*, 2019, Xu *et al.*, 2016, del Agua *et al.*, 2018)

Paredes performed an experiment comparing different experimental setups for ES specifically in regard to culture area and flow (Paredes *et al.*, 2014b). The different setups investigated were a 96-well microtiter plate, petri dish, modified CDC biofilm reactor and *ad hoc* lab tester simulating central venous port performance (Figure 5.3). All the experimental set-ups had a vertical orientation, except for the lab tester that had planar microelectrodes. Of the apparatus investigated, the 96-well plate displayed the smallest relative variation in resistance in response to *Staphylococcus epidermidis* bacterial growth versus time 0 at 15% variation at 10 Hz, with the petri dish coming at 40% variation of resistance. The biofilm reactor had the largest variation with 60% capacitance change and

the lab tester having similar 50% capacitance variation. This showed the biofilm reactor and lab tester are ideal candidates for biofilm measurements, the 40% relative change of the petri dish highlights a larger culture volume of ~50 ml is better than a smaller culture volume of 300µl for this particular measurement system and that vertical orientations can still grow bacteria and see a change in resistive features indicating biofilm growth.

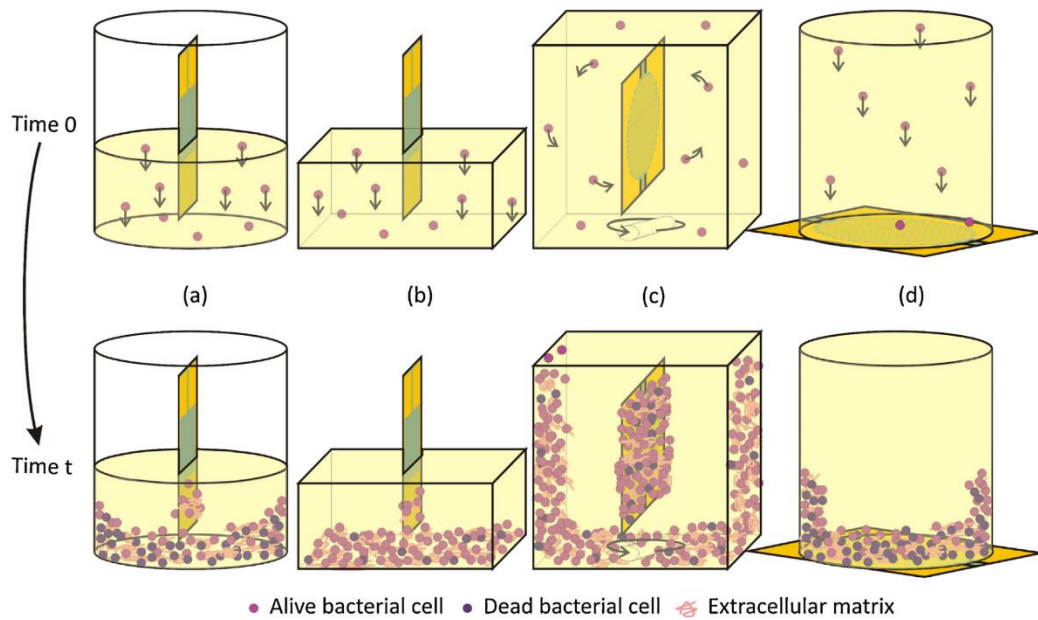


**Figure 5.3** Schematic of Paredes *et al* comparison set-up for biosensors (Paredes *et al.*, 2014a). **a)** 96-well microtiter plate, **b)** petri dish, **c)** modified CDC biofilm reactor, and **d)** lab-tester device. Time *t* represents the time at which biofilm has reached a mature stage.

Vertical electrodes have also been used for 3D impedance measurements of mammalian cells. 2D cultured EIS measurements typically have cells attaching to planar electrodes. In contrast, within 3D cultures, cells are incorporated and cultured within a scaffold structure, typically made from biopolymers (De León *et al.*, 2020). De Leon *et al* evaluated several different 3D monitoring systems, mostly through the use of vertical

electrodes three of which are displayed in Figure 5.2. They found that while such configurations can monitor cell proliferation, every device was highly customized for specific application and standardization was not easily obtained. The systems also had low resolution, only giving qualitative information at a tissue level as opposed to a cellular level. This is due to little characterisation of the effects of matrix composition like hydrogels have on cell structure and function as well as effect on impedance response. More work is needed on this characterisation before 3D impedance measurements can be taken forward and placed in more complex experiments.

#### **5.1.1.3 Non-contact**

In the above studies, the electrodes were in direct contact with the cells or the cell-scaffold interface. In this section, alternative configurations are explored in which there is no direct contact between the electrodes and the cells or substrate which could allow for measurements of surfaces without a need to contact the surface or possibly disrupt the biofilm. Such systems generally consist of an electrode that is suspended above the growing cell culture or biofilm without direct contact.

Turick *et al* 2020 used a flat patterned graphite electrode across from a glass slide supported by an aluminium coupon (Figure 5.4) and showed that the greater the bacteria density the more pronounced the EIS response, specifically an increase in  $|Z|$  with increase in bacteria biomass and increase in  $\sigma''$  which represents imaginary conductivity. This technique allowed for no disruption to measure the biofilm, indicating that bacterial attachment to the electrode is not always necessary for measurement of biofilm formation (Turick *et al.*, 2020).



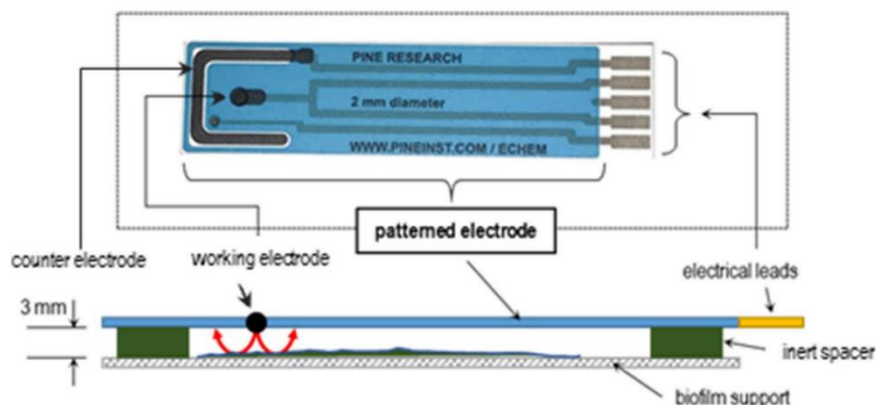


**Figure 5.4** Schematic of Turick *et al* patterned electrode used for non-contact measurements. (Turick *et al.*, 2020)

### 5.1.2 Bacteria ES analysis methods

ES data can be interpreted in various ways depending on the application being investigated. The electrode type can change magnitude of impedance and variability within measurements based on the metal properties. Similarly, the orientation of the electrodes can impact upon the measurements obtained depending on how bacteria attaches and how measurements are obtained as the resistive and capacitive features will change depending on if the bacteria is on the electrodes and how they cover the electrode.

As discussed in previous sections on impedance data analysis (Sections 2.1 and 4.2.1) a common method of analysis includes equivalent circuit modelling. Such approaches for modelling bacterial growth can rapidly become quite complex, with many assumptions having to be made to create a circuit. A study by Ben-Yoav *et al* used equivalent circuits

to model *E. coli* attachment to indium-tin-oxide electrodes. They then tracked the capacitance and resistance together assuming a solution resistance, biomaterial capacitance, biomaterial resistance, charge transfer resistance, and constant phase element for the solution-electrode interface as well as a linear diffusion boundary (Ben-Yoav *et al.*, 2011). While the resistance and capacitance they calculated could be associated with each of these elements, there could be other factors that influence those parameters that they did not consider like the potential of pellicle as mentioned by Ward *et al* (Ward *et al.*, 2018). But as mentioned, circuit equivalence makes assumptions and change based on orientation as one orientation may have cell or bacterial contact with the electrode and need a double layer capacitance value while another orientation may have no contact and need to exclude this element in a circuit. A common method used to address such potential complexities, is to use normalisation procedures when analysing the measurement data collected.

Normalising impedance and phase can highlight trends shown in impedance data. Many researchers have used this method to monitor biofilm growth. Ward *et al* used the normalisation of selected variables to track biofilm growth of *P. aeruginosa* in a co-culture with *S. aureus*. They focused on peaks occurring at certain frequencies to characterise biofilm growth at around 100 Hz. They found that addition of phenazine pigment pyocyanin, pigment used to colour *P. aeruginosa*, into bacterial culture yields distinct changes in phase depending on concentration at 100Hz (Ward *et al.*, 2014). Pennington and Van de Walle also used this method to study changes in Crandall-Rees Feline Kidney cells infected with felid herpesvirus type 1. Higher frequencies from 10 kHz to 1 MHz are

generally used in cell analysis, this is shown by their analysis of cells at 16 kHz (Pennington and Van de Walle, 2017). Paredes *et al* also investigated relative variation of impedance across 10 Hz, 100 Hz, 1 kHz, and 10 kHz (Paredes *et al.*, 2014a). They found that 10 Hz and 100 Hz showed the most variation over the 24 hour incubation period, especially in the CDC reactor and Lab tester.

Other studies have focused on a particular impedance when analysing results. Liu *et al* found the largest changes in impedance at 1-2 Hz when measuring *Salmonella* and *E. coli* while also evaluating the total impedance and comparing to an equivalent circuit (Liu *et al.*, 2018). Each of these methods allows certain changes to be highlighted depending on bacteria and cell type. The normalisation allows electrode to electrode variation to be controlled for, thereby minimising variability in the datasets generated.

## 5.2 Chapter Aims and Objectives

As described in Section 1.8, the overall aim of this chapter was to:

- design and develop an *in vitro* test system using medical device metals as electrodes that can non-invasively characterize biofilm formation

The specific objectives for the experiments used to address this aim in Chapter 5 are detailed below:

- Investigate the impedance characteristic of a Gram positive and Gram negative bacterial growth on planar gold electrode surfaces
- Develop methods to non-invasively characterise *in vitro* biofilm growth on electrodes

- Establish design criteria and critically evaluate the performance of the methods to help inform the development of an advanced test system
- Design and validate the advanced *in vitro* test system against design criteria

## 5.3 Methods

### 5.3.1 General Materials

Material	Company	Location
Lab-Tek chamber slides	Nunc	USA
Silver conductive paste	Electrolube	Leicestershire, UK
SYLGARD 184 silicone elastomer kid (PDMS)	Dow Europe	Germany
Staphylococcus aureus NCTC 4135	NCTC: National Collection of Type Cultures	Colindale, UK
<i>P. aeruginosa</i> NCTC 9009	NCTC: National Collection of Type Cultures	Colindale, UK
Nutrient/tryptone soya agar and nutrient/ tryptone soya broth	Oxoid	UK
Acetic Acid		UK
BRAND 6-well Cell Culture Insert, PC-membrane	Sigma-Aldrich	UK
Lab-Tek chamber slides	Nunc	USA
Stainless steel (SS) (304L, annealed, 0.25mm thickness)	Goodfellow	Cambridge, UK
titanium/aluminium/vanadium (Ti90) (Ti90/Al6/V4) foil	Goodfellow	Cambridge, UK

### 5.3.2 General Equipment

Equipment	Company	Location
AGAR Auto Sputter Coater	Agar Scientific	Essex
Daro UV systems	Sudbury	Suffolk

### 5.3.3 Device 1 Design Fabrication

These initial bacteria experiments focused on ideal electrodes, gold, as a reference for later experiments. Gold electrodes were sputter coated through a laser cut mask at 40 mA at 0.03 mb Argon for a thickness of 144 nm onto 35 mm diameter petri dish surfaces that had a counter electrode (100 mm<sup>2</sup>) and 4 smaller working electrodes (7 mm<sup>2</sup> each) (Holland *et al.*, 2018). A 4.2 cm<sup>2</sup> culture cube (Lab-Tek chamber slide, Nunc, USA) was then sealed onto the cell culture area using Polydimethylsiloxane (PDMS). Thin copper wires were attached to each electrode on the outside of the culture tube using silver conductive paste.

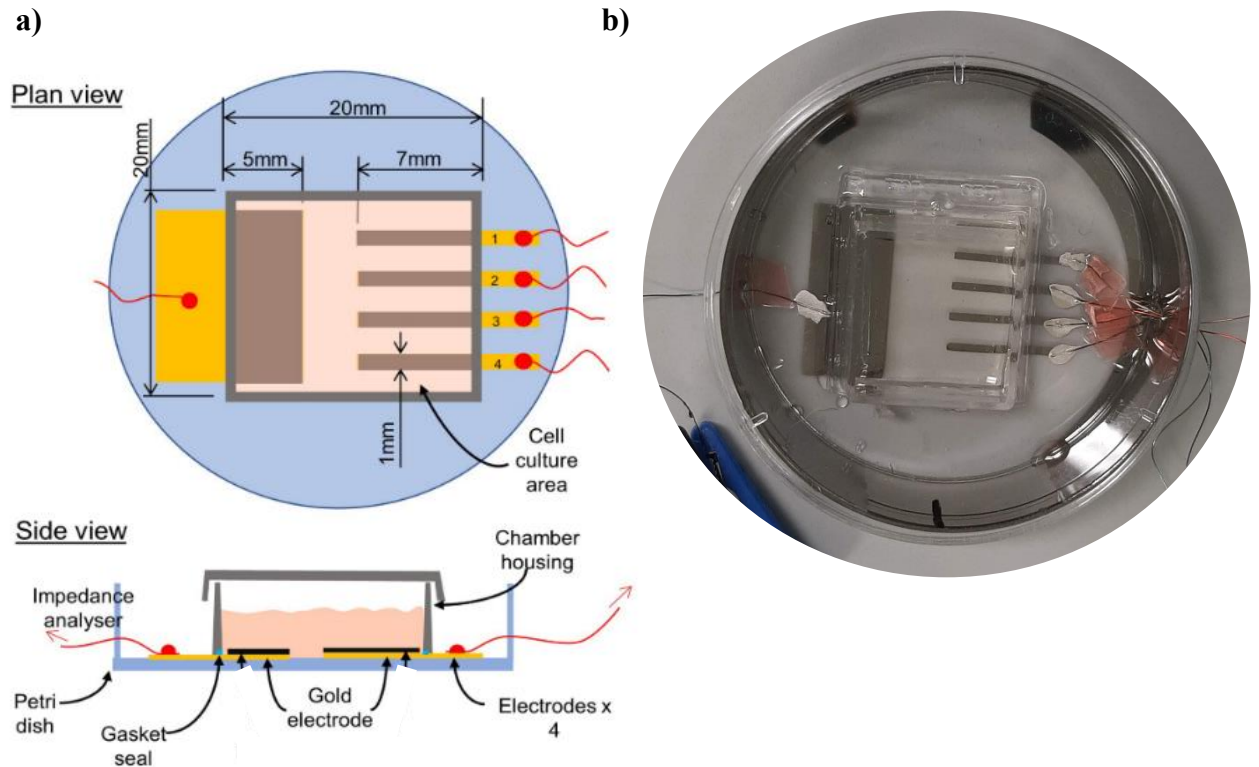


**Figure 5.5 a)** Schematic of Holland's design (Holland *et al.*, 2018). Initially used for experiments on ideal, gold, surface. Plan view shows the counter electrode on left and

*working electrodes on right with detailed measurements. The grey box and shaded area represent the culture area. b) Picture of Hollands design used within this study*

The electrodes were sterilized by UV light at 28 watts for 15 minutes prior to use in bacteria culture experiments.

### **5.3.4 Bacteria test device design 1**

#### **5.3.4.1 Bacteria Preparation**

The bacteria used for this experiment were *Staphylococcus aureus* NCTC 4135 and *Pseudomonas aeruginosa* NCTC 9009. Bacteria were cultured in 50ml nutrient broth and incubated at 37°C for 18-24 hours under rotary conditions (120 rpm). Cultures were then centrifuged at 4300 rpm for 10 minutes, and the supernatant removed and the bacterial cell pellets were re-suspended and serially diluted (1:10) in sterile PBS, to the required cell density of 10<sup>5</sup> CFU/ml for experimental use, with this final dilution being into nutrient broth.

#### **5.3.4.2 ES of Biofilm**

##### **5.3.4.2.1 Measurement of nutrient broth alone**

New sterile testing chambers were filled with 3ml of sterile nutrient broth without bacteria. ES measurements taken at time 0 then placed into incubator at 37°C. ES measurements were then performed at incubation hours 1, 3, 6, and 24 hours on sterile nutrient broth. Parameters of interest were normalised based on the equation below (Ward et al., 2014, Lind et al., 1991).

$$IPN_{t=n} = \frac{IPA_{t=n}}{IPA_{t=0}}$$

The  $IPN_{t=n}$  is the normalised impedance parameter of interest, while  $IPA_{t=n}$  is the measured impedance parameter. With data presented as mean with standard error. This data analysis and presentation was used on all following ES experiments.

#### 5.3.4.2.2 *Measurement of biofilm formation*

New sterile testing chamber were filled with 3ml of sterile nutrient broth without bacteria and ES measurements performed. Nutrient broth was removed and replaced with 3ml of  $10^5$  of either *S. aureus* or *P. aeruginosa*. ES measurements were taken immediately after addition of bacterial suspension. The chambers were placed into 37°C incubator and then ES measurements were taken at incubation hours 1, 3, 6, and 24.

At 24 hours, bacterial suspension was removed and electrodes were washed with 1 ml of sterile PBS to remove any bacterial cells not attached to electrodes. 3 ml of new sterile broth was added to the chambers, then one final ES measurement was taken with new sterile broth to determine what impedance measurement represented attached bacteria. The results were plotted as average impedance and normalised impedance with standard error.

#### 5.3.4.2.3 *Measurement of bacteria byproducts*

It was of interest to determine if anything produced by the bacteria cells would affect the ES. The supernatant of both *S. aureus* and *P. aeruginosa* was saved from the process described in Section 5.3.4.1 Bacteria Preparation above. New sterile testing chambers were filled with 3 ml of sterile nutrient broth without bacteria and ES measurements were taken immediately. Nutrient broth was removed and 3ml of supernatant of either *S. aureus*

or *P. aeruginosa* was placed into a testing chamber and an ES measurement of the supernatant was taken immediately.

#### 5.3.4.2.4 Evaluation of Biofilm

Crystal violet staining was used as a quick visual indicator of bacterial growth on chambers in initial bacterial experiments.

For biofilm staining, 400µl 0.1% crystal violet solution was added to each chamber after final incubation ES measurements were performed and all broth removed. After 15 minutes, all excess crystal violet was removed by running chambers under running tap water and allowed 15 minutes to air dry. Bound crystal violet was released by adding 500 µl of 30% acetic acid solution which was then manually agitated every 3-5 minutes for 10 minutes. All steps were carried out at room temperature (Peeters *et al.*, 2008), (Shao *et al.*, 2019). Data was shown as pictures to visually indicate bacterial growth.

As crystal violet confirmed bacterial growth in initial experiments, direct enumeration was used in further experiments to determine exact bacterial counts. After ES measurements, biofilm was recovered from chamber using a PBS moistened sterile cotton-tipped swab. The swab was rolled over all electrodes 15 times while turning and kept consistent between each testing chamber.

The swab was then submerged in 4.5 ml PBS (with 500 µl 3%Tween) and vortexed for 1 minute to resuspend the bacteria from the swab into the suspension. This suspension was then serially diluted (down to  $10^{-4}$ ) and 100 µl volumes spread in triplicate onto agar plates. The agar plates were then incubated for 24 hours at 37°C and the colony-forming units



(CFU) were then enumerated (McKenzie *et al.*, 2013). The average bacterial count was found, then used to calculate CFU/chamber given the equation below.

$$\frac{CFU}{chamber} = AVG \text{ bacterial count}(per\ 100\mu l) \times \frac{10\mu l}{mL} \times dilution\ factor$$

Data presented as CFU/chamber with standard error.

## 5.4 Bacteria Results from Chamber 1

### 5.4.1 Bacteria ES chamber 1

These initial bacteria experiments focused on the use of a previously developed electrode configuration (Holland *et al.*, 2018), with planar gold electrodes. This provides a reference for comparison to later experiments performed on bespoke electrode chambers developed as part of the current study. Impedance measurements were performed on nutrient broth alone. In Figure 5.6 (a), it can be seen that normalised impedance (Z) of nutrient broth did not change significantly over the 24 hours, with  $p > 0.05$ . There appears to be a slight peak at 10 Hz after 24 hours in the normalised impedance data.

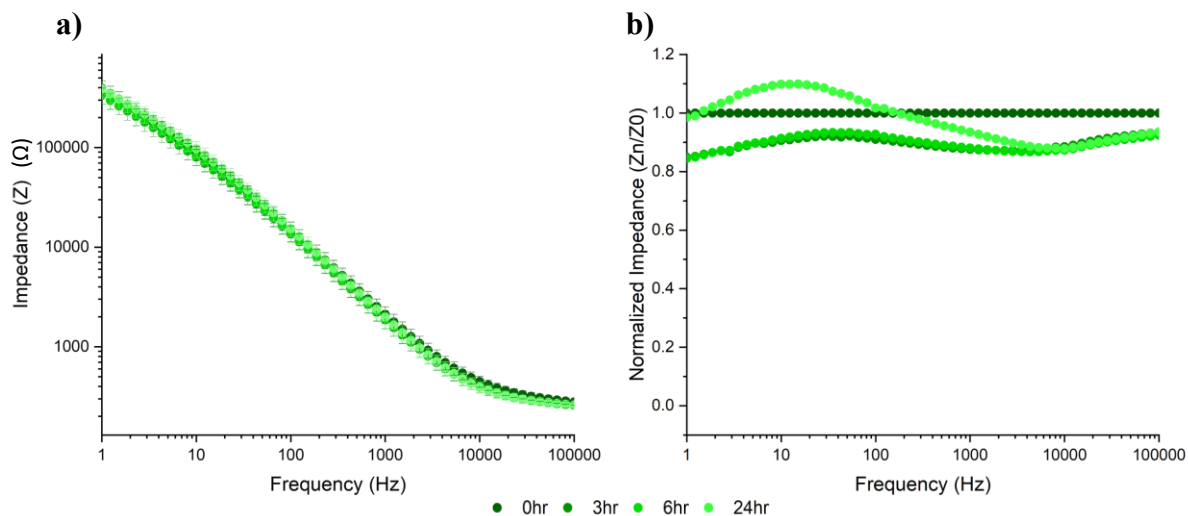


**Figure 5.6 a)** Temporal impedance profile of Nutrient broth at 0-, 3-, 6- and 24-hours incubation hours on gold electrodes. **b)** The normalised impedance of nutrient broth to time 0. Data represent the mean of data collected from three chambers, with each chamber having four replicate electrodes ( $n=3$  chambers, 12 electrodes). Error bars removed for normalised impedance for clarity of graph.

Impedance measurements were taken using a Gram- positive, *S. aureus*, and Gram-negative, *P. aeruginosa*, bacterial species to compare. The impedance appeared to decrease over the 24-hour bacteria growth for both *S. aureus* and *P. aeruginosa* as seen in Figure 5.7 (a) and (b). The impedance spectra had a linear decrease in impedance from 1 to 1000Hz that then plateaus across the higher frequencies 10,000 to 100,000Hz. The greatest change in impedance for the bacterial growth can be seen at the lower frequencies, specifically within the 1 to 100 Hz range. *S. aureus* has an overall higher starting impedance of 200,000 Ω that drops to 20,000 Ω after bacteria growth (1Hz). *P. aeruginosa* starts at a lower impedance of 60,000 Ω and drops to 20,000 Ω (1Hz). *P. aeruginosa* also

appears to have slightly more standard error at the 24-hour period (Figure 5.7 (b)), indicated by the larger error bars. The normalised impedance ( $Z$ ) was also plotted (Figure 5.7 (c) and (d)), with comparisons between broth with no bacteria incubated over 24 hours as a negative control to *S. aureus* and *P. aeruginosa*. The normalised data for both bacteria have steady normalised impedance with little change in the first 6 hours, while the 24 hour starts lower for the first 100 Hz, then has a linearly increasing slope up to the original impedance by 100,000 Hz. *S. aureus* normalised impedance changes from 0.8 to almost 0 in the first 100 Hz, while *P. aeruginosa* impedance decreases from 0.8 to 0.3 in the first 100 Hz, with peaks occurring at 10 Hz and 100 Hz for both bacteria types indicated by the dark blue vertical lines (Figure 5.7 (c) and (d)). Both the *S. aureus* and *P. aeruginosa* experienced a slight overall increase in impedance when the broth was replaced at 24 hours, and the new bacteria free broth was measured. The nutrient broth is seen to decrease initially from 1 to 0.9 before increasing slightly to 1.1 over the 24 hours at around 10 Hz.

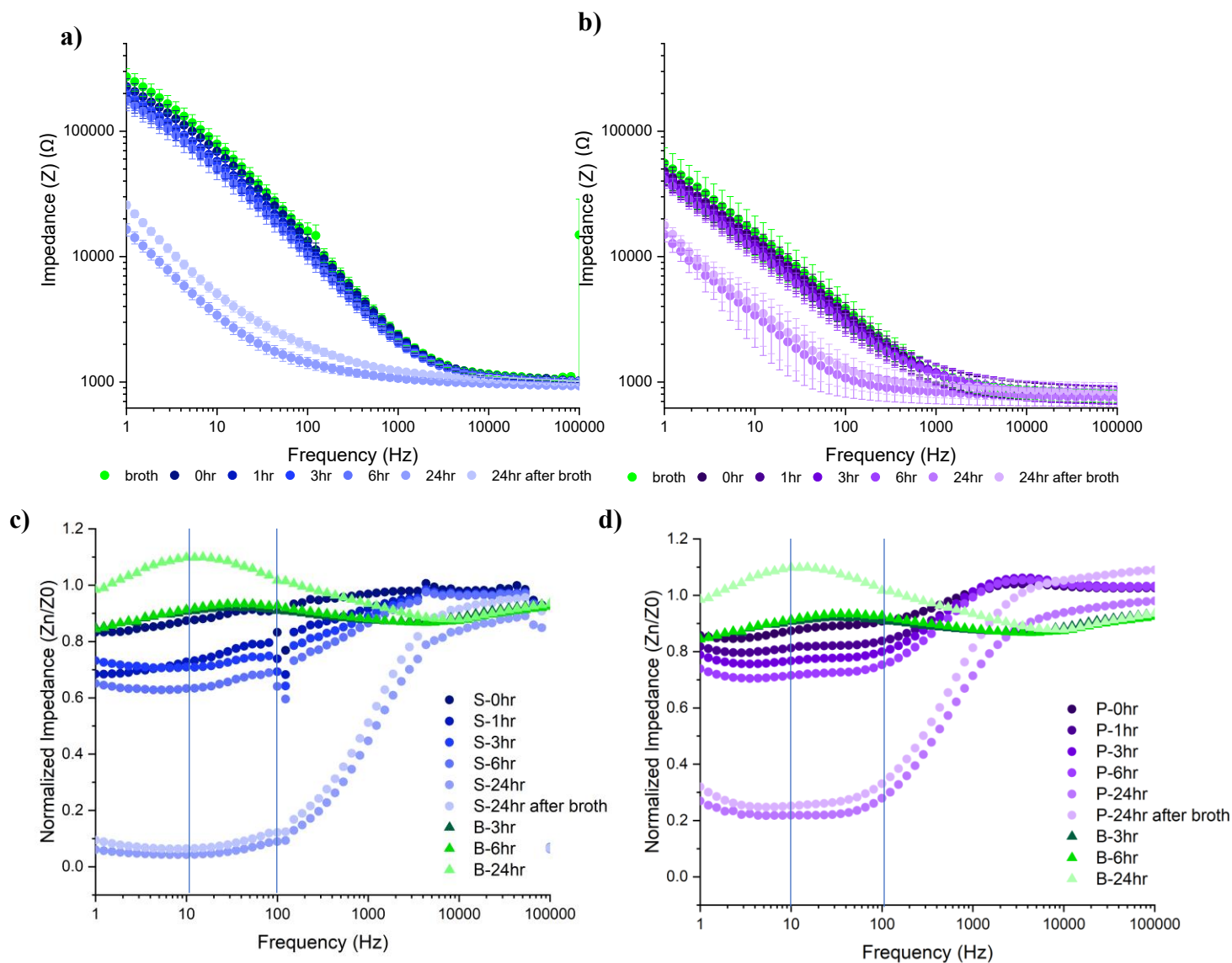


**Figure 5.7** Temporal impedance profiles of **a)** *S. aureus*(S) and **b)** *P. aeruginosa*(P) compared to nutrient broth (B) on gold electrodes with ES measurements taken with sterile nutrient broth then at  $10^5$  starting population with ES measurements taken at 0, 1-, 3-, 6-, and 24-hour incubation and one last measurement taken after switching the nutrient broth at 24 hours with fresh broth. **c)** The normalised to broth impedance *S. aureus* and **d)** *P. aeruginosa* compared to nutrient broth measurements over 24 hours

*versus the time 0 time point. Lines indicate frequencies of interest based on Ward et al procedure that are further analysed in Figures 5.5 (Ward et al., 2018). Error bars removed from (c) and (d) to ensure clarity..*

The normalised phase measurements in Figure 5.8 (c) and (d) displays the opposite trend to the normalised impedance, with the higher frequencies 100 to 100 kHz displaying the greatest decreases in phase. The first 6-hour time measurements had a stable phase until 1000 Hz then decreased linearly till 100,000 Hz. The 24-hour time measurement had a linear decrease in phase across the whole impedance spectra. The normalised phase angle had horizontal lines for the first 6 hours, then at 24 hours had a linearly decreasing phase from 1 to 1000 Hz before plateauing. Both the phase and impedance decrease down to approximately 0.2 for the normalised values of the bacteria growth, the difference being the frequency at which the phase angle peaks. The phase angle had peaks at 1 Hz and 1000 Hz indicated by the dark blue vertical lines (Figures 5.8 (c) and (d)). The broth measurements stay around 1, indicating little to no change in the phase angle, with no peaks occurring.

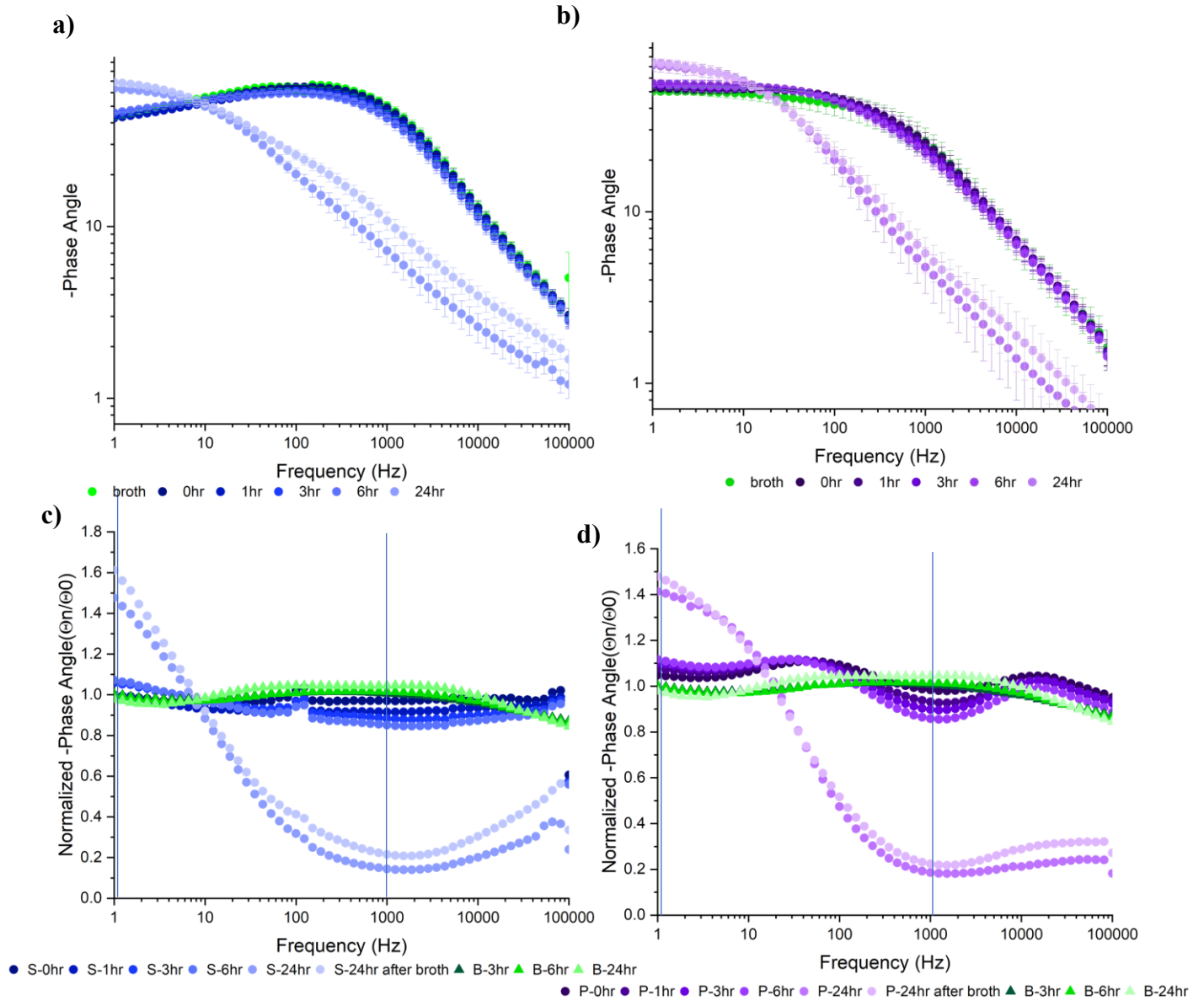


**Figure 5.8** Temporal phase angle profiles of **a)** *S. aureus*(S) and **b)** *P. aeruginosa*(P) on gold electrodes with ES measurements taken with sterile nutrient broth then at  $10^5$  starting population with ES measurements taken at 0, 1-, 3-, 6-, and 24-hour incubation and one last measurement taken after switching the nutrient broth at 24 hours with fresh broth. ( $n=3$  chambers, 12 electrodes). The normalised phase angle of the initial broth measurement **c)** *S. aureus* and **d)** *P. aeruginosa* compared to normalised nutrient broth

measurements over 24 hours versus the time 0 time point. Lines indicate frequencies of interest based on Ward *et al* procedure that are further analysed in Figures 5.5 (Ward *et al.*, 2018). *P* indicates *P. aeruginosa*, *S* indicates *S. aureus*, and *B* indicates nutrient broth.

The chosen frequencies indicated by the lines from Figures 5.7 and 5.8 were plotted in Figure 5.9 with ANOVA analysis performed between time 0 and subsequent time points. The frequencies were chosen based on the Ward *et al* procedure in finding peaks in the frequency sweep (Ward *et al.*, 2014), with impedance frequencies chosen at 10 Hz and 100 Hz and phase angle frequencies chosen at 1 Hz and 1000 Hz. All frequencies show a decrease in the normalised value for both *S. aureus* and *P. aeruginosa* when compared to broth. *S. aureus* impedance at 10 Hz and 100 Hz decreased from 0.9 to 0.1, while *P. aeruginosa* decreased from 0.9 to 0.3. Only *S. aureus* had a significant difference (\*) in impedance after 24 hours per one way ANOVA analysis, but *P. aeruginosa* did have a noticeable difference just not statistically significant. The phase angle at 1 Hz and 1000 Hz (Figure 5.9 (c) and (d)) showed a significant difference at the 24-hour time point for both bacteria (\*). At 1Hz the phase for *S. aureus* dropped from 0.6 to 0.2, while *P. aeruginosa* dropped from 0.9 to 0.2. At 1000 Hz both bacteria phases dropped from 1 to 0.2. The broth remained close to 1 for all chosen frequencies with no significant differences at any time points.

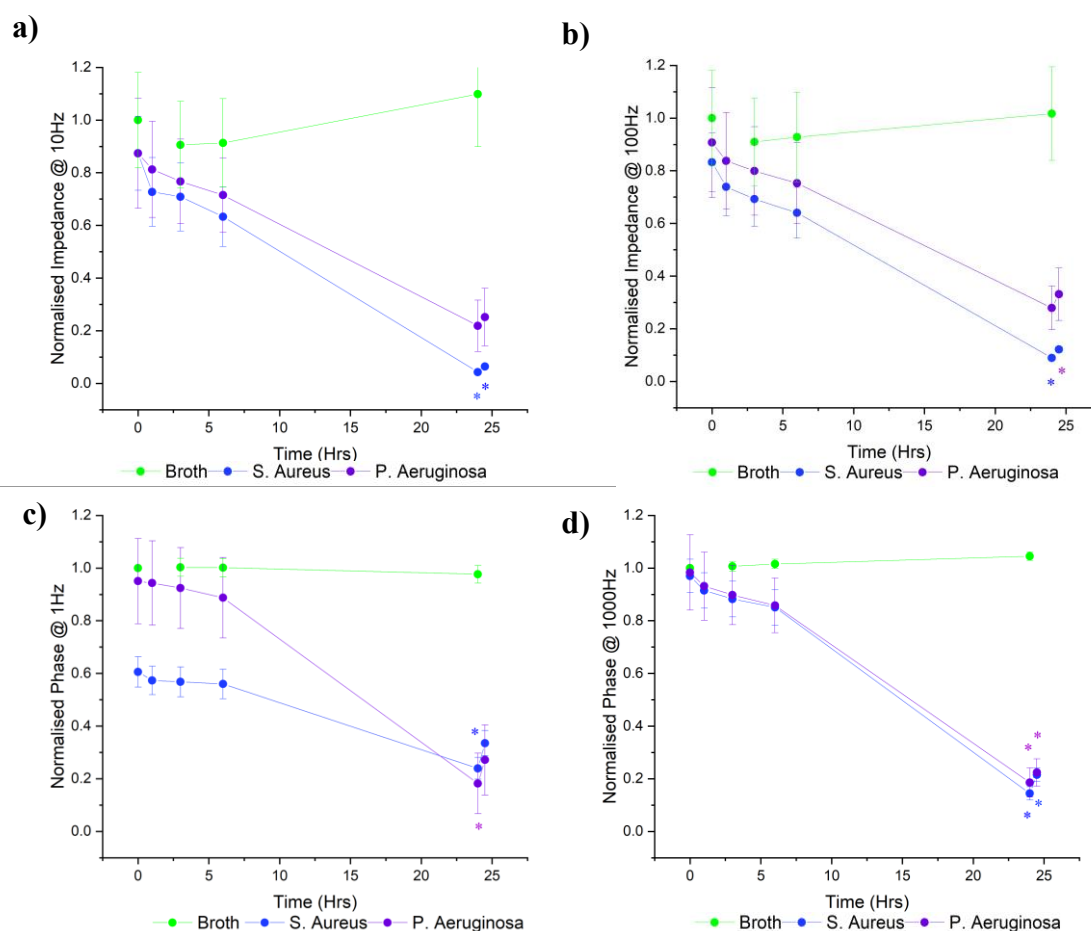


**Figure 5.9** Impedance of nutrient broth versus *S. aureus* and *P. aeruginosa* normalised to nutrient broth measurements at **a)** 10 Hz **b)** and 100Hz. Phase normalised to nutrient broth for both bacteria at **c)** 1 Hz and **d)** 1000 Hz on gold electrodes ( $n=3$  chambers, 12 electrodes). Significance was determined by ANOVA analysis, with Bonferroni post hoc between time 0 and subsequent time points (Shown by \* *Staph*, \* *Pseudomonas*)

The supernatant was investigated to determine if any by-products of the bacteria would influence the impedance measurements. Figure 5.10 indicates the supernatants have little influence on the overall impedance, with only a small decrease in impedance over the middle frequencies from 10 Hz to 10 kHz, with peaks occurring at 20 Hz and 100 Hz



plotted in Figure 5.10 (b). The impedance did not drop below a 0.7 for any normalised value unlike the bacteria growth seen in Figure 5.7 that dropped to around 0.2. This influence was mitigated through a separate measurement being taken after 24 hours growth with a replacement to sterile nutrient broth without bacteria.

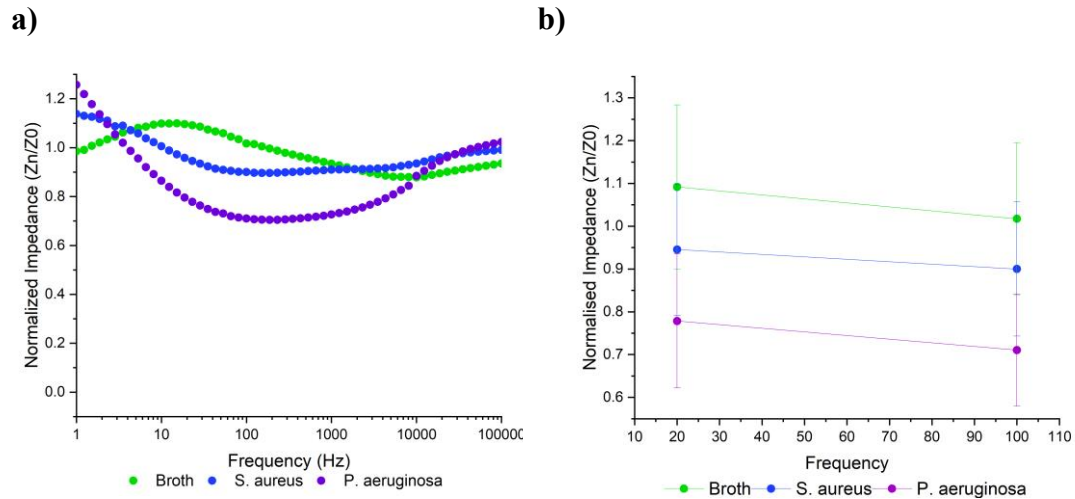


**Figure 5.10 a)** Normalised impedance spectra of Nutrient Broth over 24 hours, compared to supernatants of *S. aureus* and *P. aeruginosa* immediately after culture. Error bars removed for clarity, full graph in appendix. **b)** Normalised impedance at 20 Hz and 100 Hz of Nutrient broth after 24 hours, compared to *S. aureus* and *P. aeruginosa* immediately after culture. Significance was determined by ANOVA analysis, with Tukey post hoc performed ( $P > 0.05$ ). There were no significant differences found within this data. Data represent the mean of data collected from three chambers, with each chamber having four replicate electrodes ( $n = 3$  chambers, 12 electrodes).

#### 5.4.2 Biofilm Evaluation on device design 1

There were two different methods explored to determine biofilm formation on the electrodes: crystal violet staining and direct enumeration. Crystal violet staining was used as a quick visual indicator to determine if there was biofilm formation within the

chambers. Results from the crystal violet staining show a marked colouring of the bacteria in the incubation well (Figure 5.11) indicative of the presence of bacteria.

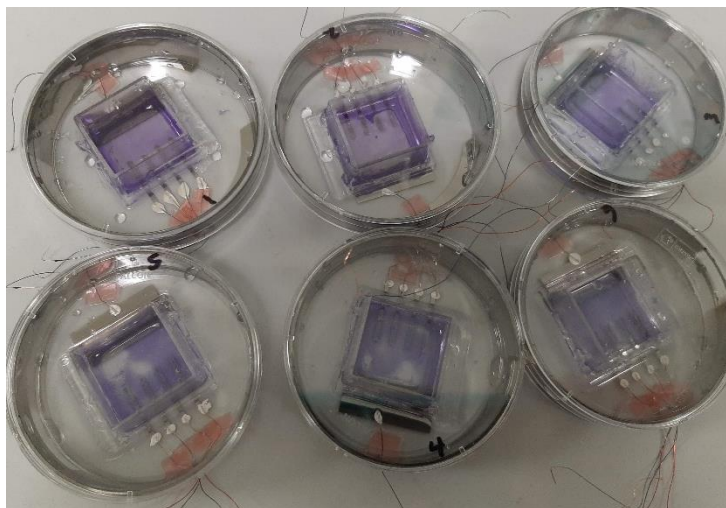


**Figure 5.11** Crystal violet-stained electrodes after 24-hour incubation period of (top row) *S. aureus* and (bottom row) *P. aeruginosa*. ( $n=3$ )

In order to provide a quantitative measure of bacterial growth, direct enumeration was employed. This involved physically swabbing the electrodes to collect the biofilm at the end of the experiment (as detailed in Section 5.3.4.3 Evaluation of Biofilm). A suspension of  $10^5$  CFU/ml of bacteria was introduced in the chambers and over a 24-hour incubation period bacterial cells attached and replicated to form biofilms. It can be seen that *S. aureus* formed a  $1.25 \times 10^7$  biofilm while *P. aeruginosa* formed a  $2.7 \times 10^7$  biofilm (Figure 5.12), with both measurements made after a 24-hour incubation period. These counts are not significantly different from each other, but it indicates that there was bacteria growth on the electrodes.

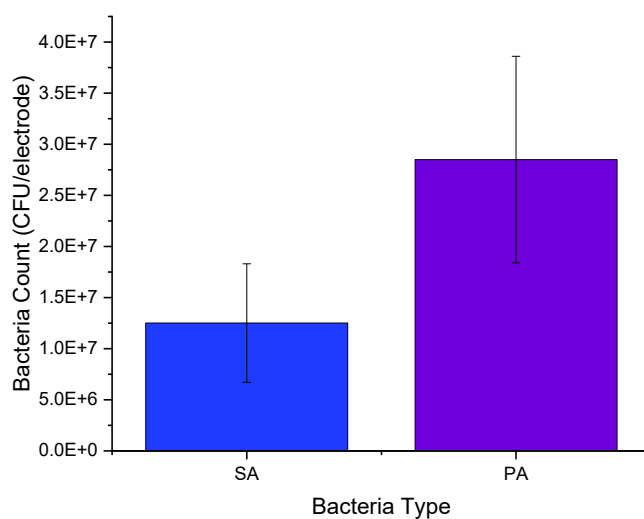


**Figure 5.12** *S. aureus* and *P. aeruginosa* biofilm formation on the electrodes after 24-hr incubation at 37°C. Bacterial suspensions of  $10^5$  CFU/ml were used to inoculate the well at time 0 ( $n = 3 \pm \text{SEM}$ ) with one way ANOVA with Tukey post hoc performed ( $P > 0.05$ )

## 5.5 Discussion

Each section will address the Chapter 5 aims and how it leads into the next section's purpose.

### 5.5.1 Electrical impedance spectroscopy on electrode design 1

Bacteria experiments were performed on ideal gold electrodes to determine factors that influenced impedance changes and to determine best analysis method for determining bacterial growth. The initial experiment was a negative control performed with broth without bacteria. Figure 5.6 shows that the broth did not change over the 24 hours incubation period, indicating the broth has little influence over impedance and phase changes and can be used as the normalisation measurement.

Two bacteria were tested in this system, *S. aureus* as a Gram-positive and *P. aeruginosa* as a Gram-negative. Both bacterial species have been associated with medical implant associated infections (Arciola *et al.*, 2018). The impedance decreased significantly for each bacteria, specifically in the lower frequency range 1 to 100 Hz which aligns with Paredes (Paredes *et al.*, 2014). This decrease is most likely attributed the change in the double layer capacitance (Cady *et al.*, 1978). Cady *et al* also proposed that the metabolic processes of the bacteria may change the conductance of the medium and influence the impedance. Paredes *et al* investigated temporal changes in impedance for *S. epidermidis* growth in many planar and vertical electrode orientations using gold and found that 10 and 100 Hz saw the most change for every electrode orientation, that also allowed for more sensitive measurements without too much noise. Ward *et al* also found the normalised resistance in the lower frequencies 1 to 1000 Hz show a decrease in resistance and normalised phase in higher frequencies from 1000 to 10,000 Hz had a decrease in phase after growing *S. aureus* on Polyethylene Terephthalate substrate cured with carbon ink electrodes(Ward *et al.*, 2014). In the present study, there was a slight decrease in impedance in the first 6 hours indicating attachment of some of the planktonic bacteria from the suspending media onto the electrodes over this period (Figure 5.7), then there is a significant drop in impedance as more bacteria attach and multiply ending in a final biofilm of  $1.25 \times 10^7$  CFU/chamber for *S. aureus* and  $2.7 \times 10^7$  CFU/chamber for *P. aeruginosa* shown in Figure 5.13. The larger decrease could be the increased presence of metabolites from more bacteria and the larger interaction between the bacteria and surface, effecting the double layer capacitance more. Yang *et al* discussed how the double-layer capacitance was influenced by the changes at the electrode interface and the absorption at

the surface of the electrode which corresponded to a larger decrease in impedance. The 10Hz and 100Hz were indicated as frequencies of interest as there was slight peaks for the broth at 10Hz and the bacteria at 100 Hz, dark blue lines on Figure 5.7(c) and (d). The peaks from this study were slightly different from Ward *et al*'s study on *P. aeruginosa* and *S. aureus* on carbon electrodes, as they found peaks at 125 Hz at 24 hours and 400 Hz at later time points. The use of one chosen frequency for analysis was used in multiple studies and in the xCelligence commercial system. The problem with pre-selecting a frequency for analysis means missing potentially relevant changes hence why a whole frequency sweep was necessary in the beginning to determine the relevant frequency to be analysed (Ward *et al.*, 2018, Paredes *et al.*, 2014a).

The normalised phase angle also showed a decrease in measurements but focused more on the higher frequency range 1000 to 100,000 Hz. These results show that normalisation of an ES parameter can give insights into biofilm formation, especially on an ideal electrode surface. The 1 Hz and 1000 Hz were highlighted in the phase because of the peaks in Figure 5.8 (c) and (d).

The chosen normalised frequencies had statistical analysis performed. The peaks were chosen just as Ward *et al* chose their frequencies, finding a peak in the data (Ward *et al.*, 2018). Both *S. aureus* and *P. aeruginosa* had statistically significant differences in normalised parameters from time 0 to time 24 hours (\* in Figure 5.9). The normalised impedance and phase did not decrease at a linear rate. This could be due to the nature of biofilm formation being exponential (Salman, 2020).

As the biofilm matures, the double-layer capacitance exhibits less changes over time even with the continued growth of the biofilm and increased bacteria count. This alludes to something other than bacterial cell body may affect impedance during monitoring like physical appendages (flagella, fimbriae) or molecular components outside the cell body including the formation of the EPS or metabolites and proteins (Kim et al., 2011c). To rule out potential influence of bacteria by-products, impedance measurements were performed on the supernatant of both bacteria species. There was a slight decrease in the middle frequency range from 10 to 10,000 Hz for both bacteria supernatants compared to broth (Figure 5.11). This may be caused by additional proteins, lipids, polysaccharides, and eDNA (Moormeier and Bayles, 2017, Thi *et al.*, 2020).

### **5.5.2 Biofilm Evaluation method**

A variety of different biofilm recovery methods were explored in the literature (Section 2.4), with two taken forwards for evaluation in the present study. The first of these methods was crystal violet staining, as this is common practice for biofilm characterisation as reported by Doll *et al* and Extremina *et al* (Doll *et al.*, 2016, Extremina *et al.*, 2011). The crystal violet results obtained in the present study did demonstrate an obvious pigmentation on the chamber that is consistent with bacterial growth. However, this provided only a quick visual indication of biofilm formation. Crystal violet could only give an approximation of biofilm formation and ideally direct counts of bacteria would be performed to determine if ES measurements are sensitive enough to distinguish between fluctuations of bacterial growth. Crystal violet is also non-ideal as this study looked at

drug concentrations released from polymers and specific counts for kill would need to be determined as well as drug measurements which may be altered by the crystal violet.

Given the limitations of the crystal violet assay, the direct enumeration with a swab was the second method evaluated. While counts were found for both bacteria types, the error bars were relatively large with  $\pm 1 \times 10^7$  standard error (Figure 5.13), indicating variability in the technique. Moreover, the collection method had a potential error as the swab used was larger than the electrode area leading to collection of bacteria that wasn't on the electrodes (but accidental collection of bacteria on the surrounding dish surface). This could cause a higher bacterial count than potentially was measured on the electrodes using ES. A more accurate method would be needed for later experiments by either having a smaller swab or using removable electrodes to allow for a sonication method.

## 5.6 Limitations

There were a few limitations to this methodology that have arisen within the discussion section. Here we will explore more in depth the limitations of the study.

This initial device design reported by Holland *et al* used planar gold electrodes sputter coated onto the bottom of the petri dish. This orientation greatly minimises the types of materials that can be used, with little opportunity for use of materials most commonly used within medical implantables, such as stainless steel. The planar electrodes were also very small, making application of polymer-drug coatings onto the electrodes very challenging, thereby making them unsuitable for addressing the ultimate focus of this study. It was also observed that the gold electrodes could become damaged during ethanol sterilization, with the gold fully lifting from the chamber surface. UV light sterilisation

was therefore employed. However, this in turn introduces a potential future limitation, since UV is known to have potentially damaging effects of polymer coatings like epoxy (Bell *et al.*, 2021) similar to those that are proposed for use in later aspects of this work. Similarly, the proposed use of Rifampicin, a light sensitive antibiotic (Angiolini *et al.*, 2019), was also likely to introduce potential challenges with UV sterilisation.

The results of the biofilm counting method led to the conclusion that crystal violet and swabbing of the current test set-up had limitations so another form of detection/quantification would be necessary. This design did not allow for removable electrodes, limiting the different methods that could be used for biofilm recovery.

A new system would need to be developed to grow bacteria and address all the issues surrounding the first electrode design. The work carried out in this pursuit forms the basis of the next section within this results chapter.

## **5.7 System Development**

### **5.7.1 Needs Analysis**

The limitations of the wire system from results chapter 4 and of the gold system in the previous section within this chapter were critically analysed against a set of performance criteria. Briefly, a needs analysis was performed based on functional and non-functional requirements analysis set by The International Council on Systems Engineering (INCOSE, 2022) for the overall goal of the new design based on the aims in Section 1.8 and discussion with key stakeholders. A list of design criteria, along with their purpose was determined either an essential or desirable criteria for the final design.



The needs analysis in Table 5.1 determined seven essential and eight desirable characteristics for the new design. This study narrowed the scope to only testing bacteria, therefore mammalian cell growth would be an additional benefit but not completely necessary for the planned experiments. The essential functional needs were based off the goal to measure effectiveness of antimicrobial coating using ES. Therefore, the system needed to allow bacterial growth and be compatible with the Palmsens, along with all essential criteria to perform ES measurements. The desirable criteria were features that would make measurements easier or be added benefits but were not required to obtain the goal. This included things like a 3-electrode design, which is used in many commercially available systems and would allow for voltammetry measurements on the Rifampicin concentration, allow flow for more accurate *in vivo* conditions, and allow cell growth for more complex studies later on.

**Table 5.1** Needs analysis for new electrode design. Design criteria listed along with the purpose of the criteria within the design, then determination if it is deemed an essential functional requirement or desirable non-functional requirement.

Design Criteria	Purpose	Essential or Desirable
Grow bacteria	Design needs to be able to grow for analysis	Essential
Palmsens- Multiplexer compatible	Run multiple measurements at once	Essential
Common medical device metals as working electrode	To determine if ES can monitor common medical device metal surfaces	Essential
Surface of electrode can be modified	Determine if ES can monitor modifications to medical device surfaces	Essential
Need Counter and working electrode	Allows current flow and able to measure impedances	Essential
Counter electrode 3X size of working electrode	Ensure no current limitations arise	Essential
Counter electrode can't affect bacteria	Ensure counter electrode does not influence bacteria growth so can accurately measure change of working electrode	Essential
Removable working electrode	Allow easy quantification of biofilm formation	Desirable
3 Electrode – design	More accurate measurements	Desirable
Grow mammalian cells	Design able to grow cells for more versatile measurements	Desirable
Allow multiple runs at once (6 or 8 well plate)	Easy replication	Desirable
Allow 2D and 3D cell growth	For more complex representation of <i>in vivo</i> conditions	Desirable
Allow flow	Mimic <i>in vivo</i> conditions more accurately	Desirable

Minimize liquid in growth chamber	Allow for easier determination of drug concentration	Desirable
Re-usable chamber	Reduce cost and waste	Desirable

An analysis of the different electrode set-ups used by others was performed to determine how many essential and desirable characteristics could be achieved in each design type.

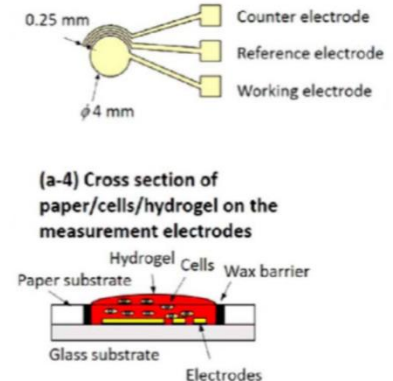
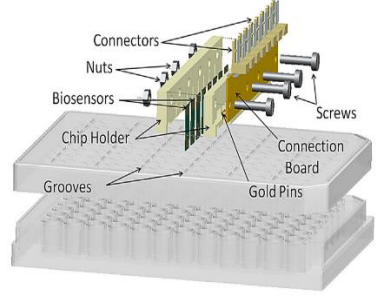
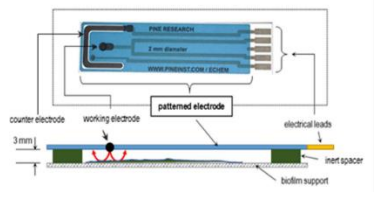
There are various advantages and disadvantages to the different electrode designs. The non-contact design would not be suitable for the present study as the bacteria needs direct contact with the electrode to determine the antimicrobial coatings effectiveness, therefore the design process focused on the planar and vertical designs.

The vertical and planar designs could allow for each essential design criteria to be met as seen in Table 5.2 but the planar design would not be ideal. The planar design is a common well-known design that has been used in many bacteria and cell experiments (Holland, 2017, Gutierrez *et al.*, 2016, Ward *et al.*, 2018). A planar approach would need the working electrode to somehow be embedded or secured onto the culture dish, which may make removal for bacterial counting more difficult. The swabbing method would need to be employed, which as stated previously, introduces a little more variability in bacterial counts.

As discussed in Section 5.1.1.2, Paredes *et al* performed a study on the different orientations of working electrode and found that the planar testing electrode with flow had the most sensitivity for detection on a fully matured biofilm while the vertical electrode in a petri dish had the least sensitivity due to larger testing area (Paredes *et al.*, 2014a). Vertical electrodes have many advantages including easier use of different electrode

materials, easy antibacterial coatings, and removable electrodes for bacterial counting. Therefore, the vertical orientation was taken forward as it allowed for more desirable criteria to be met than the planar orientation.

**Table 5.2** Table of different types of ES electrode designs currently used based on literature search and the advantages and limitations of each based on needs analysis.

Type of Electrode Set-up	Advantages	Limitations	Schematic of Design
Planar 1	<ul style="list-style-type: none"> <li>✓ Simple well-known design</li> <li>✓ Allows cell and bacteria growth</li> <li>✓ Palmsens compatible</li> <li>✓ Can allow flow</li> </ul>	<ul style="list-style-type: none"> <li>❖ Hard to remove working electrode for bacteria count</li> <li>❖ Large pellicle formation could influence measurements</li> </ul>	 <p>(a-4) Cross section of paper/cells/hydrogel on the measurement electrodes</p>
Vertical 2	<ul style="list-style-type: none"> <li>✓ Use different electrodes as metal</li> <li>✓ Allows cell(3D) and bacteria growth</li> <li>✓ Palmsens compatible</li> <li>✓ Removable working electrode</li> <li>✓ Can allow 3 electrode design</li> </ul>	<ul style="list-style-type: none"> <li>❖ Does not allow 2D cell culture</li> <li>❖ Difficult to include flow depending on design</li> </ul>	
Non-Contact 3	<ul style="list-style-type: none"> <li>✓ Easily use different electrodes as metal</li> <li>✓ Allows cell and bacteria growth</li> <li>✓ Easily modify electrode</li> </ul>	<ul style="list-style-type: none"> <li>❖ Not 3-electrode system</li> <li>❖ Non-removable electrode</li> <li>❖ Cells and bacteria do not</li> </ul>	

	✓ Palmsens compatible ✓ Can allow flow	make contact with working electrode	
References: 1. (Lei <i>et al.</i> , 2018) 2. (Paredes <i>et al.</i> , 2014a) 3. (Turick <i>et al.</i> , 2020)			

The design criteria and electrode designs were used to create new device designs for the new electrode system.

### 5.7.2 Device designs

Two designs were constructed, one with a planar orientation and one with a vertical orientation. Each design focused on use within a 6-well plate to allow multiple tests to be run simultaneously as well as minimize culture area for accurate drug concentrations to be measured.

The planar device design in Figure 5.13 had a working electrode at the bottom of the well. To optimize the area of the working electrode, the counter electrode and reference electrode would be on a well insert that would be suspended above the working electrode. A 3-electrode design was proposed for more accurate measurements. The addition of a third reference electrode allows for potential changes of the working electrode to be measured independent of changes that may occur at the counter electrode (Gamry, 2022). The bottom of the well, as seen in Figure 5.13 (c) at the impedance analyser connection,

would need a side blocked off for a connection to be made to the working electrode since liquid cannot be at that interface.

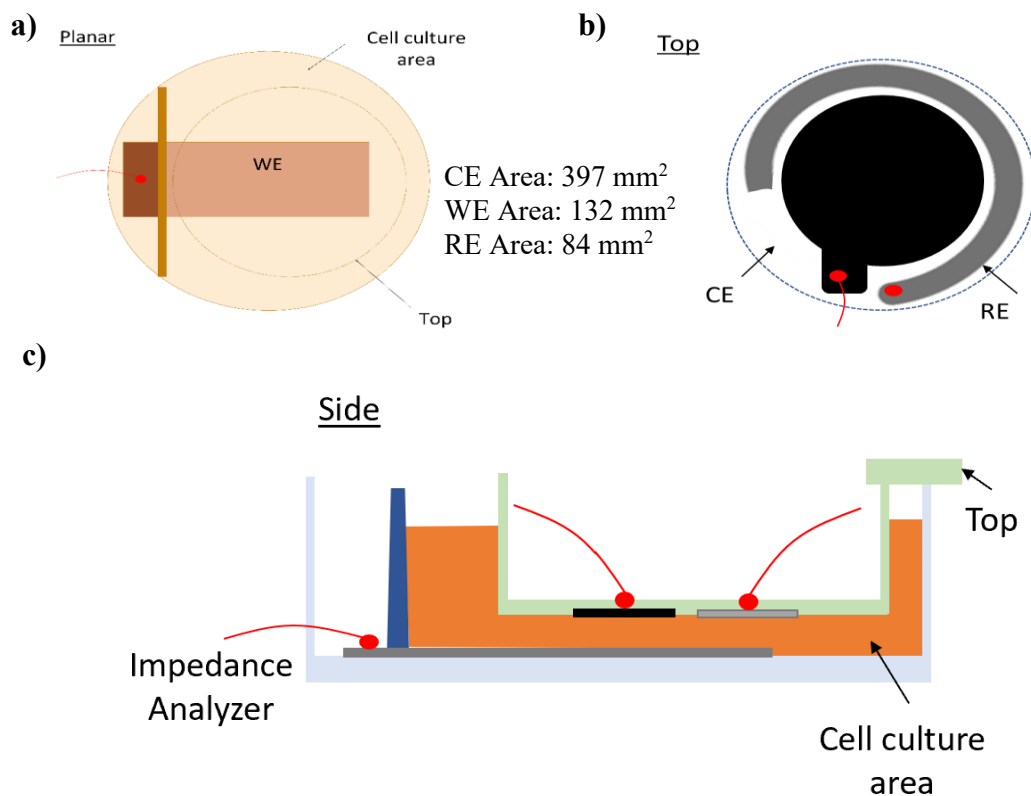


**Figure 5.13** Planar device design with **a)** planar view of working electrode on bottom of well **b)** Top view of well insert that had counter and reference electrode. **c)** Cross-sectional view of well with insert. Red lines represent wires attached to electrodes.

The vertical device design in Figure 5.14 also utilized a well insert for easy removal of electrodes and have more consistency between chambers. The device had a 2-electrode design with half the well insert coated in gold for the counter electrode and three working electrodes to allow replicates within each well. The working electrodes were also easily removable and replaceable within the insert, allowing for reuse of the device components. The working electrodes were smaller in the vertical design versus the planar design,

allowing for the counter electrode to be more than three times larger than the working electrodes. The vertical electrode could also later incorporate flow using a 6-well flow chamber without worrying about potential liquid spillage onto the connection area, as with the planar design. All these aspects were considered when choosing the final design as described in the section below.

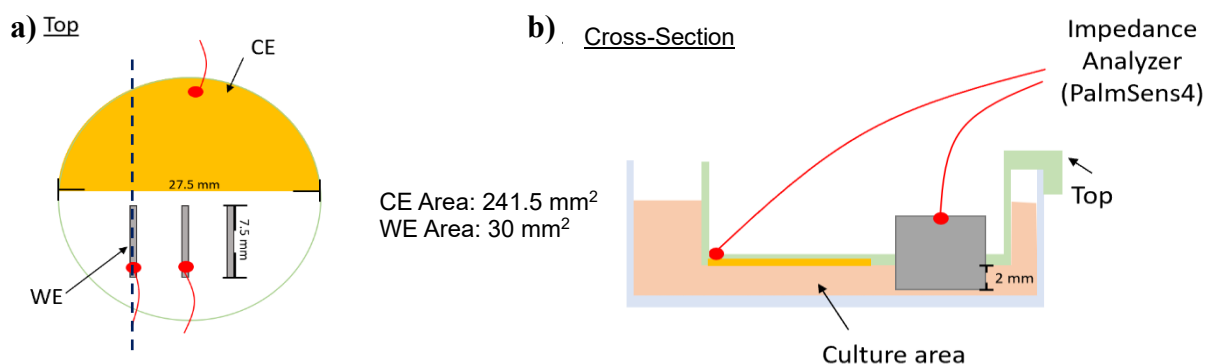


**Figure 5.14** *a) Top view of vertical device design with counter electrode and 3 working electrodes with measurements b) Cross-sectional view of new electrode design at dotted line with depth measurement and total area of electrodes given. Red lines represent wires attached to electrodes.*

### 5.7.3 Design selection

There were multiple considerations in choosing the device design to take forward for testing including how many design criteria were met, materials needed, and assembly process.

The planar design was critically evaluated, and it was found that it would need a more complicated process for assembly, with the working electrode needing to be sectioned off

for connection to a wire and would need to be sealed to the bottom to ensure no leaks which would lead to a harder removal for biofilm recovery. The silver/silver chloride reference electrode would create more cost as it is a specialized electrode. Silver also has the potential to harm bacterial growth when used within the culture area, while gold as used in the vertical design is inert and has minimal influence on bacteria (Webster, 2009). Farrow *et al* used disposable silver-silver chloride sensors from Ohmedics Ltd. that they found inhibited bacterial growth below critical cell densities (Farrow *et al.*, 2012). It has also been discussed that having planar electrodes leads to large pellicle formation at the air-surface interface that would need to be considered when making ES measurements (Ward *et al.*, 2018).

The vertical design was chosen over the planar design to take forward in this study as it would be cheaper and quicker to construct. The system utilized a 2-electrode system which would be relatively cheap and simple to fabricate, with ready access to a sputter coater for the gold counter electrode. The use of a metal foil as the working electrode increased the surface area, easier for dip coating and bacterial attachment when in a vertical position. The vertical design also had multiple working electrodes within one well allowing for easier replicates to be measured. The vertical electrodes allowed for easily removable working electrodes for biofilm quantification and for surface modification, both essential for the listed aims.



## 5.8 Device Design 2 Methods

### 5.8.1 Electrode Fabrication

Gold was sputter coated at 40 mA at 0.03 mb Argon for a thickness of 72 nm onto custom laser cut acrylic (circle with diameter 27.5 mm and three slots of 7.5 mm length) to produce the counter electrode area of 241.5 mm<sup>2</sup> (dimensions on Figure 5.7). Silver chloride paste was applied to the gold and connected to the other side of the acrylic where the wire would attach. The acrylic was then sealed onto a 6-well well insert using PDMS, with gold facing into the culture area. The stainless steel or titanium foil was cut into rectangles 7.5 mm by 10 mm to create the working electrodes. Three of the working electrodes were sealed into the laser cut slots in the acrylic using PDMS, with 2 mm of metal protruding into the culture area for a total working area of 30 mm<sup>2</sup> for each working electrode. This makes the counter electrode area greater than three times larger than the working electrode area. A copper wire was then attached to the silver chloride paste for a connection to the counter electrode while alligator clips with wires were secured onto the working electrodes that were protruding into the well insert. The working part of electrodes were cleaned with Isopropanol to ensure all PDMS residue removed. Design graphic can be seen in Figure 5.14, with final design pictures shown in Figure 5.15.

The well inserts with working electrodes were sterilized before coating by exposing to UV light for 15 minutes. Immediately prior to application of any coating, the metal working electrodes were cleaned with ethanol solution.

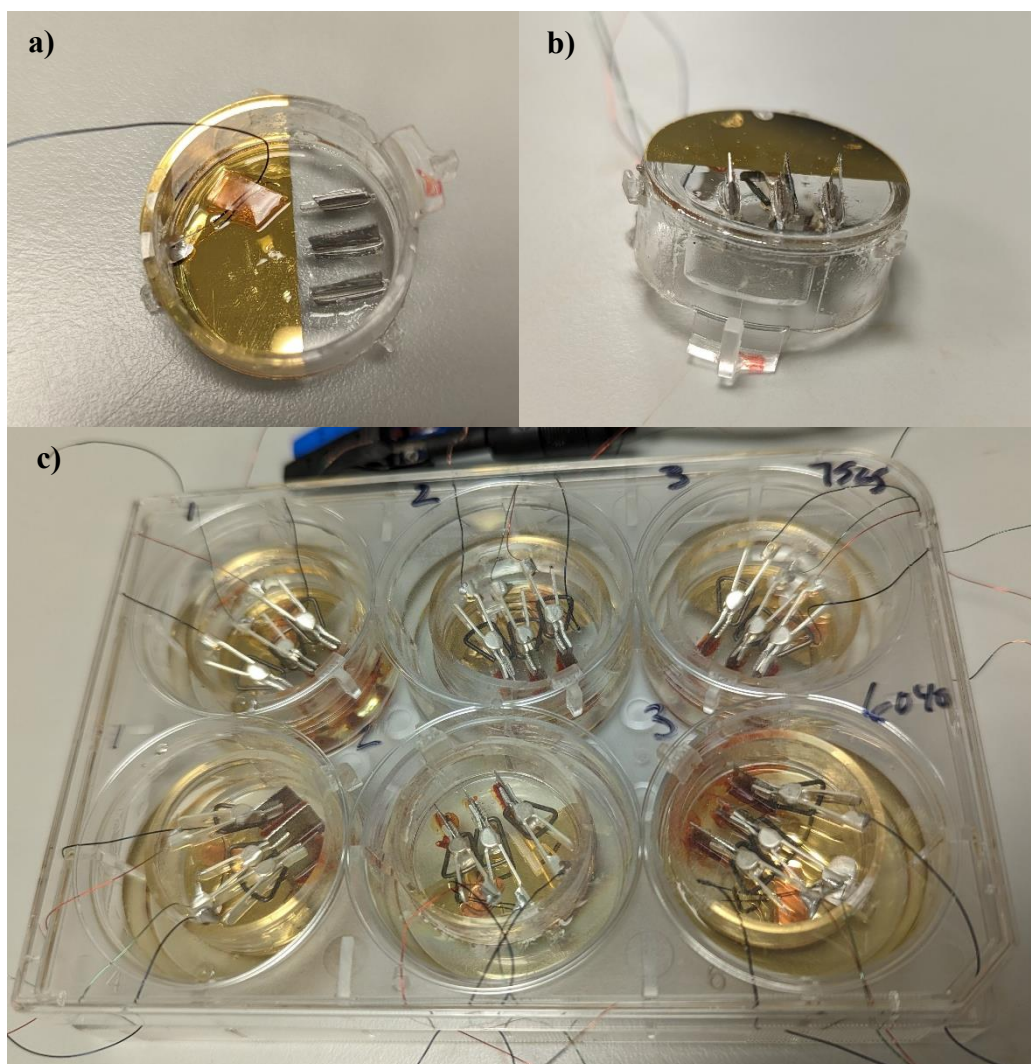
### **5.8.2 Design Evaluation**

Designs were tested for leaks to ensure the media stayed within the culture area and did not contact the wires. They also underwent an initial impedance measurement in PBS to ensure all wires were connected properly and reliable data could be collected. Impedance data collected using this new chamber design were compared to similar datasets collected from chamber design 1, to ensure data was comparable and impedance profiles similar.

## **5.9 Results**

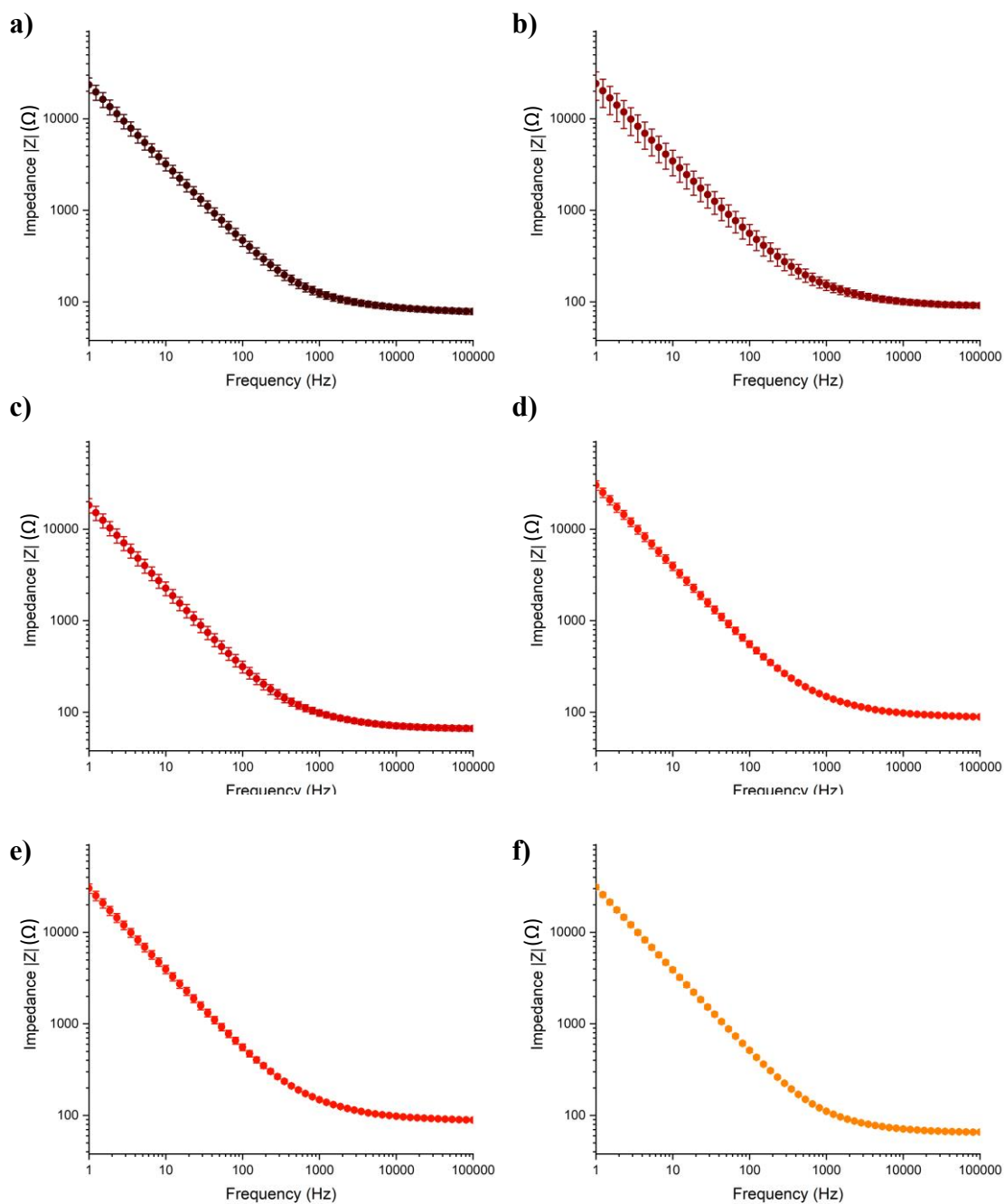
The new in vitro test system needed to be evaluated on practical design elements to ensure it worked within the context of the proposed application. The images shown in Figure 5.15 show the final chamber construction, which was confirmed to be free from leaks during the initial testing phase.

Figure 5.15 shows that the construction was carried out and the design from Figure 5.14 was achieved with no major alterations needed. The 6-well plate shows no leakage into the connection area where the alligator clips were secured for wire connection. These electrodes were then tested in PBS to ensure impedance data could be reliably collected. The results for this testing are set out in Figure 5.18 below.



**Figure 5.15** Pictures of device design 2 from **a)** top **b)** side view, and **c)** the chambers within a 6-well plate.

The impedance for the six test chambers showed some fluctuation in magnitude from chamber to chamber seen in Figure 5.16 (a-f) ( $Z$ ). The electrode-to-electrode variation within a chamber was very minimal as seen by the small error bars. The phase had less chamber variations, and even smaller electrode to electrode variation as seen in Figure 5.17.



**Figure 5.16** Impedance spectra of a) 1, b)2, c)3, d)4, e)5, and f)6 chambers of device design 2 with data representative of average of 3 electrodes  $\pm$  standard error.

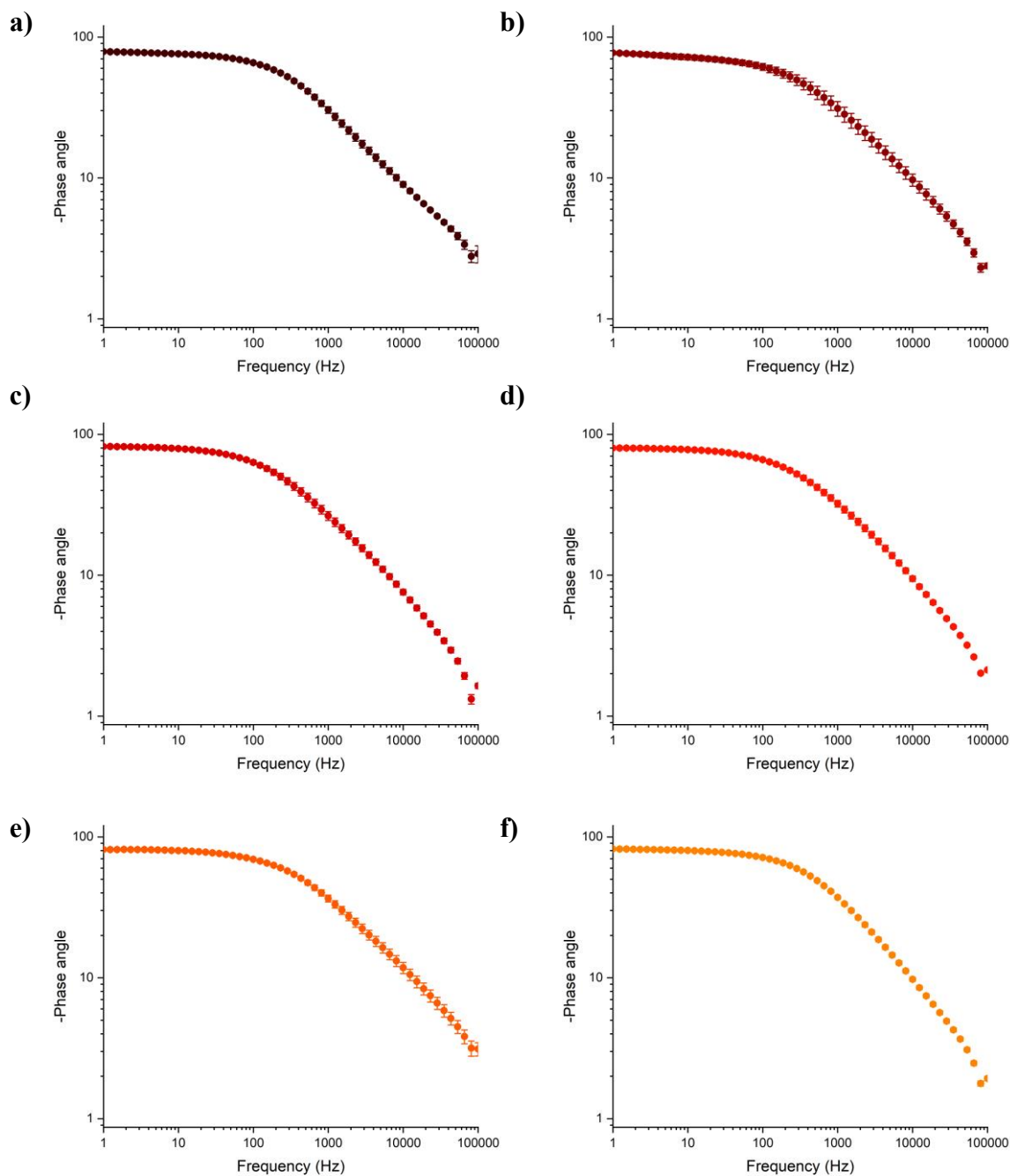


**Figure 5.17** -Phase angle of a) 1, b)2, c)3, d)4, e)5, and f)6 chambers of device design 2 with average data representative of 3 electrodes  $\pm$  standard error.

The chamber variations were taken at the frequencies of interest chosen in Section 5.4. Impedance had slightly larger deviations with  $\pm 1508 \Omega$  at 10 Hz and  $\pm 199 \Omega$  at 100 Hz, while phase had minimal standard error with  $\pm 2^\circ$  at 1 Hz and  $\pm 5^\circ$  at 1000 Hz (Table 5.3). Indicating that phase may have less variability in analysis but both impedance and phase can provide useful insights.

**Table 5.3** Table of relevant frequencies of parameters chosen from Figures 5.7 and 5.8 error and the mean and deviation calculated from the 6 test chambers used for Figures 5.18 and 5.19.

Parameter	Frequency (Hz)	Mean	Standard Error
Impedance	10	3824 $\Omega$	1508 $\Omega$
Impedance	100	542 $\Omega$	199 $\Omega$
Phase Angle	1	80°	2°
Phase Angle	1000	32°	5°

## 5.10 Discussion

The second section of this results chapter built off initial work on Device 1. It was shown that Device 1 would not allow for all aims of this study to be met, including use of medical device metals or antibacterial coatings in the design (Section 5.6). Therefore, design criteria were created and critically evaluated to develop a new advanced test system (Section 5.7.1).

As discussed in Section 5.7.3, a vertical design was taken forward in this study. The possible faults of Device 2 were tested to ensure the system achieved its intended goals. Sufficient sealing of well insert and working electrodes were tested to prevent media from

culture area from touching live wires which could cause electrical short. The connection that used the silver chloride paste from counter electrode to opposite side of well insert was tested to ensure impedance measurements could be taken. The small amount of silver paste was considered negligible in testing as it would have a very small amount in the testing chamber and would be on the counter electrode which would not affect bacterial growth on working electrodes.

Device 2 was tested for electrode-to-electrode and chamber-to-chamber variations to determine how variable measurements would be without any complicated factors like coatings and bacteria. Figures 5.18 and 5.19 showed small electrode-to-electrode variation very similar to results from Device 1 (Section 5.5), where error bars were relatively small. The magnitude and shape of the impedance profiles for Device 1 and 2 were similar with the lower frequency range starting at about 30,000  $\Omega$  at 1 Hz, with the Device 1 ending at around 1000  $\Omega$  at the 100,000 Hz and Device 2 ending around 100  $\Omega$  at 100,000 Hz. The phase also had similar shapes and magnitudes starting between 40-60° for Device 1 and 80° for Device 2, both ending around 1°. Schmiedinger found that gold, aluminium, and titanium could assess functionality of epithelial tissue but found that titanium electrodes had an elevated resistance which shifted the impedance readings due to its lower electrical conductivity (Schmiedinger *et al.*, 2020). The larger range of impedances found in this study could be due to the conductivity differences between stainless steel and gold. The variation between chambers and possible material variations can be minimised through the normalisation process described in Section 5.1.2.

This new device design created in this project had several advantages over existing impedance measurement systems. Most impedance studies on biofilm formation or rapid antibiotic treatment focus on ideal electrode materials like gold, platinum, or carbon (Ward *et al.*, 2018, Paredes *et al.*, 2014b, Swami *et al.*, 2022). This does not represent a true environment in which antibiotic coatings would be used if on medical devices implanted in the body. There are impedance systems that use medical device metals but usually within degradation studies (Fattah-alhosseini *et al.*, 2011, Kocijan *et al.*, 2004, Díaz *et al.*, 2018). Fattah-alhosseini *et al* used EIS to look at the electrochemical behaviour of anodic passive films on AISI 304 stainless steel while Kocijan *et al* showed potentiodynamic curves to show cobalt chrome alloys corrosion behaviour. They do not test for bacterial growth or the antibacterial properties of the metals or coatings on metals. Diaz *et al* investigated the change in impedance to titanium surfaces after exposure to *S. mutans* over 28 days but did not investigate if EIS could tell when bacteria grew on the titanium. There are no current publications on a system that uses medical device metals as electrodes. This presents a large gap in knowledge of if impedance can be used directly on medical device metals with coatings to determine their effectiveness against infection. This set-up will be used for this purpose and determine if ES can be used within this context in the next results chapter.

## **5.11 Limitations**

This design had some limitations, specifically in the desirable design criteria described in Section 5.7.



The chosen design would only be a 2-electrode design. A 3-electrode design would have been more accurate in measurements, but fabrication would be more complicated as well as potentially toxic to bacteria if using the silver reference most commonly used.

The design did not allow for 2D mammalian cell growth as the electrodes were vertical. Since cells adhere in monolayers and only contact cells at their border the oxygen, nutrient or waste gradients are absent, and the environment is not uniform (Antoni *et al.*, 2015). Trying to grow cells vertically can lead to hypoxia and eventually cell death if they do not have a support structure or strong adherent forces that keep them attached to the surface (McGuire *et al.*, 2018). Bacteria do not face the same problem as they can form on either horizontal or vertical surfaces without any outside influence due to their mobility and aerobic/anaerobic character (Jha *et al.*, 2022, Chang *et al.*, 2015).

This design employed medical device metals as the working electrode which meant electrode cleaning or plasma treating could not be employed to ensure fully cleaned and uniform electrodes so that it would not alter them significantly from medical device metals. The last limitation of this design was working electrodes could only be used once, as they were coated with antibacterial coatings then removed and sonicated after biofilm growth and evaluation. This meant a higher usage of material, but necessary for the scope of this project.

## **5.12 Future Work**

The current design focused on a static system, which does not accurately depict *in vivo* conditions that a medical device would be subject to. Further work could be done with a

flow system easily incorporated with an Alvetex Perfusion Plate by Reprocell or Fisher scientific.

More design criteria could also be considered and potentially added to the current design to allow for 3-electrode design or compare the impedance profiles generated by the current system to actual medical devices.

### **5.13 Summary**

It can be stated from this study that impedance spectroscopy can determine bacterial growth of both a Gram-positive (*S. aureus*) and Gram-negative (*P. aeruginosa*) bacteria on gold electrodes. The impedance profiles of both bacteria showed significant changes in phase angle at 1 Hz and 1000 Hz after 24 hours incubation. *P. aeruginosa* showed a significant change in impedance at 10 Hz and 100 Hz. The device used in the initial experiments had several limitations that made it unsuitable for future experiments in this study, specifically related to electrode material and biofilm recovery.

A needs analysis was performed based on the study aims and found seven essential criteria and eight desirable criteria that formed the basis on which new electrode designs were developed. A vertical electrode device design was taken forward as it had several advantages for this particular study including removable electrodes and easy fabrication.

This device design was evaluated and found that electrode variability and device variability was minimal. This suggests it was a suitable candidate for future testing of biofilm growth and antibacterial coating evaluation.

## **6 Chapter 6 Impedance based characterisation of drug release and biofilm formation using a novel *in vitro* platform**

### **6.1 Chapter Aims and objectives**

Chapter 4 investigated the use of ES to monitor polymer-drug coating degradation on common medical implant metals. It was shown that 50:50 and 60:40 formulations displayed distinct impedance characteristics that were potentially associated with polymer degradation and drug release kinetics. Chapter 5 critically analysed existing impedance systems, which helped inform the design and development of a novel testing device that allowed *in vitro* biofilm formation and polymer-drug coating analysis simultaneously. This chapter will utilize the newly designed system from Chapter 5 to investigate biofilm formation using medical device metals, and to characterize the polymer-drug coating effectiveness from Chapter 4 over clinically relevant time periods. It is hypothesized that inhibition of biofilm on antimicrobial-releasing medical implant surface could be successfully monitored non-invasively using impedance spectroscopy.

The specific objectives for the experiments used to address this aim and general hypothesis are detailed below.

- Investigate the impedance profiles of polymer-drug coatings within the new system
- Investigate the feasibility of using common medical device metals within the above system to detect biofilm formation

- Determine the most appropriate analysis methods that can be applied to biofilm formation with medical device metals
- Investigate the feasibility of using impedance spectroscopy to non-invasively characterize biofilm formation on polymer-drug coatings over clinically relevant time periods.

## **6.2 Methods**

### **6.2.1 Characterisation of impedance properties of polymer-drug coatings on medical implant-like surfaces**

Testing chambers were constructed as described in Section 5.8.1. Separate coating solutions of PLGA, Rifampicin, and three PLGA: Rifampicin formulations (75:25, 60:40, and 50:50) were prepared at a consistent concentration of (10% w/v). The test electrode substrate materials coated were SS and Ti, consistent with those explored in chapter 4. 5  $\mu$ l of the selected coating solutions were pipetted on to each side of the test electrode, covering the entire surface and left to dry for 15 seconds, with this process repeated a further two time in order to deposit a total of 30  $\mu$ l on each electrode, for a total of 90  $\mu$ l in each chamber for measurement of drug release.

The test chambers were sterilised through spraying of Isopropyl alcohol 5 minutes before use. The final test chambers were then incubated with 6ml of PBS within a 6-well plate, maintained static at 37°C. Impedance measurements were performed over a 6-month time-period with 1 ml samples removed periodically for drug release measurements at various time points. The PBS was fully replaced with fresh PBS at each of these time points, to

ensure a consistent volume was maintained throughout and to approximate infinite sink conditions for drug release characterisation.

UV spectrophotometry was used to estimate the Rifampicin release at each time point using the method previously described in Section 3.4.3.2. In previous studies conducted within the laboratory, it has been shown that SS and PLGA do not interfere with the UV absorbance and so for clarity, these datasets are not presented.

## **6.2.2 Characterisation of impedance properties of biofilm formation on medical implant-like surfaces**

### **6.2.2.1 *ES of biofilms***

The bacteria used for this experiment were *Staphylococcus aureus* NCTC 4135 and *Pseudomonas aeruginosa* NCTC 9009. Bacteria were cultured as described in Section 5.3.4.1.

Initial ES experiments were performed in sterile nutrient broth over 24 hours, in the absence or presence of different concentrations of bacteria ranging from  $10^2$  to  $10^9$  CFU/ml.

Each testing chamber was filled with 4ml of sterile nutrient broth without bacteria and an initial impedance measurement taken (time zero). The broth was then removed and replaced with 4ml of nutrient broth containing the bacteria. This was then incubated for 24 hours at 37°C, with impedance measurements taken at 0, 3, 6, and 24 hours. At 24 hours, the nutrient broth was removed and serially diluted in PBS, then plated and counted, as described in Section 5.3.4.2.2. This enabled the quantification of the broth and its

influence on the impedance measurements. The electrodes were washed with sterile PBS and new sterile nutrient broth was added to the chamber. After 15 minutes extra incubation in 37°C, one final impedance measurement was taken.

This procedure was repeated on 5 types of electrode samples (test electrodes): Bare SS, Bare Ti, 10% PLGA, 10% Rifampicin, and 50:50 PLGA: Rifampicin coated SS. The 50:50 formulation was selected due to its impedance having significant decreases over the selected time periods and its larger drug release. A new set of samples were incubated in PBS for each incubation period: 24 hours, 1 week, 3 weeks, and 2 months. The ES measurements with bacteria were repeated on all sample types for each time point.

#### **6.2.2.2 *Direct Enumeration from sonication***

After ES detection, the electrodes were removed and placed in 2ml of release medium. This was to release the biofilm from the electrode, which can be serially diluted and enumerated to establish biofilm populations. These were manually shaken for 20 seconds, then sonicated for 300 seconds, and a final manual shake of 20 seconds. These samples were serially diluted to desired concentration and 100 µL were plated onto nutrient agar and bacteria count obtained after 24 hours incubation. Bacteria counts for each electrode were found using the below equation.

$$\frac{CFU}{electrode} = AVG \text{ bacterial count(per } 100\mu l) \times \frac{10\mu l}{mL} \times 2 \text{ ml} \times \text{dilution factor}$$

#### **6.2.3 Data Presentation and analysis**

Unless stated otherwise, data in this chapter are presented as the mean ± one standard error of the mean from 3 repeat experiments. To investigate statistically significant differences

in impedance observed for the polymer-drug coatings, the phase angle and modulus of impedance,  $Z$ , both at 10 Hz and 10 kHz were compared using one way ANOVA analysis followed by Tukey's post-hoc between sample types and Bonferroni's post-hoc multiple comparison tests between different time points.

Similarly, to identify any statistically significant differences in biofilm formation the different test electrodes, both the phase angle and  $Z$  were compared using one way ANOVA analysis followed by Tukey's or Bonferroni's post-hoc multiple comparison tests. Values of  $p < 0.05$  were considered statistically significant. All one-way ANOVA used these parameters unless stated otherwise.

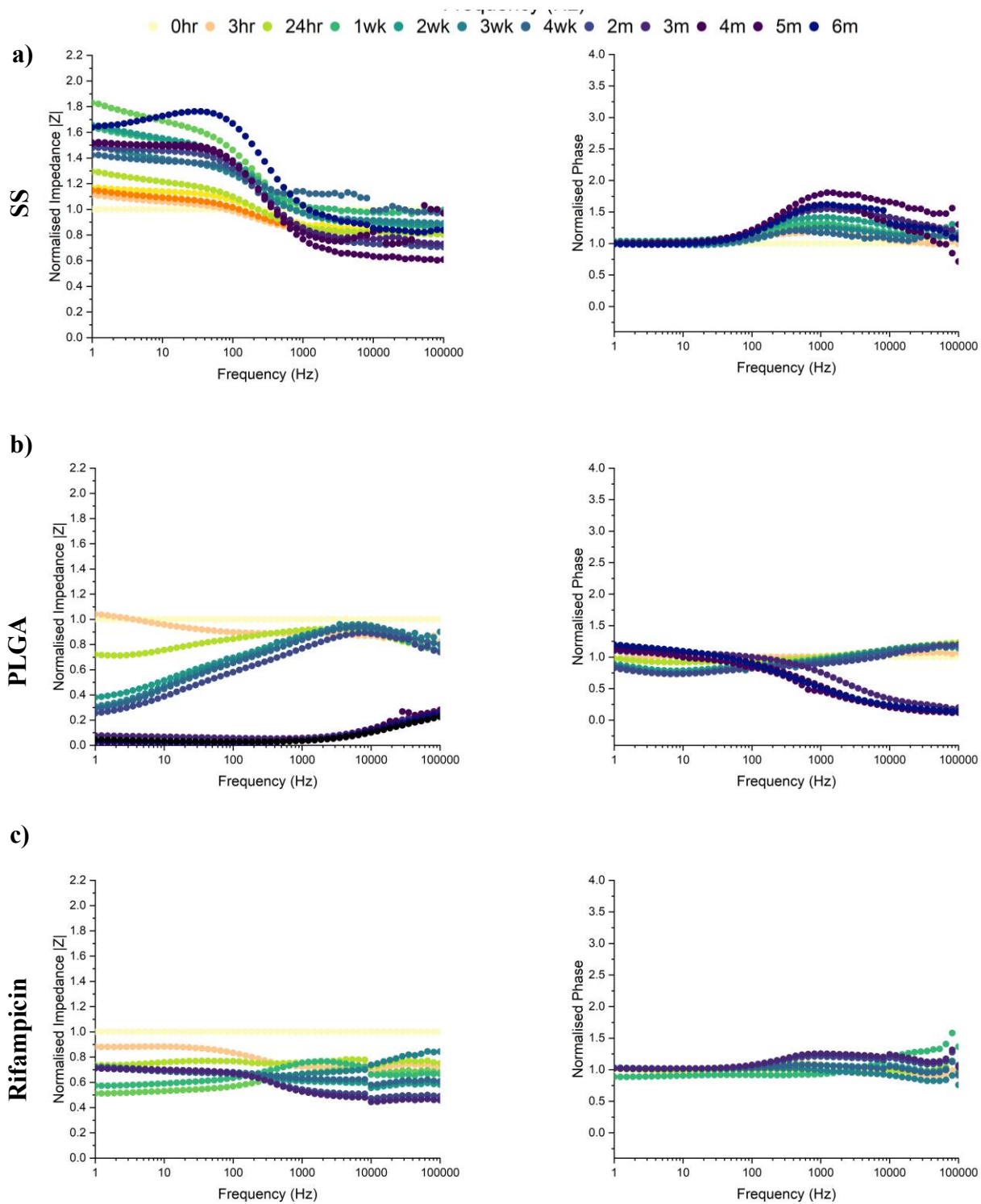
## 6.3 Results

### 6.3.1 Characterisation of impedance characteristics of polymer-drug coatings on medical implant materials

#### 6.3.1.1 *Impedance Analysis*

ES experiments were performed on the new chamber, with SS electrodes and the coatings developed in chapter 4. Measurements were recorded over a period of 6 months incubation in PBS. The results from this aspect of the study are summarised in Figure 6.1. The data was normalised to minimize chamber to chamber variations and allow direct comparison between different coatings. Each coating had distinctly different impedance profiles, which led to the selection of a chosen frequency that allowed a more direct comparison between samples. The SS impedance data increased over the 6 months, especially in the lower frequency band of 1 to 1000 Hz. It also experienced a noticeable shift in the impedance at 10 kHz, which could be due to noise influence described from Section 2.1. The PLGA impedance data experienced a decrease in impedance over the 6 months, across the entire frequency range. It can be seen that normalised impedance data at ~10 kHz showed the largest temporal differences in the coated samples, seen in Figure 6.1 d), e), and f). In contrast, the phase angle data did not exhibit as marked variations for any of the sample types.





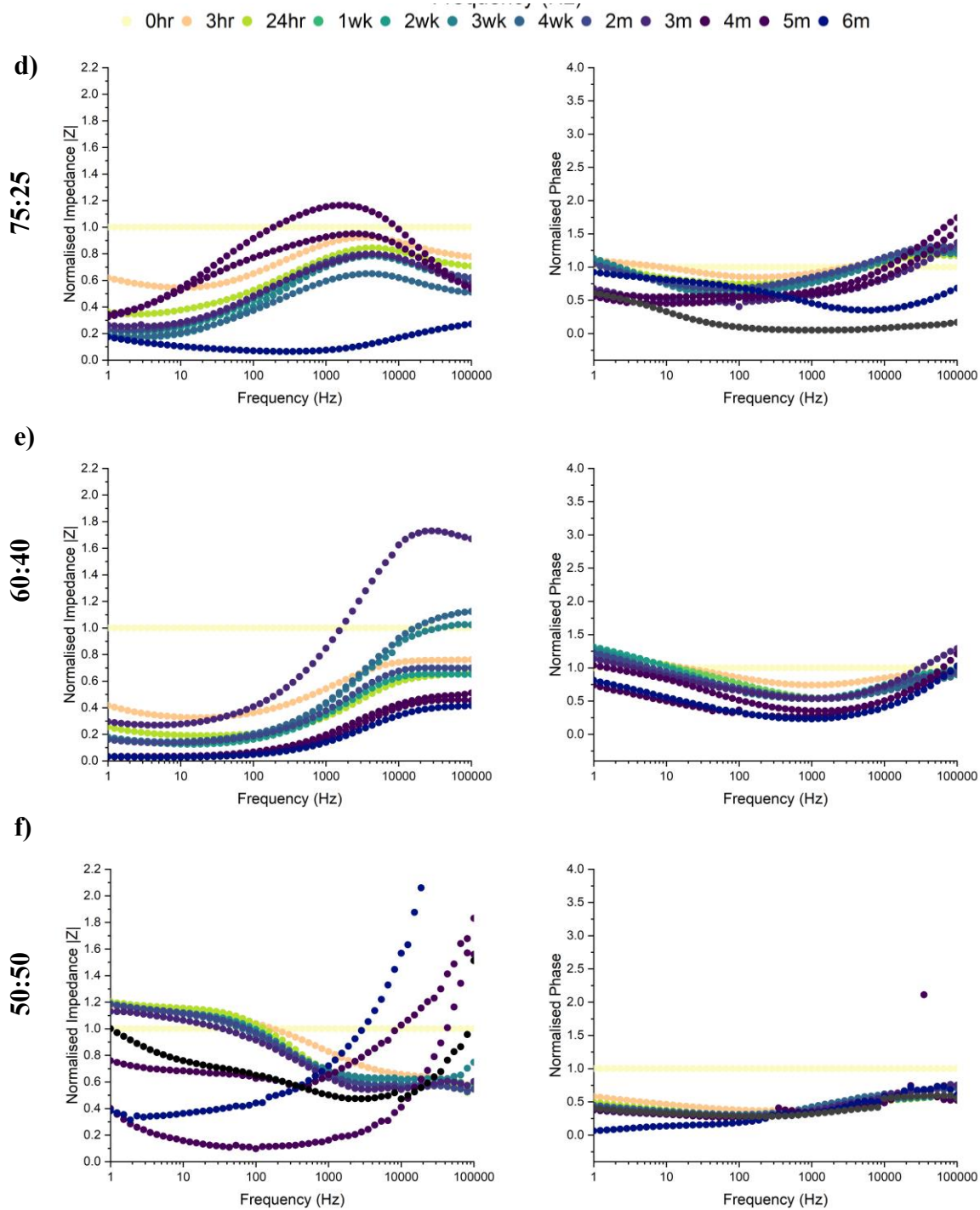


**Figure 6.1** Normalised impedance and phase angle without standard error for **a) SS b), PLGA, c) Rifampicin d) 75:25, e) 60:40, and f) 50:50** incubated in PBS over 6 months. ( $n=3$  chambers, 9 electrodes). Full data and standard error in appendix

Based on the results obtained in chapter 4, 10Hz and 10kHz were identified as frequencies of interest to monitor polymer-drug coating degradation. The same two frequencies were therefore used when analysing the datasets collected in this chapter.

The 10 Hz normalized impedance (Z) had demonstrated the greatest difference between the control SS and Ti from the coated samples (Figure 6.2). Ti and SS have a similar normalized impedance profile at 10Hz, with both starting around 1 and increasing to approximately 1.5 after 6 months. At 10 Hz, Ti displayed a significant change in impedance versus time zero at months 3-6. The impedance of the Rifampicin coated samples decreased over the first week from 0.7 to 0.5, before levelling out back at 0.7 and becoming stable for the remaining 6 months. The PLGA coating decreased linearly over the course of 1 month before drastically dropping from 0.4 to <0.1 at 2 months and remaining at <0.1 for the remaining months. The PLGA also had a significant difference in Z from 2 months to 6 months when compared to the 0-hour time point.

The 75:25, 60:40 and 50:50 coatings normalised impedance at 10Hz decreased over the 6 months at smaller linear decrease, changing around 0.2 for all coatings. Most time points were significantly different from time 0 for all the coating variations. All of the different coatings (PLGA, Rifampicin, 75:25, 60:40, and 50:50) were all significantly different from the SS and Ti bare electrodes at 10 Hz.

The 10 kHz normalised impedance data, Figure 6.2 (c) and (d), did not show a noticeable decrease in impedance over time for any of the coated wires unlike the 10 Hz. The PLGA still showed a sharp decrease at the 2-month time point, but it was not significantly different from earlier time points. The 75:25 and 50:50 coated wires still had significant

differences at almost every time point, and they were significantly different from SS but there were less time points that had significant results at the 10 kHz compared to the 10 Hz.

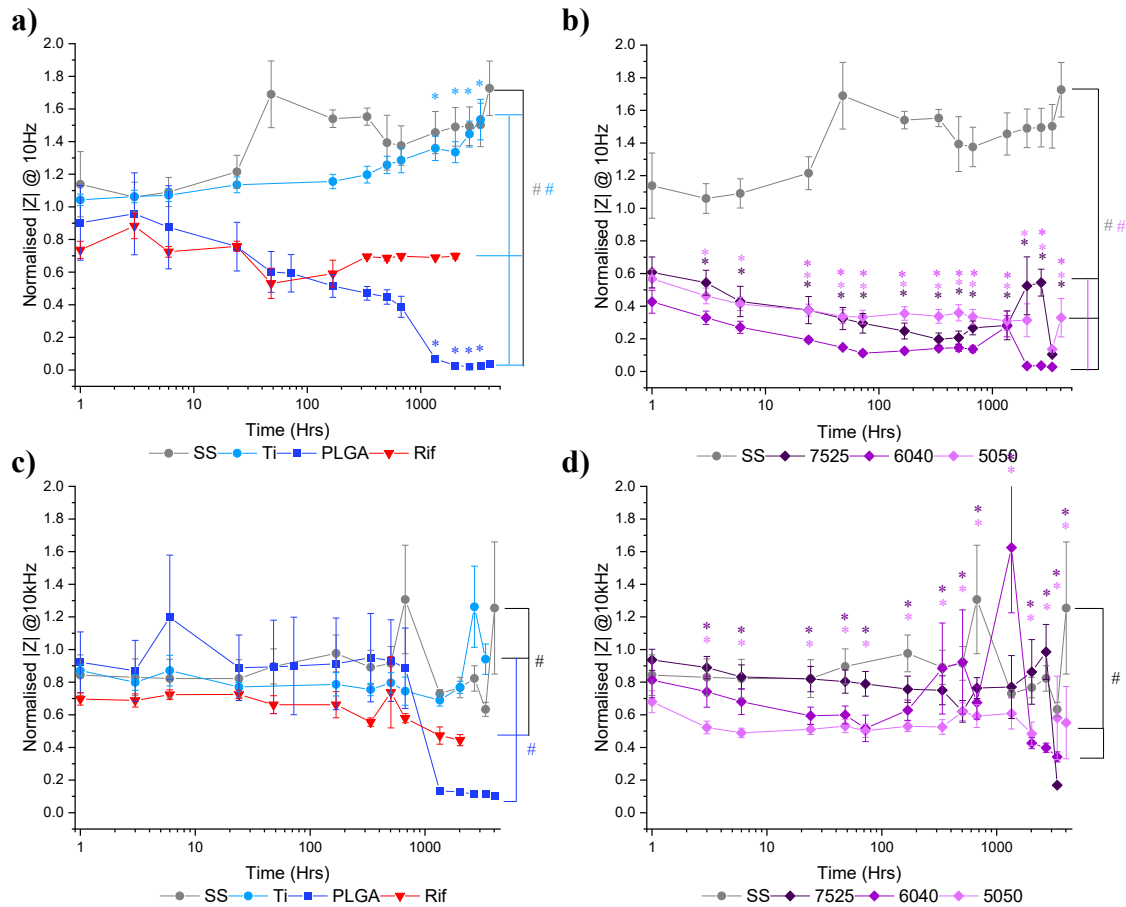


**Figure 6.2** Normalised frequency at 10Hz **a)** SS, Ti, PLGA, and Rifampicin and **b)** SS, 75:25, 60:40, and 50:50 and 10kHz **c)** SS, Ti, PLGA, and Rifampicin and **d)** SS, 75:25, 60:40, and 50:50 incubated in PBS over 6 months. Significance was determined by ANOVA analysis, with Bonferroni post hoc between time 0 and subsequent time points (Shown by \* Ti \*PLGA, \*75:25, \*60:40, \*50:50) and Tukey post hoc between trendlines (Shown by # SS, # Ti, # PLGA). (n=3 chambers, 9 electrodes)

These results were also plotted for the normalised phase angle at 10 Hz and 10 kHz, Figure 6.3. These results are similar to the normalised frequency at 10kHz, not showing a very noticeable change in phase over time. PLGA phase decreased from 1 to 0.7 at 2 weeks to 2 months with significant difference from 0-hour time point before returning to 1 for all later time points. The 75:25-coating had lower phase at 10Hz versus all other coatings and decreased from 1 to 0.3. The 60:40 and 50:50 coating decreased to around 0.3 from 1 over the months 2 to 6. These were also significantly different from the zero-hour time point and from SS control. Overall, not a clear change over 6 months for any of the coatings.

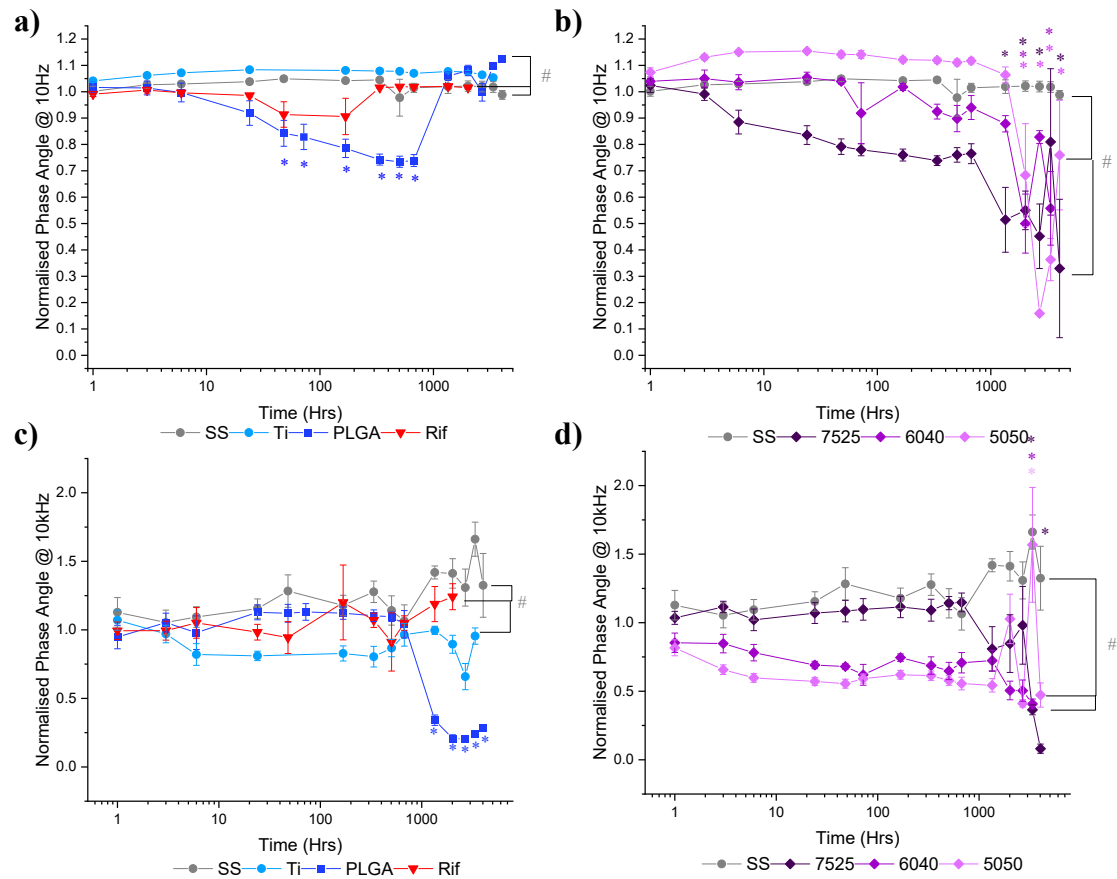


**Figure 6.3** Normalised phase angle at 10Hz **a)** SS, Ti, PLGA, and Rifampicin and **b)** 75:25, 60:40, and 50:50 and 10kHz **c)** SS, Ti, PLGA, and Rifampicin and **d)** 75:25, 60:40, and 50:50 incubated in PBS over 6 months. Significance was determined by ANOVA analysis, with Bonferroni post hoc between time 0 and subsequent time points (Shown by \*PLGA, \*75:25, \*60:40, \*50:50) and Tukey post hoc between trendlines (Shown by # SS). ( $n=3$  chambers, 9 electrodes)

### 6.3.1.2 Rifampicin drug release characterisation

The samples examined above were also tested for Rifampicin release for the different coating types. Figure 6.4 (a) shows that Rifampicin coatings displayed the greatest total amount of Rifampicin release after 6 months incubation (5.27mg), followed by 50:50 (4.49 mg), then 60:40 (3.07 mg), and finally 75:25 (1.94 mg). Figure 6.4 (b) shows the percentage released over the 6-month period. Rifampicin alone coated substrates released all drug within 1week and displayed significantly different release profiles compared to all other coating types. 50:50 coatings released 80% of their drug in the first week, then had a slow release of the remaining over the remaining 6 months. 60:40 coatings had a steady rapid release in the first 2 weeks, followed by a slow release over the remaining months. The 75:25 coating had a very small release in the first 2 months followed by a rapid release of the remaining drug over the later months.

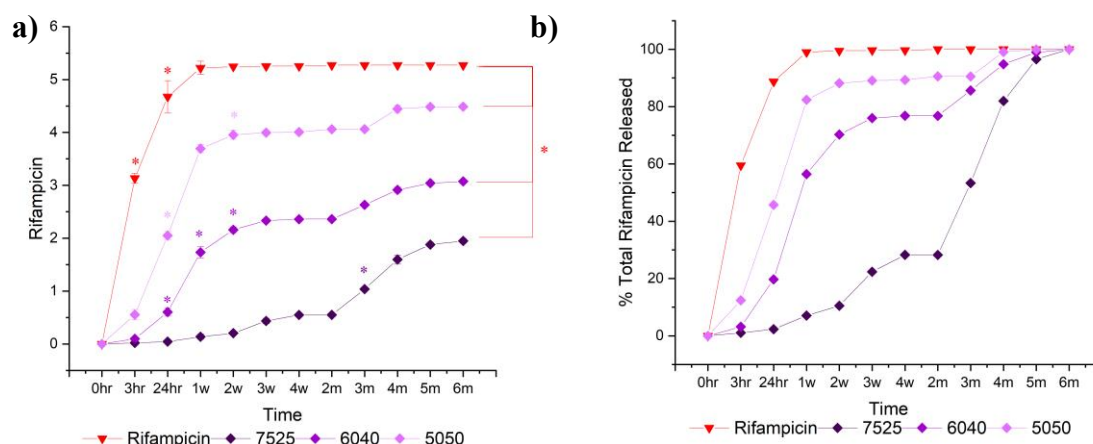


**Figure 6.4 a)** Total Rifampicin released in mg and **b)** % Total Rifampicin released from 10% Rifampicin, 75:25, 60:40, and 50:50 PLGA: Rifampicin coated samples incubated in PBS solution at 37°C (n=3). % total calculated from dividing each mass by final mass of Rifampicin per sample. Significance was determined by ANOVA analysis, with

*Bonferroni post hoc between sequential time points (Shown by \*Rif, \*75:25, \*60:40, \*50:50) and Tukey post hoc between trendlines (Shown by \*Rif). (n=3 chambers, 9 electrodes)*

These drug release profiles were directly compared to the normalised impedance profiles at 10 Hz in Figure 6.5, as the 10Hz showed the most significant changes in impedance based on Figures 6.2 and 6.3.

SS and PLGA had no drug released, but the PLGA had a decrease in normalised impedance from 1 to 0 over the first 2 months. The Rifampicin coated samples decreased in impedance from 1 to 0.5 in the first 3 weeks then remained at 0.5 for the 6 months, while the drug released almost completely within the first week then remained stable. The 75:25 coating had a decrease in impedance from 1 to 0.3 in the first 3 weeks (Figure 6.5 (d)), which corresponded to the period during which there was slow release of 30% of the drug (Figure 6.4(a)). The 75:25 then had a few changes in impedance as the remaining drug released over the later time points. The 60:40 coating had a sharp decrease in impedance over the first week, corresponding to the 60% of drug released in the first week. The impedance decreased from 0.2 to 0, at the 3-month time point correlated to a 20% more release of the drug. Finally, the 50:50 coating had a sharp decrease in impedance over the first week, along with 80% of the drug released in the first week. The impedance then remained relatively stable for the remaining 3 months, with the last release of drug occurring between 4 and 5 months that was also reflected in the impedance with a decrease of 0.2.



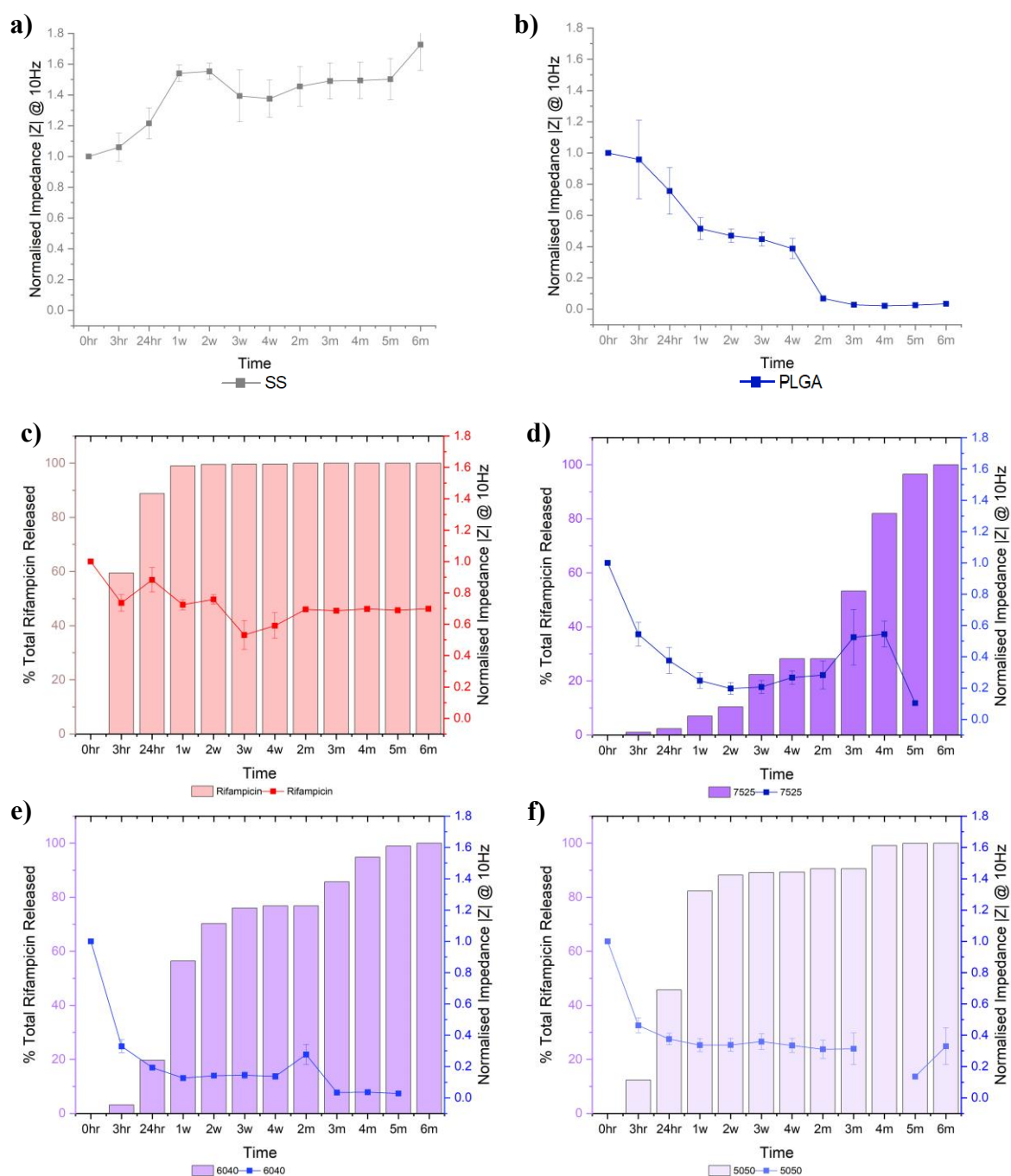


**Figure 6. 5** Normalised impedance  $|Z|$  at 10 Hz for **a)** SS samples **b)** 10% PLGA samples. Percentage of total Rifampicin released over 6-month incubation period in PBS solution, represented by bars on left hand axis, versus Normalised impedance  $|Z|$  at 10 Hz,

represented by plot points on right axis, for **c)** 10% Rifampicin samples **d)** 75:25 v/v samples **e)** 60:40 v/v samples and **f)** 50:50 v/v samples ( $n=3$  chambers, 9 electrodes).

While normalised values can provide a different insight into impedances and correct for sample-to-sample discrepancies, sometimes the actual impedance value can give useful information as well. To determine if this was the case, the unnormalised impedance value was plotted for 10 Hz and 10 kHz in Figure 6.6. It can be seen that while there is a slight difference between the different polymer-drug formulations it does not have a greater difference than the normalised data, therefore the normalised data can be used.

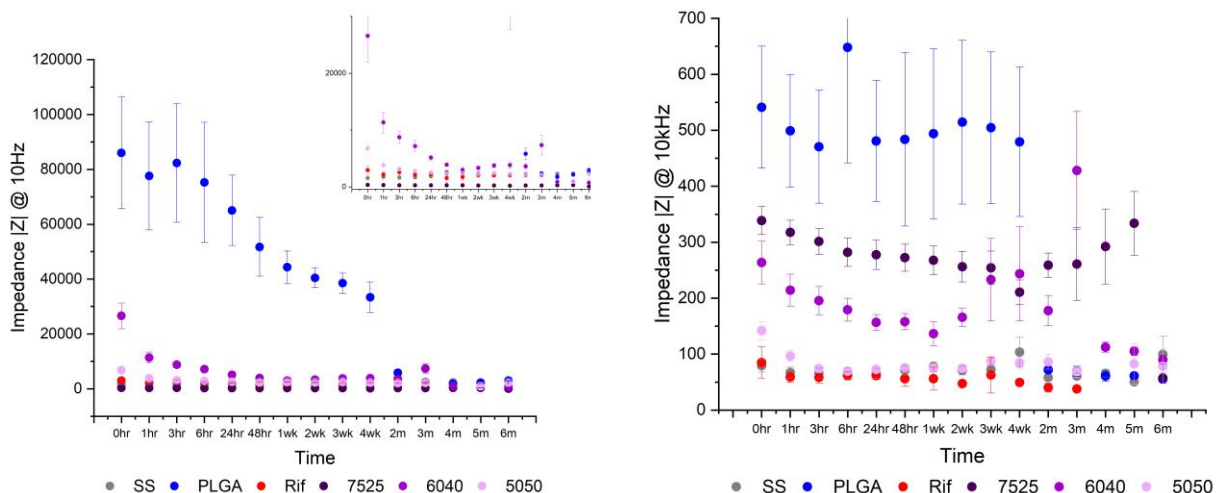


**Figure 6.6** Impedance at **a)** 10Hz and **b)** 10kHz for all sample types incubated in PBS over 6 months with zoomed in range highlighting smaller impedance differences. ( $n=3$  chambers, 9 electrodes).

### 6.3.2 Impedance characterisation of model biofilms on electrodes

The new system utilized SS as the electrode, therefore it needed to be determined if they could be used to detect biofilm growth in a similar manner to the gold electrodes used in Section 5.4. Firstly, sterile nutrient broth was tested within the system to determine if it influenced impedance. Figure 6.7 shows impedance data (normalized  $Z$ ) recorded from the SS electrodes incubated in sterile nutrient broth over 24 hours. It can be seen that there is very little change in normalized impedance, with only a slight observed at the higher frequency range 1000 to 100,000 Hz. The phase angle data demonstrated a similar profile with very little change in the normalised impedance and slight variation in the same higher frequency range as the impedance.

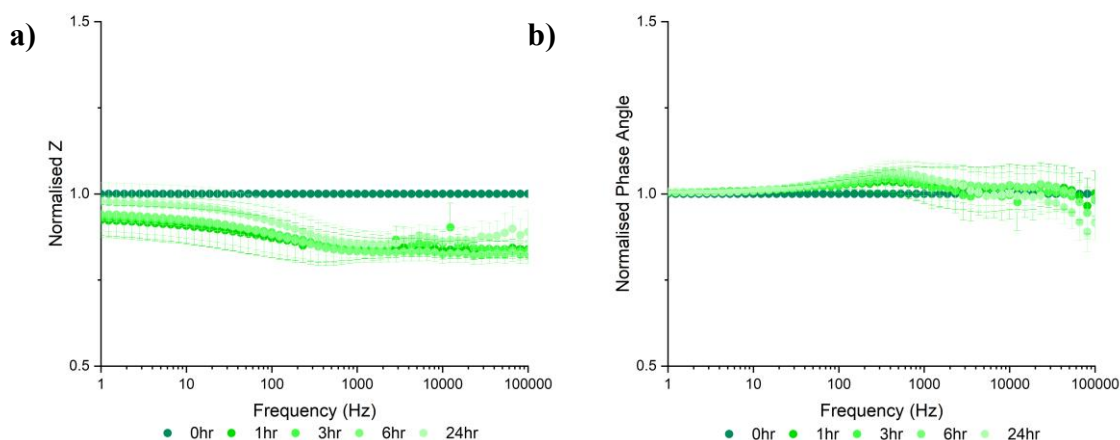


**Figure 6.7** Sterile nutrient broth incubated over 24 hours in 37°C with **a)** normalized  $Z$  and **b)** normalized phase angle from ES measurements at select time points on bare SS electrodes ( $n=3$  chambers, 9 electrodes)

The next variable tested was the bacteria concentration within the broth, since when the bacteria grow, they will attach to and colonise the electrode, but they will also be expected

to grow within the surrounding broth. Concentrations of  $10^2$  to  $10^9$  CFU/ml in nutrient broth with *S. aureus* were created through dilution after 24 hours of growth in nutrient broth. These were tested and results plotted in Figure 6.8. The impedance was found to decrease slightly with increasing bacteria concentration, especially in the 1000 to 100,000 Hz range. The phase angle was influenced by the variations in the bacteria concentration (Figure 6.8 (b)). The 100,000 Hz showed a large variation from  $10^2$  to  $10^9$  CFU/ml, going from 1.1 to 0.7. Based on bacteria growth in these experiments, a bacteria concentration of  $10^5$  CFU/ml was selected for future experiments.

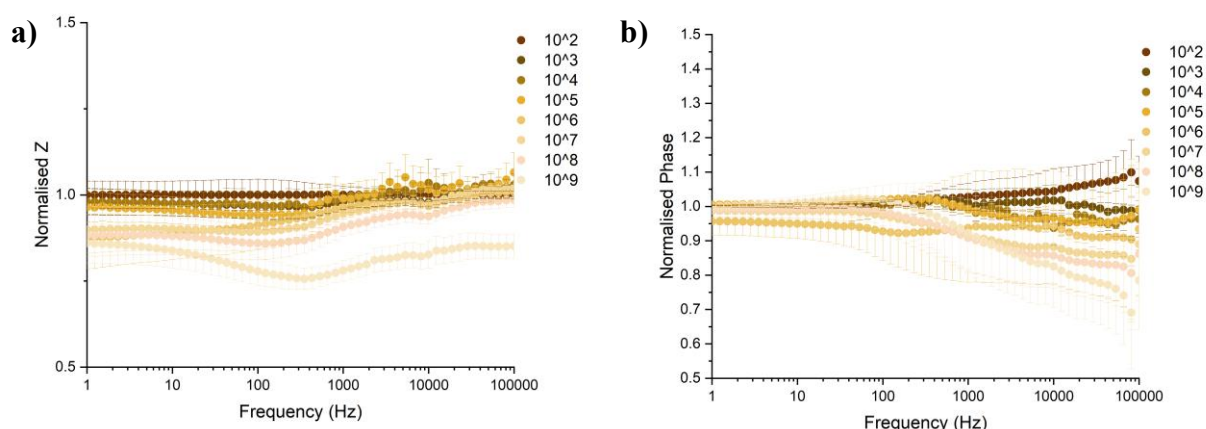


**Figure 6.8** Impedance measurements on nutrient broth with  $10^2$  to  $10^9$  CFU/ml *S. aureus* concentrations **a)** normalized Z and **b)** normalized phase angle on bare SS electrodes ( $n=3$  chambers, 9 electrodes).

ES measurements were then performed on electrodes incubated with *S. aureus* ( $10^5$  CFU) over different time periods, 24, 48 and 72 hours (Figure 6.8). The 24-hour growth had a clear difference in impedance between the 0 hour and 24 hours, specifically in the lower frequencies 1 to 100 Hz with frequencies of interest marked with solid blue lines at 10 and 100Hz. The normalised impedance dropped from 1 to 0.75, while the normalised phase

angle decreased less, having smaller differences as the bacteria grew. All impedance measurements for 24 hours had small variations between measurements. The 48- and 72-hour incubation times had similar changes, with the later incubation times having a larger drop down to  $\sim 0.6$ , but the electrode variation tended to get larger the longer the incubation time, seen specifically in Figure 6.9 e and f.

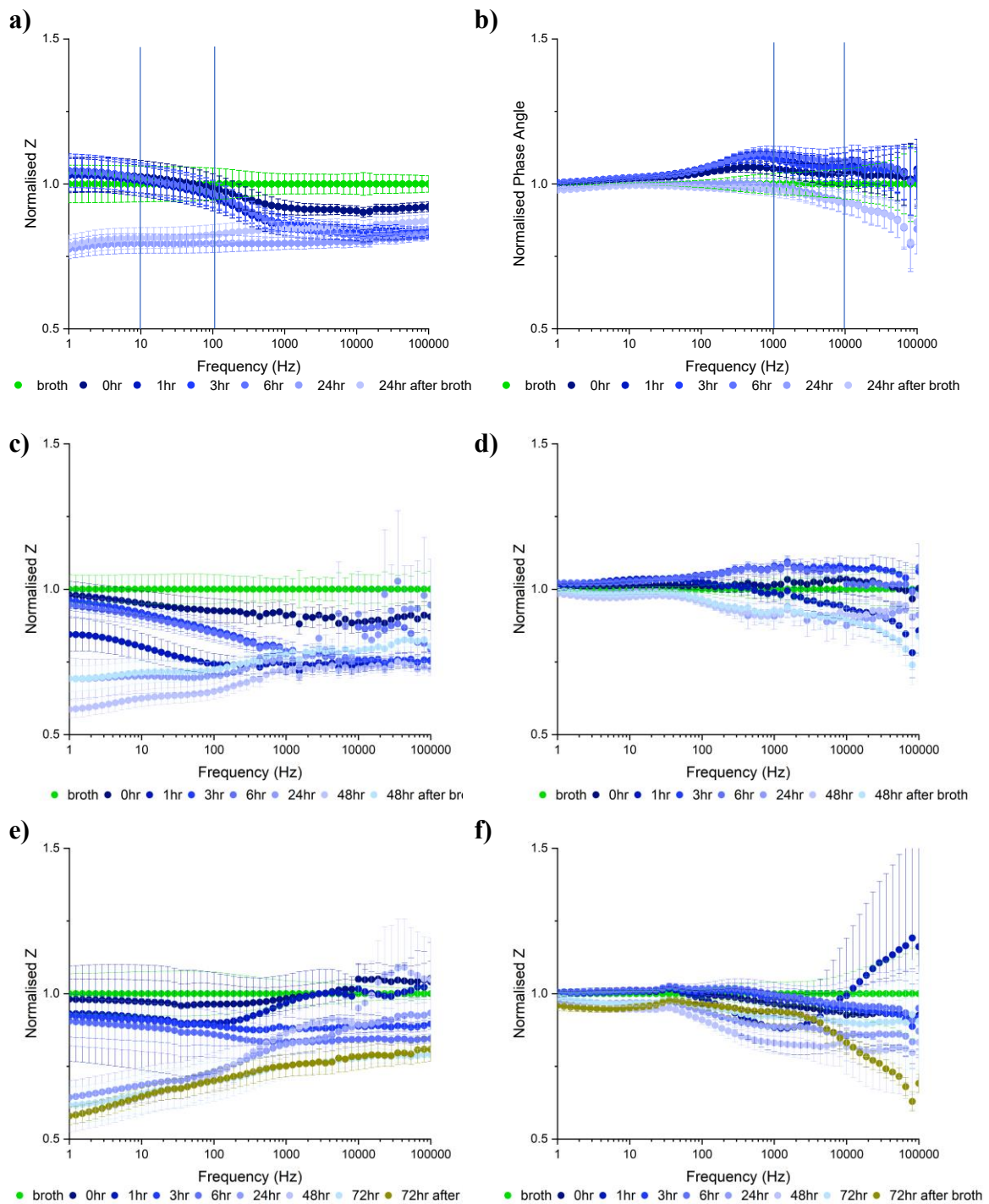


**Figure 6.9** SS electrodes with  $10^5$  CFU/ml starting population of *S. aureus* grown over 24 hours with ES measurements taken at time points across 24 hours. **a)** Normalized Z and **b)** phase angle over 24 hours, **c)** Normalized Z and **d)** phase angle over 48 hours **e)**

*Normalized Z and f) phase angle over 72 hours. Lines mark frequencies of interest based on Ward et al's procedure. After broth refers to the measurement taken after changing of broth to new sterile broth (n=3 chambers, 9 electrodes)*

The bacteria count from the surface of the electrodes for the different incubation times were plotted in Figure 6.10. This showed there was no significant difference in the bacteria counts with longer incubation. The bacteria count did not deviate significantly for longer incubation times.

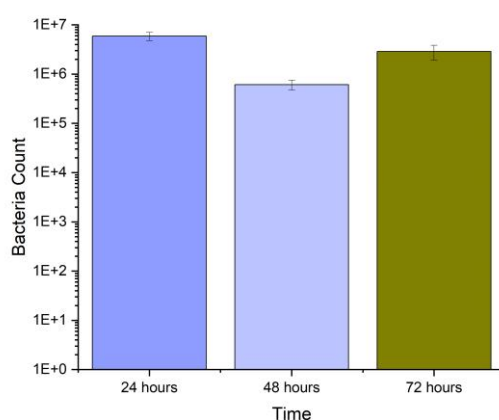


**Figure 6.10** Bacteria count of different incubation times on bare SS electrodes (n=3 chambers, 9 electrodes) with significance determine using ANOVA test.

The 24-hour results were plotted at the frequencies of interest in Figure 6.11. There is a drop in impedance and phase angle over the 24 hours, with Z experiencing a larger drop to 0.8 versus phase angle at 0.95. The 100Hz impedance did have a significant drop at the 24-hour time point versus broth.

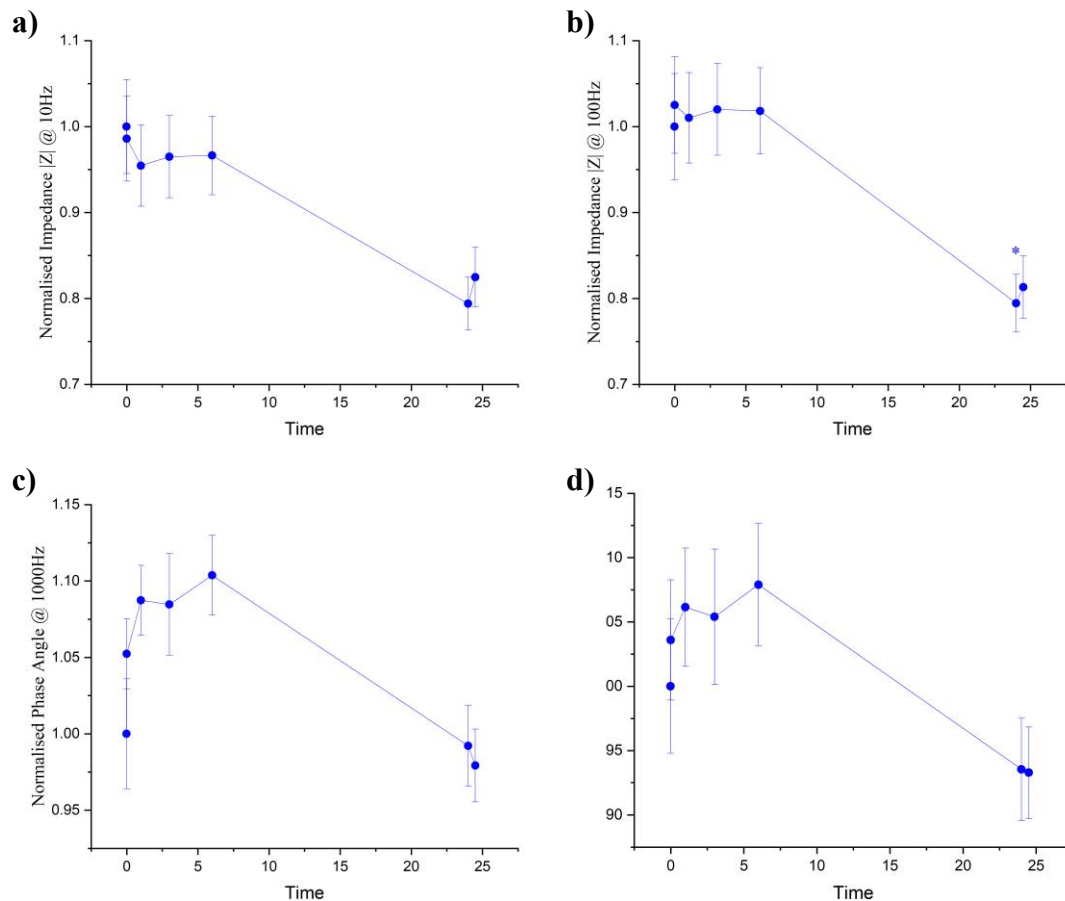


**Figure 6.11** SS electrodes with  $10^5$  CFU/ml starting population of *S. aureus* grown over 24 hours with ES measurements taken at time points across 24 hours. Normalized Z **a)** 10 Hz and **b)** 100 Hz and normalised phase angle at **c)** 1000 Hz and **d)** 10000 Hz. Significance was determined by ANOVA analysis, with Bonferroni post hoc compared between the broth measurement and all other subsequent time points.



The experiment was repeated using titanium electrodes to measure *S. aureus*. The impedance measurements had larger standard error than the SS electrodes. There is a decrease in impedance between the 1 -100 Hz range over the 24 hours, dropping to 0.75.

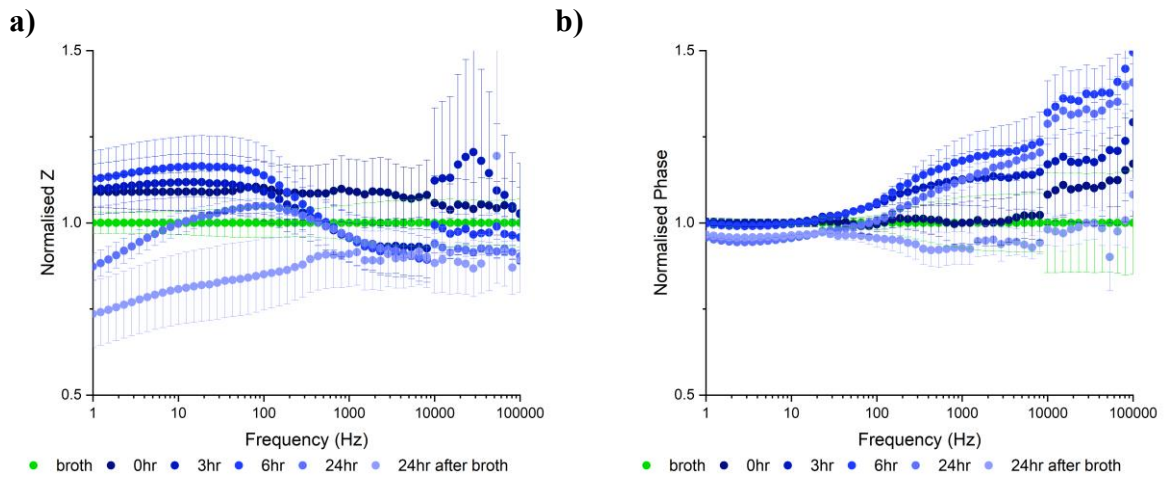


**Figure 6.12** Ti electrodes with  $10^5$  CFU/ml starting population of *S. aureus* grown over 24 hours with ES measurements taken at time points across 24 hours. **a)** Normalized Z and **b)** phase angle over 24 hours. After broth refers to the measurement taken after changing of broth to new sterile broth ( $n=3$  chambers, 9 electrodes)

The experiment was again repeated using PLGA coated electrodes to measure *S. aureus* and *P. aeruginosa*. Figure 6.13 displays the small decrease in impedance across the full spectrum for both bacteria types. The normalised data brings a clearer view of those differences observed after bacterial growth. The lower frequencies from 1 – 100 Hz has a noticeable decrease in impedance, with the largest decrease occurring between 1-10 Hz for both bacteria species. The *S. aureus* growth also had a separate peak at around 10 kHz over the 24 hours that was not in the *P. aeruginosa* data.

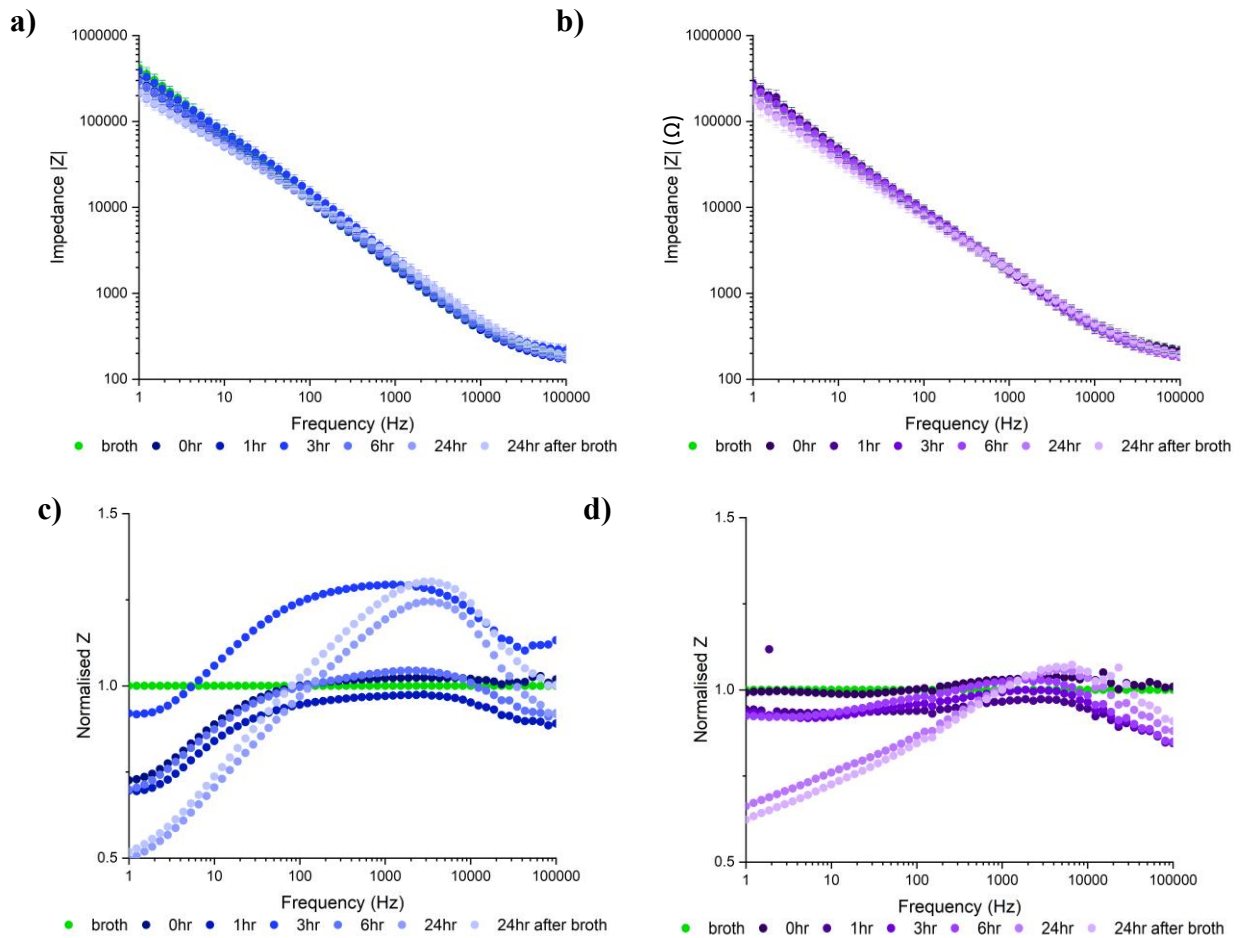


**Figure 6.13** SS electrodes with PLGA coating with  $10^5$  CFU/ml starting population of bacteria species grown over 24 hours with ES measurements taken at time points across 24 hours. **a)** Impedance spectra of *S. aureus* and **d)** *P. aeruginosa* over 24 hours. **c)** Normalized Z of *S. aureus* and **d)** *P. aeruginosa* over 24 hours. After broth refers to the measurement taken after changing of broth to new sterile broth (n=3 chambers, 9 electrodes)

### 6.3.3 ES of polymer-drug and biofilms over time

The normalized impedance and phase angle at the selected frequencies in Figure 6.11, showed a visual decrease as bacteria grew on the bare electrodes. This analysis method was applied to polymer-drug coated electrodes over clinically relevant time periods. The relative variation over 24 hours was plotted and bacteria count over time.

The relative variation of normalised impedance at 10 Hz from the impedance for broth to the 24 hour time point is shown in Figure 6.14. The bare electrodes for both *S. aureus* and *P. aeruginosa* displayed a 20% reduction in  $|Z|$  at the 24 hours, 1 week, 3week, and 2-month incubation time. The bacteria count on the electrode was in the  $10^7$  CFU range for all time periods as well. The PLGA coated electrodes had around -25% reduction in  $|Z|$  but with larger changes between measurements. The *S. aureus* bacteria count was closer to  $10^6$  CFU population, while the *P. aeruginosa* had a  $10^7$  CFU population count. The Rifampicin coated electrodes relative change went from -18% up to -10% between the 24-hour incubation and the 2-month incubation. Rifampicin had complete kill for both bacteria species in the 24-hour incubation, then *S. aureus* had partial kill still with bacteria growth only growing up to  $10^5$  CFU while *P. aeruginosa* returning back to the  $10^7$  CFU over the 2-month elution period. The 50:50 PLGA: Rifampicin coated electrodes had a -10% reduction during the 24-hour, 1 week and 3-week incubation periods. Then the final 2 month had opposite trends with *S. aureus* going to +10% and *P. aeruginosa* decreasing to -100%. *S. aureus* had complete kill after 24 hour and 1 week, then it grew up to  $10^3$  for both the 3 week and 2 months. *P. aeruginosa* had complete kill in the first 24 hours then

partial kill at 1 week with growth up to  $10^4$  before returning back to  $10^7$  for the 3 week and 2-month time points.

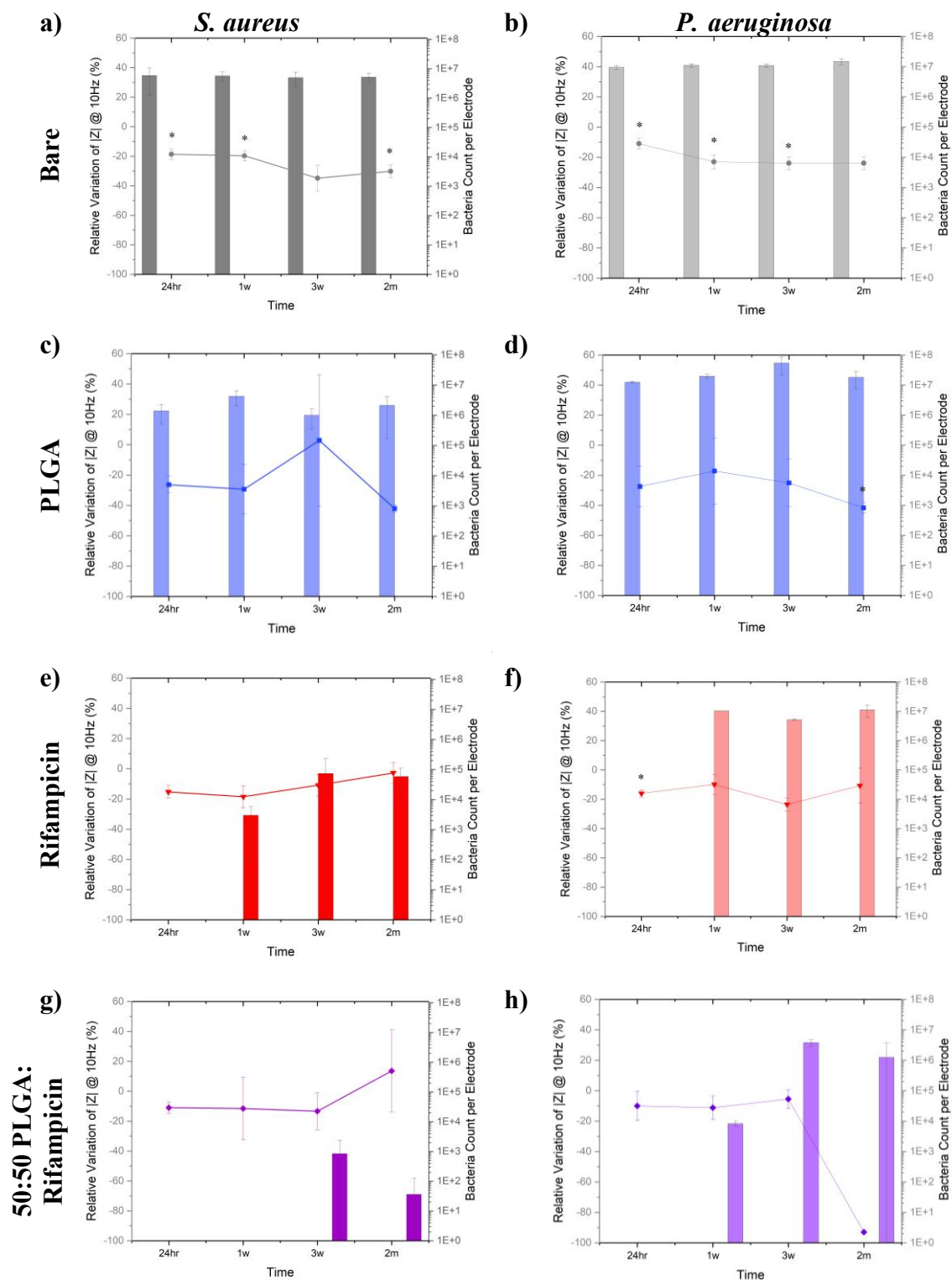


**Figure 6.14** Relative variation of normalised impedance at 10Hz in % and bacteria count per electrode for  $10^5$  CFU/ml starting population in the suspended media of *S. aureus* and *P. aeruginosa* grown over 24 hours. Bare electrode **a)** *S. aureus* **b)** and *P. aeruginosa*. PLGA coated electrode **c)** *S. aureus* **d)** and *P. aeruginosa*. Rifampicin coated electrodes **e)** *S. aureus* **f)** and *P. aeruginosa*. 50:50 PLGA: Rifampicin coated electrode **g)** *S. aureus* **h)** and *P. aeruginosa* Significance was determined by ANOVA analysis, with Bonferroni post hoc compared between the broth measurement and the 24-hour time point. (n=3)

Impedance at 100Hz, Figure 6.15, showed similar trends to 10Hz, Figure 6.13. The main difference between the two chosen frequencies was the 100Hz did not have significant impedance differences for all the bare electrodes. The *P. aeruginosa* measurements also did not have as large a reduction in the bare electrode at approximately -20%.

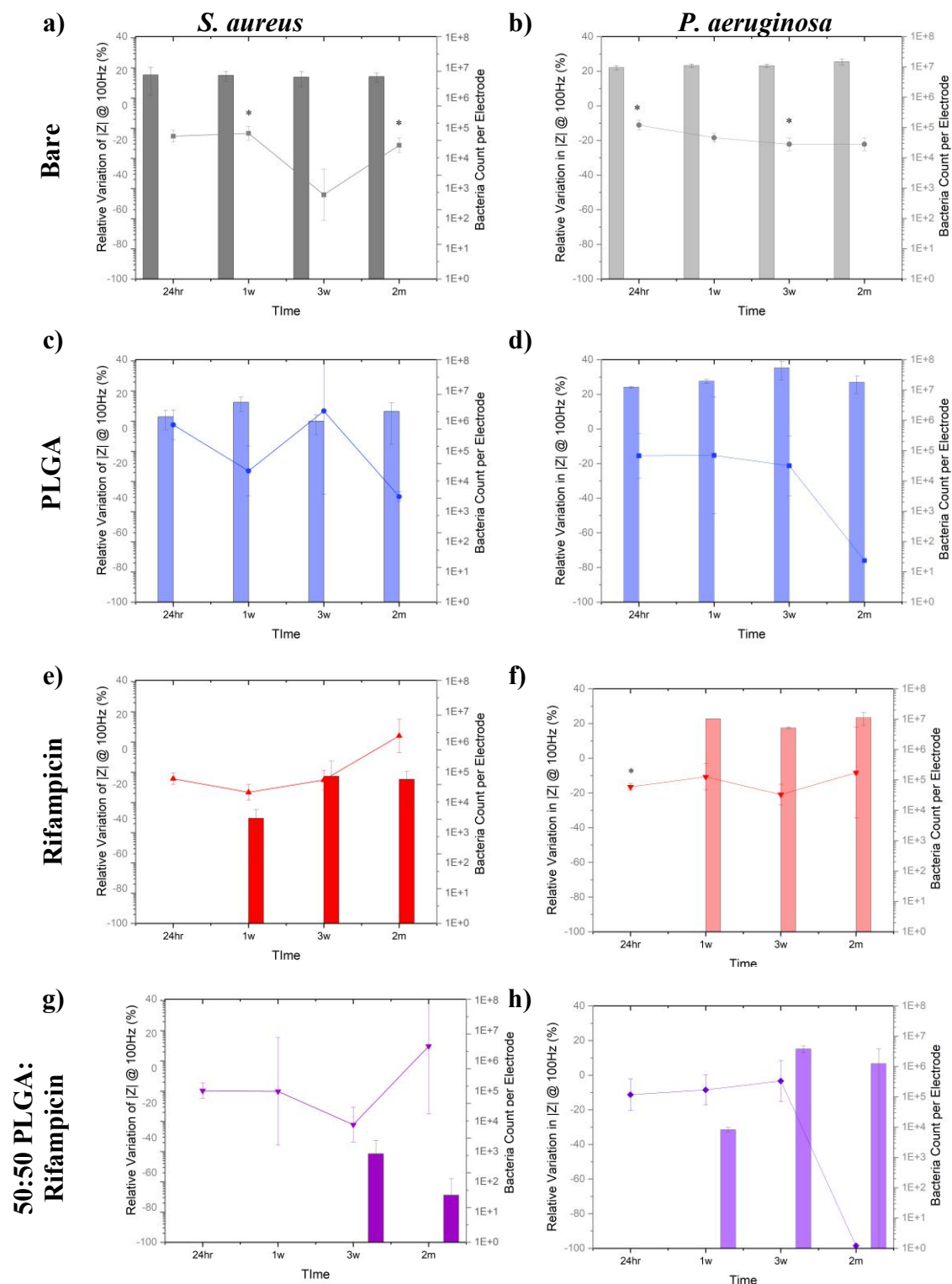


**Figure 6.15** Relative variation of normalised impedance at 100Hz in % and bacteria count per electrode for  $10^5$  CFU/ml starting population of *S. aureus* and *P. aeruginosa* grown over 24 hours. Bare electrode **a)** *S. aureus* **b)** and *P. aeruginosa*. PLGA coated electrode **c)** *S. aureus* **d)** and *P. aeruginosa*. Rifampicin coated electrodes **e)** *S. aureus* **f)** and *P. aeruginosa*. 50:50 PLGA: Rifampicin coated electrode **g)** *S. aureus* **h)** and *P. aeruginosa*. Significance was determined by ANOVA analysis, with Bonferroni post hoc compared between the broth measurement and 24-hour time point.

The normalised phase angle was also evaluated, Figure 6.16 and 6.17. At 1000 Hz, the bare electrodes had 0% change over 24 hours for all time points. The PLGA coated electrodes ranged from +20% to -20% for *S. aureus* while *P. aeruginosa* was around -10% until the 2-month period where it jumped up to +120% change in impedance. The Rifampicin coated for *S. aureus* varied from 0% to -40% over time while *P. aeruginosa* remained at 0% over all periods. The 50:50 coated electrodes also remained close to 0% change over all time periods for both bacterial species.



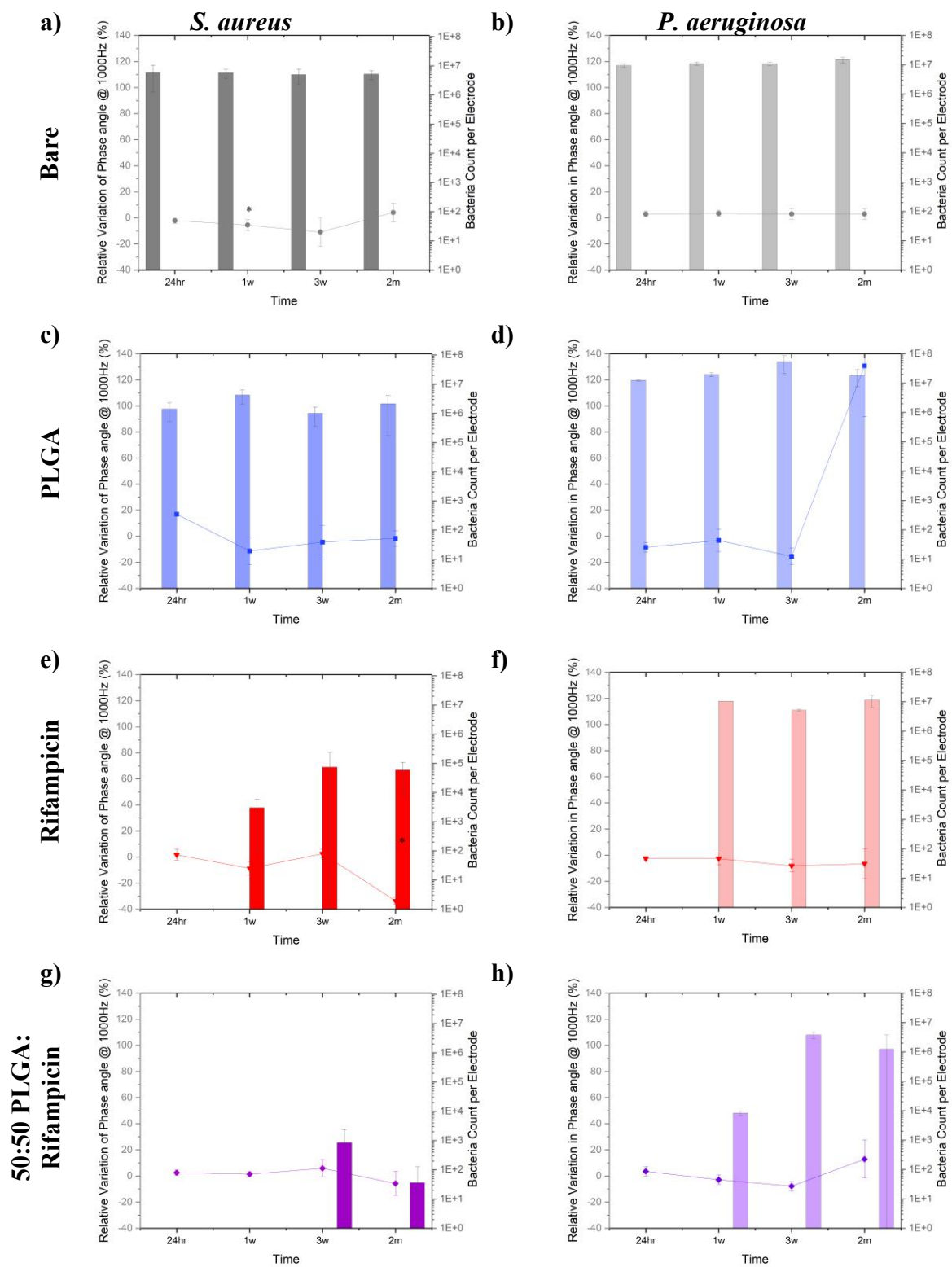


**Figure 6.16** Relative variation of normalised phase angle at 1000Hz in % and bacteria count per electrode for  $10^5$  CFU/ml starting population of *S. aureus* and *P. aeruginosa* grown over 24 hours. Bare electrode **a)** *S. aureus* **b)** and *P. aeruginosa*. PLGA coated electrode **c)** *S. aureus* **d)** and *P. aeruginosa*. Rifampicin coated electrodes **e)** *S. aureus* **f)** and *P. aeruginosa*. 50:50 PLGA: Rifampicin coated electrode **g)** *S. aureus* **h)** and *P. aeruginosa*. Significance was determined by ANOVA analysis, with Bonferroni post hoc compared between the broth measurement and 24-hour time point.

The 10 kHz normalised phase angle for the bare electrodes and 50:50 had the same trends as the 1000 Hz. The PLGA coated electrodes had varying trends for *S. aureus* while the *P. aeruginosa* decreased from 0 to -20% change in impedance over time. The Rifampicin coated electrodes also decreased over time, going from 0 to -100% for *S. aureus* and 0 to -30% for *P. aeruginosa*.

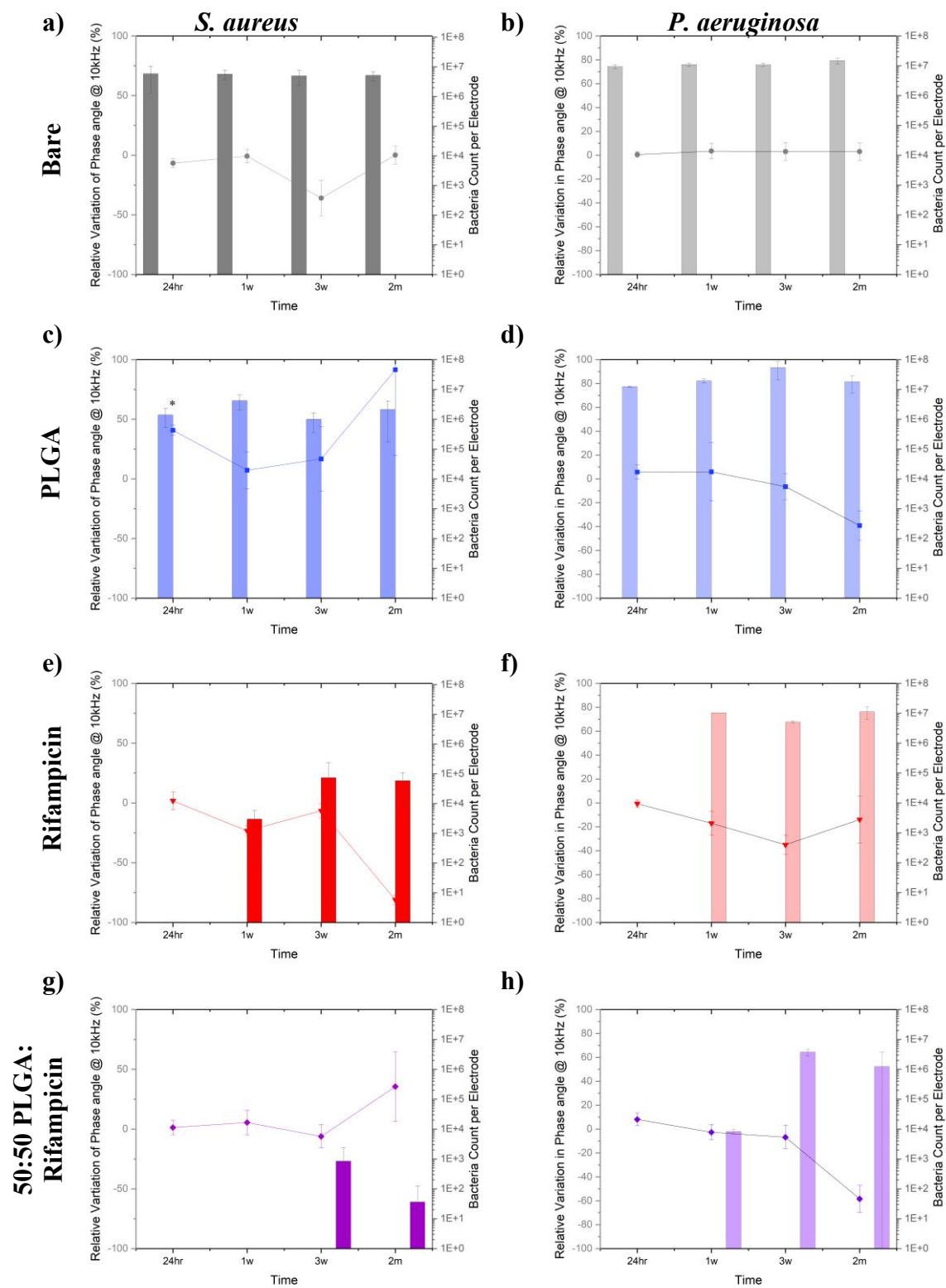


**Figure 6.17** Relative variation of normalised phase angle at 10,000 Hz in % and bacteria count per electrode for  $10^5$  CFU/ml starting population of *S. aureus* and *P. aeruginosa* grown over 24 hours. Bare electrode **a)** *S. aureus* **b)** and *P. aeruginosa*. PLGA coated electrode **c)** *S. aureus* **d)** and *P. aeruginosa*. Rifampicin coated electrodes **e)** *S. aureus* **f)** and *P. aeruginosa*. 50:50 PLGA: Rifampicin coated electrode **g)** *S. aureus* **h)** and *P. aeruginosa* Significance was determined by ANOVA analysis, with Bonferroni post hoc compared between the broth measurement and 24-hour time point.

The impedance data was plotted against the bacterial count to understand if there was a correlation between bacteria and impedance or phase angle normalised data. Figure 6.18 shows that while the bacteria count may change the impedance value does not correlate to the actual bacteria attachment to the coated electrodes.

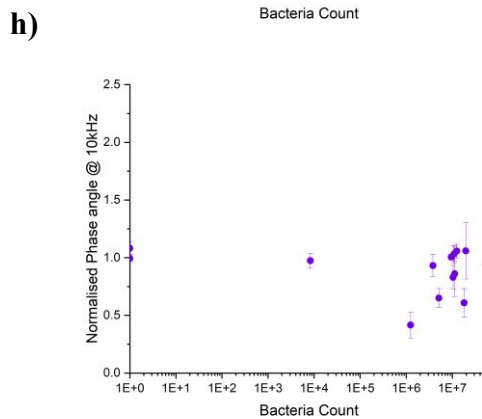
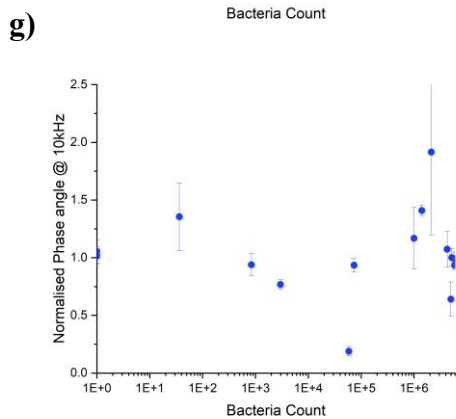
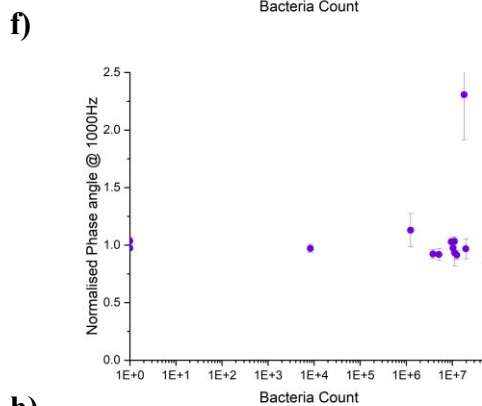
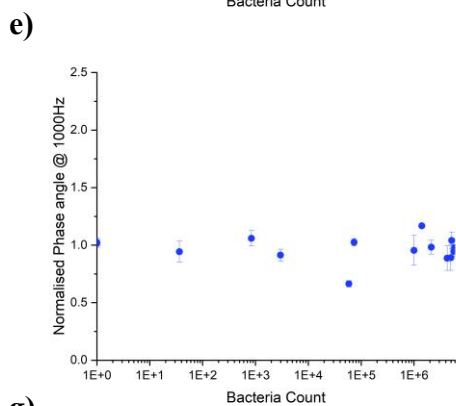
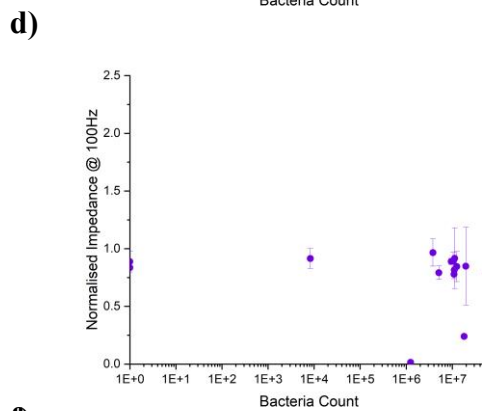
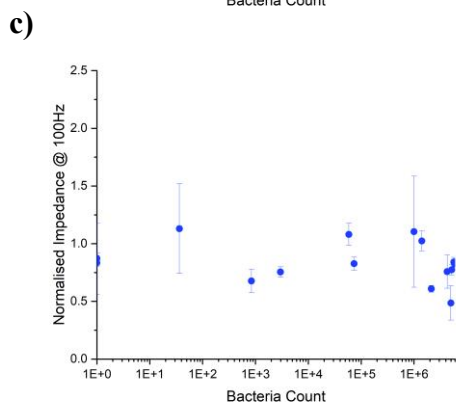
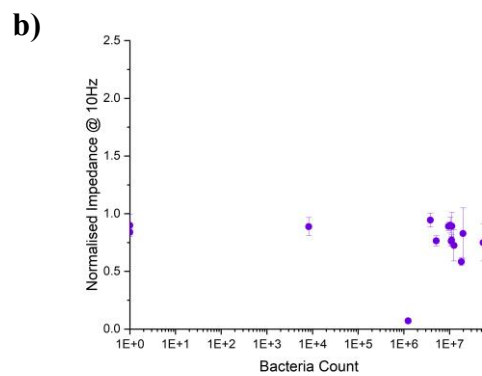
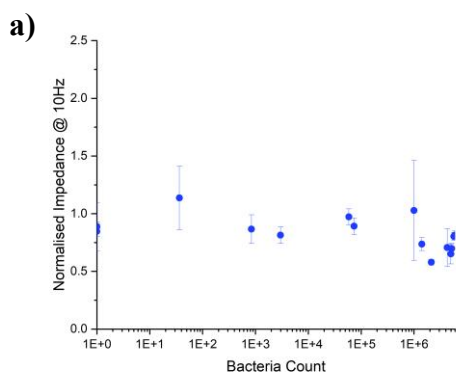


**Figure 6.18** Bacteria count of biofilm in CFU versus normalised impedance at 10 Hz **a)** *S. aureus* **b)** *P. aeruginosa*, and at 100 Hz **c)** *S. aureus* **d)** *P. aeruginosa*. Bacteria count versus normalised phase angle at 1000 Hz **e)** *S. aureus* **f)** *P. aeruginosa*, and at 10 kHz **g)** *S. aureus* **h)** *P. aeruginosa*. ( $n=3$ , electrodes=9)

The drug release profile was compared to the biofilm inhibition, calculated by bacteria count at time 0 versus bacteria count after 24 hours, for the different time points tested, Figure 6.19. The Rifampicin coated samples had a rapid release profile in the first 24 hours with 98% elution by 1 week time point. The 50:50 coating had a rapid release in the first week, with around 80% releasing then a slower release profile over the next 4 months. *S. aureus* had complete kill for both the Rifampicin and 50:50 coatings across all time points. *P. aeruginosa* had complete kill in the first 24 hours for Rifampicin coatings, then less kill over the other time points. The 50:50 coating *P. aeruginosa* had complete kill at 24 hour and 1 week, then a decrease in inhibition over the 3 week and 2-month time points.

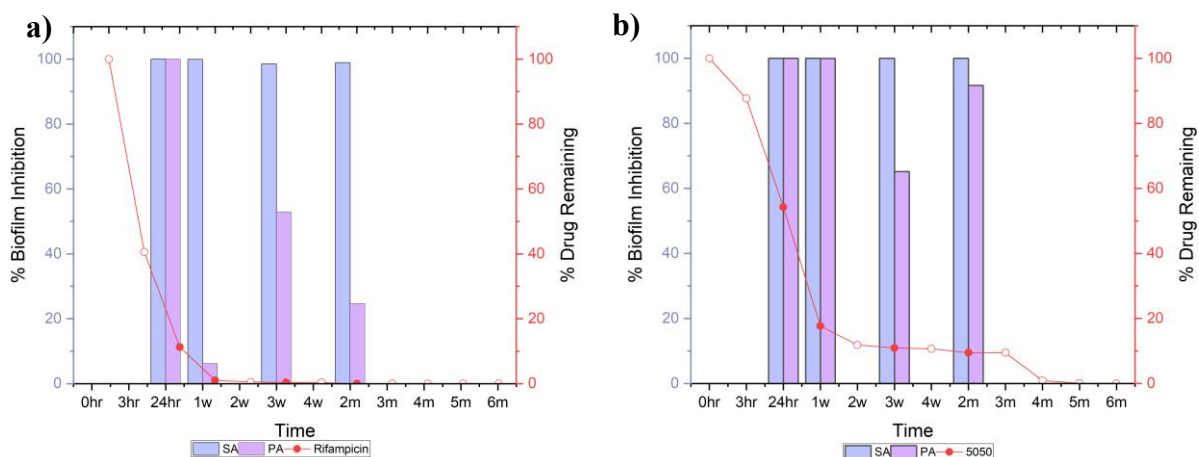


**Figure 6.19 a)** Biofilm inhibition versus drug remaining on Rifampicin coated electrodes  
**b)** biofilm inhibition versus drug remaining on 50:50 PLGA: Rifampicin coated electrodes  
 (n=9)

## 6.4 Discussion

Each section will address the main aims (Section 6.1), with focus on the different contributions that this study has made within the context of the wider literature.

The key aims of this chapter were to measure the impedance characteristics of polymer-drug coatings within a novel test cell ('new system'), the feasibility of using this system to monitor biofilm formation, develop an analysis method for measurement of biofilm formation, and determine if impedance could characterize polymer-drug coatings and biofilm formation within the same system over time.

### 6.4.1 Impedance profiles of polymer-drug coatings within new system

In chapter 4, it was determined that polymer-drug coatings could potentially be characterized through impedance spectroscopy, with changes in impedance and phase

angle observed at 10 Hz and 10 kHz consistent with expected changes within the drug-polymer coating layer. This same method was applied to the new system, with a full 6-month release study performed to determine if it could be used for such long term studies. The full impedance spectra in Figure 6.1 showed a decrease in impedance over time, but each spectrum was distinctly different for each coating type. Therefore, the chosen frequency of 10 Hz and 100 Hz for impedance and 1000 Hz and 10 kHz for phase angle allowed for more direct comparison between sample types.

The normalised impedance at 10 Hz displayed the most significant differences between the bare electrodes, SS and Ti, from all the coated electrodes in Figure 6.2. SS displayed no significant differences between the zero-hour time point and later time points but did show a slight trend of increased impedance over time. This is consistent with results reported in chapter 4 and may also be due to oxide layer formation (Kurup et al., 2021, Jelovica Badovinac et al., 2019, Wang et al., 2020). The increase occurred within the first 2 weeks then stabilizes, which coincides with the time needed for a thickened oxide layer to form (Harun et al., 2018).

The PLGA-alone coating had an almost linear decrease in impedance over the first month, with a sharper drop at the 2-month time point that then stabilizes. PLGA has an initial uptake of water, with significant degradation over 18 days then a slower degradation over 6 months to a year to fully degrade (Gentile *et al.*, 2014). This uptake of water and significant degradation may coincide with the decrease in impedance, as the water could affect the impedance through the coating and then the degradation could lead to the steady decrease. It then stabilizes as the coating slows in degradation. The Rifampicin-alone



coated electrodes had reductions in impedance over the first 3 weeks before stabilization, which corresponds to a rapid elution of the Rifampicin from the surface with 100% eluted within the first week seen in Figure 6.5. This may be due to the concentration build up in the release media, leading to the diffusion gradient to be reduced and so flux of the drug away from the surface reduces. Another possibility could be the drug finds its way into grain boundary layers within the substrate, which makes it less accessible to the aqueous phase thereby slowing release (Vo et al., 2018).

The different formulations of PLGA: Rifampicin displayed very similar impedance properties at 10 Hz and 10 kHz, with the steadily decreasing values observed over the 6 months potentially corresponding to thin film degradation profiles of PLGA (Visan, 2021). They also had significant differences between most time points and time 0 (Figure 6.2) which could be due to the release of drug opening up further porosity within the polymer coating, alongside degradation of the PLGA.

The 10 kHz normalised impedance, Figure 6.2 c and d, had similar significant levels as the 10 Hz, but the magnitude of the differences in normalised  $Z$ , between the control and the coated electrodes, were less marked than the 10 Hz datasets. This could be due to the lower frequency highlighting resistive features at the electrode-electrolyte interface as described by Shedden *et al* (2010). The normalised phase angle did not have noticeable correlation between phase angle changes and the degradation of the coating. The phase angle represents the lag of the system while impedance represents the resistive and capacitive elements of a system. In this case the impedance at 10 Hz gives greater insight into the coatings. It is common for commercial impedance systems to choose a frequency

of interest for certain applications based on the area of interest as described in Section 2.1. For this reason, the normalised impedance at 10Hz was compared directly to the drug release profiles of each sample type.

The release profiles in Figure 6.4 showed that 50:50 had the most amount of drug released, ~4.5 mg, followed by 60:40, ~3 mg, then 75:25, ~1.75 mg. Figure 6.4 b) showed that 50:50 released almost 90% of its drug within the first week, while 60:40 only released 75% and the 75:25 only released 10%. The increase in polymer delays drug release due to the coating thickness and total amount of drug encapsulated (Visan, 2021). These drug amount differences did not manifest in the normalised impedance data or the raw impedance data, with direct comparisons between normalised impedance and drug release shown in Figure 6.5 and raw impedance data compared in Figure 6.6. The drop in normalised impedance for 75:25 and 50:50 was similar at around 0.3 change in normalised impedance in the first week, while 60:40 dropped to 0.2. These impedance profiles were not significantly different from each other even though the elution profiles were very different between both quantity of drug and elution time. A noteworthy aspect to all the impedance data for these electrodes is the standard error associated with measurements are very small, indicating that electrode variations are low and so the datasets are robust.

The work of Zhong *et al* 2015, which has been discussed in detail in previous chapters, used an incubation time of 50 days. This is an important limitation, given that the grade of PLGA, PURASORB PDLG 5004, used is expected to degrade over a period of 6 months to a year. When a polymer-drug coating is made with PLGA, drug could be released months later, and it could have some effect on the antimicrobial activity. While

the overall effect of polymer-drug coatings may be evaluated through a decrease in normalised impedance, subtle differences between different polymer-drug formulations may not be easily assessed using normalised or raw impedance values.

#### **6.4.2 Impedance using medical device metals to detect biofilm formation**

Chapter 5 found that gold electrodes could be used to monitor in vitro biofilm formation, with significant characteristic changes in impedance at 10 Hz and 100 Hz. While this ideal surface can allow insight into non-invasive biofilm characterization, it does not mimic the true environment, a surface that is made of the same material as the implant with a coating, of the bacteria when forming a biofilm on an implant. This work sets out to address this gap by determining if a medical implant metal could be used to monitor biofilm formation.

A few factors were evaluated to determine what could affect the impedance measurements for the new system. Nutrient broth was evaluated for its influence on SS impedance over 24 hours, which is the longest period of time the electrodes would be incubated in nutrient broth. The 6-month incubation was performed in PBS to enable the continued use of UV-spectroscopy for easy drug concentration measurements, and only the growth of bacteria would occur in nutrient broth. Figure 6.7 shows minimal influence of the nutrient broth on the system impedances, with only a very slight decrease in the higher frequencies 1000 to 100,000 Hz possibly due to the presence of nutrients in the broth.

The impact of bacterial concentration in broth on the impedance of the system was also evaluated (Figure 6.8). The bacteria concentration in nutrient broth did not have a noticeable effect on impedance, but did appear to influence the normalised phase in the higher frequency range. The phase decreased in increments as the bacterial concentration

increased. To take this into account, impedance measurements were taken after 24 hours of growth then a second measurement was taken after refreshing the media to have measurements without free-floating bacteria. Another awareness that needed to be taken forward would be potential pellicle formation. Van Duuren *et al* showed that the cell index at 10 kHz could be influenced by pellicle formation or biofilm formers and controls which might coincide with pellicle formation (van Duuren *et al.*, 2017). The orientation of the electrodes in the new system minimizes pellicle formation as there is little air fluid contact with the well insert, this is also minimized through changing of the media after 24 hours of growth.

The growth period for bacteria was determined through evaluation of impedances after 24 hours, 48 hours, and 72-hour incubation times. This study showed that after 24 hours the biofilm had reached its full growth at  $10^7$  CFU/ml and that the longer the incubation had minimal influence on biofilm growth, or the impedance seen in Figure 6.10. The 48 hour and 72-hour impedances did not change significantly more than the 24-hour incubation impedance, as there was no additional bacteria growth this showed that biofilm maturation mainly finished after 24 hours. A study conducted by Ben-Yoav *et al* found indium-tin-oxide electrode coverage and bacteria density affected the impedance measurements, specifically the capacitance increased and resistance decreased in the first 24 hours before levelling back to the original measurements due to the biofilms composition and porosity (Ben-Yoav *et al.*, 2011). Babushkina *et al* grew enterobacteria and *P. aeruginosa* and *Acinetobacter spp* for 24 hours, 48 hours, and 72 hours finding that most strains had a significant increase in optical density of gentian violet extracts within the first 24 hours.

Enterobacteria tended to decrease in optical density significantly at 72 hours, while the *P. aeruginosa* and *Acinetobacter spp* remained relatively the same (Babushkina *et al.*, 2020). This supports that the longer incubation period might not benefit the growth of biofilms as most of the mass is produced within the first 24 hours.

Using the same method as Chapter 5, the peaks for the impedance differences was chosen and evaluated based on Ward *et al's* 2014 procedure. The impedance was evaluated at 10 Hz and 100 Hz, a frequency below 10 Hz was not chosen even with the larger impedance difference because lower frequencies can have more noise as discussed in Section 2.1. The phase angle was evaluated at 1000 Hz and 10,000 Hz, Figure 6.10. The impedance and phase angle decreased over the 24-hour incubation period but only the 100 Hz normalised impedance had a significant drop compared to the broth measurement. Farrow *et al* found that normalised impedance and phase could detect the presence of *S. aureus* in different culture media using Ag-AgCl electrodes by finding peaks within the normalised data (Farrow *et al.*, 2012). The 24-hour *S. aureus* growth was repeated on Ti electrodes and showed a decrease in impedance at 10Hz as well as a higher frequency 10,000 Hz. From the data in this study, it shows the potential of using SS and Ti as an electrode to non-invasively detect biofilm formation at specific frequencies based on peaks within the frequency range. Roughening the surface of the electrodes could enhance sensitivity of measurements and would correspond to antimicrobial techniques. Another possible technique to improve the electrode sensitivity and reduce possible noise would be to optimize the set-up including possibly altering the geometry of the electrodes, both the working and counter electrode and having more stable connections by ensuring the clips

do not rust or move. The differences in peaks for SS and Ti suggests that peak frequencies need to be chosen after a full frequency sweep as different metals may have different peaks.

#### **6.4.3 Characterize polymer-drug coatings and biofilm formation in same system over time**

The previous section concluded that medical implant metals could potentially be used to monitor biofilm growth. While this is useful for simple studies of biofilm formation, a major aim of this study was to determine if ES could also evaluate antimicrobial coating effectiveness on medical implants. This study focused on polymer-drug coatings as an antibacterial coating, specifically 50:50 PLGA: Rifampicin coatings as Section 6.3 found the impedance decrease similar and significant for all different coating formulations but 50:50 had the most drug release therefore would potentially have greater antimicrobial effects. The coatings were evaluated on both *S. aureus* and *P. aeruginosa* to potentially show Gram-negative versus Gram-positive bacterial differences, especially since Rifampicin is more effective against *S. aureus*.

Four different elution times were evaluated between 24 hours and 2 months, as the Rifampicin coating released 98% of its drug in the first week, and the 50:50 coating released 75% of drug within the first 2 months based on data in Figure 6.4.

The chosen frequencies from Section 6.3.2 were evaluated with direct comparisons to bacteria formation on the electrodes. The SS showed significant change in impedance over the 24 hours with both bacteria species for all time points at 10Hz and 100Hz. This is to be expected from the previous Section results, as both bacteria species grew up to  $10^7$  per

electrode. The PLGA coated samples had approximately the same reduction in impedance with bacteria growth up to  $3 \times 10^6$  for *S. aureus* and  $2 \times 10^7$  for *P. aeruginosa*. The reduction in impedance was not significant unlike the SS which could be due to the larger error that the PLGA coating introduced. There is still a reduction in impedance as the biofilm grows, specifically in the 10 Hz. The PLGA coating at 100 Hz had fluctuations in impedance differences for *S. aureus* which could be due to several factors like uneven biofilm growth on a coated surface or different biofilm densities since variations can also be seen in the SS electrode at 100Hz (Ben-Yoav *et al.*, 2011).

The normalised phase angle did not show a difference in magnitude over time, for SS or PLGA. This is consistent with the previous section results where phase did not show reliable trends for what was happening on the surface of the electrode.

The Rifampicin and 50:50 results did not show a trend in impedance variation versus bacterial growth. The Rifampicin and 50:50 coating had almost the same reduction in impedance but did not have bacteria growth. For the Rifampicin coating, the variation could be associated with the release of Rifampicin from the surface, since it is during the first week that most of the Rifampicin is being released, meaning that the reduction could be associated with that versus the lack of biofilm growth. The 50:50 coating also had a rapid release of Rifampicin in the first month that could attribute to the variation in impedance observed. The variation in impedance at 10 Hz and 100 Hz is approximately -10% for 50:50 versus SS and PLGA which is a larger decrease at -20%. The 50:50 coating had larger error in the variations in the longer elution time points as well which could be due to the degradation of the coating for different samples being different. This suggests

there could be overlap between the polymer-drug monitoring and biofilm growth monitoring as both show differences at 10 Hz and 100 Hz.

To investigate whether that the variation in impedance was a true representation of the impact of biofilm formation, adherent bacteria count versus normalised impedance was plotted in Figure 6.16. The bacteria count did not directly correlate to the normalised impedance, it remained relatively consistent between no bacteria or  $10^7$  bacteria formation. The impedance not reflecting the bacteria attachment for the coated electrodes may be due to the polymer-drug coating insulating the electrode and masking the bacteria effects because its influence on the impedance is greater than that of the bacteria.

When comparing drug remaining on the samples versus biofilm inhibition there is a clear correlation between kill and drug. Consistent with what is already known about its antibacterial profile (Thornsberry et al., 1983), Rifampicin exerted a greater inhibitor effect on *S. aureus* than *P. aeruginosa*. The Rifampicin coating was effective for the first week against both bacteria species then being more effective against the Gram-positive bacteria at all later time points. The impedance had a similar decrease in impedance over the full 2 months. The early 24 hour and 1 week time point decrease could be due to the drug releasing, then later time points due to the bacteria growth. For the 50:50 coating, even though very little was being eluted between 3 weeks and 2 months, there was still complete kill of the *S. aureus* species and upwards of 80% inhibition of *P. aeruginosa*. The drug could therefore have been anchored within the PLGA at the surface, thereby exerting a local antimicrobial effect. The impedance again had similar decreases in impedance across all time points which could have corresponded to the polymer-drug



degradation or the biofilm formation. A more in-depth evaluation would need to be performed in order to separate the different effects.

## **6.5 Limitations**

This study had a few limitations that will be considered in this section.

With the system design, the alligator clip connection to the electrodes experienced a significant challenge, with ~45% failure occurring by the 4-month incubation time point. This failure was typically caused by condensation onto the clip and it leading to corrosion over time. This could have affected the long term polymer-drug impedance measurements. A potential solution to this would be to remove the connectors while the samples are incubating in between time points or coating the clips to reduce moisture contact.

This study only used drug release as an evaluative method for the polymer-drug coatings as it would be most relevant to biofilm formation. An additional piece of information that could contribute to better understanding of the polymer-drug coatings would be evaluation of polymer degradation, including pitting or roughness, with the use of AFM providing potential utility for future studies.

While there were some precautions within electrode design and media change to reduce pellicle formation there might be potential for it to influence impedance measurements. A separate experiment looking specifically for pellicle formation and understanding how much it influences would be beneficial.

The last experiments performed only used the 50:50 PLGA: Rifampicin formulation on bacteria growth. These final experiments also only investigated the first 2 months of

polymer-drug coatings effectiveness on bacteria, but it was seen that the 50:50 coating was still almost 100% effective against *S. aureus*. A longer time study up to one year would therefore yield important new insights, determining how effective ES can monitor degradation and antimicrobial effectiveness.

## **6.6 Future Work**

With the limitations mentioned, there are some aspects of the study that could be expanded on in future work. This work focused on PLGA and Rifampicin as the antimicrobial methods but ideally the system would be tested on multiple types of antimicrobial coating materials and methods, to determine how effective ES would be in determining antimicrobial effectiveness.

The current study also only goes to 2 months for the PLGA: Rifampicin coatings, but there was still complete kill for the *S. aureus* therefore longer time periods could be evaluated to determine when exactly the coating is completely ineffective against the target species.

This study focused on bacteria inhibition, but there is always a chance that an antimicrobial technique may affect the surrounding cells. A testing chamber that could also grow and test cells would be a benefit to scientists as it would be multi-functional in testing the antibacterial methods against bacteria and how it affects cells.

The experiment also lacked flow; therefore, it was not an ideal mimic of the medical implant environment. It has been previously shown by Gomes and Mergulhao (Gomes and Mergulhão, 2021) that shear stress, induced by flow, significantly impacts upon biofilm formation. Future experiment with the incorporation of flow would therefore

create a better model. This study also focused on using SS as the main electrode type with some Ti experiments, but other metals such as CoCr and Nitinol would also be materials that could be evaluated as electrode materials.

The experiments focused on high bacteria starting concentration at  $10^6$  CFU/ml which produced a larger biofilm. A study on the calibration of bacteria concentrations attaching to the electrode would be a study that would provide more insight into the relationship between bacteria attachment concentration and impedance measurements, along with the influence of EPS on impedance.

## **6.7 Summary**

From this study, it can be stated that the novel system developed may be able to non-invasively characterise degradation of polymer-drug coatings on SS. It was found that 10 Hz was the best frequency to characterize polymer-drug coatings, with significant differences between time points for all polymer-drug combinations but also a significant difference between the bare metal and the coatings. However, there was only a significant difference between the highest polymer-drug formulation and the lower two formulations. The impedance measurements at 10Hz did closely follow the trends of drug release when directly compared, specifically within the first week where most of the drug was released for most of the formulations. This means the subtleties between drug quantities would be hard to differentiate using solely impedance measurements but has the potential to relate general drug release to impedance changes. A possible route to differentiate the drug measurements would be to introduce a third reference electrode to allow for voltammetry measurements that would measure drug concentrations.

Impedance spectroscopy using SS and Ti can also be used to monitor biofilm growth after 24 hours of incubation for both Gram-positive (*S. aureus*) and Gram-negative (*P. aeruginosa*) bacteria species, with 10Hz and 100Hz showing visual decreases in impedance as bacteria grew on the electrodes. The amount of incubation time did not influence impedance nor the bacterial count. There is also minimal influence on impedance from the nutrient broth or free-floating bacteria within the media.

When looking at polymer-drug and biofilm growth within the same system there was not a noticeable or significant trend between the variation in impedance over the 24 hours and bacteria growth. The bare SS electrode did have a significant variation versus the bacteria growth but the variation for the 50:50 PLGA: Rifampicin did not change as less drug was released and more bacteria grew. Therefore, at shorter time points, impedance cannot be the sole measurement method for both polymer-drug degradation and release and biofilm growth but could still provide a different insight potentially in longer time points.

This study focused on fast evaluation of biofilm and coating degradation, specifically on total impedance. Another possibly route for differentiating the different processes could be creating equivalent models and breaking the impedances into different components and seeing how those components change. Another technique could be to perform both ES and voltammetry within the same system, which could give different insights on the two different processes.

## **7 General Discussion**

### **7.1 Introduction**

Whilst medical implants have proven to be a tremendous medical innovation, serving to save lives and restore function to many people over many decades, the less common but highly problematic challenge of implant infection remains. The work described in this thesis set out to develop new knowledge in support of addressing this challenge. A review of both the clinical and wider scientific literature revealed that the development and translation of new implant materials is limited by many barriers. Fundamentally, there are important gaps in understanding of the factors that influence biofilm formation on medical implant surfaces, which in turn impedes the development of advanced materials and indeed local drug delivery strategies. There is currently no accurate way to non-invasively characterise polymer-drug coatings under conditions that match the *in vivo* environment of the devices including the material and coating. In response to these gaps in knowledge and capability, this study sought to utilize ES as a non-destructive, near real time monitoring method that would more accurately model *in vivo* conditions of an antibacterial coated implant. The main aim was for the system to simultaneously monitor polymer-drug coatings and their effect on bacteria adhesion and growth. These aims were pursued using a range of techniques, with the development of a novel impedance-based monitoring system ultimately resulting from this work. Using this system, it has been shown that the novel system can monitor bacterial adhesion on medical implant-like surfaces, including stainless steel 316L. Moreover, the degradation of polymer-drug coatings could be characterised by the system, with impedance changes observed at

specific frequencies being indicative of changes within the coating. Bacterial adhesion could also be tracked on coated surfaces, although the impedance-based method did not detect significant differences in bacteria attachment, except after the coated surfaces had incubation periods of greater than 2 months. These contributions summarised above, combined with the new knowledge and insights fully reported within chapters 4-6, can help advance understanding of medical implant infection, thereby providing opportunities to accelerate progress towards more effective treatments in future. This chapter briefly contextualises the key findings from each results chapter, with critical analyses helping to identify the most important contributions and indeed some important limitations. Taken together, this helps inform the final part of this chapter, which explores potential future directions for this work.

## **7.2 Impedance monitoring of the medical implant surfaces**

Inspired by the work first described by Shedden *et al*, 2008, a basic two-electrode system was developed and characterised. The impedance measurements made using this system were sensitive to temperature and solution mixing, consistent with previous studies (Gamry, 2022), providing confidence in the basic methodology being used and helping inform the subsequent experimental conditions adopted. Previous studies of this type in the literature have relied on the use of electrode materials that are often far removed from the materials found at the surface of medical implant materials, with the use of platinum and gold electrodes commonly reported (Magar et al., 2021, Randviir and Banks, 2013). It was therefore important to determine whether the system could provide meaningful results when medical implant materials were used as electrodes. The evidence that medical

implant materials could be used as an electrode opens up many possibilities of using implant metals as an actual electrode in different electrical monitoring systems.

Importantly, impedance profiles of varying polymer-drug formulations showed distinct variations, with higher PLGA concentrations having higher impedances which has not been previously reported and is novel from this study. The impedance also decreased over time as the polymer degraded and drug was released, with the 50:50 and 60:40 formulations showing significant differences from the control electrode. Previous studies, for example by Zhong et al (2015) have only reported impedance profiles of polymer coatings, with the present study being the first to report the use of impedance spectroscopy in analysis of polymer-drug coatings. This study has therefore provided insight into the potential relationship between physical changes within the polymer-drug coatings and the overall impedance profiles. This opened up potential opportunities for application of this system to the characterisation of a wide range of implant coatings. If an implant coating can be monitored using a non-invasive technique many more viability studies could be performed and allow for easier translation from research to clinical use.

Given the importance of the challenge of medical implant infections, it was decided to go on to determine if impedance could simultaneously monitor polymer-drug antimicrobial coatings and bacteria attachment. However, the relatively basic apparatus first investigated within this study did not allow for consistent monitoring of bacteria growth. A new system was needed to be developed to achieve all project requirements, with this forming the basis of subsequent result chapters.

### **7.3 Development of novel system for near continuous monitoring of the medical implant-bacteria interface**

Inspired by the approach to mammalian cell characterisation first reported by Holland et al, 2018, a new system was developed to simultaneously monitor antibacterial coatings and bacterial growth. Holland et al's system, in common with commercial systems (Gutierrez et al., 2016, Ward et al., 2018) and other similar systems reported in the literature (Paredes et al., 2014a, Farrow et al., 2012) were deemed unsuitable for the current study as they did not incorporate electrodes that were made from medical device metals, did not permit for easy coating of the electrodes, and did not permit easy removal of electrodes for bacteria quantification. The present study initially showed that gold and/or platinum electrodes could show significant impedance changes with growth of *S. aureus* and *P. aeruginosa* at certain frequencies. This theory was then taken forward when designing a novel system. The needs analysis provided design criteria and allowed for the development of a novel electrode system that was evaluated and found electrode variability and device variability minimal. This system was then taken forward for further testing.

### **7.4 An optimised system for exploring antimicrobial medical implant-bacteria interfaces**

The novel system developed found impedance decreased as polymer-drug coatings degraded over time. There were no distinct impedance trends between the different drug formulations that would allow for different formulations to be distinguishable from each other solely based on impedance, but general polymer-drug degradation could be



monitored with impedance. The study did show that more complex coatings could be monitored, as no previous studies had looked into impedance changes of polymer-drug coatings.

The system also showed that impedance decreased as biofilms developed on the surface of the stainless steel and titanium electrodes, including the PLGA coated electrodes. This gave novel findings into monitoring of biofilms and showed the fast evaluation method of chosen frequencies could be applied to different electrode types.

Most importantly, when combining polymer-drug monitoring with biofilm monitoring there was not a trend in impedance measurements to biofilm formation. The system could not accurately decipher between coating changes and biofilm changes within the same system using the PLGA Rifampicin coating, specifically in shorter time measurements. It therefore cannot be the sole measurement method yet within this type of scenario.

A potential route to allow for the simultaneous measurement of biofilm and polymer-drug degradation would be multiple different techniques performed on the same system, including impedance and voltammetry. Each could give different information of the surface and allow for the distinction between the two processes. If this were to be fully developed, it could be used to differentiate the effectiveness of different polymer-drug combinations would affect bacterial growth and at what time the coatings stop being as effective.

## **7.5 General Study Limitations and Future Work**

This study had a few limitations within the overall study. It focused on PLGA: Rifampicin coatings as the antimicrobial technique, but there are a wide range of antimicrobial coatings that could be studied. The simultaneous readings were also performed only to the 2-month time point, but it is known that PLGA can take up to months to degrade.

Future work could be done on the same system taken to further time points. The system could also utilize various drugs and polymers to characterize their impedance profiles. This study gave a solid understanding of PLGA: Rifampicin coatings and biofilm formation on medical implant like surfaces in a short time period.

The use of impedance in combination with voltammetry could be used not only to measure biofilm or PLGA: Rifampicin, but many other antimicrobial techniques. If each of the different techniques were characterized with biofilm growth, industry could focus on the most effective treatments. They could also find what treatments work in short term versus long term and choose the best antimicrobial technique for the specific application on implants whether that would be a long term hip replacement or short term fixation screw.

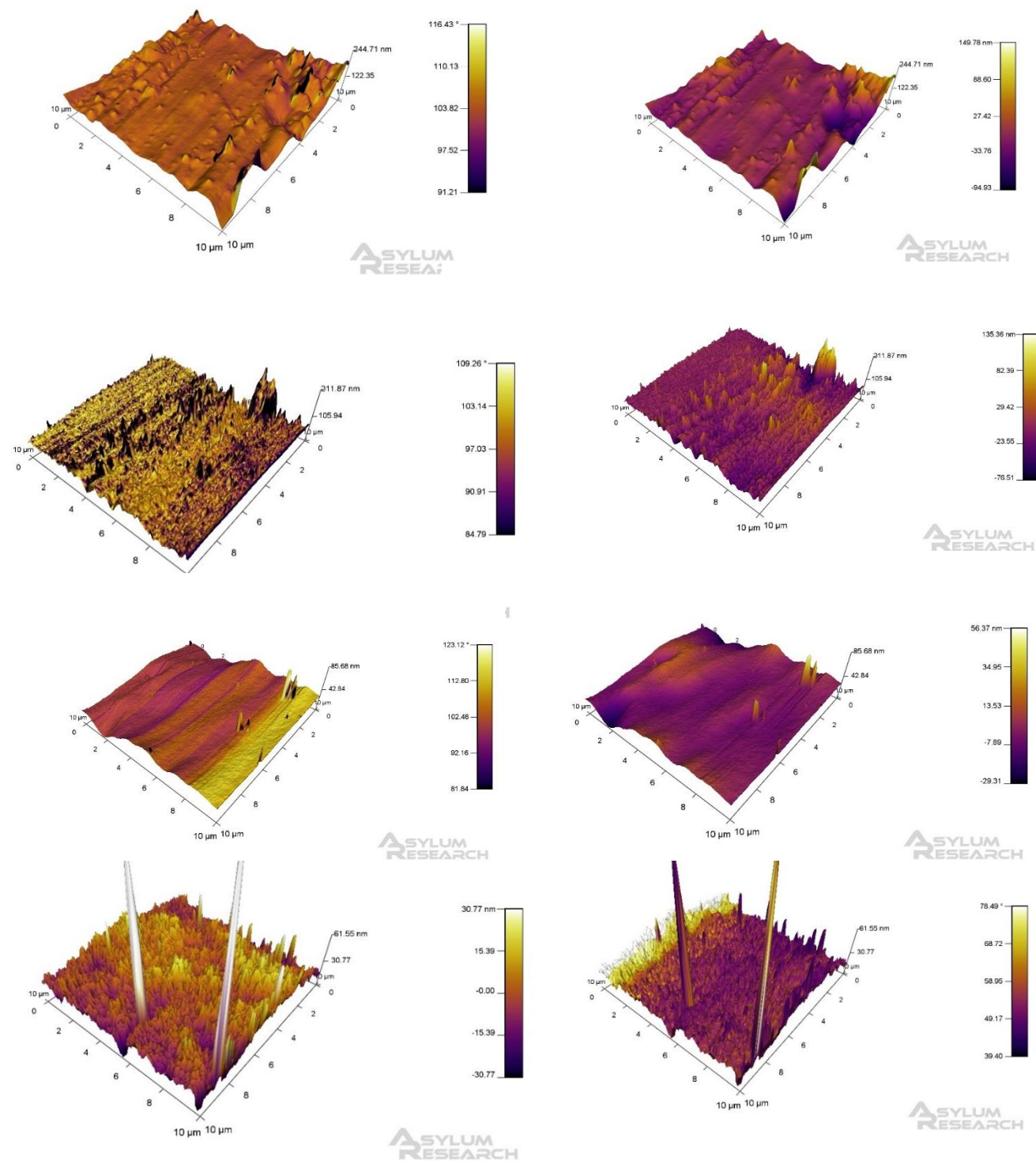
This study has potential to be further developed into a real-time assessment for implants within the body specifically any implant with a metal feature, including artificial joints, stents, or aortic graft. The implant could provide real time information on healing and potential infection to help doctors with stubborn infections before they become biofilms that are hard to treat. If this were attempted today, there would need to be an electrical connection to the implant which would introduce another possible site for infection. If a wireless system were created, this would be ideal as it would allow measurements to be

taken without the need for physical connections allowing for an implant with full ‘smart’ capabilities.

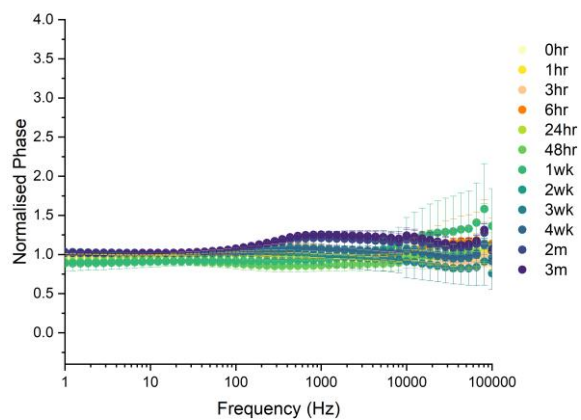
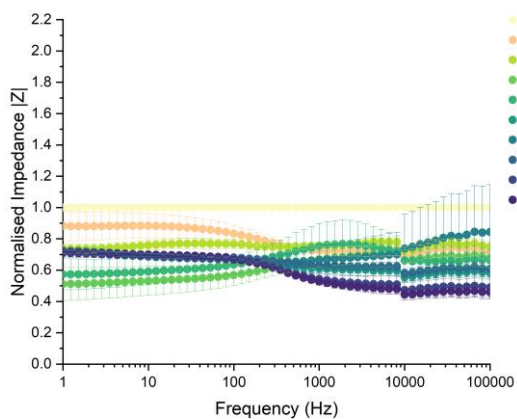
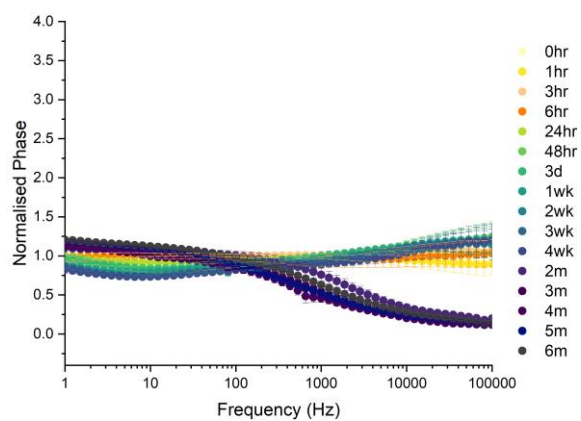
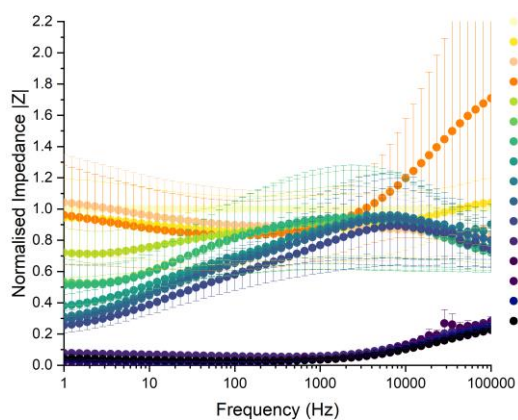
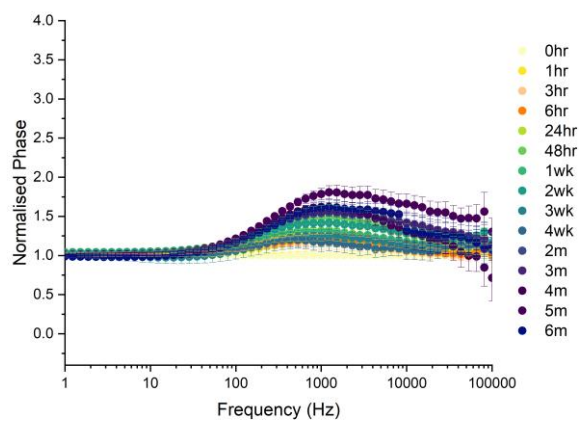
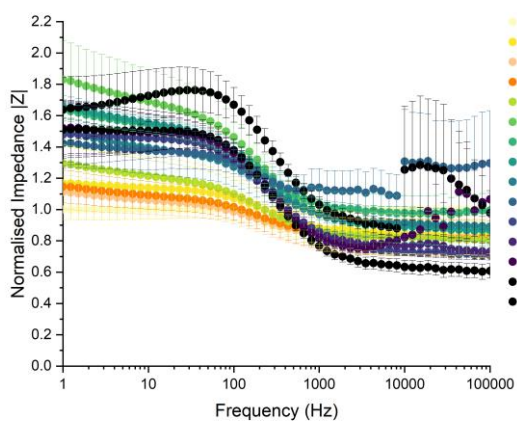
## **7.6 Summary of Contribution**

This study is the first to investigate the use of impedance spectroscopy as a means of directly tracking the response of bacteria to medical implant surfaces. Moving beyond the idealised in vitro conditions and materials used in prior work, the novel system has been used to generate new insights into the bacteria-metal implant interface. Showing that medical device metals can be used to non-invasively characterize polymer degradation and drug release. Importantly, the system may allow the investigation of bioactive polymeric coatings as the study showed that biofilm could be monitored using ES. Taken together, these contributions may be used to help accelerate progress towards the development of more effective implant materials in future through screening the effectiveness of antimicrobial techniques in real time.

8 Appendix



**Figure 8.1** AFM 3D renderings of height data and phase data. a) Bare electrode, b) 75:25 PLGA: Rifampicin, c) 60:40 PLGA: Rifampicin, and d) 50:50 PLGA: Rifampicin



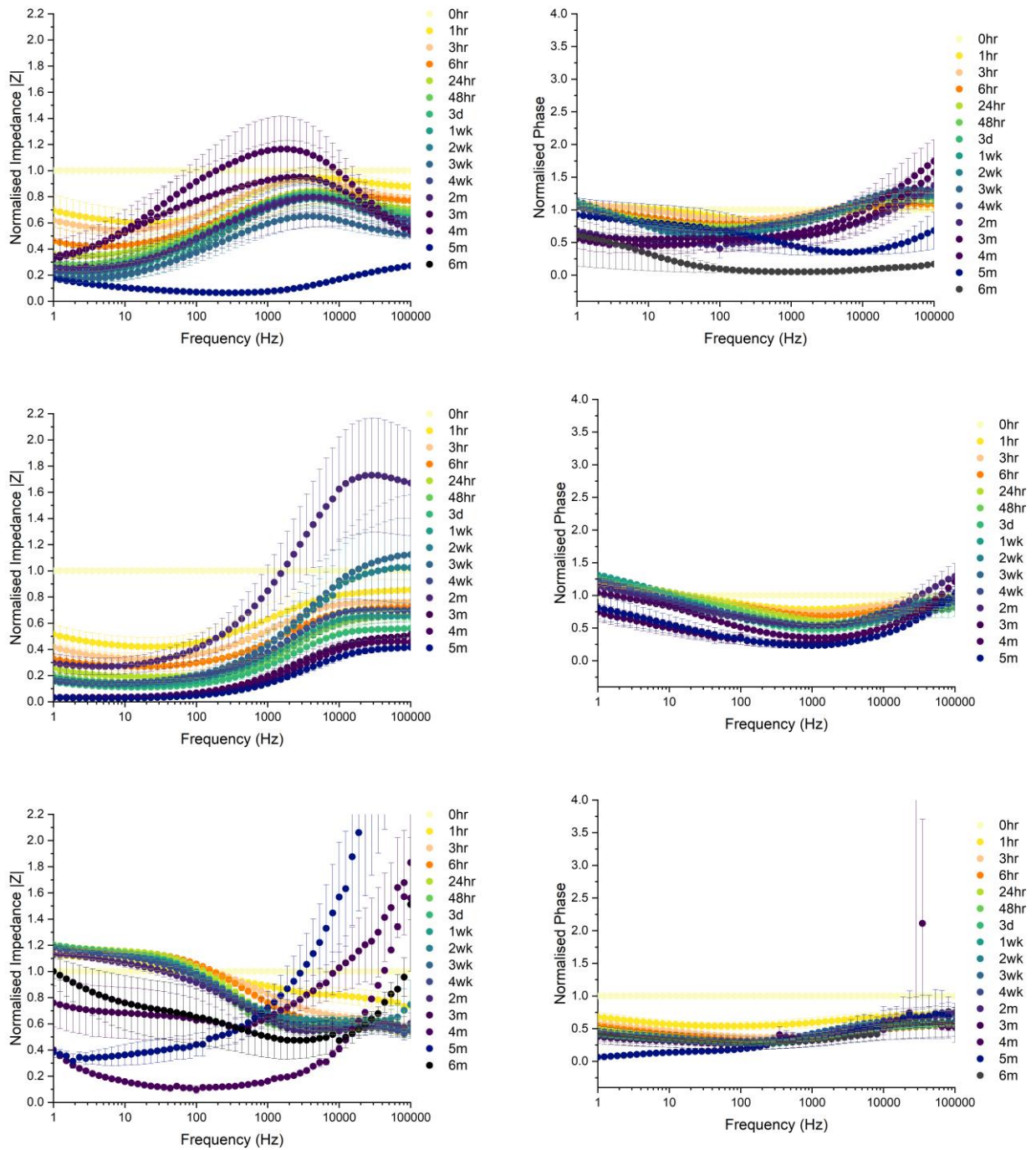


**Figure 8.2** Normalised impedance and phase angle with standard error for **a) SS b),** PLGA, **c) Rifampicin d) 75:25, e) 60:40, and f) 50:50** incubated in PBS over 6 months. ( $n=3$  chambers, 9 electrodes).

## 9 References

- ACHARYA, G. & PARK, K. 2006. Mechanisms of controlled drug release from drug-eluting stents. *Advanced Drug Delivery Reviews*, 58, 387-401.
- AKSHAYA, S., ROWLO, P. K., DUKLE, A. & NATHANAEL, A. J. 2022. Antibacterial Coatings for Titanium Implants: Recent Trends and Future Perspectives. *Antibiotics (Basel)*, 11.
- AMIDI, S., ARDAKANI, Y. H., AMIRI-AREF, M., RANJBARI, E., SEPEHRI, Z. & BAGHERI, H. 2017. Sensitive electrochemical determination of rifampicin using gold nanoparticles/poly-melamine nanocomposite. *RSC Advances*, 7, 40111-40118.
- ANGIOLINI, L., COHEN, B. & DOUHAL, A. 2019. Ultrafast dynamics of the antibiotic Rifampicin in solution. *Photochemical & Photobiological Sciences*, 18, 80-91.
- ANTONI, D., BURCKEL, H., JOSSET, E. & NOEL, G. 2015. Three-dimensional cell culture: a breakthrough in vivo. *Int J Mol Sci*, 16, 5517-27.
- ARCIOLA, C. R., CAMPOCCIA, D. & MONTANARO, L. 2018. Implant infections: adhesion, biofilm formation and immune evasion. *Nature Reviews Microbiology*, 16, 397-409.
- ARPAIA, P., CLEMENTE, F. & ZANESCO, A. 2007. Low-Invasive Diagnosis of Metallic Prosthesis Osseointegration by Electrical Impedance Spectroscopy. *IEEE Transactions on Instrumentation and Measurement*, 56, 784-789.
- ASWATHY, S. H., NARENDRAKUMAR, U. & MANJUBALA, I. 2020. Commercial hydrogels for biomedical applications. *Heliyon*, 6, e03719.
- AYYUBI, S. A. S., REHMAN, A., FATIMA, L., AHMED, M., REHMAN, M. U., ZAMEER, R. & MALIK, J. 2023. Coronary Stent Infection: A Systematic Review of Literature. *Cardiol Rev.*
- BABCOCK, K. & PRATER, C. J. D. I., SANTA BARBARA, CA 1995. Phase imaging: beyond topography.
- BABUSHKINA, I. V., BONDARENKO, A. S., ULYANOV, V. Y. & MAMONOVA, I. A. 2020. Biofilm Formation by Gram-Negative Bacteria during Implant-Associated Infection. *Bull Exp Biol Med*, 169, 365-368.
- BASIAGA, M., KAJZER, W., WALKE, W., KAJZER, A. & KACZMAREK, M. 2016. Evaluation of physicochemical properties of surface modified Ti6Al4V and Ti6Al7Nb alloys used for orthopedic implants. *Materials Science and Engineering: C*, 68, 851-860.
- BEGLY, C., ACKART, D., MYLIUS, J., BASARABA, R., CHICCO, A. J. & CHEN, T. W. 2020. Study of Real-Time Spatial and Temporal Behavior of Bacterial Biofilms Using 2-D Impedance Spectroscopy. *IEEE Transactions on Biomedical Circuits and Systems*, 14, 1051-1064.
- BEKMURZAYEVA, A., DUNCANSON, W. J., AZEVEDO, H. S. & KANAYEVA, D. 2018. Surface modification of stainless steel for biomedical applications: Revisiting a century-old material. *Materials Science and Engineering: C*, 93, 1073-1089.



- BELL, A. M., KELTSCH, N., SCHWEYEN, P., REIFFERSCHIED, G., TERNES, T. & BUCHINGER, S. 2021. UV aged epoxy coatings - Ecotoxicological effects and released compounds. *Water Res X*, 12, 100105.
- BEN-YOAV, H., FREEMAN, A., STERNHEIM, M. & SHACHAM-DIAMAND, Y. 2011. An electrochemical impedance model for integrated bacterial biofilms. *Electrochimica Acta*, 56, 7780-7786.
- BHATTACHARYA, M., WOZNAK, D. J., STOODLEY, P. & HALL-STOODLEY, L. 2015. Prevention and treatment of *Staphylococcus aureus* biofilms. *Expert review of anti-infective therapy*, 13, 1499-1516.
- BIAN, H., ZHOU, S., LIANG, X., LI, Q. & HAN, W. 2012. In vitro study of poly(ethylene carbonate) as a drug-eluting stent coating. *Progress in Natural Science: Materials International*, 22, 295-302.
- BING, L. X., AT; LIANG, YS; HUANG, Z; QIAO, ZX; XIA, DH 2012. Evaluation on protective performance of organic coatings by analyzing the change rate of phase angle at high frequency. *Int J Eletrochem*, 7.
- BOHINC, K., DRAŽIĆ, G., ABRAM, A., JEVŠNIK, M., JERŠEK, B., NIPČ, D., KURINČIČ, M. & RASPOR, P. 2016. Metal surface characteristics dictate bacterial adhesion capacity. *International Journal of Adhesion and Adhesives*, 68, 39-46.
- BORDBAR-KHIABANI, A. & GASIK, M. 2022. Smart Hydrogels for Advanced Drug Delivery Systems. *Int J Mol Sci*, 23.
- BRACERAS, I., PACHA-OLIVENZA, M. A., CALZADO-MARTÍN, A., MULTIGNER, M., VERA, C., BRONCANO, L. L., GALLARDO-MORENO, A. M., GONZÁLEZ-CARRASCO, J. L., VILABOA, N. & GONZÁLEZ-MARTÍN, M. L. 2014. Decrease of *Staphylococcal* adhesion on surgical stainless steel after Si ion implantation. *Applied Surface Science*, 310, 36-41.
- BRYERS, J. D. 2008. Medical biofilms. *Biotechnology and Bioengineering*, 100, 1-18.
- BUSSCHER, H. J., ALT, V., VAN DER MEI, H. C., FAGETTE, P. H., ZIMMERLI, W., MORIARTY, T. F., PARVIZI, J., SCHMIDMAIER, G., RASCHKE, M. J., GEHRKE, T., BAYSTON, R., BADDOUR, L. M., WINTERTON, L. C., DAROUICHE, R. O. & GRAINGER, D. W. 2019. A Trans-Atlantic Perspective on Stagnation in Clinical Translation of Antimicrobial Strategies for the Control of Biomaterial-Implant-Associated Infection. *ACS Biomaterials Science & Engineering*, 5, 402-406.
- CADY, P., DUFOUR, S. W., SHAW, J. & KRAEGER, S. J. 1978. Electrical impedance measurements: rapid method for detecting and monitoring microorganisms. *J Clin Microbiol*, 7, 265-72.
- CASEY FOX, W. & MILLER, M. A. 1993. Osseous implant for studies of biomaterials using an in vivo electrochemical transducer. *Journal of Biomedical Materials Research*, 27, 763-773.
- CHANG, Y.-W., FRAGKOPOULOS, A. A., MARQUEZ, S. M., KIM, H. D., ANGELINI, T. E. & FERNÁNDEZ-NIEVES, A. 2015. Biofilm formation in geometries with different surface curvature and oxygen availability. *New Journal of Physics*, 17, 033017.

- CONNAUGHTON, A., CHILDS, A., DYLEWSKI, S. & SABESAN, V. J. 2014. Biofilm Disrupting Technology for Orthopedic Implants: What's on the Horizon? *Frontiers in medicine*, 1, 22-22.
- DAROUICHE, R. O. 2004. Treatment of Infections Associated with Surgical Implants. *New England Journal of Medicine*, 350, 1422-1429.
- DAVIDSON, D. J., SPRATT, D. & LIDDLE, A. D. 2019. Implant materials and prosthetic joint infection: the battle with the biofilm. *EFORT Open Rev*, 4, 633-639.
- DE LEÓN, S. E., PUPOVAC, A. & MCARTHUR, S. L. 2020. Three-Dimensional (3D) cell culture monitoring: Opportunities and challenges for impedance spectroscopy. *Biotechnology and Bioengineering*, 117, 1230-1240.
- DE MEO, D., CECCARELLI, G., IAIANI, G., LO TORTO, F., RIBUFFO, D., PERSIANI, P. & VILLANI, C. 2021. Clinical Application of Antibacterial Hydrogel and Coating in Orthopaedic and Traumatology Surgery. *Gels*, 7.
- DEL AGUA, I., MARINA, S., PITSALIDIS, C., MANTIONE, D., FERRO, M., IANDOLO, D., SANCHEZ-SANCHEZ, A., MALLIARAS, G. G., OWENS, R. M. & MECERREYES, D. 2018. Conducting Polymer Scaffolds Based on Poly(3,4-ethylenedioxythiophene) and Xanthan Gum for Live-Cell Monitoring. *ACS Omega*, 3, 7424-7431.
- DEL POZO, J. L. & PATEL, R. 2007. The Challenge of Treating Biofilm-associated Bacterial Infections. *Clinical Pharmacology & Therapeutics*, 82, 204-209.
- DÍAZ, I., PACHA-OLIVENZA, M., TEJERO, R., ANITUA, E., GONZÁLEZ-MARTÍN, M. L., ESCUDERO, M. L. & GARCÍA-ALONSO, M. C. 2018. Corrosion behavior of surface modifications on titanium dental implant. In situ bacteria monitoring by electrochemical techniques. *J Biomed Mater Res B Appl Biomater*, 106, 997-1009.
- DOLL, K., JONGSTHAPHONGPUN, K. L., STUMPP, N. S., WINKEL, A. & STIESCH, M. 2016. Quantifying implant-associated biofilms: Comparison of microscopic, microbiologic and biochemical methods. *Journal of Microbiological Methods*, 130, 61-68.
- DONLAN, R. M. & COSTERTON, J. W. 2002. Biofilms: survival mechanisms of clinically relevant microorganisms. *Clinical microbiology reviews*, 15, 167-193.
- ELTORAI, A. E., HAGLIN, J., PERERA, S., BREA, B. A., RUTTIMAN, R., GARCIA, D. R., BORN, C. T. & DANIELS, A. H. 2016. Antimicrobial technology in orthopedic and spinal implants. *World J Orthop*, 7, 361-9.
- ENGINEER, C., PARIKH, J., RAVAL, A. J. T. I. B. & ORGANS, A. 2011. Review on hydrolytic degradation behavior of biodegradable polymers from controlled drug delivery system. 25.
- EVANS, H. E. 2001. Oxidation. In: BUSCHOW, K. H. J., CAHN, R. W., FLEMINGS, M. C., ILSCHNER, B., KRAMER, E. J., MAHAJAN, S. & VEYSSIÈRE, P. (eds.) *Encyclopedia of Materials: Science and Technology*. Oxford: Elsevier.
- EXTREMINA, C. I., COSTA, L., AGUIAR, A. I., PEIXE, L. & FONSECA, A. P. 2011. Optimization of processing conditions for the quantification of enterococci biofilms using microtitre-plates. *Journal of Microbiological Methods*, 84, 167-173.

- FAN, C., LIU, Y., YIN, X., SHI, J. & DILGER, K. 2021. Electrochemical Behavior and Interfacial Delamination of a Polymer-Coated Galvanized Steel System in Acid Media. *ACS Omega*, 6, 20331-20340.
- FARROW, M. J., HUNTER, I. S. & CONNOLLY, P. 2012. Developing a real time sensing system to monitor bacteria in wound dressings. *Biosensors (Basel)*, 2, 171-88.
- FATTAH-ALHOSSEINI, A., TAHERI SHOJA, S., HEYDARI ZEBARDAST, B. & MOHAMADIAN SAMIM, P. 2011. An Electrochemical Impedance Spectroscopic Study of the Passive State on AISI 304 Stainless Steel. *International Journal of Electrochemistry*, 2011, 152143.
- FEARING, B. V., AFETSE, K. E., SEYMOUR, R. B., WENKE, J. C. & HSU, J. R. 2022. Orthopaedic Implant Coatings: Recent Approaches and Clinical Translation. *J Surg Orthop Adv*, 31, 169-176.
- FERGUSON, R. J., PALMER, A. J., TAYLOR, A., PORTER, M. L., MALCHAU, H. & GLYN-JONES, S. 2018. Hip replacement. *Lancet*, 392, 1662-1671.
- GAMRY. 2022. *Basics of Electrochemical Impedance Spectroscopy* [Online]. Gamry Instruments. Available: <https://www.gamry.com/application-notes/EIS/basics-of-electrochemical-impedance-spectroscopy/> [Accessed].
- GAO, X. & WHITE, H. 1995. Rotating microdisk voltametry. *Anal Chem.*, 67:4057-64.
- GENTILE, P., CHIONO, V., CARMAGNOLA, I. & HATTON, P. V. 2014. An overview of poly(lactic-co-glycolic) acid (PLGA)-based biomaterials for bone tissue engineering. *Int J Mol Sci*, 15, 3640-59.
- GEORGAKOPOULOS-SOARES, I., PAPAZOGLU, E. L., KARMIRIS-OBRATAŃSKI, P., KARKALOS, N. E. & MARKOPOULOS, A. P. 2023. Surface antibacterial properties enhanced through engineered textures and surface roughness: A review. *Colloids and Surfaces B: Biointerfaces*, 231, 113584.
- GIAEVER, I. & KEESE, C. R. 1986. Use of Electric Fields to Monitor the Dynamical Aspect of Cell Behavior in Tissue Culture. *IEEE Transactions on Biomedical Engineering*, BME-33, 242-247.
- GIAEVER, I. & KEESE, C. R. 1993. A morphological biosensor for mammalian cells. *Nature*, 366, 591-592.
- GOMES, L. C. & MERGULHÃO, F. J. M. 2021. A Selection of Platforms to Evaluate Surface Adhesion and Biofilm Formation in Controlled Hydrodynamic Conditions. *Microorganisms*, 9.
- GUTIERREZ, D., HIDALGO-CANTABRANA, C., RODRIGUEZ, A., GARCIA, P. & RUAS-MADIEDO, P. 2016. Monitoring in Real Time the Formation and Removal of Biofilms from Clinical Related Pathogens Using an Impedance-Based Technology. *PLoS One*, 11, e0163966.
- HANAWA, T. 2012. Research and development of metals for medical devices based on clinical needs. *Science and technology of advanced materials*, 13, 064102-064102.
- HANNAH, S., ADDINGTON, E., ALCORN, D., SHU, W., HOSKISSON, P. A. & CORRIGAN, D. K. 2019. Rapid antibiotic susceptibility testing using low-cost, commercially available screen-printed electrodes. *Biosensors and Bioelectronics*, 145, 111696.

- HANSEN, E. 2020. *Total Hip Replacement Surgical Procedure* [Online]. Arthritis-health. Available: <https://www.arthritis-health.com/surgery/hip-surgery/total-hip-replacement-surgical-procedure> [Accessed 07/12 2020].
- HARUN, W. S. W., MOHD ASRI, R., RAHMAN, F., SHARIF, S., MOHD JAN, N. H. & TSUMORI, F. 2018. Surface characterisation and corrosion behaviour of oxide layer for SLMed-316L stainless steel. *Journal of Alloys and Compounds*, 748.
- HOLLAND, I. 2017. Towards non-invasive characterisation of reendothelialisation and restenosis following coronary stenting: an in vitro investigation using impedance spectroscopy.
- HOLLAND, I., MCCORMICK, C. & CONNOLLY, P. 2018. Towards non-invasive characterisation of coronary stent re-endothelialisation - An in-vitro, electrical impedance study. *PLoS One*, 13, e0206758.
- HU, C. Y. & YOON, T.-R. 2018. Recent updates for biomaterials used in total hip arthroplasty. *Biomaterials research*, 22, 33-33.
- HUOTARI, K., PELTOLA, M. & JÄMSEN, E. 2015. The incidence of late prosthetic joint infections: a registry-based study of 112,708 primary hip and knee replacements. *Acta Orthop*, 86, 321-5.
- INCOSE. 2022. *INCOSE Guide to Writing Requirements V3.1 – Summary Sheet* [Online]. Available: [https://www.incose.org/docs/default-source/working-groups/requirements-wg/rwg\\_products/incose\\_rwg\\_gtwr\\_summary\\_sheet\\_2022.pdf?sfvrsn%3Da95a6fc7\\_2](https://www.incose.org/docs/default-source/working-groups/requirements-wg/rwg_products/incose_rwg_gtwr_summary_sheet_2022.pdf?sfvrsn%3Da95a6fc7_2) [Accessed].
- JACKSON, B. M. & CARPENTER, J. P. 2009. Devices used for endovascular aneurysm repair: past, present, and future. *Semin Intervent Radiol*, 26, 39-43.
- JAHANMARD, F., CROES, M., CASTILHO, M., MAJED, A., STEENBERGEN, M. J., LIETAERT, K., VOGELY, H. C., VAN DER WAL, B. C. H., STAPELS, D. A. C., MALDA, J., VERMONDEN, T. & AMIN YAVARI, S. 2020. Bactericidal coating to prevent early and delayed implant-related infections. *Journal of Controlled Release*, 326, 38-52.
- JELOVICA BADOVINAC, I., KAVRE PILTAVER, I., PETER, R., SARIC, I. & PETRAVIC, M. 2019. Formation of oxides on CoCrMo surfaces at room temperature: An XPS study. *Applied Surface Science*, 471, 475-481.
- JHA, P. K., DALLAGI, H., RICHARD, E., DELEPLACE, M., BENEZECH, T. & FAILLE, C. 2022. Does the vertical vs horizontal positioning of surfaces affect either biofilm formation on different materials or their resistance to detachment? *Food Control*, 133, 108646.
- JIAO, J., ZHANG, S., QU, X. & YUE, B. 2021. Recent Advances in Research on Antibacterial Metals and Alloys as Implant Materials. *Front Cell Infect Microbiol*, 11, 693939.
- KARGUPTA, R., BOK, S., DARR, C. M., CRIST, B. D., GANGOPADHYAY, K., GANGOPADHYAY, S. & SENGUPTA, S. 2014. Coatings and surface modifications imparting antimicrobial activity to orthopedic implants. *Wiley Interdiscip Rev Nanomed Nanobiotechnol*, 6, 475-495.
- KHAN, A. U., SHAH, F., KHAN, R. A., ISMAIL, B., KHAN, A. M. & MUHAMMAD, H. 2021. Preconcentration of rifampicin prior to its efficient spectroscopic

- determination in the wastewater samples based on a nonionic surfactant. *Turk J Chem*, 45, 1201-1209.
- KHATOON, Z., MCTIERNAN, C. D., SUURONEN, E. J., MAH, T. F. & ALARCON, E. I. 2018. Bacterial biofilm formation on implantable devices and approaches to its treatment and prevention. *Heliyon*, 4, e01067.
- KIM, T., KANG, J., LEE, J.-H. & YOON, J. 2011a. Influence of attached bacteria and biofilm on double-layer capacitance during biofilm monitoring by electrochemical impedance spectroscopy. *Water Research*, 45, 4615-4622.
- KIM, T., KANG, J., LEE, J. H. & YOON, J. 2011b. Influence of attached bacteria and biofilm on double-layer capacitance during biofilm monitoring by electrochemical impedance spectroscopy. *Water Res*, 45, 4615-22.
- KIM, T., KANG, J., LEE, J. H. & YOON, J. 2011c. Influence of attached bacteria and biofilm on double-layer capacitance during biofilm monitoring by electrochemical impedance spectroscopy. *Water Research*, 45, 4615-22.
- KOCIJAN, A., MILOSEV, I. & PIHLAR, B. 2004. Cobalt-based alloys for orthopaedic applications studied by electrochemical and XPS analysis. *J Mater Sci Mater Med*, 15, 643-50.
- KUL, D. 2020. Electrochemical Determination of Rifampicin Based on Its Oxidation Using Multi-Walled Carbon Nanotube-Modified Glassy Carbon Electrodes. *Turkish journal of pharmaceutical sciences*, 17, 398-407.
- KURUP, A., DHATRAK, P. & KHASNIS, N. 2021. Surface modification techniques of titanium and titanium alloys for biomedical dental applications: A review. *Materials Today: Proceedings*, 39, 84-90.
- LEE, S. M., HAN, N., LEE, R., CHOI, I. H., PARK, Y. B., SHIN, J. S. & YOO, K. H. 2016. Real-time monitoring of 3D cell culture using a 3D capacitance biosensor. *Biosens Bioelectron*, 77, 56-61.
- LEI, K. F., LIU, T. K. & TSANG, N. M. 2018. Towards a high throughput impedimetric screening of chemosensitivity of cancer cells suspended in hydrogel and cultured in a paper substrate. *Biosens Bioelectron*, 100, 355-360.
- LI, B. & WEBSTER, T. J. 2018. Bacteria antibiotic resistance: New challenges and opportunities for implant-associated orthopedic infections. *Journal of orthopaedic research : official publication of the Orthopaedic Research Society*, 36, 22-32.
- LI, H., WANG, D., ZHANG, W., XU, G., XU, C., LIU, W. & LI, J. 2023a. Potential side effects of antibacterial coatings in orthopaedic implants: A systematic review of clinical studies. *Frontiers in Bioengineering and Biotechnology*, 11.
- LI, P., YIN, R., CHENG, J. & LIN, J. 2023b. Bacterial Biofilm Formation on Biomaterials and Approaches to Its Treatment and Prevention. *Int J Mol Sci*, 24.
- LIN, M. C., HU, D., MARMOR, M., HERFAT, S. T., BAHNEY, C. S. & MAHARBIZ, M. M. 2019. Smart bone plates can monitor fracture healing. *Sci Rep*, 9, 2122.
- LIND, R., CONNOLLY, P., WILKINSON, C. D. W., BRECKENRIDGE, L. J. & DOW, J. A. T. 1991. Single cell mobility and adhesion monitoring using extracellular electrodes. *Biosensors and Bioelectronics*, 6, 359-367.
- LIU, J., XU, Y., LIU, S., YU, S., YU, Z. & LOW, S. S. 2022. Application and Progress of Chemometrics in Voltammetric Biosensing. *Biosensors*, 12, 494.

- LIU, L., XU, Y., CUI, F., XIA, Y., CHEN, L., MOU, X. & LV, J. 2018. Monitoring of bacteria biofilms forming process by in-situ impedimetric biosensor chip. *Biosensors and Bioelectronics*, 112, 86-92.
- LOVEDAY, D. P., P. ; RODGERS, B. 2004. Evaluation of Organic Coatings with Electrochemical Impedance Spectroscopy Part 2: Application of EIS to Coatings.
- LU, X., WU, Z., XU, K., WANG, X., WANG, S., QIU, H., LI, X. & CHEN, J. 2021. Multifunctional Coatings of Titanium Implants Toward Promoting Osseointegration and Preventing Infection: Recent Developments. *Frontiers in bioengineering and biotechnology*, 9, 783816-783816.
- MAGAR, H. S., HASSAN, R. Y. A. & MULCHANDANI, A. 2021. Electrochemical Impedance Spectroscopy (EIS): Principles, Construction, and Biosensing Applications. *Sensors (Basel)*, 21.
- MAGILL, S. S., EDWARDS, J. R., BAMBERG, W., BELDAVS, Z. G., DUMYATI, G., KAINER, M. A., LYNFIELD, R., MALONEY, M., MCALLISTER-HOLLOD, L., NADLE, J., RAY, S. M., THOMPSON, D. L., WILSON, L. E. & FRIDKIN, S. K. 2014. Multistate point-prevalence survey of health care-associated infections. *N Engl J Med*, 370, 1198-208.
- MAHDAVIAN, M. & ATTAR, M. 2006. Another approach in analysis of paint coatings with EIS measurement: Phase angle at high frequencies. *Corrosion Science*, 48, 4152-4157.
- MARQUES, I. D., BARÃO, V. A., DA CRUZ, N. C., YUAN, J. C., MESQUITA, M. F., RICOMINI-FILHO, A. P., SUKOTJO, C. & MATHEW, M. T. 2015. Electrochemical behavior of bioactive coatings on cp-Ti surface for dental application. *Corros Sci*, 100, 133-146.
- MCGUIRE, A. F., SANTORO, F. & CUI, B. 2018. Interfacing Cells with Vertical Nanoscale Devices: Applications and Characterization. *Annu Rev Anal Chem (Palo Alto Calif)*, 11, 101-126.
- MCKENZIE, K., MACLEAN, M., TIMOSHKIN, I. V., ENDARKO, E., MACGREGOR, S. J. & ANDERSON, J. G. 2013. Photoinactivation of bacteria attached to glass and acrylic surfaces by 405 nm light: potential application for biofilm decontamination. *Photochem Photobiol*, 89, 927-35.
- MEDILANSKI, E., KAUFMANN, K., WICK, L. Y., WANNER, O. & HARMS, H. 2002. Influence of the surface topography of stainless steel on bacterial adhesion. *Biofouling*, 18, 193-203.
- METROHM Electrochemical Impedance Spectroscopy (EIS)
- Part 2 – Experimental Setup.
- MOORMEIER, D. E. & BAYLES, K. W. 2017. Staphylococcus aureus biofilm: a complex developmental organism. *Mol Microbiol*, 104, 365-376.
- MU, M., LIU, S., DEFLORIO, W., HAO, L., WANG, X., SALAZAR, K. S., TAYLOR, M., CASTILLO, A., CISNEROS-ZEVALLOS, L., OH, J. K., MIN, Y. & AKBULUT, M. 2023. Influence of Surface Roughness, Nanostructure, and Wetting on Bacterial Adhesion. *Langmuir*, 39, 5426-5439.
- MUFTY, H., VAN DEN BERGH, M., MEURIS, B., METSEMAKERS, W. J. & FOURNEAU, I. 2022. Clinical Studies Reporting on Vascular Graft Coatings for

- the Prevention of Aortic Graft Infection: A Systematic Review and Meta-Analysis. *Eur J Vasc Endovasc Surg*, 63, 112-118.
- NAVARRO, P., OLMO, A., GINER, M., RODRÍGUEZ-ALBELO, M., RODRÍGUEZ, Á. & TORRES, Y. 2022. Electrical Impedance of Surface Modified Porous Titanium Implants with Femtosecond Laser. *Materials (Basel)*, 15.
- O'BRIEN, B., ZAFAR, H., IBRAHIM, A., ZAFAR, J. & SHARIF, F. 2015. Coronary Stent Materials and Coatings: A Technology and Performance Update. *Ann Biomed Eng*, 44, 523-535.
- OLMO, A., HERNÁNDEZ, M., CHICARDI, E. & TORRES, Y. 2020. Characterization and Monitoring of Titanium Bone Implants with Impedance Spectroscopy. *Sensors (Basel, Switzerland)*, 20, 4358.
- PAN, C., ZHOU, Z. & YU, X. 2018. Coatings as the useful drug delivery system for the prevention of implant-related infections. *J Orthop Surg Res*, 13, 220.
- PAN, Y., HU, N., WEI, X., GONG, L., ZHANG, B., WAN, H. & WANG, P. 2019. 3D cell-based biosensor for cell viability and drug assessment by 3D electric cell/matrigel-substrate impedance sensing. *Biosensors and Bioelectronics*, 130, 344-351.
- PAREDES, J., BECERRO, S. & ARANA, S. 2014a. Comparison of real time impedance monitoring of bacterial biofilm cultures in different experimental setups mimicking real field environments. *Sensors and Actuators B: Chemical*, 195, 667-676.
- PAREDES, J., BECERRO, S. & ARANA, S. 2014b. Label-free interdigitated microelectrode based biosensors for bacterial biofilm growth monitoring using Petri dishes. *J Microbiol Methods*, 100, 77-83.
- PEETERS, E., NELIS, H. J. & COENYE, T. 2008. Comparison of multiple methods for quantification of microbial biofilms grown in microtiter plates. *J Microbiol Methods*, 72, 157-65.
- PENNINGTON, M. R. & VAN DE WALLE, G. R. 2017. Electric Cell-Substrate Impedance Sensing To Monitor Viral Growth and Study Cellular Responses to Infection with Alphaherpesviruses in Real Time. *mSphere*, 2.
- PERMEH, S., LAU, K. & DUNCAN, M. 2019. Characterization of Biofilm Formation and Coating Degradation by Electrochemical Impedance Spectroscopy. *Coatings*, 9, 518.
- RADHI, M., ISMAEL, A., AL-HAIDAIRE, Y., ALASADI, S. & ALMULLA, E. 2019. Rifampicin: Electrochemical Effect on Blood Component by Cyclic Voltammetry Using Nano-Sensor. *Nano Biomedicine and Engineering*, 11, 150-156.
- RAHMAN, Z. U., SHABIB, I. & HAIDER, W. 2016. Surface characterization and cytotoxicity analysis of plasma sprayed coatings on titanium alloys. *Materials Science and Engineering: C*, 67, 675-683.
- RANDVIIR, E. P. & BANKS, C. E. 2013. Electrochemical impedance spectroscopy: an overview of bioanalytical applications. *Analytical Methods*, 5, 1098-1115.
- RAPOSO, M., FERREIRA, Q. & RIBEIRO, P. 2007. A Guide for Atomic Force Microscopy Analysis of Soft Condensed Matter. *Modern Research and Educational Topics in Microscopy*, 1.

- ROMANÒ, C. L., SCARPONI, S., GALLAZZI, E., ROMANÒ, D. & DRAGO, L. 2015. Antibacterial coating of implants in orthopaedics and trauma: a classification proposal in an evolving panorama. *Journal of orthopaedic surgery and research*, 10, 157-157.
- ROMERO, M. C., RAMOS, G., GONZÁLEZ, I. & RAMÍREZ, F. 2021. A Novel Method to Reveal a Ureolytic Biofilm Attachment and In Situ Growth Monitoring by Electrochemical Impedance Spectroscopy. *Applied Biochemistry and Biotechnology*, 193, 1379-1396.
- SAEED, S., RAFIQ, M., BALOACH, Q.-U.-A., NAQVI, S. H., TAHIRA, A., KHAN, H., HULLIO, A., MALLAH, A., WILLANDER, M., AKHTAR, M. & IBUPOTO, Z. 2017. Vanillin Assisted Synthesis of Co<sub>3</sub>O<sub>4</sub> Nanostructures for the Development of Sensitive and Selective Peptone Biosensor. *Sensor Letters*, 15, 536-544.
- SALMAN, H. 2020. Bacterial Growth: Cell-Cycle Dependent Growth-Rate Homeostasis. *Curr Biol*, 30, R703-r704.
- SCHMIEDINGER, T., PARTEL, S., LECHLEITNER, T., EITER, O., HEKL, D., KASEMAN, S., LUKAS, P., EDLINGER, J., LECHNER, J. & SEPPI, T. 2020. Interdigitated aluminium and titanium sensors for assessing epithelial barrier functionality by electric cell-substrate impedance spectroscopy (ECIS). *Biomedical microdevices*, 22, 30-30.
- SCHWARTZ, R. S., EDELMAN, E., VIRMANI, R., CARTER, A., GRANADA, J. F., KALUZA, G. L., CHRONOS, N. A., ROBINSON, K. A., WAKSMAN, R., WEINBERGER, J., WILSON, G. J. & WILENSKY, R. L. 2008. Drug-eluting stents in preclinical studies: updated consensus recommendations for preclinical evaluation. *Circ Cardiovasc Interv*, 1, 143-53.
- SHAO, X., XIE, Y., ZHANG, Y. & DENG, X. 2019. Biofilm Formation Assay in *Pseudomonas syringae*. *Bio-protocol*, 9, e3237-e3237.
- SHEDDEN, L., KENNEDY, S., WADSWORTH, R. & CONNOLLY, P. 2010. Towards a self-reporting coronary artery stent—Measuring neointimal growth associated with in-stent restenosis using electrical impedance techniques. *Biosens Bioelectron*, 26, 661-666.
- SILVA, R. R. A., MARQUES, C. S., ARRUDA, T. R., TEIXEIRA, S. C. & DE OLIVEIRA, T. V. 2023. Biodegradation of Polymers: Stages, Measurement, Standards and Prospects. 3, 371-399.
- SINGH, R., TIWARI, S. K., MISHRA, S. K. & DAHOTRE, N. B. 2011. Electrochemical and mechanical behavior of laser processed Ti-6Al-4V surface in Ringer's physiological solution. *J Mater Sci Mater Med*, 22, 1787-96.
- STEWART, P. S. & BJARNSHOLT, T. 2020. Risk factors for chronic biofilm-related infection associated with implanted medical devices. *Clinical Microbiology and Infection*, 26, 1034-1038.
- SURGEONS, A. A. O. H. A. K. 2023. *Infection and Your Joint Replacement* [Online]. Available: [https://hipkneeinfo.org/hip-care/infection-and-your-joint-replacement/#:~:text=LATE%20\(6%20weeks%20or%20more,late%20as%20a%20late%20infection.](https://hipkneeinfo.org/hip-care/infection-and-your-joint-replacement/#:~:text=LATE%20(6%20weeks%20or%20more,late%20as%20a%20late%20infection.) [Accessed].



- SWAMI, P., VERMA, G., HOLANI, A., KAMARAJU, S., MANCHANDA, V., SRITHARAN, V. & GUPTA, S. 2022. Rapid antimicrobial susceptibility profiling using impedance spectroscopy. *Biosensors and Bioelectronics*, 200, 113876.
- SZULCEK, R., BOGAARD, H. J. & VAN NIEUW AMERONGEN, G. P. 2014. Electric cell-substrate impedance sensing for the quantification of endothelial proliferation, barrier function, and motility. *J Vis Exp*.
- THI, M. T. T., WIBOWO, D. & REHM, B. H. A. 2020. Pseudomonas aeruginosa Biofilms. *Int J Mol Sci*, 21.
- THORNSBERRY, C., HILL, B. C., SWENSON, J. M. & MCDUGAL, L. K. 1983. Rifampin: Spectrum of Antibacterial Activity. *Reviews of Infectious Diseases*, 5, S412-S417.
- TRIPATHI, N. & SAPRA, A. 2024. Gram Staining. *StatPearls*. Treasure Island (FL) ineligible companies. Disclosure: Amit Sapra declares no relevant financial relationships with ineligible companies.: StatPearls Publishing
- Copyright © 2024, StatPearls Publishing LLC.
- TURICK, C. E., COLON-MERCADO, H., BAGWELL, C. E., GREENWAY, S. D. & AMOROSO, J. W. 2020. Non-contact electrochemical evaluation of biofilms. *SN Applied Sciences*, 2, 389.
- VAN DUUREN, J., MÜSKEN, M., KARGE, B., TOMASCH, J., WITTMANN, C., HÄUSSLER, S. & BRÖNSTRUP, M. 2017. Use of Single-Frequency Impedance Spectroscopy to Characterize the Growth Dynamics of Biofilm Formation in Pseudomonas aeruginosa. *Sci Rep*, 7, 5223.
- VANEPPS, J. S. & YOUNGER, J. G. 2016. Implantable Device-Related Infection. *Shock*, 46, 597-608.
- VISAN, A. 2021. Degradation Behavior of Polymers Used as Coating Materials for Drug Delivery—A Basic Review. *Polymers*.
- VO, T. T. N., MORGAN, S., MCCORMICK, C., MCGINTY, S., MCKEE, S. & MEERE, M. 2018. Modelling drug release from polymer-free coronary stents with microporous surfaces. *International Journal of Pharmaceutics*, 544, 392-401.
- WANG, L., SEYEUX, A. & MARCUS, P. 2020. Thermal stability of the passive film formed on 316L stainless steel surface studied by ToF-SIMS. *Corrosion Science*, 165, 108395.
- WARD, A. C., CONNOLLY, P. & TUCKER, N. P. 2014. Pseudomonas aeruginosa can be detected in a polymicrobial competition model using impedance spectroscopy with a novel biosensor. *PLoS One*, 9, e91732.
- WARD, A. C., HANNAH, A. J., KENDRICK, S. L., TUCKER, N. P., MACGREGOR, G. & CONNOLLY, P. 2018. Identification and characterisation of Staphylococcus aureus on low cost screen printed carbon electrodes using impedance spectroscopy. *Biosensors and Bioelectronics*, 110, 65-70.
- WEBSTER, T. 2009. *Safety of Nanoparticles: From Manufacturing to Medical Applications*.
- WELCH, K., CAI, Y. & STRØMME, M. 2012. A method for quantitative determination of biofilm viability. *J Funct Biomater*, 3, 418-31.

- WU, D. W., YU, M. Y., GAO, H. Y., ZHANG, L., SONG, F., ZHANG, X. Y. & WU, Y. J. 2015. Polymer-free versus permanent polymer drug eluting stents in coronary artery disease: A meta-analysis of 10 RCTs with 6575 patients. *Chronic Dis Transl Med*, 1, 221-230.
- WU, M., KLEINER, L., TANG, F.-W., HOSSAINY, S., DAVIES, M. C. & ROBERTS, C. J. 2010. Surface characterization of poly(lactic acid)/everolimus and poly(ethylene vinyl alcohol)/everolimus stents. *Drug Delivery*, 17, 376-384.
- XIA, D.-H., SONG, S., WANG, J., BI, H. & HAN, Z. 2012. Fast evaluation of degradation degree of organic coatings by analyzing electrochemical impedance spectroscopy data. *Transactions of Tianjin University*, 18, 15-20.
- XU, Y., XIE, X., DUAN, Y., WANG, L., CHENG, Z. & CHENG, J. 2016. A review of impedance measurements of whole cells. *Biosens Bioelectron*, 77, 824-36.
- YU, X., JIANG, G., LI, H., ZHAO, Y., ZHANG, H., ZHAO, L., MA, Y., COULTER, C. & HUANG, H. 2011. Rifampin stability in 7H9 broth and Löwenstein-Jensen medium. *Journal of clinical microbiology*, 49, 784-789.
- ZHANG, H., KONG, F., DUN, Y., CHEN, X., CHEN, Q., ZHAO, X., TANG, Y. & ZUO, Y. 2023. Degradation of Carbon Fiber-Reinforced Polymer Composites in Salt Water and Rapid Evaluation by Electrochemical Impedance Spectroscopy. *Materials (Basel)*, 16.
- ZHAO, L., CHU, P. K., ZHANG, Y. & WU, Z. 2009. Antibacterial coatings on titanium implants. *Journal of Biomedical Materials Research Part B: Applied Biomaterials*, 91B, 470-480.
- ZHENG, T.-X., LI, W., GU, Y.-Y., ZHAO, D. & QI, M.-C. 2022. Classification and research progress of implant surface antimicrobial techniques. *Journal of Dental Sciences*, 17, 1-7.
- ZHONG, Q., MAO, Q., YAN, J., LIU, W., ZHANG, T. & LIU, J. 2015. Real-time in situ monitoring of poly(lactide-co-glycolide) coating of coronary stents using electrochemical impedance spectroscopy. *Society for Biomaterials*, 103, 691-699.
- ZHU, Y., LIU, W. & NGAI, T. 2022. Polymer coatings on magnesium-based implants for orthopedic applications. *Journal of Polymer Science*, 60, 32-51.
- ZUO, Y., PANG, R., LI, W., XIONG, J. P. & TANG, Y. M. 2008. The evaluation of coating performance by the variations of phase angles in middle and high frequency domains of EIS. *Corrosion Science*, 50, 3322-3328.